Early Age Characterization and Microstructural Features of Sustainable Binder Systems for Concrete

by

Kirk Vance

A Dissertation Presented in Partial Fulfillment
of the Requirements for the Degree
Doctor of Philosophy

Approved May 2014 by the
Graduate Supervisory Committee:

Narayanan Neithalath, Chair
Barzin Mobasher
Subramaniam Rajan
Nikhilesh Chawla
Robert Marzke

ARIZONA STATE UNIVERSITY

August 2014

ABSTRACT

Concrete is the most widely used infrastructure material worldwide. Production of portland cement, the main binding component in concrete, has been shown to require significant energy and account for approximately 5-7% of global carbon dioxide production. The expected continued increased use of concrete over the coming decades indicates this is an ideal time to implement sustainable binder technologies. The current work aims to explore enhanced sustainability concretes, primarily in the context of limestone and flow. Aspects such as hydration kinetics, hydration product formation and pore structure add to the understanding of the strength development and potential durability characteristics of these binder systems.

Two main strategies for enhancing this sustainability are explored in this work: (i) the use of high volume limestone in combination with other alternative cementitious materials to decrease the portland cement quantity in concrete and (ii) the use of geopolymers as the binder phase in concrete. The first phase of the work investigates the use of fine limestone as cement replacement from the perspective of hydration, strength development, and pore structure. The nature of the potential synergistic benefit of limestone and alumina will be explored. The second phase will focus on the rheological characterization of these materials in the fresh state, as well as a more general investigation of the rheological characterization of suspensions.

The results of this work indicate several key ideas. (i) There is a potential synergistic benefit for strength, hydration, and pore structure by using alumina and in portland limestone cements, (ii) the limestone in these systems is shown to react to some extent, and fine limestone is shown to accelerate hydration, (iii) rheological characteristics of

cementitious suspensions are complex, and strongly dependent on several key parameters including: the solid loading, interparticle forces, surface area of the particles present, particle size distribution of the particles, and rheological nature of the media in which the particles are suspended, and (iv) stress plateau method is proposed for the determination of rheological properties of concentrated suspensions, as it more accurately predicts apparent yield stress and is shown to correlate well with other viscoelastic properties of the suspensions.

To Asha, for her support, encouragement and understanding

ACKNOWLEDGEMENTS

The completion of this dissertation would not have been possible without the support and assistance of many friends and colleagues. Firstly I would like to thank my family: Asha, my mother, my father, and sister for all of their support, encouragement and assistance throughout.

I would further like to gratefully acknowledge the guidance, support and motivation offered by my advisor, Prof. Neithalath without whom this dissertation surely would not have been possible. I would additionally like to thank my committee members: Profs. Rajan, Mobasher, Marzke, and Chawla for dedicating their time and guidance to this work.

I would additionally like to thank the many with whom I worked on this project. Specifically I am grateful to those that directly contributed to this work: Matthew Aguayo, Akash Dakhane, and Aashay Arora. I would like to also acknowledge the other students who helped along the way: Deepak, Sundar, Sumanta, Ben, Vikram, Ussala, Kingsten, Sateesh, Pu, and Breeann.

I would further like to thank the laboratory support staff: Kenneth Witczak and Peter Goguen for all their assistance throughout this project.

Finally, I would like to thank the National Science Foundation and the Ira A. Fulton Schools of Engineering Dean's Fellowship for the financial support provided which enabled the completion of this project.

TABLE OF CONTENTS

Page

CHAPTER Page

CHAPTER Page

CHAPTER Page

CHAPTER Page

CHAPTER Page

LIST OF TABLES

Table Page

Table Page

LIST OF FIGURES

Figure Page

Figure Page

Figure Page

Figure Page

Figure Page

Figure Page

Figure Page

Figure Page

Figure Page

Figure Page

1. INTRODUCTION

The expected continued increase in worldwide demand of concrete (P. Kumar Mehta and Monteiro 2005) indicates this is an ideal time to focus on the sustainability of these systems. Concrete is composed of portland cement, water, and aggregates. Portland cement undergoes hydration reactions with water to form a cement paste which binds the aggregates together to form concrete. Portland cement production is an energy intensive process which requires heating of limestone and other raw materials to a very high temperature, after which the products of this process, the portland cement clinker, are ground to the desired fineness. Production of concrete thus requires significant energy, approximately 4600 MJ/ton of cement (Government of Canada 2009). Further, it has been shown that portland cement production accounts for approximately 5% of global anthropogenic CO_2 emissions (Worrell et al. 2001). These carbon dioxide emissions are both a product of the energy production required as well as the calcination that occurs when limestone is heated to a high temperature (Worrell et al. 2001; P. Kumar Mehta and Monteiro 2005). The inherent chemical production of CO_2 can be as high as 60% of total carbon emissions from portland cement production (Worrell et al. 2001). This fact indicates that while gains may be possible from the use of low heat cements or increased efficiency, since a majority of the CO_2 emissions result from portland cement manufacture are a direct result of the chemical process itself, alternative strategies are required to further reduce carbon emissions associated with portland cement manufacture. These issues have motivated the current work to explore two possible strategies for enhanced sustainability in concrete: (i) replacement of portland cement by limestone and limestone in combination with waste stream alumina sources, and (ii) the use of cement-free binder systems, also

known as geopolymers, wherein the binder phase in the concrete is composed entirely of aluminosilicate waste stream materials such as fly ash or slag. The first phase of the project is devoted to the hydration, strength development, and microstructural features of limestone replaced portland cement systems with and without additional alumina sources. The second phase of the project is devoted to determination of the rheological characteristics of both plain and blended portland cement systems, as well as fly ash and slag based geopolymer systems.

1.1 Objectives

Determine the synergistic benefits of the use of limestone in combination with alumina sources (metakaolin, fly ash, sodium aluminate) as partial cement replacement materials on the hydration kinetics, product formation, and strength development of cement pastes.

Investigate the microstructure of these modified cementitious systems through the use of mercury porosimetry.

Determine the influences of fine blended and interground limestone with or without an alumina source on the flow characteristics of fresh portland cement suspensions.

Investigate the applicability of the generalized Bingham models to portland cement based suspensions as well as fly ash and slag geopolymer suspensions. Also, to investigate methods for determining the rheological yield stress in concentrated cementitious suspensions and use rheology to investigate influences of limestone and additives on the property (storage and loss moduli) development of these suspensions.

Investigate the influences of silica modulus, alkali-to-binder ratio, activator type, and molarity on the rheological properties of fly ash and slag based geopolymer materials, so

as to better tailor chemical admixture systems for geopolymer mixtures, which are non-existent currently.

1.2 Dissertation Layout

This dissertation is composed primarily of the seven papers that have been or will be submitted for publication as part of this work, with in some cases additional data that is not presented in the published papers. These papers can be found in Chapters 4-10. The first section of this dissertation is composed of Chapters 4 and 5, which focuses on the hydration, strength development, and pore structure of limestone replacement portland cement pastes. The second section composed of the remaining chapters is devoted to the rheological characterization of sustainable binder systems in the fresh state, including: limestone replacement portland cement, fly ash geopolymer, and slag geopolymer suspensions.

Chapter 2 provides an extensive literature review into the following key topics: (i) the use of limestone in portland cement systems, (ii) the use of rheology to characterize the flow behavior of cementitious suspensions and concentrated suspensions in general.

Chapter 3 provides a brief exploration of the experimental methodologies and materials used in the study. As a large number of experiments were completed as part of this study using a wide variety of experimental techniques and procedures, more in-depth discussions of methods used for the individual chapters is presented in their corresponding chapters.

Chapter 4 explores the influences of limestone replacement of portland cement with or without additional alumina sources on the hydration kinetics, compressive strength development, and hydration product formation.

Chapter 5 presents an analysis of the influence of limestone replacement of portland cement on the pore structure of the hardened pastes as determined using mercury intrusion porosimetry. The pore structure of the pastes is investigated using both intrusion and extrusion curves, and the influence of limestone is disconnected from packing and surface area influences by replacing cement with particle size distribution matched limestone.

Chapter 6 presents rheological exploration of ternary blended portland cement, limestone, and metakaolin or fly ash suspensions in the fresh state. The nature of the rheological performance of these suspensions is explored through the use of the Bingham model, and particle size and surface area effects are fully explored in this analysis.

Chapter 7 presents an exploration of experimental influences on the rheological characterization of portland cement suspensions in the fresh state. The effect of gap, mixing technique, surface roughness, and shear rate range of the study are thoroughly explored. Further, an investigation of the relevance of several rheological models is included, namely: Bingham, Herschel-Bulkley, and Casson. Further, this model investigation is extended to other concentrated suspensions including suspensions of fly and limestone in water, as well as fly ash and slag suspended in various alkali-activated solutions.

Chapter 8 further explores the rheological nature of limestone replaced portland cement suspensions using the techniques as determined in Chapter 7. The nature of limestone in these suspensions is disconnected from particle size and surface area effects through the use of size-matched limestone as a cement replacement material. The viscoelastic nature of these suspensions is explored using small amplitude oscillatory shear experiments.

Chapter 9 investigates the influence of alkali activator type and concentration on the rheological performance of fly ash suspensions in the alkali activated solution. Characterization of these suspensions was completed for both alkali-hydroxide activator solutions and alkali-silica-hydroxide activator solutions, where the selected alkalis are Na or K.

Chapter 10 provides a similar investigation as Chapter 9, however for the case of slag based geopolymers in the fresh state. A similar comparison of activator solution effects is explored and presented.

2. LITERATURE REVIEW

The proceeding literature review is divided into two distinct sections, one focused on the historical and current use of limestone as a portland cement replacement material, and the second a review of rheological characterization of suspensions, with a particular focus on cementitious suspensions.

2.1 Limestone as Cement Replacement Material

2.1.1 Overview and Background

Portland cement concrete (PCC) is the most widely used infrastructure material globally. PCC is primarily composed of aggregates (rock and sand), water, and portland cement. Portland cement, the main binding component in concrete is manufactured by heating raw materials such as limestone and clay in a kiln at temperatures of approximately 1500 °C. The high heat requirement for portland cement production requires a significant quantity of energy, approximately 4600 MJ/ton (Government of Canada 2009). Further the production of portland cement releases a significant quantity of CO_2, accounting for approximately 5% of global anthropogenic carbon dioxide production (Worrell et al. 2001; Hendriks et al. 2002). These factors, combined with the predicted increases in concrete use over the coming decades indicate this is an ideal time to focus on enhancing the sustainability of concrete (P.K. Mehta 2002; P. Kumar Mehta and Monteiro 2005). Two primary methods are currently used for enhancing concrete sustainability: (i) decrease the energy demand required for cement production or increase efficiency and (ii) partial replacement of cement by inert fillers or reactive pozzolanic materials. Strategies for decreasing energy requirements include enhancing efficiency of production facilities and the use of low energy cements (Popescu, Muntean, and Sharp 2003), cements which require

lower temperatures to produce cement. However, more than 50% of the carbon dioxide released during cement production is a result of the calcination of limestone (Worrell et al. 2001), thus advances in efficiency may not be able to have a significant impact on greenhouse gas emissions. Pozzolanic materials are aluminosilicate materials which chemically react with the portlandite phase in cement hydration to produce additional C-S-H gel. Traditional pozzolanic replacement materials used to enhanced concrete sustainability include the use of aluminosilicate waste stream materials such as fly ash and slag from coal fired power plants and steel production respectively. However, the availability of these materials is limited, and the increased use of natural gas extracted using hydraulic fracturing may limit the availability of fly ash in particular (Texas Department of Transportation 2012).

Over the past decades there has been increased interest in the use of limestone as a partial cement replacement material in portland cement concrete. This interest is motivated by a desire to increase the sustainability of concrete by reducing the required portland cement content, thereby reducing the CO_2 emissions and energy requirements associated with portland cement production. To achieve full hydration, it has been shown that chemically a minimum water-to-cement (w/c) ratio of approximately 0.25 is required (P. Kumar Mehta and Monteiro 2005), however the hydration model proposed by Powers indicates that the lack of capillary porosity in low w/c ratio concretes restricts the ultimate degree of hydration further, and a minimum w/c ratio of 0.36 is required for complete hydration of cement (Powers and Brownyard 1947). Thus, in modern high performance concretes (HPCs) which are commonly manufactured using very low w/c ratios, below this limit proposed by Powers, there remains unhydrated portland cement even at very late ages.

Given that this remaining unreacted cement is acting primarily as a filler material and increasing the microstructural packing, it has been proposed that partial replacement of cement by an inert filler may achieve comparable mechanical performance while concurrently decreasing the financial and environmental costs associated with concrete production (D. Bentz et al. 2009a; V. Bonavetti et al. 2003; Dale P. Bentz 2006). Thus, inclusion of the relatively inert limestone in as a cement replacement material could act to raise the effective w/c ratio, increasing the degree of hydration and replacing the unreacted cement at later ages.

2.1.2 Influence of Limestone on Cement Hydration

Typical portland cement hydration is a series of exothermic reactions consisting of a dissolution phase, an induction period, a subsequent acceleration phase, followed finally by diffusion controlled regime. The resultant heat flow curve is typically a two peak system, the first peak representing the dissolution peak and the second peak corresponding to the main hydration peak. A typical presentation of the heat evolution of the cement hydration reactions is presented in Figure 2-1. The dissolution phase corresponds to the initial heat release associated with the dissolution of aluminates and sulfates and the early hydration of the aluminate phase, and lasts on the order of minutes (Irassar et al. 2011; P. Kumar Mehta and Monteiro 2005). The induction period typically lasts on the order of a few hours, and is proceeded by the main hydration peak. The main hydration peak corresponds to the reaction of the calcium phases in the portland cement to form C-S-H gel and other hydration products. A shoulder is typically present on the main hydration peak indicating the secondary formation of ettringite (Bullard et al. 2011). At early ages in ordinary portland cement ettringite is formed in a reaction between the C_3A phases and the

sulfates added in the form of gypsum to control setting. After the sulfates have been consumed, ettringite reacts with the remaining C_3A to form monosulfate. The final phase in portland cement hydration is the diffusion controlled phase, represented by a slow downward slope of the main hydration peak, where further reaction of the C_3S and C_2S is controlled by the diffusion of water through the hydration shell that has formed on the portland cement grains.

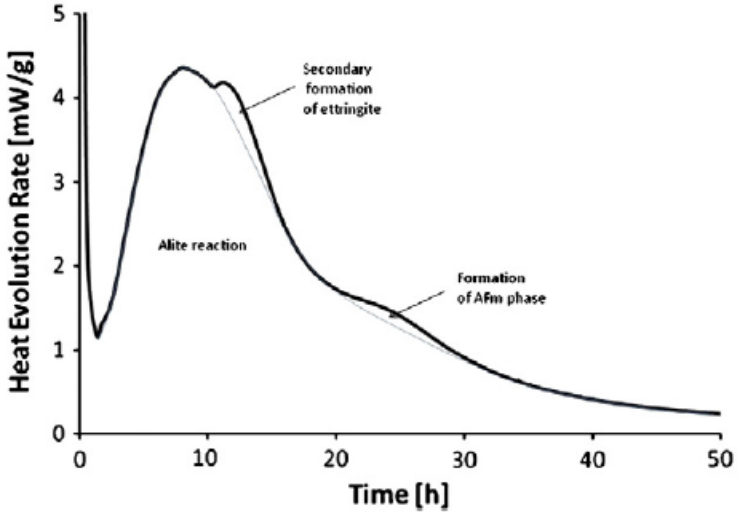

Figure 2-1: Typical cement heat evolution curve (Bullard et al. 2011)

Extensive work has been completed on the influences of limestone replacement on portland cement hydration. Some works on the heat evolution of portland cement replaced by limestone tended to indicate that the inclusion of limestone had a negligible effect, or even a slight reduction in the heat flow response of the paste (Irassar et al. 2011; Hooton 1990; Livesey 1991). However, it is noted that these experiments were either conducted semi-adiabatically or appear to be measuring the heat flow response of the entire composite system. Other works by both Bonavetti (V. Bonavetti et al. 2003) and Bentz (Dale P. Bentz 2006) found that the replacement of cement by limestone raised the degree of hydration of

the resultant cement paste. These results appear contradictory to the works described above, however there are multiple possible causes for the discrepancy: (i) normalization of heat flow based on cement content rather than sample mass provides a more accurate picture of the degree of hydration and (ii) the effect of fineness of the limestone used as replacement material may be crucial. Similarly, reports on the effect of limestone on heat of hydration in self compacting concrete systems indicated a significantly accelerated hydration (Ye et al. 2007). It is thus appears generally agreed that the influence of fine limestone on cement hydration is one to accelerate the hydration reactions, as it acts as a nucleation site for hydration product formation (Soroka and Setter 1977).

Several studies have investigated the influence of limestone on hydration product formation. It has been shown that limestone reacts to some extent with the C_3A phase in portland cement (Soroka and Stern 1976; Ingram et al. 1990), and in a pure C_3A system limestone has been shown to react significantly with this phase, while not as significantly with pure C_3S (Kakali et al. 2000). Limestone powder interacts chemically with the C_3A phase in the cement stabilizing carboaluminate and reducing the formation of monosulfoaluminate (Matschei, Lothenbach, and Glasser 2007b). Subsequently the reaction of ettringite with the C_3A phase to form monosulfate is prevented due to the increased stability of carboaluminate as compared to monosulfate (Matschei, Lothenbach, and Glasser 2007b; De Weerdt, Haha, et al. 2011). This stabilized ettringite in the paste, and due to the lower density of ettringite as compared to other hydration products may potentially lead to a reduction of porosity and enhanced strength in the hardened paste. These results have been confirmed by the determination that ettringite remained present in significant volumes even in later age pastes (Kakali et al. 2000; Hoshino, Yamada, and

Hirao 2006). There have been varying results with regard to investigations of the quantities of calcium carbonate that is consumed in these systems, with some believing that in low volume replacement almost all of it may be consumed (Matschei, Lothenbach, and Glasser 2007b), while most reporting limestone consumption on the order of 5-10% of limestone by mass. Further, the reactivity of limestone in portland cement systems has indicate an overall decrease in bound water in the system, indicated a decrease in degree of hydration, as limestone quantity is increased, however, when the value is normalized by the quantity of cement the bound water can be seen to increase (De Weerdt, Kjellsen, et al. 2011). This indicates that the degree of hydration of the portland cement is higher, supporting the idea that limestone is accelerating the hydration reactions. These effects are attributed primarily to the dilution of cement in the system resulting in a higher effective w/c ratio and limestone acting as a nucleation site for hydration products.

Based on the noted interaction between limestone and the alumina phases in portland cement, several studies have been completed to investigate possible synergistic benefits of the addition of alumina sources to portland limestone cements. The hydration of binary systems of portland cement and alumina sources such as fly ash, slag, or metakaolin have been well documented in the literature. Pozzolanic materials such as fly ash, metakaolin and slag have been shown to react with the portlandite phase in cement hydration. This in turn results in enhanced durability and mechanical strength in these concretes due to a reduction in the water soluble calcium hydroxide phase, and replacement with less soluble hydration products. In fly ash-cement blends, fly ash has been shown to have a low reactivity until later ages (Fajun, Grutzeck, and Roy 1985; Fraay, Bijen, and de Haan 1989; Sakai et al. 2005), typically remaining unreacted in the system until later ages when it

reacts with the portlandite (calcium hydroxide) to form C-(A)-S-H gel. The influence of low calcium fly ash is seen to be primarily a dilution effect on heat evolution, due to this low early age reactivity (Sánchez de Rojas et al. 1993), decreasing the heat evolved in the paste, however when normalized by cement content remaining comparable to portland cement. Metakaolin, a calcined clay aluminosilicate material, has indicated enhanced reactivity at early ages (Wild and Khatib 1997; Sabir, Wild, and Bai 2001) as compared to fly ash, typically increasing the heat evolution when replacing portland cement (M. Frías, de Rojas, and Cabrera 2000). Like other pozzolans, metakaolin reacts with the portlandite that is formed as part of cement hydration reactions to form alternative reaction products including C-S-H and C-(A)-S-H gels. However, it is noted that due to the higher reactivity of metakaolin at early ages, the quantity of portlandite will vary based on how much has been produced and how much is consumed, often with local minima in portlandite content present as the paste ages.

Based on the Pozzolanic activity of added aluminosilicate materials in combination with the reactivity of limestone with the alumina species in cement, there is interest in possible synergistic benefits of replacement of cement in ternary blends of limestone and alternate alumina sources. Several studies have been completed on the hydration mechanisms in these systems, including hydration models of ternary limestone-fly ash systems (De Weerdt, Haha, et al. 2011), where a potential synergistic benefit was noted with enhanced formation of C-(A)-S-H gel in the presence of limestone, as well as the stabilized ettringite as discussed above. Figure 2-2 presents the results of this hydration modelling.

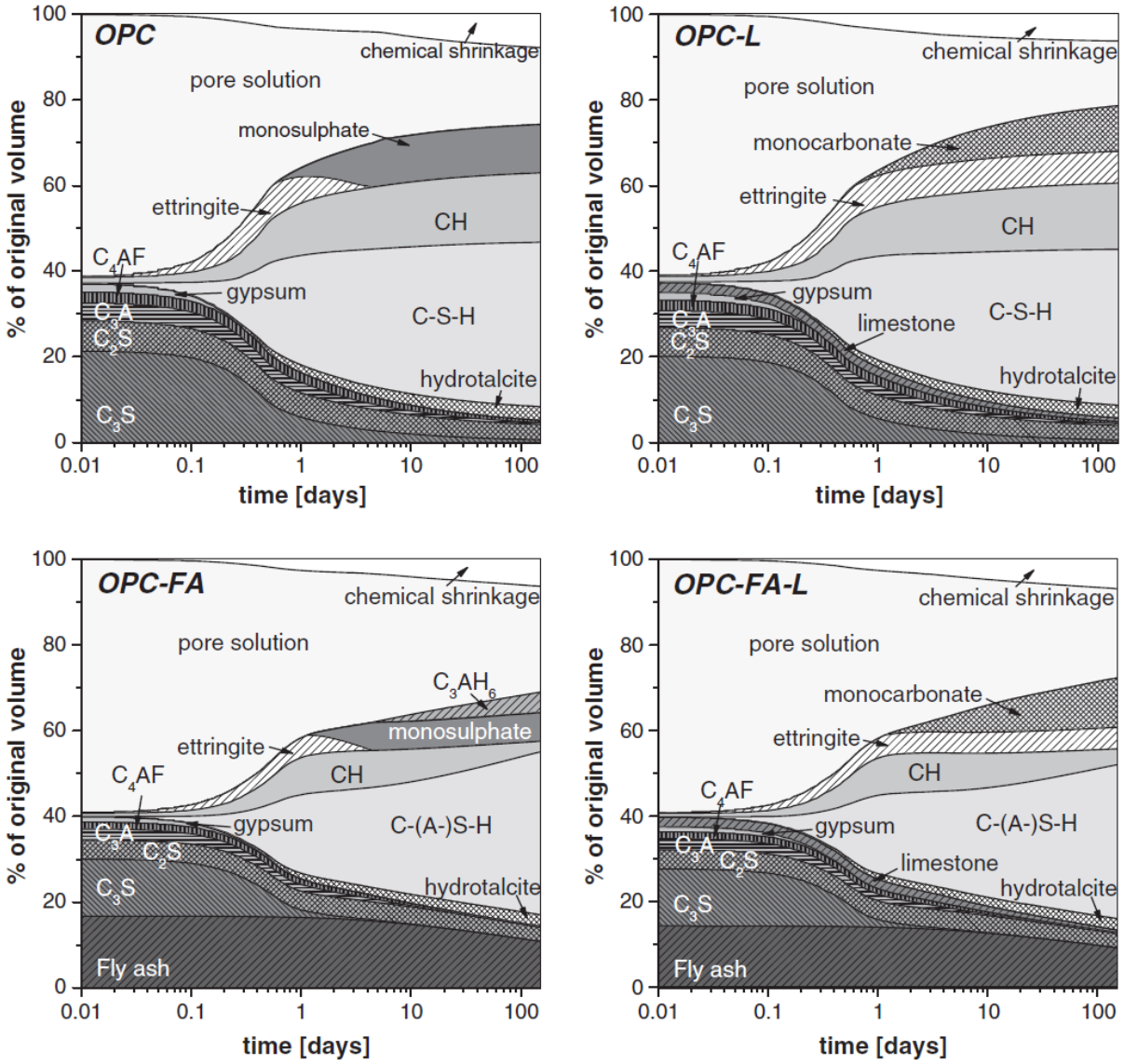

Figure 2-2: Predicted hydration products for ternary blends of limestone and fly ash (De Weerdt, Haha, et al. 2011).

The results of this hydration modeling have been partially verified, with De Weerdt (De Weerdt et al. 2010) noting both a reduction in portlandite and an increased bound water content as compared to binary limestone mixtures. Other investigations into the hydration influence of these ternary systems have noted limestone can be used to regulate the hydration of high volume fly ash mixtures (D. P. Bentz et al. 2011). Similarly, the inclusion of metakaolin in portland limestone cement systems has indicated a possible synergistic

benefit, with respect to hydration, where the main hydration peak has been shown to be significantly accelerated in blends of limestone and metakaolin, and the reaction rate of metakaolin is seen to be enhanced in the presence of limestone (Antoni et al. 2012).

2.1.3 Influence of Limestone on Mechanical Properties

Extensive work has been completed investigating the influences of limestone on the mechanical properties of portland cement pastes, mortars, and concretes. It is notable that many of these studies have contradictory results, possibly attributed to the fineness of the selected limestone, replacement ratio and type of cement used. Tsivilis found that limestone replacement by intergrinding with the clinker at ratios of up to 10% had limited effects on the compressive strengths of pastes, however at higher replacement ratios there was a noted decline in strength (Tsivilis, Chaniotakis, Badogiannis, et al. 1999). It was further noted that increased intergrinding time in the ball mill decreased the strength reduction in these pastes. Similarly, Bentz (D.P. Bentz 2005) noted that replacement of the coarser fraction of portland cement with limestone allowed for mechanical properties that were comparable to OPC. Similarly, Voglis (Voglis et al. 2005) found that hardened portland limestone cement pastes had comparable properties to OPC pastes, with noted higher early age strength in the limestone system. Bentz further studied the influence of limestone fineness on the compressive strength of both mortars and concretes and found that there was no apparent influence of fineness (Dale P. Bentz and Peltz 2008), as limestone of either fineness used resulted in comparable strength reductions, however both sizes of limestone used in this study were comparable in size or coarser than the portland cement used in the study. Irasser noted similar results, with limestone replacement resulting in a strength reduction in mortar specimens, with further reductions as

replacement ratio is increased; however, the limestone size was not noted (Irassar 2001). For more information on the influences of limestone on the mechanical properties of portland cement pastes, mortars and concrete, the author directs readers to a comprehensive review of limestone behavior in portland cement systems (Hawkins, Tennis, and Detwiler 2003). It is generally noted from this review that limestone replacement results in decreased mechanical properties, further decreasing as the replacement ratio is increased.

The influence of ternary blends of limestone and other alumina sources, including: slag, fly ash, and metakaolin, has not been as extensively studied in the literature as the influence of binary limestone. Elkhadiri (Elkhadiri et al. 2002) noted that inclusion of fly ash in interground limestone systems resulted in comparable mechanical behavior to OPC. De Weerdt (De Weerdt, Haha, et al. 2011; De Weerdt, Kjellsen, et al. 2011) noted a beneficial effect of inclusion of limestone and fly ash. The inclusion of fly ash in portland limestone cements was shown to recover the compressive strength loss associated with limestone inclusion, and further shown to increase the flexural strength loss associated with the inclusion of fly ash. These two studies both indicated potential synergistic benefits of combined replacement of portland cement by limestone and fly ash. Similarly, metakaolin has shown to enhance the compressive strength of portland cement-limestone blends (Antoni et al. 2012). Metakaolin alone significantly enhances the strength of portland cement mixes, particularly at early ages (Ambroise, Maximilien, and Pera 1994; Wild, Khatib, and Jones 1996), and its inclusion in limestone cement systems helps to recover some of the strength lost associated with limestone inclusion. Similarly, the inclusion of slag in limestone replaced portland cements was found to recover some of the strength loss

associated with limestone inclusion, although there were still noted strength deficits, these were typically recovered by later ages (Menéndez, Bonavetti, and Irassar 2003).

2.1.4 Influence of Limestone on Durability

The development of sustainable concrete systems also requires the development of portland cement concretes with equivalent or better durability characteristics. Enhancing the durability of portland cement concrete would increase the service life of structures, as well as decrease associated rehabilitation and repair costs. The durability of concrete can be divided into several key components, but primarily: (i) resistance to corrosion, and (ii) resistance to chemical attack. The current section will review the influence of limestone on the resistance to corrosion, as determined via the pore structure of the portland cement paste. The proceeding section provides a brief overview of some concerns with limestone with respect to chemical attack. The estimated cost of corrosion, just in reinforced concrete highway bridge infrastructure is between $64.3 and $101.5 billion annually (Yunovich and Thompson 2003), and the overall cost of corrosion in the United States is further estimated to be approximately 27% of the gross domestic product (Koch et al. 2002). For corrosion of steel reinforcing to occur in reinforced concrete, only two things are required: water and oxygen. However, due to the highly alkaline pore solution in cementitious systems, corrosion typically will not occur below a certain critical concentration of chloride ions required to break the passive layer on the steel (Alonso et al. 2000; Moreno et al. 2004). Thus, the presence of chloride ions in concrete allows for the initiation of corrosion, and the transport of chloride ion in the sample is crucial to resistance to corrosion. Corrosion resistance of a portland cement concrete has been shown to be dependent on both the chloride ion permeability (Halamickova et al. 1995) and the chloride binding of the

portland cement paste (Geiker, Nielsen, and Herfort 2007; Yuan et al. 2009). As a key focus of this dissertation is the microstructural features of portland limestone cement pastes, the influences of limestone on the chloride ion binding capabilities of the hardened cement paste are not included in this literature review.

In general, the permeability and diffusivity of concrete is dominated by the portland cement paste phase, due to the fact that the portland cement paste is significantly more porous than materials typically used as aggregates. The permeability of the cement paste is influenced by several factors, including the degree of hydration (Halamickova et al. 1995; Atahan, Oktar, and Tasdemir 2009), the pore structure of the cement paste (Bágel' and Živica 1997), and the constitution of the cement paste (Dale P. Bentz et al. 1999). The pore structure of cement pastes is similarly influenced by the degree of hydration of the paste, and the constitution of the cement paste, particularly with regard to the w/c ratio and the particle size distribution of the species in the paste (Dale P. Bentz et al. 1999; Winslow and Diamond 1970a). These effects are illustrated in Figure 2-3.

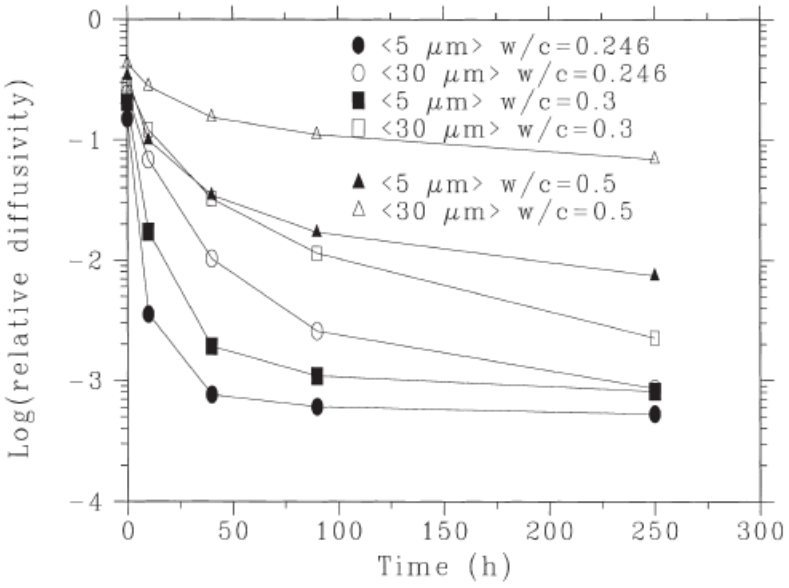

Figure 2-3: Influence of particle size distribution, degree of hydration, and fineness on diffusivity (Dale P. Bentz et al. 1999)

Several studies are found in the literature on the influence of limestone on the pore structure of hardened cement pastes. Ye (Ye et al. 2007) noted comparable porosities between limestone blended systems for self-compacting concrete; however, due to the fact that solids ratios were inconsistent it is difficult to discern any trends from the pore size distributions in this study. Tsivilis found a reduction in porosity as determined when limestone was interground with portland cement at very late age (9 months) at replacement levels of up to 35% by mass, however the w/c ratio used in these mixtures was very high at 0.50 (Tsivilis et al. 2000). An additional study by Tsivilis indicated little influence on porosity when limestone is included at replacement ratios up to 15%; however, again a relatively high w/c ratio was used (Tsivilis et al. 2003). Pipilikaki noted that the replacement of cement by limestone in interground limestone systems resulted in increased capillary pore size and an increase in overall porosity (Pipilikaki and Beazi-Katsioti 2009). Again, the inclusion of limestone is shown to have varying influences, this variability is

likely attributed to changes in limestone size distribution, varying w/c ratios and different methodologies of limestone replacement.

As a final note in the discussions of durability of limestone cement systems, it is important to note that limestone has been shown to have some potential influences on chemical attack in portland cement concrete. There is concern in the literature that portland limestone cement systems may be susceptible to sulfate attack due to the stabilization of more voluminous hydration products in the microstructure. Sulfate attack is a form of deterioration in portland cement systems where the stabilization or delayed formation of less dense hydration products results in expansive cracking in the microstructure and decreased mechanical performance. The stability of less dense ettringite in portland limestone cement systems leads to increased volume of hydration products (Matschei, Lothenbach, and Glasser 2007b) which has been proposed to increase packing, however may also lead to cracking. Further, several authors have noted the potential of sulfate attack due to thaumasite formation (Bensted 1999; Hartshorn, Sharp, and Swamy 1999; Justnes 2003; Kakali et al. 2003), and is of particular concern at lower temperatures and environments where the concrete is exposed to sulfates.

2.2 Rheology of Cementitious Suspensions

2.2.1 Overview and Background

Rheological studies are the study of flow in a material, typically a fluid (Barnes, Non-Newtonian, and Mechanics 2000). Rheological studies of fluids typically consist of investigations of the response of the fluid to changes in stress or strain, applied in both linear and oscillatory studies. The rheological behavior of cementitious suspensions is a crucial area of investigation, as it gives insight into the ease of casting, pumping, and

finishing of concrete structures. Further, exploration of the rheological nature of cementitious materials gives insight into the underlying physicochemical interactions between the various suspended species as well as potential interactions with the suspending media itself.

2.2.2 The Rheology of Suspensions

The study of the flow of suspensions is a broad discipline, including investigations into food processing (Bayod, Willers, and Tornberg 2008; Steffe 1996), blood (Cerny, Cook, and Walker 1962; Dintenfass 1976), and construction materials such as asphalt (Chomton and Valyer 1972; Gaskins et al. 1960) and concrete (Banfill and others 2003). The rheological behavior of suspensions is a complex system, dependent on solid loading, particle size, particle interaction effects, and the nature of the suspending media. Particle interaction effects include particle contact forces, electrostatic forces, and van der Waals forces. Colloidal stability and the behavior of colloidal suspensions has been proposed to be dominated by DLVO theory (named for Derjaguin, Landau, Verwey, and Overbeek) which relates repulsion and coagulation through electrostatic repulsive forces and attractive van der Waals forces respectively. The electrostatic forces result from the adsorption of charged particles in the electric double layer (EDL). A graphical representation of the EDL is depicted in Figure 2-4, where the stern layer is the layer closest to the particle consisting of strongly held ions of opposite charge to the surface of the particle and the diffuse layer is the outer shell layer consisting of less strongly held ions with the same charge as the particle. DLVO theory proposes that the electrostatic interaction at particle surfaces results in a repulsive force which is balanced by van der Waals attractive forces. Where van der Waals forces are proportional to $1/r^2$ and electrostatic repulsion forces are proportional to

exp[-κ(r-2a)] where r is the distance from the center of the particle, κ is the Debye length, and a is the particle diameter (Hunter and White 1987; Neubauer, Yang, and Jennings 1998). Thus, it can be seen that electrostatic repulsive forces fall off faster than van der Waals attractive forces. The effect of these two forces and the net interaction potential is noted in Figure 2-4(b). It is noted, however, that the DLVO theory does not account for Brownian motion or hydrodynamic forces resultant from mixing or hydration.

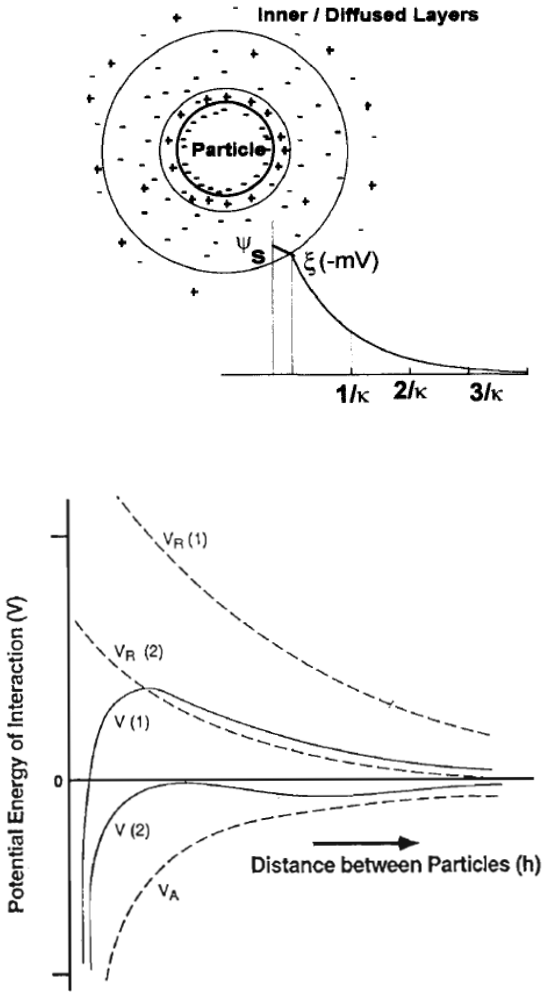

Figure 2-4: Electric double layer model (left) (Yang, Neubauer, and Jennings 1997) and interaction potential between two surfaces based on DVLO theory (Shaw 1992).

The influence of solid loading on the rheological behavior of suspensions has been rigorously studied for various suspensions; a typical depiction of this effect is presented in Figure 2-5 (Mueller, Llewellin, and Mader 2010). Noted from this figure is the transition in the flow curve (shear rate, shear stress response) as the solid loading is increased. The initial behavior, at a very low volume fraction indicates Newtonian behavior, with a linear flow curve and a zero stress intercept. As the solid loading is increased, the particle interaction become more prevalent and the flow transitions to a shear thinning behavior, as indicated by the formation of curvature in the figure; however, a zero stress intercept remains. Shear thinning behavior in suspensions is related to a competition between shear stresses causing particle reorganization and Brownian motion restoring the original particle configuration. As shear rates increase or particle size distributions are increased out of the colloidal regime, the effect of local particle rearrangement is dominant, resulting in a decreasing viscosity with increasing stress (Lootens et al. 2004; Loose and Hess 1989; Poslinski et al. 1988). As solid loading further increases, networks of particles form, and particle interactions become even more prevalent. At this loading, an apparent yield stress is developed, indicated by a non-zero stress intercept. Finally, at the highest loading, the apparent yield stress is maintained, and the network of particles is further refined. At this solid loading level, the initiation of flow requires significant local particle reorganization or migration and formation of localized areas of low particle concentration, sometimes referred to as the formation of shear bands (Herle, Fischer, and Windhab 2005; Callaghan 2008; Schall and van Hecke 2009).

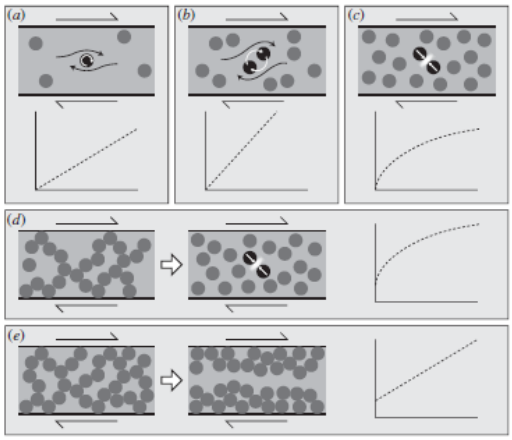

Figure 2-5: Graphical depiction of the influence of solid loading on the flow behavior of suspensions (Mueller, Llewellin, and Mader 2010).

Rheological studies of suspensions can thus be seen as very complex systems. The strong influence of particle concentration, particle shape, and particle interaction can significantly affect the flow of suspensions.

Rotational rheological studies of concentrated suspensions are commonly divided into two types of studies, linear shear rate responses and oscillatory shear studies. Shear rate (or stress) ramp studies investigate the flow of concentrated suspensions producing flow curves as presented above. From these flow curves, several rheological parameters are commonly extracted, including the apparent yield stress and plastic viscosity. Several models are commonly used to extract these parameters, including the Bingham (Bingham 1922), Casson (Casson 1959), and Herschel-Bulkley (Herschel and Bulkley 1926) models. These three models are generally classified as the generalized Bingham models. Further discussions of the relevance and influence of these models can be found in Chapter 7. Oscillatory shear studies, on the other hand are typically conducted at very low strains, and are used to investigate the viscoelastic nature of the suspensions (Barnes, Non-Newtonian, and Mechanics 2000).

2.2.3 Rheology and Flow of Fresh Cement and Concrete

As mentioned previously, the study of flow of fresh cement in concrete is crucial to providing insight into effects on pouring, finishing, casting, and pumping of fresh concrete. Studies on the flow of concrete range from empirical tests such as the slump test ("ASTM C143 - 12. Standard Test Method for Slump of Hydraulic-Cement Concrete" 2012) to experiments using viscometers and rheometers. The slump test is a field test commonly used to determine the workability of a concrete, wherein a concrete specimen is placed in a cone, and then the cone is withdrawn and the distance the concrete settles is recorded as the slump. Thus, a higher slump indicates a mixture that is more fluid and a lower slump indicates one that is stiffer. The results of the slump test are generally considered to be a measurement of the yield stress of the concrete (Saak, Jennings, and Shah 2004; Nicolas Roussel 2006; N. Roussel and Coussot 2005); however, relationships between determined yield stress and slump often have a fair amount of scatter. This is likely due to the fact that the flow of concrete cannot be effectively modelled by a single parameter, and thus slump estimations of yield stress are prone to error.

The second method of investigating the rheological properties of concrete and portland cement suspensions is through the use of rotational viscometers or rheometers. The majority of rheological studies of cementitious systems involve rheological studies of the cement pastes, rather than of the concrete, and relate the properties of the paste to the properties of concrete. This is due to the increased complexity and size requirements of measuring the rheological characteristics of the concrete itself. It is noted that concrete is a suspension of rock and sand, where the suspending fluid is a paste, while the suspending fluid itself is also a suspension of portland cement, gypsum, and hydration products in

water. The range of scales from the macro – aggregate in paste, to micro – cement in water, make investigations of the concrete itself a challenging endeavor. Some studies have developed large scale viscometers to perform these types of investigations (Banfill and others 2003; C. F Ferraris and de Larrard, Francois; Ferraris and Gaidis 1992); however, the use of this equipment was not available as part of this dissertation, so the focus here will be on the rheological characterization of cementitious pastes.

Rheological studies of cementitious systems are common in the industry and have been completed dating back several decades. Several comprehensive reviews have been performed on this topic, and the author directs the reader to one of these reviews for a more complete discussion (Banfill 2006). In general rheological studies have been focused on two key areas: the influence of cement constitution on the rheological performance of cementitious suspensions (Ferraris, Obla, and Hill 2001; Park, Noh, and Park 2005; D. P. Bentz et al. 2012; Grzeszczyk and Lipowski 1997) and the influence of admixtures on these suspensions (Burgos-Montes et al. 2012; Asaga and Roy 1980; Daimon and Roy 1979; Lachemi et al. 2004). As the work completed in this dissertation is focused primarily at the physicochemical changes in suspensions that result from changes in cement constitution, the focus of this literature review will be primarily aimed at these influences.

Several key factors have been noted to influence the rheological behavior of cementitious suspensions when admixtures are present: the inclusion of mineral admixtures, the inclusion of pozzolanic materials, and the size and shape distribution of the particles present in the suspension. Investigations of these key factors provide insight into the overall behavior of these systems, as well as provide background for the discussions in this paper. As solids content in portland cement is increased, there is a corresponding increase

in the determined rheological properties, as would be expected from the discussions above (Justnes and Vikan 2005). The influence of the surface area of portland cement was studied by Vikan (H. Vikan et al. 2007), where it was noted that increasing the specific surface area by additional grinding of the portland cement clinker led to an increased flow resistance due to decreased particle spacing.

It is notable that there have been many conflicting reports with respect to the influence of cement replacement on the rheological properties of portland cement suspensions. For example, at a water-to-powder (w/p) ratio of 0.5, Nehdi (Nehdi and Rahman 2004a) showed reductions in yield stress for most models used with 25% fly ash replacement; however, at a lower w/p ratio (0.4), an increase in yield stress was noted. Further, significant variability was noted in the determined yield stress based on the selected model. Ferraris (Ferraris, Obla, and Hill 2001) generally showed enhanced flowability when cement was replaced by ultrafine fly ash indicated by the reduced need for high range water reducing admixtures (HRWR). However, in neither of the above cases was the class of fly ash indicated. Rudzinski noted an increase in determined rheological properties when fly ash is included; however, the fly ash was added, not used as cement replacement, thereby decreasing the w/p ratio of the suspension. The use of Class C, or high calcium fly ash, resulted in a general decrease in flowability of the suspension (Grzeszczyk and Lipowski 1997). The inclusion of Class F fly ash on the other hand, has been shown to reduce both the yield stress and plastic viscosity of the suspension. Park noted a decrease in yield stress but increase in plastic viscosity when portland cement was replaced by fly ash (Park, Noh, and Park 2005). The cause of these varied results may be attributed to material variability,

differences in experimentation, differences in chemical admixtures, and possibly issues with the rheological models themselves.

The reported influences of limestone on the rheological properties of portland cement suspensions was also varied. Yahia reported that up to a certain dosage the inclusion of limestone had no influence of the flowability of the paste; however, limestone was replaced by mass in this study and the limestone size was not specified (Yahia, Tanimura, and Shimoyama 2005). Similarly Sakai reported improved flowability with replacement of low heat cement by fine limestone (Sakai et al. 2009). Ultrafine fly addition was shown to reduce yield stress and plastic viscosity at inclusion values up to 10% (X. Zhang and Han 2000); however, several results in this study indicated a zero yield stress, and further it appeared this was an addition rather than replacement to a portland cement suspension.

2.2.4 Rheology of Alkali Activated Geopolymer Suspensions

Alkali activated geopolymers are cement-free binder systems for concrete composed of aluminosilicate materials which are activated by a highly alkaline solution, typically of Na or K (Davidovits 1991). The aluminosilicate materials typically used as the binders in these systems are slag, fly ash, and metakaolin. As the focus of this dissertation is on the early age flow characteristics of these systems, a further review of geopolymers is not provided; however, the author directs the reader to several papers on the topic (Davidovits 1991; Provis et al. 2007; Phair, Smith, and Van Deventer 2003) which more thoroughly review the nature of these materials including polymerization reactions and hydration. A review of the literature found very little work done on the rheological characterizations of geopolymer solutions. The majority of the studies found were focused on investigations of the influence of chemical admixtures on these suspensions (Bakharev, Sanjayan, and

Cheng 2000; Criado et al. 2009; Palacios and Puertas 2005; Palacios et al. 2009a), with the majority of the studies indicating admixtures had variable or inconsistent effects in these systems. The rheological nature of metakaolin based geopolymers was studied; however, this was a study of the viscoelastic development of metakaolin over time, rather than an investigation of the flow of the fresh paste (Poulesquen, Frizon, and Lambertin 2013a). The influence of the type of activator, the influence of activator concentration, and the influence of activator cation on the rheological performance of these suspensions has not studied in the literature, thus there remains a significant gap in the understanding of these systems.

3. MATERIALS AND EXPERIMENTAL METHODS

3.1 Materials

This study was completed using a wide variety of materials, including: portland cement, limestone, metakaolin, fly ash, and ground granulated blast furnace slag. As these materials varied for each section of the project, the author directs the reader to the individual materials sections in each chapter for information on the materials used in this work.

3.2 Experimental Methods

As with materials, experimental methods varied significantly, particularly with respect to rheological characterization of these materials. Based on this, a broad overview of the experimental methods used in this dissertation is provided. For a more in depth look that the experimental methods used in each section, the author directs the reader to the experimental methods sections in each chapter.

3.3 Curing Conditions and Mixing for Tests on Hardened Cement Pastes

Mixing for tests on hardened concrete specimens was performed in accordance with ASTM C305. All powders were dry blended prior to adding water. All mixes in this study were completed without the use of chemical admixtures to distinguish the effects of mixture constitution without influence of admixtures.

For tests on hardened cement pastes, two different curing regimes were used in this study. The first method was for samples for compression testing and thermal analysis. Samples were cast and the cured until the desired testing age in a humidity chamber with a relative humidity $\geq$ 95% at a temperature of 23±1 °C. At the desired testing age, samples were removed from the chamber and blotted dry with a towel. Compressive test samples were cured for the first 24 hours loosely covered with plastic, after which they were demolded

and cured for the duration in the humidity chamber. For mercury intrusion experiments, samples were cured in a 50 ml sealed vessel until the desired testing age.

3.3.1 Isothermal Calorimetry

Isothermal calorimetry is a technique to measure the heat evolution associated with endothermic or exothermic reactions. In cementitious systems it is used to monitor the progression of the hydration reaction, as well as investigate the influence of mixture proportioning on early age heat evolution. These characteristics can help in the identification of the acceleration/deceleration of hydration reactions, as well as distinguish individual phenomena. For example, in portland limestone cement systems with fine limestone, a more pronounced secondary peak on the main hydration peak is noted, which is indicative of secondary formation of ettringite which is more pronounced when additional calcium carbonate is included in the system.

The instrument used for these experiments was a Calmetrix ICal 8000 isothermal calorimeter. This instrument is an eight channel calorimeter, and is pictured in Figure 3-1. The instrument functions by measuring the heat flow required to maintain isothermal conditions, recorded in watts, this data, when normalized by the mass of portland cement present, provides information on the changes in heat evolution in the binder as mixture constitution is modified.

Figure 3-1: ICal 8000 isothermal calorimeter

3.3.2 Simultaneous Thermal Analysis (STA/TGA)

Simultaneous thermal analysis is an instrument which measures the mass loss through thermogravimetry and associated heat flow as a sample is heated over a specified temperature range. The resultant heat flow peaks can be used to determine individual decomposition processes associated with the heating of the sample, and can be used to determine the quantity of some hydration products in a cementitious sample. In a typical cementitious sample, there are three major heat flow peaks, the first corresponds to the loss of evaporable water, and the bound water in C-S-H and ettringite. The second corresponds to the dehydroxilization of calcium hydroxide. The final peak corresponds to decarbonation of calcium carbonate. The temperature bounds of the mass loss peaks are defined by the onsets of the peaks in the heat flow curve, the associated mass of calcium hydroxide and calcium carbonate are determined by the stoichiometric mass ratios associated with the respective decomposition.

The thermal analysis instrument used was a Perkin Elmer STA 6000 simultaneous thermal analyzer with a maximum operating temperature of 1000 °C. The STA 6000 used in this research project is shown in Figure 3-2.

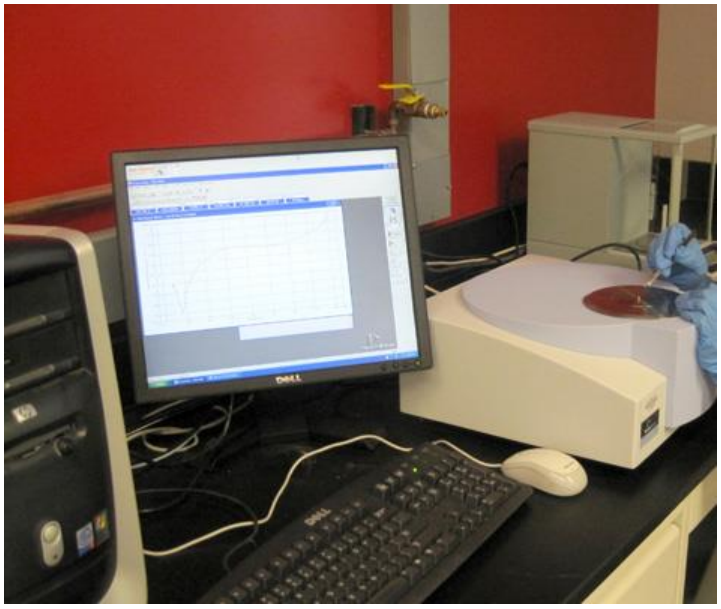

Figure 3-2: Perkin Elmer STA 6000 instrument setup

3.3.3 Mercury Intrusion Porosimetry

Mercury intrusion porosimetry is a commonly used technique for pore structure investigations in porous materials. In mercury intrusion porosimetry, mercury is forced into a sample at variable pressure, and the pore diameter is determined using the pressure-pore diameter relationship established in the Washburn equation, which relates the pressure to diameter, mercury contact angle, and mercury surface tension. The instrument used for intrusion measurements in this study is a Quantachrome Instruments PoreMaster, capable of a maximum pressure of approximately 415 MPa, which corresponds to a pore diameter of about 3 nm, depending on the intrusion parameters of the sample. The instrument used in these experiments is presented in Figure 3-3.

Figure 3-3: Quantachrome PoreMaster mercury intrusion porosimeter

It bears noting that there are several noted disadvantages of mercury intrusion porosimetry. A brief review of these disadvantages will be presented here, for a more in depth review please see the discussions in Chapter 5. Mercury intrusion porosimetry has several possible sources of error: (i) the so-called ink-bottle effect, wherein a pore with a smaller entrance to a larger pore is recorded as a large volume of the smaller pore, (ii) mercury intrusion porosimetry is unable to determine porosity if there are large unconnected pores, (iii) the act of running an intrusion experiment at such high pressures may damage the underlying pore structure, and (iv) sample drying is required, and different techniques will result in different results due to potential damage to the pore structure as a result evaporative pressure.

3.3.4 Rheology

A wide variety of rheological experiments was conducted as part of this study, for detailed information on the individual experiments the author directs the reader to the respective chapters where those experiments were completed. Thus, to avoid confusion relating which experiment was conducted as a part of which test, the discussions here will focus on the instrument and geometries used in these experiments.

The rheometer used in this study is a TA Instruments AR2000EX dynamic shear rheometer, the instrument is pictured in Figure 3-4.

Figure 3-4: TA Instruments AR2000EX used in this study, shown in parallel plate configuration.

Two different geometries were used in this study, the first a parallel plate configuration and the second a cup-and-bob configuration. The parallel plate configuration consists of a 50 mm diameter stainless steel upper geometry which is serrated to a depth of 1 mm to minimize the effects of slip. Two different lower geometries were used in this study, both utilizing a Peltier plate element which is set to a surface temperature of 25 °C: (i) Peltier plate element with adhesive backed resin coated sandpaper, and (ii) a Peltier cover plate

with a surface serrated to a depth of 0.15 mm. Both surface treatments were provided to minimize the influence of slip in the study. The cup-and bob geometry used in thus study consists of a stainless steel cup and stainless steel bob, both of which were grit blasted to increase surface roughness and minimize the influence of slip. The cup-and-bob geometries used in this study are pictured in Figure 3-5.

Figure 3-5: Cup-and-bob geometries used in study

PART I – HYDRATION AND PORE STRUCTURE

4. HYDRATION AND STRENGTH DEVELOPMENT IN TERNARY PORTLAND CEMENT BLENDS CONTAINING LIMESTONE AND FLY ASH OR METAKAOLIN

4.1 Introduction

In recent years there has been increased interest in the use of limestone powder as a partial cement replacement material. Limestone has the advantages of being abundant, inexpensive, and without the environmental costs associated with Portland cement. Portland limestone cements have been in extensive use in Europe and Canada since the 1990s. ASTM standards historically allowed only up to 5% limestone (mass basis) in cement, and it has been shown that such low replacement levels can result in comparable or better properties as compared to plain cements (Tsivilis, Chaniotakis, Badogiannis, et al. 1999; Voglis et al. 2005). Recently ASTM C 595-12 has defined a Type IL cement that can include up to 15% of limestone powder as a cement replacement material (Tennis, Thomas, and Weiss 2011).

The incorporation of limestone powder modifies the hydration process in low water-to-cement ratio (w/c) cement systems where a substantial fraction of the cement remains unhydrated (V. Bonavetti et al. 2003; D. Bentz et al. 2009a). The use of appropriate size ranges of limestone powder as a filler material has been reported to result in similar/better fresh properties in self-consolidating concretes, inspite of reduced cement contents (Felekoğlu et al. 2006). The use of fine limestone powder (finer than OPC) provides nucleation sites and thus accelerates C_3S hydration (Oey et al. 2012; V. Bonavetti et al. 2003; Lothenbach et al. 2008), while participating to a limited extent in the cement hydration reactions (L. Opoczky 1992). For this reason, fine limestone powder has been

used to limit delays in setting in high volume fly ash mixtures (D. P Bentz and Ferraris 2010). The use of limestone powder has been shown to slightly increase compressive strength (Tsivilis, Chaniotakis, Badogiannis, et al. 1999), while contrary results have also been reported (D. Bentz et al. 2009b; Voglis et al. 2005; Dhir et al. 2007). The likely cause of these discrepancies is the use of limestone powders of different fineness, the dosage of limestone powder, water-to-powder ratios, and the type/fineness of cement used. Fine fillers have been shown to decrease the capillary porosity of the paste, which may account for some of the strength gain reported (D. Bentz et al. 2009a). It has been shown that by increasing the fineness of Portland cement or decreasing the water-to-solids ratio (w/s), some of the strength loss associated with limestone additions can be mitigated (V. Bonavetti et al. 2003; Tsivilis, Chaniotakis, Badogiannis, et al. 1999; Cam and Neithalath 2010).

Limestone powder has been shown to chemically interact with the aluminate phases in cement (Ingram et al. 1990) to stabilize a carboaluminate phase at the expense of monosulfoaluminate (Matschei, Lothenbach, and Glasser 2007b). This action can, within limits, increase the quantity of ettringite formed which leads to an increase in solid volume, and thus slightly improved mechanical properties. In pure C_3A systems, it has been shown that a significant portion of the carbonate will be consumed after 24 hours (V. L. Bonavetti, Rahhal, and Irassar 2001). In the case of OPC pastes, limestone is expected to react with the aluminous clinker phases (Kakali et al. 2000), ensuring that, at low replacement levels (< 5%, mass basis) much if not all of the calcite will be consumed through the course of hydration (Matschei, Lothenbach, and Glasser 2007b).

The synergy between fly ash and limestone powder has recently been elucidated (De Weerdt, Kjellsen, et al. 2011) to show that composite cements containing a low amount of limestone powder (5%) and high amounts of fly ash (30%) perform similarly to a cement containing no limestone powder. However, a common issue with high levels of fly ash incorporation is the delay in setting observed in these systems (Langan, Weng, and Ward 2002; Fajun, Grutzeck, and Roy 1985; Sakai et al. 2005). The use of small amounts of a more reactive cement replacement material with appropriate chemical characteristics could facilitate the use of higher levels of limestone powder without attendant property loss. However, a systematic investigation of the effects of limestone fineness on the behavior of binders containing supplementary cementing materials (SCMs) is missing. This study develops a more detailed understanding of the influence of limestone fineness and additions on the behavior of ternary binder systems (i.e., cement + limestone + SCM), containing SCMs of differing chemical reactivity. As such, these investigations are focused on clarifying the role of limestone fineness and the type of cement replacement material (i.e., metakaolin or a Class F fly ash) on early, and later age behavior to understand if it may be possible to proportion ternary binder formulations which would display properties similar to traditional OPC systems.

4.2 Experimental Program

4.2.1 Materials and Mixture Proportions

The materials used in this study include: a commercially available Type I/II ordinary portland cement (OPC) conforming to ASTM C 150, a Class F fly ash, and metakaolin conforming to ASTM C 618, and limestone powder conforming to ASTM C 568. Limestone powders with three different median particle sizes - 0.7 μm, 3 μm, and 15 μm

were used. The particle size distributions of the cement, limestone, fly ash, and metakaolin are shown in Figure 4-1 and their chemical composition in Table 4-1. Cement was replaced by volume percentages of limestone powder varying between 0-40 % in increments of 10% (increments of 5%, up to a total replacement of 10% for the 0.7 μm limestone), and metakaolin and fly ash between 0-10% in increments of 5%. In the remainder of this paper, the percentages of limestone or other cement replacement materials reported are all on a volumetric basis, unless otherwise noted. The volumetric water-to-solids ratio (w/s_V) used for the mixtures is 0.55; however since replacement was done by volume and all of the replacement materials are less dense than Portland cement, the effective water to powder ratio of the blended mixtures varies between 0.35 and 0.38 (mass basis). Ternary blends comprising combinations of limestone and metakaolin or fly ash were also proportioned. Fly ash and metakaolin are used as OPC replacement materials because the aluminous nature of these materials favors the formation of the carboaluminate phases (Matschei, Lothenbach, and Glasser 2007b). OPC replacement levels of up to 20% by limestone and up to 10% by fly ash or metakaolin were attempted. These selections were made to attain a 28-day compressive strength within 10% of the reference (i.e., plain cement) system. Overall, 42 different paste mixtures were proportioned and evaluated as part of this study.

Table 4-1: Chemical composition of the component materials

Component (%)	Cement	Limestone	Fly ash	Metakaolin
SiO_2	21.0		58.4	51.7
Al_2O_3	3.61		23.8	43.2
Fe_2O_3	3.47		4.19	0.5
CaO	63.0		7.32	--
MgO	3.26		1.11	--
SO_3	3.04		0.44	--
Na_2O	0.16		1.43	--
K_2O	0.36		1.02	--
LOI	2.13		0.50	0.16

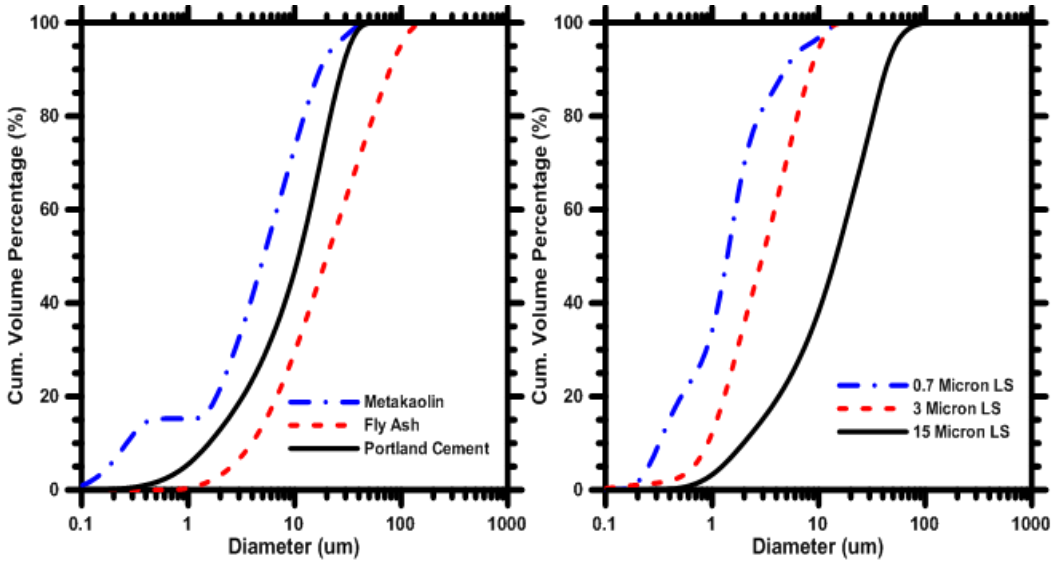

Figure 4-1: Particle size distributions of: (a) limestone powders and (b) cement, fly ash, and metakaolin

4.2.2 Experimental Methods

Isothermal calorimetry was carried out as per ASTM C 1702. The pastes were mixed externally as described in ASTM C305 prior to being loaded into the calorimeter. The time elapsed between the instant water was added to the powder(s) and the paste loaded into the calorimeter was approximately 2 minutes. Isothermal calorimetry was performed over a period of 48 to 72 hours. The powders were dry-blended using a hand mixer at low speed prior to adding water.

Compressive strengths were determined in accordance with ASTM C109 on 50 mm cubes stored in saturated limewater until the age of testing. Simultaneous thermal analysis (thermogravimetric analysis (TGA) and differential thermal analysis (DTA)) was carried out on selected pastes at ages of 1, 7, and 28 days to determine the calcium hydroxide (CH) and calcium carbonate (CC) contents. The tests were carried out in a pure nitrogen environment, at a flow rate of 20 ml/s. A heating rate of 10^{o}C/min was employed and the pastes were heated from ambient to 950^{o}C. The non-evaporable water content (w_n) was

calculated as the difference between the mass measurements at 950°C and 105°C, normalized by the mass at 950°C, and corrected for the loss on ignition of the cement powder (based on its mass fraction in the paste) and the calcium carbonate content (650-800°C). The CH contents were determined based on the mass change measured between temperatures in the DTA curve corresponding to the CH peak (Dweck et al. 2000).

4.3 Results and Discussions

4.3.1 Early-Age Behavior of Binary and Ternary Cementitious Pastes

Isothermal calorimetry was carried out on binary and ternary paste blends containing several dosages of limestone powder of different particle sizes. The following sections provide insights into the influence of limestone fineness, dosage, and the synergistic effects of limestone powder and metakaolin or fly ash on the calorimetric response. The timing of the primary and secondary hydration peaks, their amplitudes, and the slopes of the acceleration and deceleration regimes are used to describe the influence of blend composition on the calorimetric response. Since a large set of mixtures is evaluated, a computer program was developed to extract these parameters from the calorimetric curves to expedite analysis. To keep the discussions succinct, the data reported is limited to OPC replacements levels of 10 and 20% by limestone and 10% by fly ash or metakaolin.

4.3.1.1 Effect of limestone fineness and dosage on the progress of reactions

Figure 4-2 depicts the heat release curves of the plain cement paste as well as those modified using 10% limestone powder, for three different median particle sizes. It is immediately evident that finer limestone powders accelerate reactions; increasing the magnitude of the heat release peak and shifting the peaks to earlier times. For example, for the finest limestone powder, i.e., 0.7 μm, the main hydration peak is 15% higher than that

of the OPC paste, it appears 25% sooner, and the slopes of the acceleration and deceleration regions are about 40% higher. The calorimetric response of the paste incorporating fine limestone also demonstrates a more pronounced shoulder on the main hydration peak. These effects are attributable to the limestone powder accelerating hydration (Ramachandran 1988; Lothenbach et al. 2008) by enhancing the number of nucleation sites for the hydration products, as described in (Soroka and Setter 1977). With increasing coarseness of limestone powder, the heat release curve begins to mimic that of the plain paste. The differences in surface areas of the particles has implications in their dissolution rates, which reflect in the changes in the heat release response as observed. The effects of limestone size-dependent acceleration are supported by 1-day compressive strength datasets (Figure 4-3) which show that the mixture containing finer limestone powder has a higher 1 day strength than the OPC paste. Previous studies have reported that up to 5% limestone powder (by mass) can be used without compromising early age strength (Lothenbach et al. 2008; D. Bentz et al. 2009b). However, with increasing limestone coarseness and dosage, the compressive strength is noted to reduce due to effects including increasing porosity and a progressively reducing mineral acceleration effect.

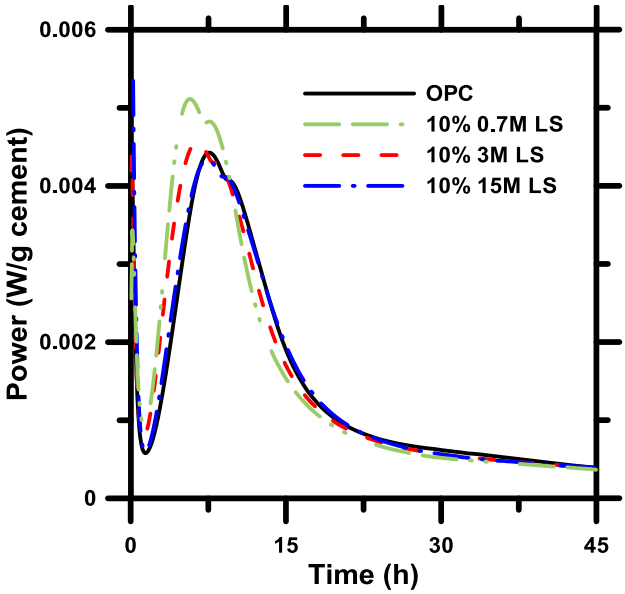

Figure 4-2: Influence of limestone fineness on the heat release rate. Representative heat flow curves are shown. The uncertainty in the heat flow is less than 2% based on measurements on triplicate specimens.

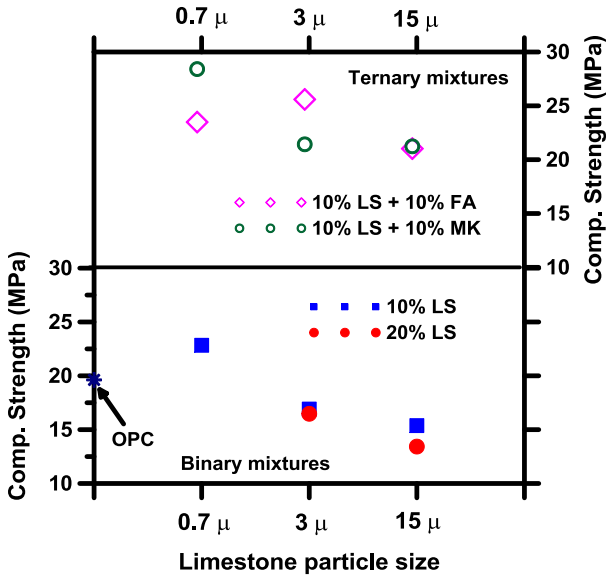

Figure 4-3: 1-day compressive strengths of binary and ternary blends of limestone and fly ash/metakaolin

The influence of limestone dosage for varying particle sizes on the calorimetric response is shown in Figures 4-4 (a), (b), and (c). For the 0.7 μm and 3 μm size powders, an increase in the limestone content is found to significantly influence early reactions, with a larger peak amplitude, earlier occurrence of the peak, and increase in the slope of the acceleration and deceleration regions being noted in comparison to the plain cement paste (Péra, Husson, and Guilhot 1999). However, the calorimetric signatures are not substantially influenced by the presence of coarser limestone powders, irrespective of their contents in the paste. It is additionally noted that pastes proportioned at different water contents (dilution) to mimic water content increase with cement replacement show overlapping curves (Figure 4-5). Notwithstanding the changes in w/c, the heat response curves are largely identical, suggesting that the reaction kinetics at early ages is largely a filler effect rather than an influence of a change in the effective *w/c* (Oey et al. 2012).

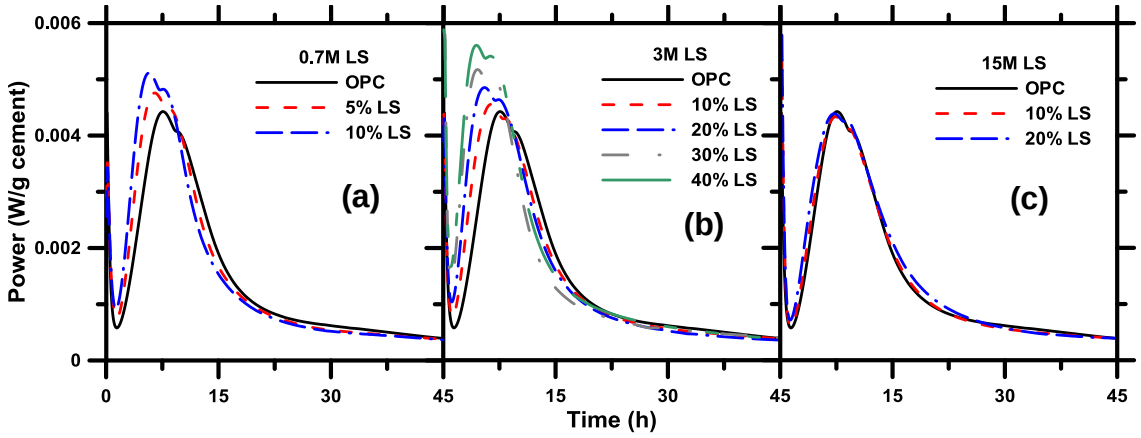

Figure 4-4: Influence of limestone dosage on heat release rates for pastes containing: (a) 0.7 μm limestone powder, (b) 3 μm limestone powder, and (c) 15 μm limestone powder. Representative heat flow curves are shown. The uncertainty in the heat flow is less than 2% based on measurements on triplicate specimens.

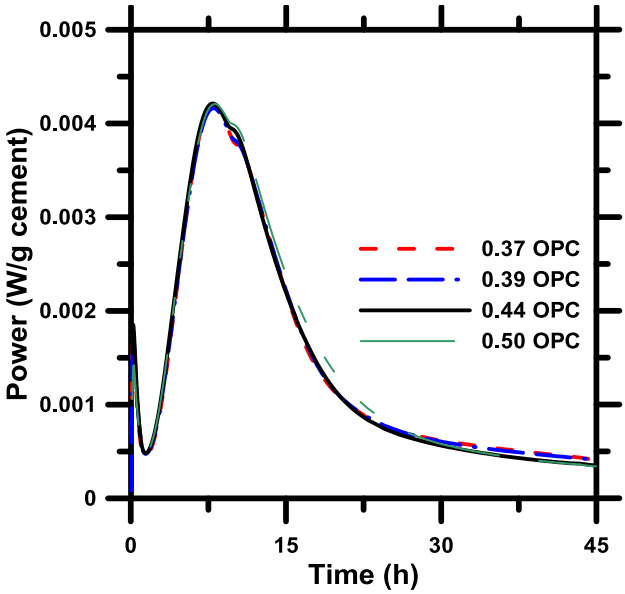

Figure 4-5: Influence of w/c ratio on the calorimetric response of OPC pastes. Representative heat flow curves are shown. The uncertainty in the heat flow is less than 2% based on measurements on triplicate specimens.

Figure 4-6 shows 1-day CH contents of selected pastes normalized by the mass fraction of OPC in the pastes. The normalized 1-day CH contents are higher for the 0.7 μm and 3 μm limestone containing pastes, consistent with the acceleration effects noted in Figures 4-4(a) and (b). For the paste containing 15 μm limestone powder, the normalized CH is similar to that of the plain paste (not shown in graph) indicating no acceleration effects as supported by Figure 4-4(c).

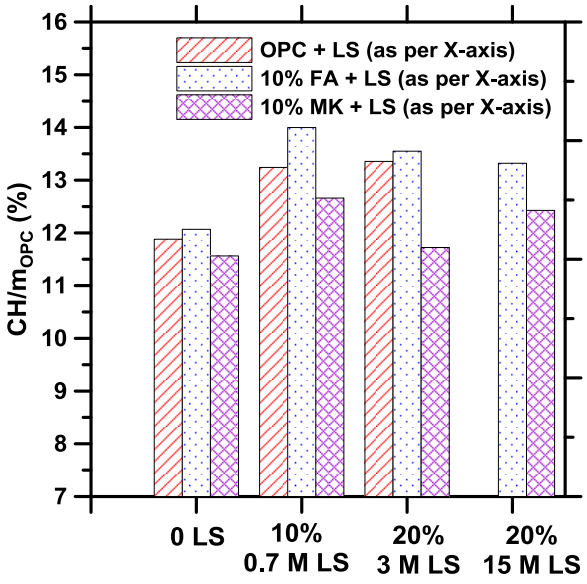

Figure 4-6: 1 day CH contents for selected binary and ternary pastes

4.3.1.2 Influence of fly ash and metakaolin replacements on the progress of reactions

It is instructive to examine the influence of aluminous cement replacement materials such as fly ash and metakaolin (bulk Al_2O_3 contents of 24% and 43% respectively, mass basis) on the early-age heat release response of pastes containing limestone powder. Figures 4-7(a) and (b) show heat release for binary pastes containing 5% or 10% of fly ash or metakaolin as the only cement replacement materials. The calorimetric response of fly ash modified pastes is very similar to that of the OPC paste (total heat released after 48 hours of 233 J/g cement compared to 236 J/g for OPC). In this regard, fly ash performs similarly to the coarser limestone powder (15 µm). This is unsurprising, as the fly ash is not expected to react substantially at early times. However, in the presence of metakaolin, the amplitude of the peak and the slope of the curve during the acceleration region increases with an increase in the metakaolin content, similar to results reported in (Kadri et al. 2011). In addition, increasing the metakaolin dosage is also found to result in a more pronounced shoulder in the heat release response.

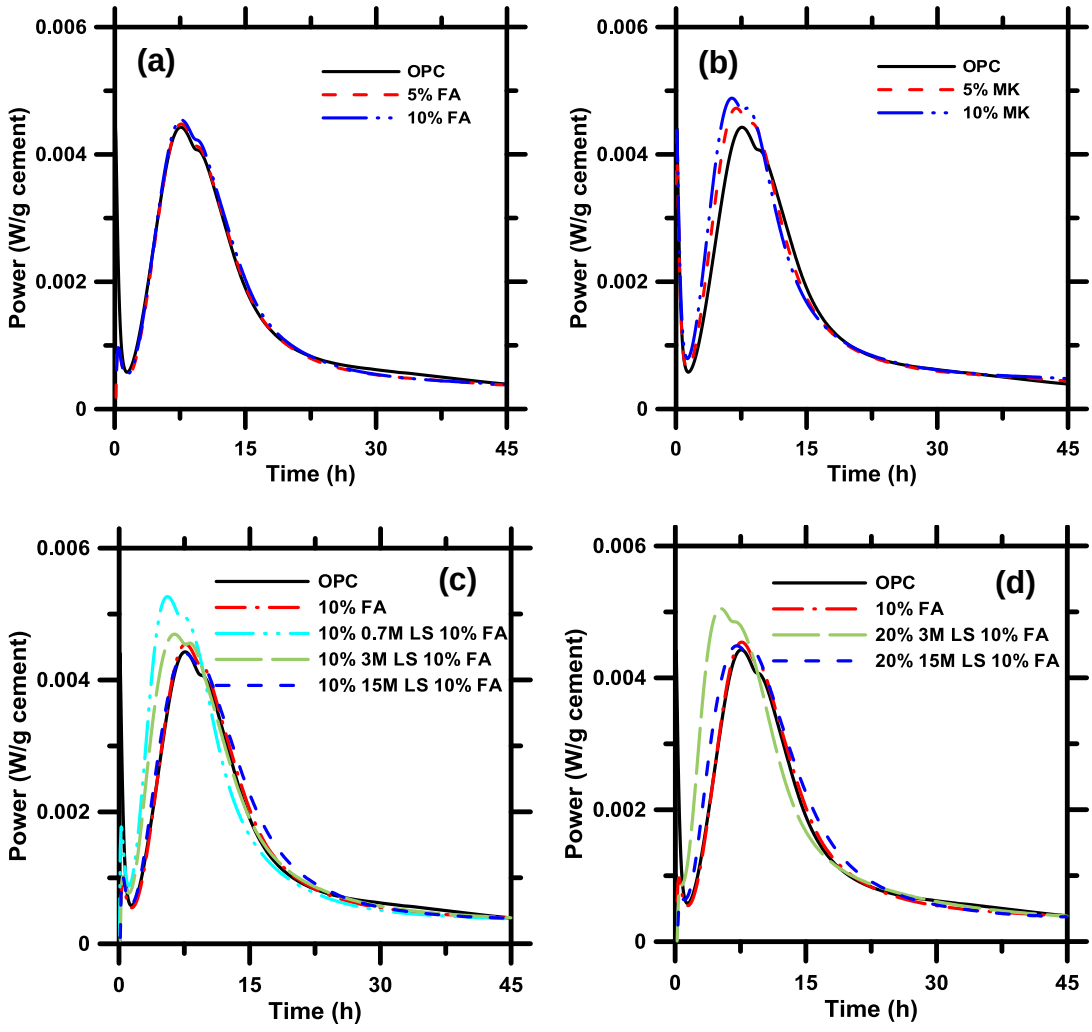
(a)
OPC
5% FA
10% FA
(b)
OPC
5% MK
10% MK
(c)
OPC
10% FA
10% 0.7M LS 10% FA
10% 3M LS 10% FA
10% 15M LS 10% FA
(d)
OPC
10% FA
20% 3M LS 10% FA
20% 15M LS 10% FA
Power (W/g cement)
Time (h)
0.006
0.004
0.002
0
0
15
30
45

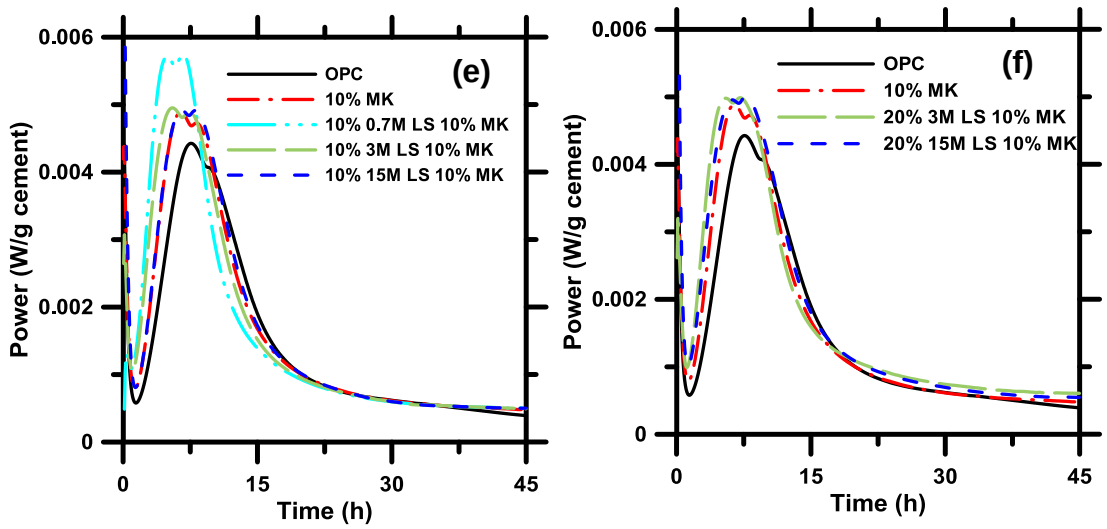

Figure 4-7: Calorimetric response of: (a) fly ash modified pastes, (b) metakaolin modified pastes, (c) ternary mixtures of 10% limestone and 10% fly ash, (d) ternary mixtures of 20% limestone and 10% fly ash, (e) ternary mixtures of 10% limestone and 10% metakaolin, and (f) ternary mixtures of 20% limestone and 10% metakaolin. Representative heat flow curves are shown. The uncertainty in the heat flow is less than 2% based on measurements on triplicate specimens.

An analysis of the response of pastes containing fly ash or metakaolin requires considerations of their particle sizes and reactivity. Fly ash has a median particle size similar to the coarsest limestone powder whereas the median particle size of metakaolin is much smaller (5 μm). When the heat release parameters for the 10% metakaolin modified paste are compared to those of the OPC paste with 10% of 3μm limestone powder, they are quite similar, demonstrating the influence of particle size. The peak amplitude is slightly higher for the metakaolin modified paste, but the peaks appear at virtually the same time. The normalized CH contents of the fly ash and metakaolin modified pastes are similar to that of the OPC paste at age of 1 day as observed from Figure 6, suggesting that at early times, their hydration behavior is rather similar. For example, the 10% fly ash modified paste (7.5% by mass) produces a 7% reduction in the 1-day actual (unnormalized) CH content, whereas for the 10% metakaolin modified paste (7.9% by mass), the reduction in CH is about 11%. In other words, the reduction roughly scales with the OPC replacement

level even though metakaolin incorporation results in a slightly higher reduction of CH. Figures 4-7(a) and (b) show that, while the incorporation of fly ash does not change the reaction kinetics considerably, the use of metakaolin results in an acceleration of reactions. This is likely due to the early age pozzolanic reactions and CH consumption in metakaolin blended pastes, which are expected to be more reactive than fly ash or silica fume modified pastes (Poon et al. 2001).

4.3.1.3 Progress of reactions in fly ash/metakaolin containing limestone containing pastes

The calorimetric response of ternary blends containing up to 10% of fly ash or metakaolin with different particle sizes/dosages of limestone powder are discussed in this section. Figures 4-7 (c) and (d) represent the effects of a combination of limestone powder and fly ash on the heat release response of cement pastes. Figure 4-7(c) depicts the calorimetric response of systems containing 10% of limestone and fly ash whereas Figure 4-7(d) shows the response of the systems containing 20% limestone powder augmented with 10% fly ash. From both the figures, it can be noticed that the behavior of the ternary systems are different from those containing fly ash as the sole cement replacement material. When the response of the systems containing 10% fly ash and 10% limestone powder of varying sizes shown in Figure 4-7(c) is compared to those containing 10% limestone powder alone (Figure 4-2), it is noticed that the early age behavior of limestone powder modified pastes is not significantly modified by the presence of fly ash. To better facilitate these comparisons, Table 4-2 shows the parameters of the heat release curves of the plain, binary, and ternary mixtures. Comparing the 10% limestone powder modified pastes with and without fly ash, the time of appearance of the main hydration peak and the shoulder, the peak amplitudes, and the slopes of the acceleration and deceleration regions are found to

be very similar. While it has been reported that small amounts of limestone powder have an influence on the reaction products and properties of OPC-fly ash blended systems (De Weerdt, Kjellsen, et al. 2011; De Weerdt, Haha, et al. 2011), these are predominant at later ages as driven by the somewhat slow, time dependent dissolution of fly ash which releases aluminate species into the pore solution (Deschner et al. 2012). Increasing the limestone content of the ternary blends to 20% as shown in Figure 4-7(d) results in a behavior fairly similar to that of the 20% limestone powder pastes without fly ash; although a small enhancement in the peak amplitude and slightly earlier appearances of the main hydration peak and the shoulder peak are noted.

Table 4-2: Parameters of the calorimetric response for binary and ternary cement pastes

OPC	FA	MK	LS	LS size (μm)	Main hydration peak				Slopes	
					Peak 1		Peak 2		Accel. (W/g-h)	Decel. (W/g-h)
					Time (h)	P (W/g)	Time (h)	P (W/g)		
100	0	0	0	--	7.5	0.0044	--	--	0.0009	-0.0005
90	0	0	10	0.7	5.7	0.0051	7.6	0.0048	0.0013	-0.0007
				3	6.4	0.0046	8.2	0.0043	0.0010	-0.0005
				15	7.4	0.0044	9.1	0.0041	0.0008	-0.0004
90	10	0	0	--	7.6	0.0046	--	--	0.0009	-0.0004
80	10	0	10	0.7	5.6	0.0053	7.4	0.0050	0.0014	-0.0007
				3	6.3	0.0047	8.1	0.0045	0.0010	-0.0005
				15	7.6	0.0044	9.4	0.0042	0.0009	-0.0004
90	0	10	0	--	6.4	0.0048	8.2	0.0047	0.0011	-0.0006
80	0	10	10	0.7	4.9	0.0057	6.7	0.0057	0.0017	-0.0009
				3	5.5	0.0050	7.4	0.0050	0.0012	-0.0005
				15	6.5	0.0049	8.0	0.0049	0.0011	-0.0006

or the pastes containing limestone powder along with 10% fly ash, Figure 4-6 shows that increasing the limestone content increases the normalized CH content as expected. Expectedly, increasing coarseness of the limestone powder and increasing dosage reduces the normalized 1-day CH contents. However, it can be noticed that a further cement reduction of 10% through fly ash incorporation in limestone powder modified concretes does not result in a corresponding change in the normalized CH contents, suggesting that the addition of fly ash does not influence early age behavior. A comparison of the isothermal calorimetry results for limestone powder modified pastes with and without fly ash (Figure 4-4 and Figures 4-7(c),(d)) also indicate that the benefits of low amounts of fly ash addition, in conjunction with limestone powder, up to 20% are not readily observed at early ages. This observation highlights the need to select a more reactive aluminous cement replacement material, metakaolin, to be used in limestone powder modified systems so as to induce changes in early age behavior.

Figure 4-7(e) shows the heat release response of pastes containing 10% limestone and 10% metakaolin as (partial) cement replacement materials while Figure 4-7(f) shows the response of pastes containing 20% limestone powder augmented with 10% metakaolin. The synergistic early age effects of small amounts of metakaolin in conjunction with 10% or 20% cement replacement by limestone powder are evident from these figures. For example: from Figure 4-7 (e), it is noted that limestone powder in combination with metakaolin results in two distinct peaks (corresponding to C_3S and C_3A hydration) of similar magnitudes – indicating that aluminate hydration is potentially enhanced in the presence of metakaolin. These peak heights increase with decreasing median particle size of the limestone powder. The parameters of the heat release peaks of these ternary blends

for a limestone replacement level of 10% are shown in Table 4-2. The acceleration in hydration reaction in the presence of finer limestone powder and metakaolin as compared to limestone alone can be quantified based on the time of appearance of the peaks and the peak amplitudes provided in Table 4-2. The fact that the secondary peak related to the aluminate reaction is equal in magnitude to the primary peak in the ternary metakaolin blends (note that when limestone or metakaolin alone is used as a cement replacement material – Figure 4-4 and 4-7 (b) – the primary and secondary peak amplitudes are different) suggests that the combination of finer limestone powder and metakaolin enhances the reaction kinetics at early ages in a more direct fashion than any other combination of binary or ternary blends evaluated here.

The normalized 1-day CH contents of metakaolin modified pastes are found to be consistently lower than those of pastes containing only limestone or limestone/fly ash as OPC replacement materials. The reaction of carbonate from limestone with Al from the OPC and metakaolin results in the formation of the mono/hemi-carboaluminate hydrates. Thermodynamic calculations suggest that the formation of the carboaluminates initiates as early as 1 day in limestone containing systems (Lothenbach et al. 2008; De Weerdt, Haha, et al. 2011), a point confirmed by XRD (Voglis et al. 2005; Ipavec et al. 2011). The formation of carboaluminates (specifically, hemicarboaluminate) consumes CH (V. L. Bonavetti, Rahhal, and Irassar 2001; Matschei, Lothenbach, and Glasser 2007b; Lothenbach et al. 2008). While this action partly explains the reduced CH content observed in ternary blends containing metakaolin, an additional contribution of the pozzolanic action of metakaolin at ages as early as 1 day (Lagier and Kurtis 2007; Poon et al. 2001) may be another factor to consider.

4.3.2 Compressive Strength Development

The compressive strengths of plain, binary, and ternary cement paste blends up to 28 days of hydration are shown in Figure 4-8. The compressive strengths for the OPC-limestone powder pastes are shown in Figure 4-8(a). The paste containing 10% of 0.7 μm limestone powder shows the highest strengths until 14 days of age, after which it shows strengths similar to that of the plain paste. The enhancement in cement hydration facilitated by the fine particles of limestone powder is responsible for this effect. Similar results are reported for limestone powder modified cement pastes in (Tsivilis, Chaniotakis, Badogiannis, et al. 1999; Voglis et al. 2005; De Weerdt, Haha, et al. 2011). With increasing limestone content and median particle size, the compressive strengths at all ages are found to reduce, as expected. The reduction is not very prominent at early ages except for the higher replacement levels with the coarser limestone powder, due in part to mineral acceleration effects being able to partially compensate for the effects of OPC replacement. However, for the 15 μm limestone powder modified paste, a 20% replacement of cement by limestone powder results in a 21% strength loss at 28 days, attesting to the effects of OPC by coarse limestone powder on mechanical properties.

The compressive strength development of ternary blends containing fly ash or metakaolin along with limestone powder is provided in Figures 4-8(b) and (c) respectively. The use of metakaolin with 10% of the finer limestone powder provides compressive strengths similar to or higher than that of 10% metakaolin modified cement pastes at the ages considered. Note that similar or higher strengths are achieved in this case even when the cement replacement level in the ternary blend is double that of the binary blend. However, for a similar paste in which fly ash is used, the compressive strengths are generally substantially

lower than the 10% metakaolin modified paste - demonstrating the synergistic effects of the use of fine limestone powder with metakaolin. A comparison of Figures 4-8(b) and (c) shows that for the same level of cement replacement with limestone powder of a given particle size, mixtures containing metakaolin have marginally higher strengths (of the order of 5%) at all ages than the plain paste. For a given total cement replacement level, the ternary blends (containing fly ash/metakaolin with limestone powder) demonstrate higher 28 day strengths than the corresponding OPC-limestone blends. This can be attributed to the combined effects of: (1) carboaluminate formation and ettringite stabilization and (2) the pozzolanic reactions, which would increase the solid volume of the hydrates and reduce the porosity in the system (Lothenbach et al. 2008; V. L. Bonavetti, Rahhal, and Irassar 2001; Marsh and Day 1988).

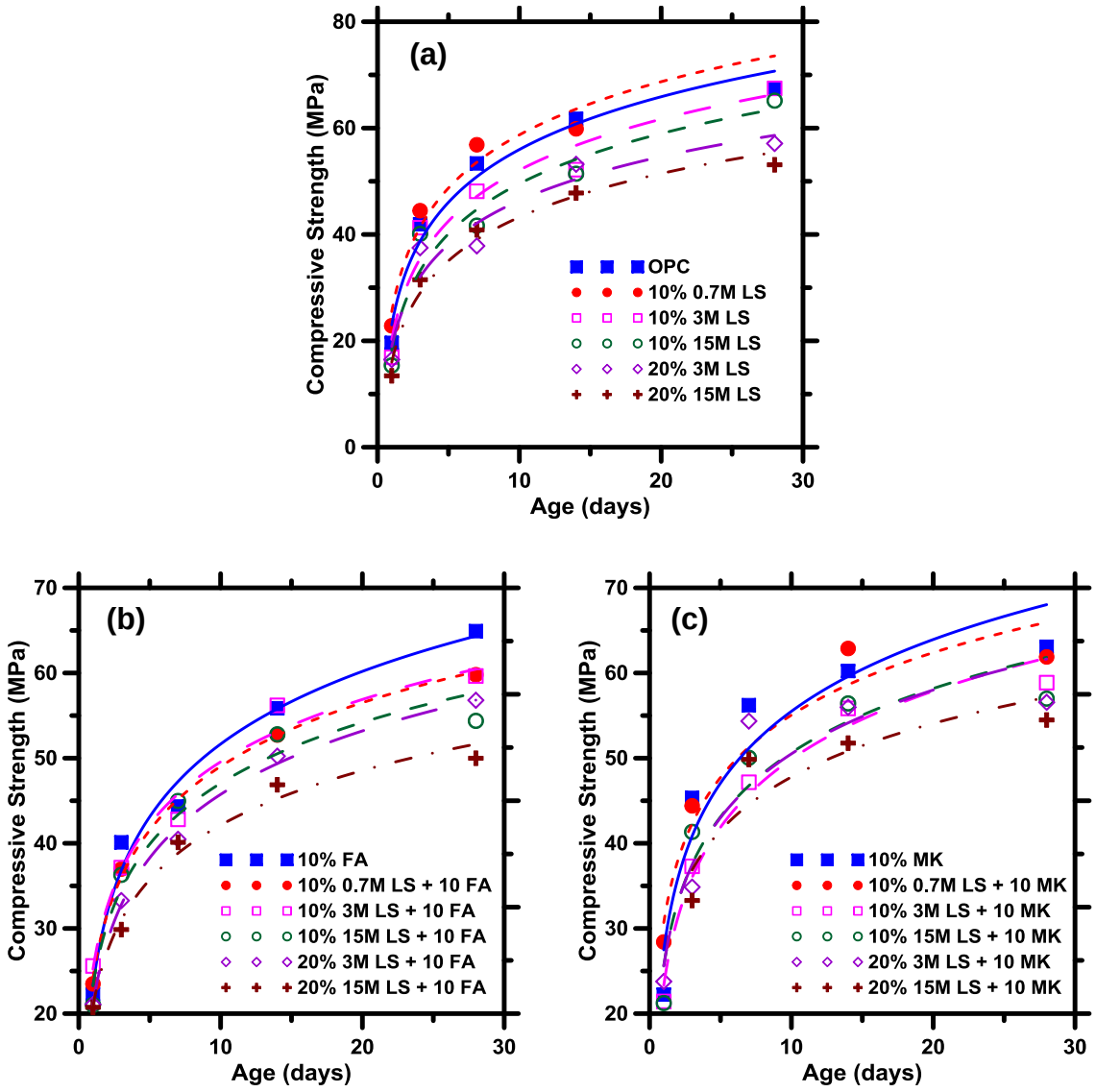

Figure 4-8: Compressive strength development of: (a) OPC- limestone pastes, (b) OPC-limestone-fly ash pastes, and (c) OPC-limestone-metakaolin pastes. The standard deviation in compressive strengths ranged from 0.5 MPa at early ages to 4.5 MPa at later ages, but are not shown in the graphs to avoid cluttering.

4.3.3 Thermal Analysis of Pastes: Influence of Limestone and Fly Ash/Metakaolin

4.3.3.1 Analysis of TG and DTG Curves

The discussions provided earlier suggest that fine limestone powder in combination with a small amount of metakaolin results in higher heat release and strength as compared to pastes composed with fine limestone and fly ash. Thermogravimetric (TG) and differential

thermogravimetric (DTG) curves for the 1 day hydrated systems are provided in Figure 4-9(a). It is noted that the residual mass fraction at 600°C is similar for the OPC paste and the 10% 0.7 µm limestone powder modified paste with and without fly ash, indicating similarities in their w_n contents. The w_n is the highest for the ternary blend with metakaolin, indicating the enhanced reactivity of metakaolin + limestone blends at early ages- as also supported by the strength gain response and normalized CH contents.

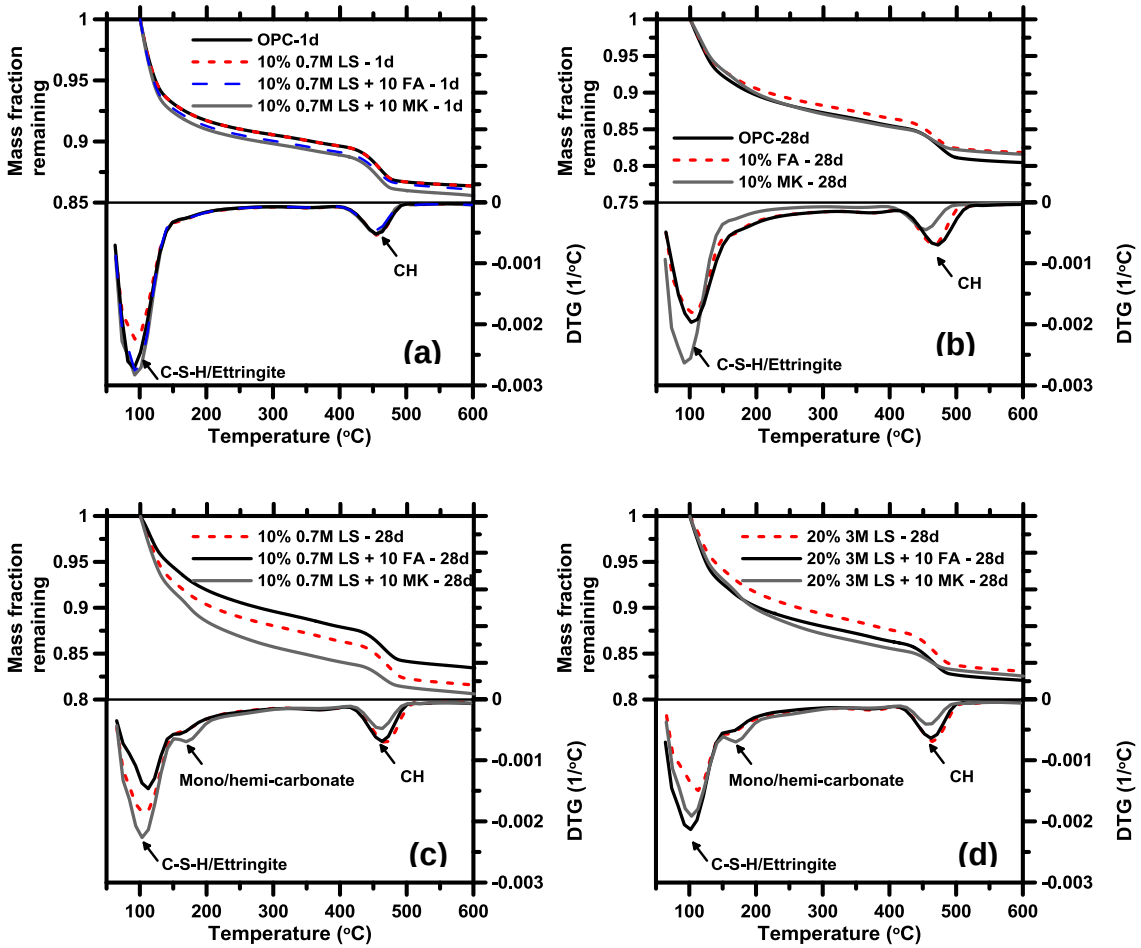

Figure 4-9: TG and DTG curves of: (a) 1 day hydrated binary and ternary pastes containing limestone and fly ash/metakaolin, (b) 28 day hydrated pastes containing fly ash/metakaolin, (c) 28 day hydrated ternary blends with 10% 0.7 µm limestone, and (d) 28 day hydrated ternary blends with 20% 3 µm limestone. Representative data is shown. The uncertainty in the mass loss was less than 5% for duplicate measurements made at the same age.

The peak at 100°C, linked to the decomposition of C-S-H and ettringite (De Weerdt, Kjellsen, et al. 2011; De Weerdt, Haha, et al. 2011) is slightly higher for the ternary blend containing metakaolin, potentially suggesting increased amounts of C-S-H and/or the stabilization of ettringite in the presence of limestone. However, no monocarbonate is observed in the 1 day DTG curves, though slight (if any) formation is only expected at such early ages (Voglis et al. 2005).

The TG and DTG curves of OPC, fly ash, and metakaolin modified pastes cured for 28 days are shown in Figure 4-9(b). The OPC and fly ash modified pastes show similar behavior at 28 days. The beneficial effects of metakaolin in terms of increasing the C-S-H content and decreasing the CH contents can be clearly seen in this figure. This figure provides context to the TG and DTG analysis of ternary blends shown in Figures 4-9(c) and (d). From the DTG curve of the ternary blend of 10% 0.7 μm limestone and metakaolin shown in Figure 4-9(c), a distinct peak around 180°C corresponding to the carboaluminate phases (De Weerdt, Haha, et al. 2011; Lothenbach et al. 2008) is observed. The formation of the carboaluminates, in conjunction with the pozzolanic reaction decreases the CH content even though the w_n (and hence anticipated CH production) is the highest among all the three pastes shown in this figure. The formation of carboaluminate phases can be quantified using the residual amounts of $CaCO_3$ in the pastes. Figure 4-10 shows the residual mass fraction of $CaCO_3$ in the pastes hydrated for 1 and 28 days, obtained by dividing the mass fraction of $CaCO_3$ from TG analysis by the initial mass fraction of $CaCO_3$ in the paste. It can be readily noticed from this figure that the residual calcium carbonate content is lower for the limestone modified pastes containing metakaolin, confirming the increased consumption of limestone to form carboaluminate phases. For example, in the

paste containing 10% 0.7 μm limestone by volume (8.7% by mass), 14% of all the limestone added (or 1.21% by mass of cement) reacts after 28 days. This value increases to 16% (1.4% by mass of cement) and 19% (1.65% by mass of cement) if the binder contains 10% of fly ash or metakaolin by volume respectively in addition to limestone. For the paste containing 20% 3μm limestone by volume (17.4% by mass), 17% of all the limestone added (3% by mass of cement) is consumed after 28 days whereas this value increases to 17.5% (3.1% by mass of cement) and 18.2% (3.3% by mass of cement) in the presence of additional 10% fly ash or metakaolin by volume. The amounts of limestone reacted are in the general range reported in (Kakali et al. 2000; Taylor 1997).

The TG and DTG results for a larger replacement level of cement with 3 μm limestone powder along with metakaolin or fly ash is shown in Figure 9(d), which also shows a DTG peak corresponding to the presence of carboaluminates. Note that even at higher limestone replacement levels, the intensity of the carboaluminate peak is relatively unchanged as compared to Figure 4-9(c). This qualitatively shows that a higher replacement level of the 3μm size limestone powder is able to provide the same effect as a lower replacement level of the 0.7μm limestone powder as far as carboaluminate formation is concerned. Figure 10 confirms this observation where the residual carbonate contents in 10% 0.7μm limestone powder and 20% 3μm limestone powder are found to be similar. Such an effect was not noticed for the 15 μm size limestone powder as can be noted from Figure 4-10.

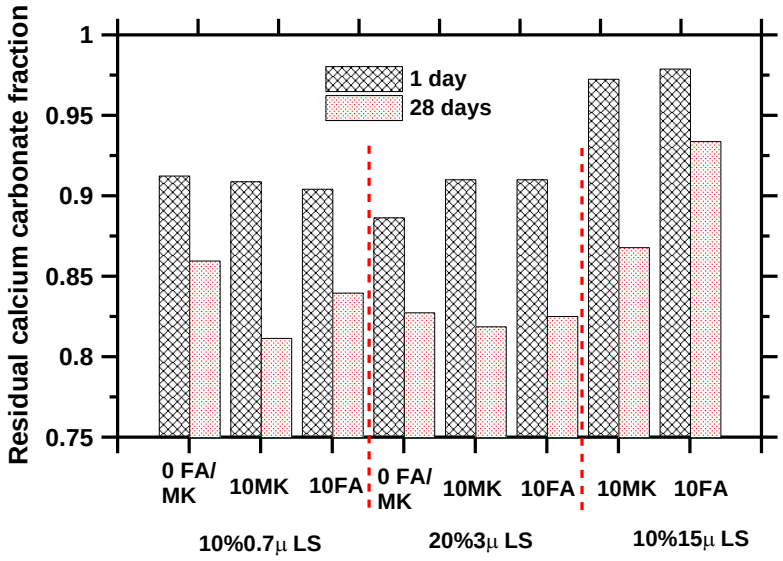

Figure 4-10: Residual calcium carbonate contents in the limestone powder modified pastes after 1 and 28 days of hydration.

For the limestone-fly ash ternary blends shown in Figure 4-9(c) and (d), only a very small peak is seen in the DTG curve corresponding to carboaluminate phases. In order to clearly distinguish between the effects of fly ash and metakaolin in limestone powder modified pastes, the heat flow corresponding to the thermal decomposition of the pastes is shown in Figure 4-11. The thermal signature corresponding to carboaluminates is clearly observed in this figure, with a noticeable minor peak at around 180^{o}C for the OPC-limestone-metakaolin blend. The minor peak is similar in size and much smaller for the limestone powder modified pastes with and without fly ash, and for the OPC paste. The fly ash content in these pastes is only 10%, which proves insufficient to form a significant volume of carboaluminates. It has been shown in previous publications that a much higher cement replacement level with fly ash (30- 35%), which in turn means higher amount of aluminates, coupled with small amounts of limestone (5%) result in a detectable peak in the DTG curves at around 180^{o}C (De Weerdt, Kjellsen, et al. 2011; De Weerdt, Haha, et al. 2011). It was also shown that higher amounts of fly ash in conjunction with smaller

amounts of limestone powder can result in later-age (beyond 28 days) properties, comparable to OPC mixtures. However the disadvantage of using such high volumes of fly ash is the lack of early-age property development. In this study, it is shown that the combination of a reactive aluminate source with fine limestone powder can provide 1-and 28-day properties comparable to OPC mixtures for cement replacement levels of 20% (by volume).

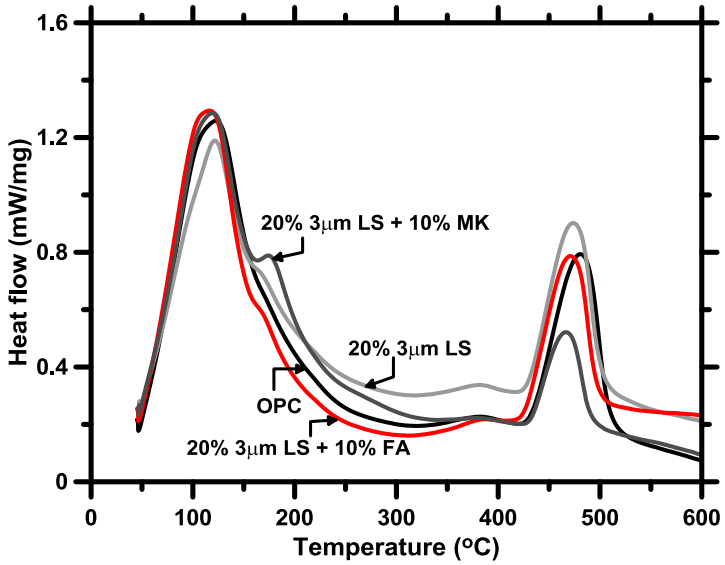

Figure 4-11: Heat flow curves for the limestone modified pastes at 28 days of hydration

4.3.3.2 Bound Water and CH Contents

If the total mass loss value at 600°C (w_n) is assumed indicative of taken as a reasonable measure of the volume of reaction products, then the increased reaction product volume (even at 20% less cement in the paste, and a reduced CH content) can be considered to be contributed by (i) accelerations in hydration facilitated by the filler effect of limestone powder, (ii) higher reactivity of metakaolin to form pozzolanic C-S-H, and (iii) the formation of carboaluminates through the reaction between the aluminates from metakaolin and carbonates from limestone powder. These effects compensate for the

reduced cement content in ternary blend with metakaolin (and limestone) to enable a compressive strength similar to that of the OPC paste (Figure 4-8).

The non-evaporable water contents (w_n) and the CH contents after 1, 7, and 28 days of hydration, normalized by the mass fractions of cement in the pastes are shown in Figures 4-12(a) and (b) for selected binary and ternary blend pastes. For all the pastes considered, a major fraction of the water is bound in the first 7 days of hydration. The OPC paste has the lowest normalized w_n at all ages among all the binary pastes considered in Figure 4-11(a). The 10% 0.7 μm limestone powder and the 20% 3 μm limestone powder modified pastes show higher normalized w_n and normalized CH contents at 1 and 28 days, attesting to the effect of fineness and amount of limestone powder on accelerating cement hydration (Figures 4-4 and 4-8). The 10% fly ash modified paste shows a higher normalized w_n than the OPC paste at 1 day, and similar w_n at later ages. The enhancement in reactivity of cement provided by metakaolin and its own reaction at early ages result in the metakaolin modified paste showing a higher normalized w_n than the OPC paste at all ages. It is also important to note from the lower panel of Figure 4-12(a) that this paste has the lowest content of normalized CH, with a significant lowering of CH contents at 28 days as compared to the other pastes. Higher w_n and lower CH contents are an indication of the effective pozzolanic reaction of metakaolin starting at very early ages. For all the other pastes, the CH contents follow trends similar to that of w_n. The normalized w_n and CH contents of the ternary blend pastes are shown in Figure 4-12(b). Immediately evident from this figure are the higher normalized w_n values for the ternary blends as compared to the binary blends shown in Figure 4-12(a). The paste with overall 30% cement replacement by volume (20% 3 μm limestone powder and 10% metakaolin or fly ash) show higher

normalized w_n at later ages, closely followed by the metakaolin modified 10% 0.7 µm limestone powder paste. The normalized CH content of the limestone-metakaolin blends shown here reduces or remain fairly constant with age while the normalized w_n values for the corresponding pastes are seen to increase. For cement hydration, an increase in w_n generally means an increase in CH. The reduction in CH can be construed as an indication of the change in reaction products, i.e., due to pozzolanic reactions and the formation of the carboaluminate hydrates as shown in Figure 4-9 through the TG and DTG curves. Evidence of reaction product modification at 28 days of hydration can be seen in both 0.7 µm and 3 µm size limestone powder pastes containing metakaolin. A total cement replacement of 20% (10% 0.7 µm limestone and 10% metakaolin) results in a much higher 1 day compressive strength and comparable 28 day compressive strength as compared to the OPC paste. Such a beneficial effect is not observed for OPC-limestone-fly ash blends. Even cement replacement at 30% level (20% 3 µm limestone powder, 10% metakaolin), results in only a 15% strength reduction as compared to the plain OPC paste. Small amounts of monocarboaluminate, shown to have a high modulus (Moon et al. 2011), could also play a role in mitigating strength loss in these mixtures. The incorporation of small amounts of metakaolin is thus found to be highly beneficial in improving the properties of limestone powder modified systems at ages up to 28 days.

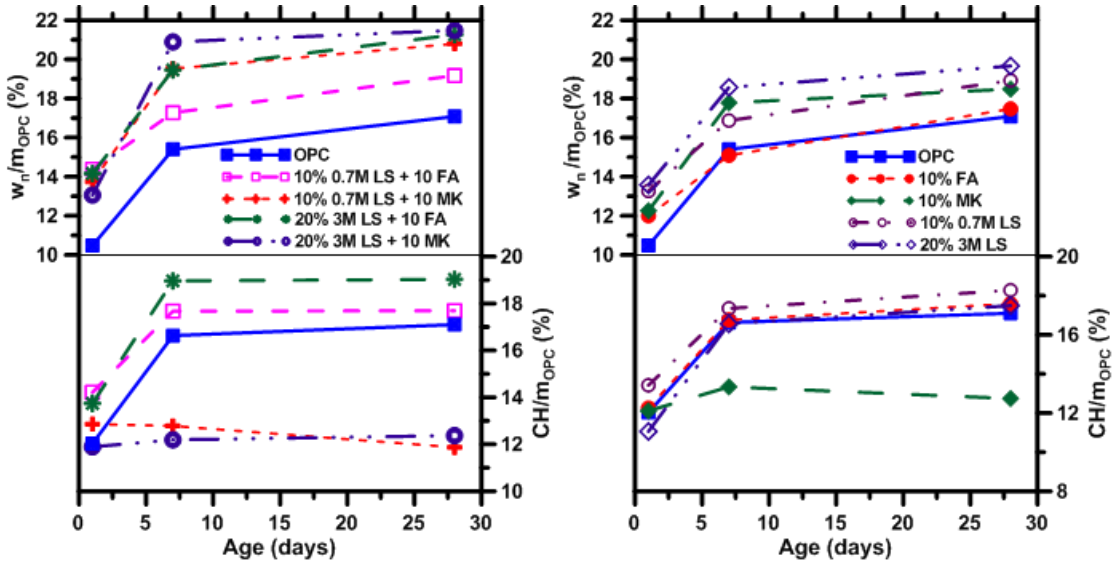

Figure 4-12: Non-evaporable water and CH contents of: (a) binary mixtures containing limestone or fly ash/metakaolin, and (b) ternary blends of limestone and fly ash/metakaolin

4.4 Conclusions

This paper describes the influence of limestone fineness and the reactivity of the alumina source on the early-age heat release response, the compressive strength and hydration products formed until 28 days for cement pastes containing limestone powder of three different median particle sizes or a combination of limestone powder and small amounts (10%) of fly ash or metakaolin. Fine limestone powders (0.7 and 3 µm) were found to accelerate the early-age cement hydration at all the dosages studied. The paste with 10% of 0.7 µm limestone powder was found to have better 1 day strength and increased normalized non-evaporable water (w_n) and CH contents than the OPC paste. Increasing limestone coarseness and dosage reduced the compressive strength as expected. Cement replacement by metakaolin in binary blends resulted in a higher heat release rate while replacement by fly ash did not produce large changes in the calorimetric response.

The calorimetric response of the pastes containing limestone was not considerably modified by the presence of fly ash whereas significant changes in the calorimetric response was observed when metakaolin was used in conjunction with fine limestone powder (0.7 and 3 μm). The enhanced reaction kinetics in ternary blends containing 10% 0.7 μm limestone powder and 10% metakaolin resulted in the highest 1 day compressive strength and the 1-day normalized CH content was among the lowest of all the evaluated pastes. While CH reduction could also be partially attributed to carboaluminate formation, it was not detected in the thermal decomposition signatures of these pastes. It could also be that the enhanced aluminate phase reaction contributed to increased incorporation of Al^{3+} in the C-S-H at early ages rather than forming carboaluminates.

The fine limestone powder (0.7 and 3 μm) modified pastes at 10% cement replacement level showed compressive strengths comparable to those of OPC pastes until 28 days. The ternary blend of metakaolin along with 10% 0.7 μm limestone powder resulted in compressive strengths that were higher than either of the corresponding binary blends, even at a higher overall cement replacement level. Such a response was not observed in the case of fly ash. The normalized w_n at 28 days for the ternary blends of 0.7 and 3 μm limestone powder and metakaolin was higher than that of the OPC paste, the binary blends, and the ternary blends containing fly ash. While the normalized w_n of these pastes increased with age, the normalized CH contents were found to reduce or remain unchanged with age, indicating changes in reaction products. The DTG curves for the 28 day cured ternary pastes with both 0.7 and 3 μm limestone powder confirmed this through the observation of the presence of carboaluminates. Thus, this paper considers the role of the overall chemical compatibility of OPC replacement materials, with a view towards selecting replacement

material to produce synergistic effects and optimal OPC replacement efficiency. As such, this work advances approaches to utilize multiple material solutions based on limestone and metakaolin to proportion ternary binders, dedicated to reducing the use of OPC in concrete.

5. COMPARATIVE INVESTIGATION OF TERNARY LIMESTONE AND FLY ASH OR METAKAOLIN BLENDED CEMENT PASTE MICROSTRUCTURE VIA MERCURY INTRUSION POROSIMETRY

5.1 Introduction

There continues to be a growing interest in the use of limestone as a cement replacement material, acting as a filler increasing particle packing (V. Bonavetti et al. 2003), a location for cement hydration product nucleation, and reacting to some extent with the aluminate phases in cements (Lothenbach et al. 2008). Limestone replacement in portland cement has generally been shown to result in some strength reduction (Hawkins, Tennis, and Detwiler 2003), acceleration of hydration reactions (Lothenbach et al. 2008) and Chapter 4, and decrease setting time (Irassar et al. 2011) Recent work (De Weerdt, Kjellsen, et al. 2011; De Weerdt, Haha, et al. 2011) and in Chapter 4, has noted the synergistic benefit of limestone and alumina inclusion in portland cement systems, including the use of fly ash, metakaolin, and slag. Several benefits have been noted, including acceleration of cement hydration reactions (De Weerdt, Haha, et al. 2011) and Chapter 4, improving the reactivity of limestone in cement (De Weerdt, Haha, et al. 2011) and Chapter 4, offsetting potential strength losses associated with limestone replacement as noted in Chapter 4, and possible improvement to early age rheological performance as noted in the proceeding chapters, and setting performance.

The current work aims to explore the potential benefits of ternary blended limestone and metakaolin or fly ash on the pore structure of these systems. It has been proposed that fine limestone inclusion may increase particle packing, thereby decreasing the porosity of the resultant hardened cement paste. The current exploration is completed in the context of

mercury intrusion porosimetric investigations of these materials. Extensive work has been completed on the use of mercury intrusion porosimetry (MIP) to investigate the pore structure of micro-porous materials such as cement paste including (Zeng et al. 2012; Beaudoin 1979; Cook and Hover 1999). Several recent concerns about this type of study have recently been raised, including potential concerns from the so-called "ink bottle" effect, wherein a pore with a small opening opens to a much larger pore is recorded as a large volume of the small pore associated with the pore opening. This results from the necessary assumption in mercury intrusion experiments that pores are all cylindrical in shape, and have a constant diameter throughout their depth. Further, several recent studies have investigated the influence of sample pre-treatment on the experimental results from an MIP investigation. Pretreatment, or drying, of MIP samples is required to remove pore water from the sample to ensure mercury is able to fully intrude into the sample. Several common strategies are used including vacuum and oven drying as well as solvent exchange (Gallé 2001; Cook and Hover 1999). The primary concern noted with these techniques was changes to the pore structure induced as part of the drying process, potentially resulting in significant error in the determination of the porosity of the material.

There have been several studies investigating the influence of limestone on the pore structure of portland cement pastes, mortars and concretes (Tsivilis et al. 2003; Ye et al. 2007; Tsivilis, Chaniotakis, Batis, et al. 1999; Pipilikaki and Beazi-Katsioti 2009), however these studies have been largely focused on interground portland limestone cements and portland limestone cements with a coarser limestone phase. It has been proposed that the stabilization of AFt phases, primarily ettringite, in hardened portland limestone cement paste due to favored monocarbonate formation may result in a more

refined structure due to increased volume of hydration products resultant from the stabilized less dense ettringite (Matschei, Lothenbach, and Glasser 2007a; Lothenbach et al. 2008; De Weerdt, Haha, et al. 2011). However, it is generally reported in studies that limestone replacement increases porosity, permeability, intruded volume and critical pore diameter, and that increasing the replacement percentage further increases these parameters. The current work aims to expand on these studies by investigating fineness effects in limestone, as well as potential benefits of inclusion of alumina in portland limestone cements.

5.2 Experimental Program

5.2.1 Materials

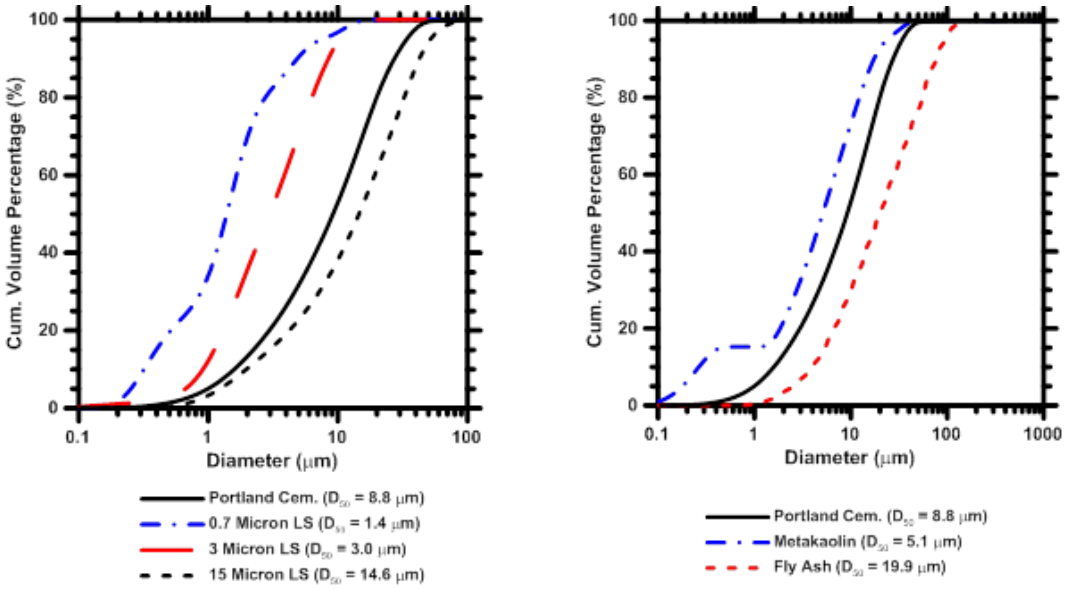

Figure 5-1: The particle size distributions (PSDs) of: (a) the OPC and limestone powders, and (b) the OPC, fly ash, and metakaolin powders.

The materials used include: a commercially available Type I/II ordinary portland cement (OPC) conforming to ASTM C150 ("ASTM C109 / C109M - 12 Standard Test Method for Compressive Strength of Hydraulic Cement Mortars (Using 2-In. or [50-Mm] Cube

Specimens)" 2012), a Class F fly ash and metakaolin conforming to ASTM C618 ("ASTM C109-13. Standard Test Method for Compressive Strength of Hydraulic Cement Mortars Using 2-In. Cube Specimens" 2013), and a nominally pure limestone powder (purity > 95% $CaCO_3$, by mass) of three different median particle sizes denoted as 0.7 µm, 3 µm, and 15 µm, conforming to ASTM C568 ("ASTM C568 / C568M - 10. Standard Specification for Limestone Dimension Stone" 2012). Figure 5-1 shows the particle size distributions (PSD) of the limestone, metakaolin and fly ash, as measured using laser diffraction, along with their median particle sizes.

The compositions of the portland cement and the cement replacement materials are presented in Table 5-1. Binary blends were prepared wherein: OPC was replaced by limestone of different particle sizes at levels ranging from 0-20%, by fly ash from 0-10% and by metakaolin from 0-10%; all by volume. Ternary blends containing limestone powder and fly ash or metakaolin were also prepared. Table 5-2 shows the proportions of the different mixtures evaluated. All pastes were proportioned at a fixed volumetric water-to-solids ratio, $(w/s)_v = 1.26$, corresponding to a mass based water-to-solids ratio $(w/s)_m = 0.40$ for the OPC mixture to allow for the comparison of the pore structure of the resultant cement pastes.

Table 5-1: Composition and specific surface areas (m^2/kg) of the materials used in this study as determined using XRF and the Blaine's air permeability apparatus per ASTM C205-11

Phase (%)	OPC	Class F Fly Ash	Metakaolin
SiO_2	21.06	58.4	51.7
Al_2O_3	3.86	23.8	43.2
Fe_2O_3	3.55	4.19	0.5
CaO	63.75	7.32	--
MgO	1.83	1.11	--
SO_3	2.93	0.44	--
Na_2O	0.12	1.43	--
K_2O	0.48	1.02	--
LOI	1.99	0.5	0.16
SSA (m^2/kg)	470	218	3255

Limestone powder contains 95-97% $CaCO_3$ as per the manufacturer. The Blaine specific surface areas are 4970 m^2/kg, 2400 m^2/kg, and 613 m^2/kg for the limestone powders having median particle sizes of 0.7 μm, 3 μm, and 15 μm respectively.

Table 5-2: The proportions of the paste mixtures evaluated in this study

		Replacement level (Vol. %)		
Mix Type	Volumetric Water-to-solids ratio $(w/s)_v$	Limestone (0.7, 3, and 15 μm)	Metakaolin	Fly Ash
OPC	1.26	0	0	0
OPC + LS	1.26	10,20	0	0
OPC + FA	1.26	0	0	10
OPC + MK	1.26	0	10	0
OPC + LS + FA	1.26	10,20	0	10
OPC + LS + MK	1.26	10,20	10	0

5.2.2 Experimental Parameters

Suspensions were prepared by dry blending powders prior to adding water and then hand mixed using a kitchen mixer. Samples of approximately 100g were cured for 28 days under sealed conditions at a constant temperature of 23±1 °C. At the desired age of testing, the samples were crushed to an approximate size of 2mm, and then dried in accordance with the pretreatment procedure described below. Approximately 1g of material was selected and weighed using a high precision scale accurate to 0.001g. Testing was completed using a 0.5 cc cell in a Quantachrome Instruments PoreMaster mercury intrusion porosimeter to a maximum testing pressure of approximately 414 MPa. Mercury intrusion values were extracted from the Quantachrome Instruments PoreMaster software package and used for analysis. The relationship between pore diameter and intrusion pressure was determined internally in the Quantachrome software package using the Washburn equation (Washburn 1921) (Equation 1), where d is the apparent diameter, P is the applied pressure and γ is the surface tension of mercury and, φ is the intrusion mercury contact angle which are assumed to be 0.48 N/m and 117° respectively. 117° was selected as the intrusion contact angle is typically used for oven dried samples (Winslow and Diamond 1970b; Bager and Sellevold 1975; R. Kumar and Bhattacharjee 2003)

$$d = \frac{-4\gamma \cos \varphi}{P} \qquad \text{Equation 5-1}$$

Finally, the extrusion pore size distribution was attained using the methodology presented in (Zeng et al. 2012). In porous media, the intrusion and subsequent extrusion of mercury results in a hysteresis, where the extrusion curve lies above the intrusion curve, indicating mercury is retained in the sample. The volume of mercury retained has been attributed to two effects: (i) the change in mercury contact angle in extrusion cycle versus the intrusion

cycle and (ii) the pore structure of the sample, in particular pores with small diameter openings which open to larger pores, often referred to as the ink bottle effect (Zeng et al. 2012). The extrusion curve typically has a plateau at high pressure, where the intruded volume of mercury remains constant; a behavior which has been assumed to be primarily due to the decrease in contact angle from intrusion to extrusion. Based on this principle, the change in the contact angle was determined by the determination of contact angle modification factor (Zeng et al. 2012), as presented in Equation 5-2.

$$\alpha_\theta = \frac{\Delta P}{P} \qquad \text{Eq. 5-2}$$

Where ΔP is determined as the change in pressure before extrusion begins, selected in this study to be the point at which the extrusion rate exceeds 0.001 cc/g. This modification factor is then used to determine the extrusion contact angle as:

$$\theta_{ex} = \cos^{-1}\left(\cos(\theta_{in})\,(1-\alpha_\theta)\right) \qquad \text{Eq. 5-3}$$

The extrusion contact angles determined with this methodology in this study varied by sample, but were typically about 106°. After the extrusion contact angle was determined, the extrusion distribution was determined using the modified angle in Eq. 5-1, and the total volume retained determined as the volume remaining at the end of the extrusion cycle. The retained volume is proposed to be related to the tortuosity of the pore structure, as it measures the quantity of mercury that is "trapped" in the sample after pressure has been removed. The retained volume in this paper is reported as a fraction of the total volume intruded, as this ratio gives a better idea of the complexity of the pore structure in the sample.

There has been significant recent discussion on the influence of pretreatment on determined parameters in mercury intrusion porosimetry, including (Gallé 2001; Winslow and Diamond 1970b). It has been noted that methods such as heating at high temperature effect the pore structure of the sample due to the internal pressure resultant from the phase transformation of water. A preliminary study was performed as part of this study on a fly ash and OPC sample to determine an appropriate drying method for use in the experimentation. The results of this preliminary study for the OPC sample are presented in Figure 5-2. It is noted from these figures that the use of no pretreatment resulted in a significant decrease in intruded mercury, while drying for long durations or at high temperatures resulted in significant increases in the volume of mercury intruded. Drying at lower temperature or vacuum drying resulted in comparable pore size distribution curves. The critical (percolation) pore diameter is defined as the diameter at which the maximum rate of intrusion occurs, as illustrated by the earliest major peak (Atahan, Oktar, and Tasdemir 2009) as shown in Figure 5-2(b). Noted from this figure for both 60°C for 2 hours and vacuum drying comparable peak locations are determined. Based on this analysis, the drying methodology of 60°C for 2 hours was selected for this study. As this study is comparative in nature, and investigating relative differences, this was determined to be sufficient for this study.

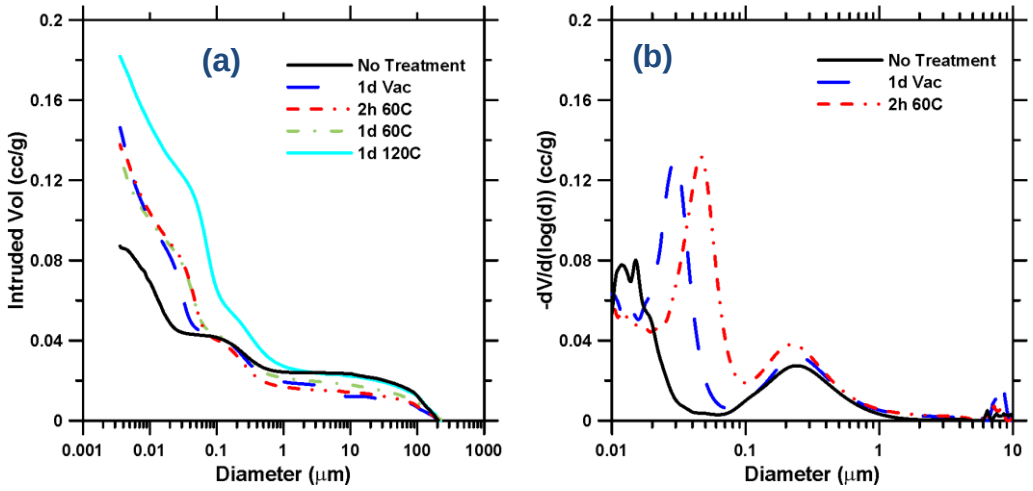

Figure 5-2: Preliminary study of influence of drying techniques on (a) determined pore size distribution and (b) critical pore diameter values.

5.2.3 Experimental Design

The experimental design for this project consists two phases, (i) the investigation of the effects of limestone fineness and replacement ration on microstructure, and (ii) the investigation of potential synergistic benefits of additional alumina in limestone blended cements. The first phase consists of three single factor experiments with one replicate (for the three sizes of limestone) at three levels: 0, 10 and 20% replacement by volume. The second phase consists of multiple concurrent fully randomized 2^2 factorial experiments with one replicate, where the effects investigated are limestone replacement ratio (2 levels, 0 and 10% by volume) and alumina source replacement ratio (2 levels, 0 and 10% of fly ash or metakaolin by volume). A tabular representation of the experimental design if presented in Table 5-3, where the minus represents a replacement ratio of 0 and the plus a replacement ratio of 10. An individual 2^2 factorial experiment was completed for each limestone size, resulting in 6 individual 2^2 factorial experiments (three sizes with two sources of alumina). Statistical analysis to determine the influence of limestone addition, alumina addition, and interaction effects between limestone and fly ash or metakaolin was

conducted using analysis of variance (ANOVA). Additional investigations were completed at higher limestone volumetric replacement ratios to further examine the influences of limestone as part of the randomized experiment but external to the ANOVA statistical analysis. A p-value of less than 0.05 was used to define statistical significance to reject the null hypothesis: there is no effect.

Table 5-3: Experimental Design Table

	LS	FA/MK
OPC	-	-
10 LS	+	-
10 FA/MK	-	+
10 LS 10 FA/MK	+	+

ANOVA analysis was completed on the response variables of volume intruded, critical pore diameter, and volume fraction retained. These parameters were determined as discussed in the previous section.

5.3 Results and Discussions

5.3.1 Influence of limestone replacement ratio and fineness on pore structure

Mercury intrusion experiments were conducted on binary blended limestone cements as outlined in Section 5-2, the resultant determined intruded and extruded pore size distributions are presented in Figure 5-3. The extrusion portion of these curves was determined using the modified extruded mercury contact angle as determined using Equation 5-3. Immediately evident from these figures is that the fineness of limestone appears to have very little influence on the intrusion curves or the total volume of mercury intruded. Further, it is noted that increasing the replacement ratio further increases the total intruded volume, and appears to increase it at approximately the same ratio regardless of

limestone fineness. This result is consistent with the results for interground portland limestone cements reported elsewhere. As noted previously, the pore size distributions determined from mercury intrusion experiments have been shown to be inaccurate due to several effects including: pore mouth opening effects and pore tortuosity, thus the discussions of Figure 5-3 have been limited and this figure is provided more to present experimental results.

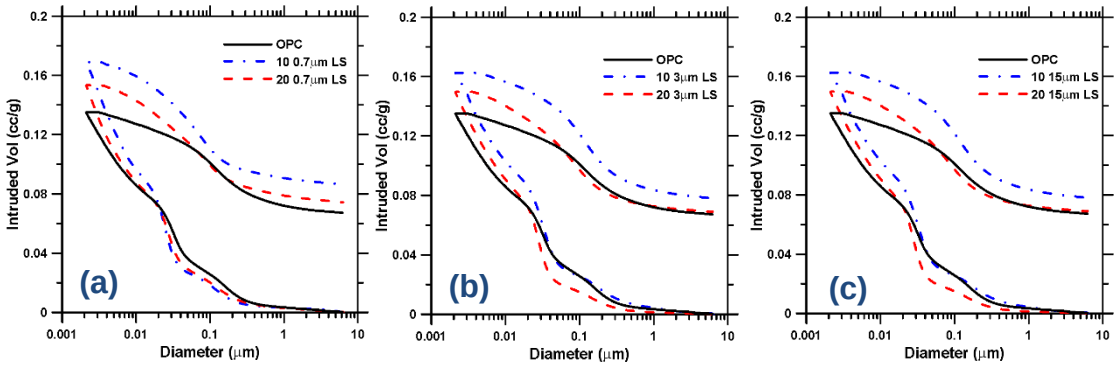

Figure 5-3: Determined intrusion and extrusion (higher curve) pore size distributions for: (a) 0.7 μm, (b) 3 μm, and (c) 15 μm limestone replacement

To further explore the influence of limestone fineness and replacement ratio on binary blended portland cement pastes, several key parameters were determined as discussed in Section 5-2: (i) the porosity of the sample, (ii) the critical pore diameter, and (iii) the retained volume after extrusion. These parameters are likely to be more accurate in discussions of intrusion experiments, as these parameters have been shown to be minimally effected by the sources of error discussed above. The results of this analysis are presented in Figure 5-4.

Noted from the porosity values (Figure 5-4(a)) is the same trend as noted from Figure 5-3. Statistical analysis of these determined values indicated that the effect of limestone replacement ratio was significant ($p<0.05$), however the effect of fineness was not

significant ($p>0.10$). From Figure 5-4(a), these results can be confirmed, as increasing limestone replacement ratio increases porosity at a relatively steady rate, and does so independent of limestone fineness. The porosity results appear intuitively correct for volumetric replacement of cement by a relatively inert filler material such as limestone. Increasing the fineness of limestone has been shown to accelerate hydration and increase the reactivity of limestone, however at later ages, it has been shown that the volume of limestone consumed is relatively low, and the progression of the hydration reaction becomes roughly equivalent regardless of fineness. Thus, the dominant factor effecting the porosity in these samples is the higher effective water-to-cement ratio resultant from limestone replacement, where in plain cement pastes it has been extensively shown that increasing the water-to-cement ratio increases the porosity of the resultant paste by increasing the volume of capillary water present in the paste.

Figure 5-4(b) shows the influence of limestone fineness and replacement ratio on the critical pore diameter of these pastes. Statistically analysis of these data indicates the effect of limestone replacement ratio for larger limestones (3 and 15 μm) are not significant ($p > 0.1$) over the replacement ranges used in this study, while for the fine limestone this effect is significant. The critical pore diameter, is the threshold diameter at which mercury percolates into the interior of the sample, and thus is thought to be a measure of ion permeability of a porous material, a measure of the concrete's durability and corrosion resistance (Halamickova et al. 1995). The replacement of cement by the finest limestone (0.7 μm) decreases the critical pore diameter by acting more effectively as a nucleation site, creating more fine hydration product spheres which refines the pore structure, resulting in an increased critical pore diameter. Further, it is notable that the volumetric

ratio of solids-to-water is constant in these samples, however the increased presence of fines randomly distributed in the microstructure would act to break-up the connected pore structure, creating blockages which limit the further intrusion of mercury (Beaudoin 1979). Finally, it has been reported that the presence of limestone may stabilize ettringite or other AFt phases in the microstructure at later ages (Lothenbach et al. 2008; De Weerdt, Haha, et al. 2011). This effect would result in an increased hydration product volume due to the lower density of AFt phases, potentially refining the pore structure and decreasing porosity.

It is important to note here, that the inclusion of limestone results in an increase in effective mass based water-to-cement ratio from 0.40 for OPC to 0.44 and 0.50 for 10 and 20% volumetric replacement by limestone respectively. The results by Cook (Cook and Hover 1999) indicate an increase in porosity of about 30% for a water-to-cement ratio increase from 0.40 to 0.50. The increase in porosity corresponding to the comparable increase in effective water-to-cement ratio due to limestone replacement found in this study was comparable to that determined by Cook, at about 25%. The slight reduction in porosity is likely attributed to limestone replacing portland in cement, resulting in a decrease volume occupied by cement hydration products. This result indicates that the inclusion of limestone in these systems likely does not have a significant influence on porosity, and that the porosity increases as a result of limestone inclusion can be primarily attributed to the increase in effective water-to-cement ratio associated with that replacement. As discussed previously, limestone inclusion in portland cement systems is thought to stabilize ettringite at later ages, which would be expected to result in an increase in hydration product volume and a subsequent reduction in porosity. This analysis appears to contradict that assessment, and indicate that the influence of ettringite stabilization on the porosity in these systems is

minimal. It may be that there are competing effects resultant from ettringite stabilization in these systems, including: (i) reduced production of ettringite due to decreased sulfates available in the system as the quantity of gypsum is decreased due to cement replacement and (ii) possible formation of microcracks due to expansive ettringite in the microstructure.

The inclusion of coarse limestone has little effect on the critical pore diameter due to a similar but opposing effect: coarse limestone powder less effectively acts as a location of hydration product formation due to comparable specific surface area to portland cement particles, and as it is comparably sized to the cement particles that would normally be present, and thus has little meaningful impact on pore refinement. Cook (Cook and Hover 1999) noted a significant increase in critical pore diameter with increasing water to powder ratio, increasing by about 100% as the water-to-cement ratio was increased from 0.40 to 0.50. Unlike the discussions above with respect to porosity, the results here do not indicate the same effect when considering effective water-to-cement ratios resultant from limestone replacement. Fine limestone in particular shows the opposite trend, with decreasing critical pore diameter with increasing effective water-to-cement ratio. This indicates that critical pore diameter is more strongly influenced by the solid volume fraction in the paste and the particle size distribution of those solids. As the solid volume fraction is constant across all samples investigated here, the decrease in critical pore diameter with fine limestone can be attributed to the inclusion of the fine limestone phase. Similarly, the relatively constant critical pore diameter in the 3 and 15 μm samples are likely due to negligible changes in particle surface area and sizes in the composite system.

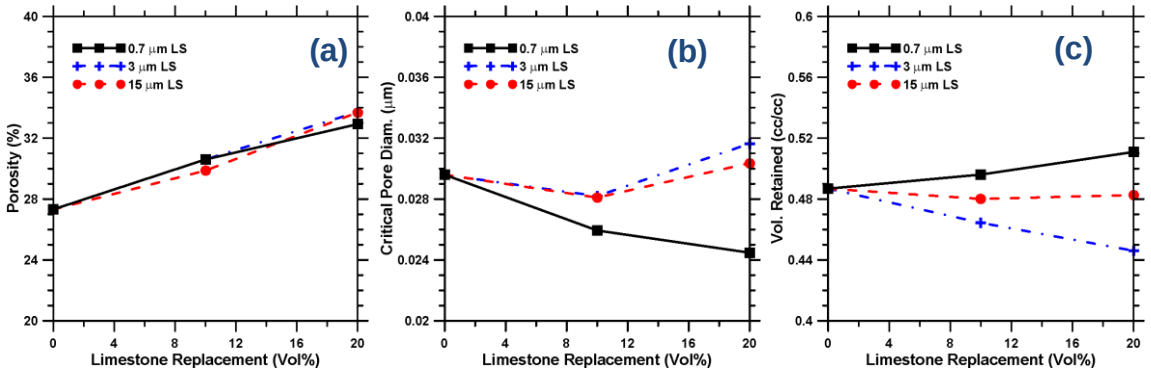

Figure 5-4: Influence of limestone fineness and replacement ratio on determined (a) mercury porosity, (b) critical pore diameter, and (c) retained volume ratio.

mercury porosity, (b) critical pore diameter, and (c) retained volume ratio.

A similar parameter used to characterize the tortuosity of the pores, the volume retained after extrusion, is presented in Figure 5-4(c). Statistical analysis of these results indicate the replacement ratio is statistically significant for limestone sizes of 0.7 and 15 μm, and insignificant at 3 μm over the range of replacement ratios investigated in this study. This analysis further supports the discussions in the previous paragraph, indicating that the fine limestone is make the pore structure of the sample more tortuous, resulting in a higher retained volume, due to the effects described above. The inclusion of the coarse limestone, combined with a higher effective water-to-powder ratio results in a less refined pore structure with larger pores, as the specific surface area of the particles present in the paste is decreased.

5.3.2 Influences of alumina addition on the pore structure of portland limestone cement paste

Statistical analysis of the influences of alumina additions (fly ash or metakaolin) on the pore structure of hardened cement pastes at 28 days was completed using the ANOVA methodology as presented in Section 5-2. This analysis was completed on several key

parameters: (i) the sample porosity, (ii) the critical pore diameter of the sample, and (iii) the volume fraction retained after extrusion. The results of the sample porosity and critical pore diameter determinations are presented in Figure 5-5 for limestone and fly ash or metakaolin ternary blended hardened pastes.

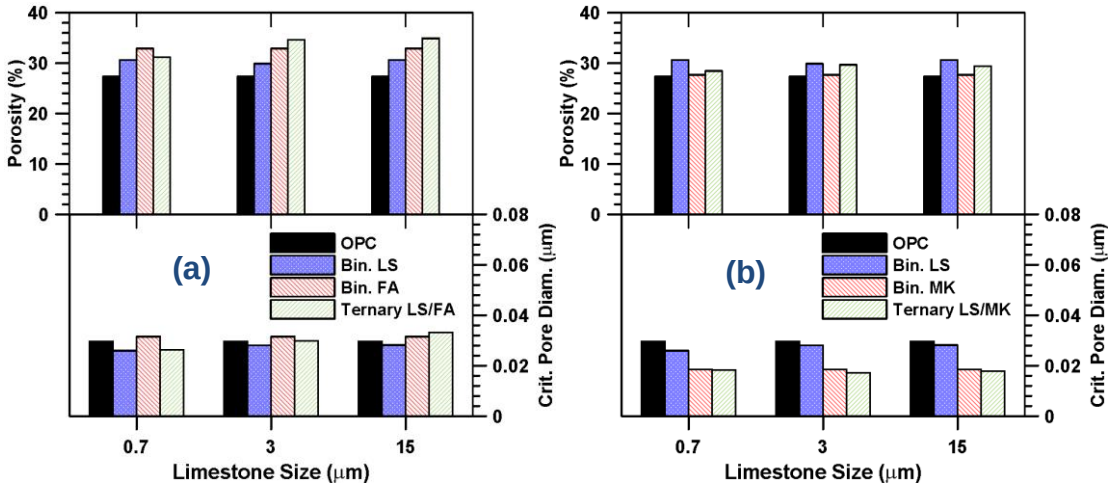

Figure 5-5: Influence of inclusion of alumina sources in hardened portland limestone cement pastes on critical pore diameter and porosity for (a) fly ash, and (b) metakaolin.

For the fly ash based pastes, there is a noted trend in porosity with the coarse limestone replacement (3 and 15 μm), where the OPC has the lowest porosity and the ternary blend of limestone and fly ash has the highest. Statistical analysis of the results for coarse limestone indicate both limestone and fly ash presence are significant factors, however the interaction effect between limestone and fly ash is not significant. Thus the continued increase in porosity as fly ash and limestone are incorporated into the paste is a result merely of the additive individual effects of limestone and fly ash replacement. At early ages, hardened cement pastes partially replaced by fly ash have been shown to have increased porosity (Chindaprasirt, Jaturapitakkul, and Sinsiri 2005; Fraay, Bijen, and de Haan 1989) due to the presence of large unreacted fly ash particles in the microstructure

and the low pozzolanic reactivity of fly ash at relatively early ages, a result which is confirmed in this study. Further, inclusion of coarse limestone particles results in a further increase of porosity due to the increased effective water-to-powder ratio as described above.

The combination of fine limestone (0.7 μm) and fly ash shows a different trend, however. Both binary fly ash and binary limestone mixes are shown to increase the porosity of the sample, for reasons discussed previously. When both fly ash and fine limestone replace cement, the additive effect seen with coarse limestones is not present, and a reduction in porosity as compared to the binary fly ash sample is noted. Statistical analysis of effects indicates that fly ash and the interaction effect of fly ash and limestone are significant, while the influence of limestone is less significant. This indicates there is a potential synergistic benefit on porosity between fine limestone and fly ash. As discussed previously, studies have indicated that fine limestone in combination with fly ash enhances the reactivity of limestone (De Weerdt, Haha, et al. 2011) and in Chapter 4, and further stabilizes ettringite at later ages. These two factors would increase hydration product volume as compared to the binary fly ash mixture, resulting in a decrease in porosity.

The ternary blends of the coarsest limestone and fly ash shows a similar behavior for critical pore diameter (lower panel of Figure 5-5(a)) as for porosity. Statistical analysis of these results, however, indicate that none of the effects are statistically significant, as the p-value is in excess of 0.10 for all tests. Observing the results in Figure 5(a), the coarsest limestone shows a slight continued increase in critical pore diameter when limestone and fly ash replace cement, likely attributed to the low pozzolanic activity of fly ash at the age investigated and the increased effect water-to-cement ratio of the system. The finest and

median limestone (0.7 and 3 μm) show a different trend, with the inclusion of limestone reducing the critical pore diameter as compared to OPC or binary fly ash. This is likely resultant from the enhanced reactivity of limestone, combined with the increased fines present in the sample and stabilization of ettringite leading to a more refined pore structure.

For metakaolin replacement pastes (Figure 5-5(b)), the addition of metakaolin is shown to result in no significant change as compared to the OPC paste at the tested age which is generally consistent with (Moisés Frías and Cabrera 2000), while the addition of metakaolin to limestone blends can be seen to result in a slight reduction in porosity as compared to the binary limestone sample. This is a noted difference from the fly ash sample, where there was no apparent synergistic benefit except in the case of the finest limestone used. This is attributed to the enhanced pozzolanic activity of metakaolin at earlier ages as compared to fly ash (M. Frías, de Rojas, and Cabrera 2000) resulting in increased hydration product formation, reducing the porosity of the sample. With respect to critical pore diameter (lower panel of Figure 5-5(b)), the inclusion of metakaolin results in a significant decrease as compared to both the OPC and binary limestone samples for all sizes tested. Statistical analysis of this data indicated that metakaolin was the only significant factor. Metakaolin results in a significant refinement of the pore structure of the sample, particularly at later ages (Moisés Frías and Cabrera 2000).

The presence of mono/hemi-carbonate in ternary blends of limestone and metakaolin, as noted in Chapter 4, indicates the presence of stabilized ettringite as the formation of monocarbonate is favored preventing or delaying the transformation of ettringite to monosulfate (De Weerdt, Haha, et al. 2011; Matschei, Lothenbach, and Glasser 2007a; Kakali et al. 2000). The presence of less dense ettringite would be expected to indicate a

refined pore structure and decrease in porosity, with a decreased critical pore diameter and porosity due to the increased volume of reaction products, however no such decrease is noted in the critical pore diameter data in Figure 5-5(b) and only a slight decrease is indicated in the overall porosity. This may be due to the less dense ettringite causing microcracking in the sample, thus the increased volume of hydration products is balanced by increased microcracking in the sample. It is further noted that statistical analysis of the critical pore diameter data indicates metakaolin is a very significant influence and both the inclusion of limestone and the limestone metakaolin interaction terms are not significant.

To explore these influences further, the volume fraction of mercury retained has been determined for the ternary blends. The retained volume fraction of mercury is related to the tortuosity of the pore structure, where a more tortuous structure makes full evacuation of the pore structure more difficult resulting in an increased fraction of retained mercury. The results of this analysis are shown in Figure 5-6. For the fly ash based suspensions (Figure 5-6(a)), several trends are immediately evident. The binary mix of fly ash shows the lowest volume fraction retained for all mixtures. The binary mixes of limestone show differing trends, with the finest limestone showing an increase in retained volume fraction, while the two coarser limestones show a reduction. The inclusion of both fly ash particles and coarse limestone, in combination with their limited participation in cement hydration at this age, gives rise to a less refined, less tortuous pore structure. In contrast, fine limestone more effectively acts as a nucleation site for hydration products as well as more effectively disperses in the microstructure, resulting a more tortuous pore structure and a higher retained volume fraction of mercury. Ternary blends of limestone and fly ash all show increased retained volume as compared to the binary fly ash mixtures, with the 0.7

μm paste with fly ash showing the highest overall retained volume fraction. Statistical analysis of these results indicate that both fly ash and the fly ash-limestone interaction effects are significant for all the pastes investigated, with the limestone effect indicating statistical significance only for the 0.7 μm limestone. As with critical pore diameter, this indicates a synergistic benefit of replacement of cement by both limestone and fly ash on the pore structure of these hardened pastes. Though fly ash has limited reactivity in the first 28 days, a previous study has indicated that the combined replacement of OPC by fly ash and fine limestone beneficially effects the development of hydration products as compared to limestone or fly ash alone as a replacement material, this enhanced hydration product formation refines the pores, limits pore connectivity, resulting in increased retained volume.

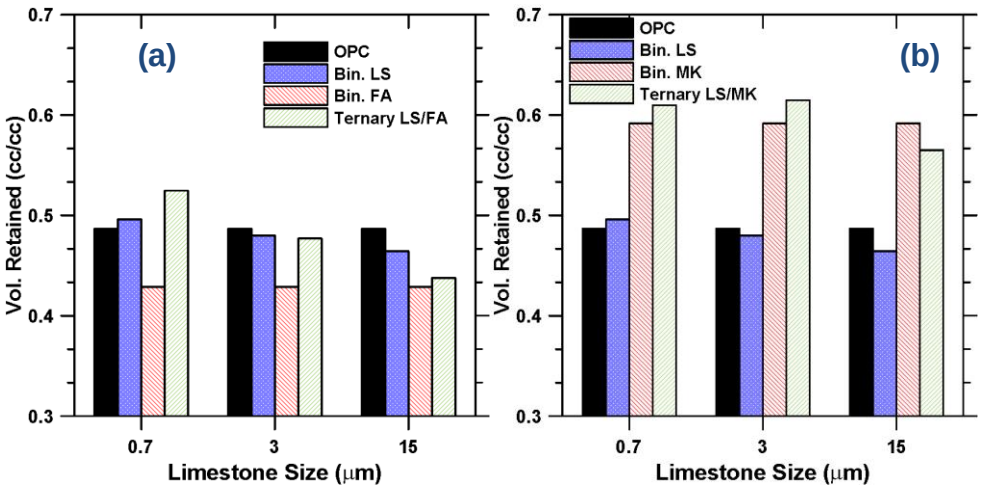

Figure 5-6: Retained mercury volume fraction after extrusion for (a) fly ash, and (b) metakaolin.

The retained volume fraction for metakaolin mixes shows a similar synergistic benefit in the inclusion of metakaolin with fine limestone as indicated by the higher volume fractions retained for the ternary blends of metakaolin and fine limestone. Further, these mixes show a significantly more dominant influence of metakaolin as compared to fly ash. The

inclusion of metakaolin results in a significant increase in volume fraction retained. As discussed previously, metakaolin has significantly higher pozzolanic activity at early ages as compared to fly ash, due in part to the higher surface area and alumina content (M. Frías, de Rojas, and Cabrera 2000; Ambroise, Maximilien, and Pera 1994). This increased reactivity results in a more tortuous structure, with hydration products blocking connected paths.

5.3.3 Influences of limestone dosage on pore structure of cement pastes with metakaolin or fly ash

A mercury intrusion porosimetric investigation was completed using 3 µm limestone at an additional cement replacement level of 20% by volume with a fly ash or metakaolin replacement ratio of 10% by volume. The results of this investigation showing the influence of limestone dosage on mercury porosity, critical pore diameter, and volume fraction retained are presented in Figure 5-7. It is first noted from these figures that the trends for metakaolin or fly ash are nearly identical, although offset vertically. This supports the concept that limestone is not significantly participating in the hydration reactions, except primarily to dilute the portland cement content in the mixture, raising the water-to-cement ratio. The porosity results indicate a behavior that would be expected given the previous discussions on the influence of limestone dosage in binary limestone systems. As the limestone dosage is increased, the effective water-to-cement ratio is increased resulting in an increase in porosity. There does not appear to be a synergistic benefit of limestone inclusion with additional alumina sources on the porosity of these systems. The critical pore diameter (Figure 5-7(b)) shows a continued trend from what is depicted above, continued replacement by limestone finer than OPC results in a continued

decrease in the critical pore diameter. Further, as discussed previously, critical pore diameter is shown to be more dependent on solid loading and specific surface area, whereas porosity is more strongly dependent on effective water-to-cement ratio. Thus, inclusion of limestone finer than portland cement refines the pore structure by increasing the surface area, while also acting as a nucleation site for hydration products. The retained volume of mercury after extrusion indicates an initial increase followed by a subsequent decrease as limestone content is increased. As limestone volume is initially increased, the pore structure of the system is refined due to the increased surface area and fine limestone acting to block the connected path of the pore structure, thereby increasing the retained volume of mercury. However, as limestone volume is further increased, the effective water-to-cement ratio begins to dominate, resulting a higher pore volume in the microstructure and more possible connected paths, reducing the retained volume fraction.

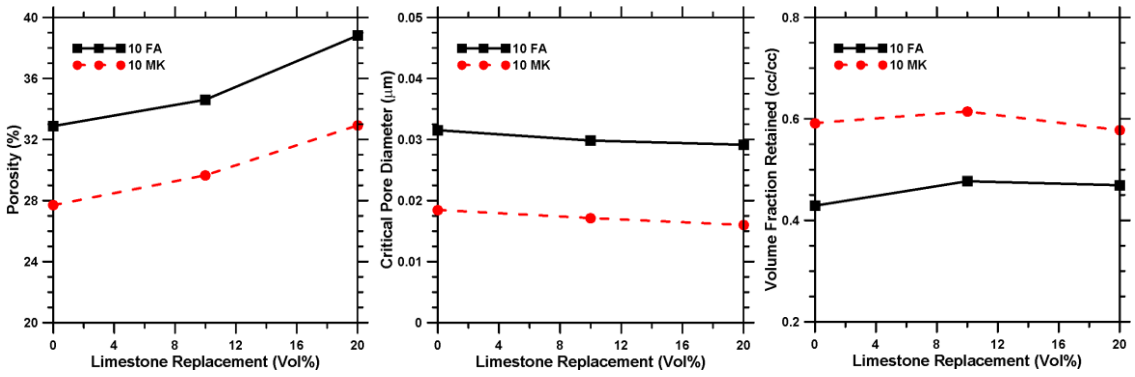

Figure 5-7: Influence of 3 μm limestone replacement ratio in ternary blends with fly ash or metakaolin on (a) porosity, (b) critical pore diameter, and (c) volume fraction retained.

5.4 Comparing Interground and Blended Limestone Pore Structure

Mercury intrusion investigations were also performed on interground and blended limestone portland cements to compare the effects of intergrinding and blending. The blended cements were prepared using particle size distribution matched limestone to

precisely match the particle size distributions and limestone replacement ratios of the interground samples. More information in this size matching procedure can be found in Chapter 8.

5.4.1 Interground and Blended Pore Structure

The influence of limestone on the pore structure in these systems was determined using mercury intrusion porosimetry and the methodology presented in Section 5-2. The resultant intrusion curves at 3 and 28 days are presented in Figure 5-8. As previously noted, pore size distribution curves determined using mercury intrusion porosimetry have been shown to be prone to error due to the assumptions required in the Washburn equation, thus these figures are presented primarily for reference. However, it is generally noted that the pore structure development is generally as would be expected. At the later age investigated, the pore volume intruded decreases, and the pore structure becomes more refined. This is due to the progression of the hydration reaction, as more hydration products are incorporated into the paste and the degree of hydration increases, the pore volume decreases and the pore structure becomes more refined. Further, from Figure 5-8(a), it is noted that OPC has a lower intruded volume than the size matched limestone replacement cement at both ages tested. This is likely due to the decrease in volume of material which participates in the hydration reactions as well as an increase in effective water-to-cement ratio. The increase in the effective water-to-cement ratio would lead increase the pore solution as well as decrease the relative quantity of hydration products, resulting in an increase in porosity. From Figures 5-8(b) and (c) it is noted that the blended limestone sample has a higher intruded volume at all ages and diameters than the interground limestone. It was previously noted that limestone is a softer material than portland cement

clinker (R. Kumar and Bhattacharjee 2003), thus as limestone is interground with cement the limestone will achieve a finer particle size distribution than the clinker. Thus, though the replacement volume is the same for both interground and blended limestone cements, the finer limestone present in the interground PLCs accelerate the hydration reaction more effectively as noted in Chapter 4, resulting in an increase in the particle packing in the system, leading to a decrease in porosity as compared to the blended system where the limestone particle size distribution matches that of portland cement.

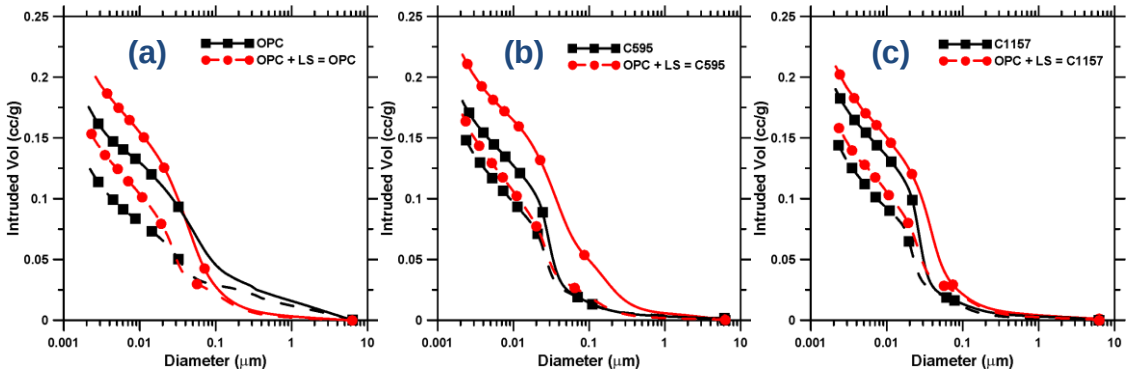

Figure 5-8: Intrusion curves comparing interground to blended PLCs, solid lines are 3 day, dashed are 28 day for: (a) OPC, (b) C595, and (c) C1157

To explore the influences of limestone on the pore structure of these systems, the porosity and critical pore diameters were determined as presented in Section 2.2.4. The results of this analysis are presented in Figure 5-9. Several key aspects of these samples are noted from the upper panel of this figure: (i) the OPC mixture has a lower porosity than all other mixtures at all ages, (ii) the interground mixes have lower porosities than their blended counterpart at all ages, and (iii) all mixes show approximately equivalent reduction in porosity between 3 and 28 days of about 25%. The overall lower porosity for OPC compared to any of the PLC mixtures is attributed to the effects described above, the

limestone filler raises the effective water-to-cement ratio resulting in a greater porosity within the cement paste. The lower porosity for interground samples as compared to blends is similarly attributed to the same effects as above. The interground samples are noted to have higher bound water contents than the size matched blended samples, indicating an increase in reaction product formation, which would decrease the porosity of the sample.

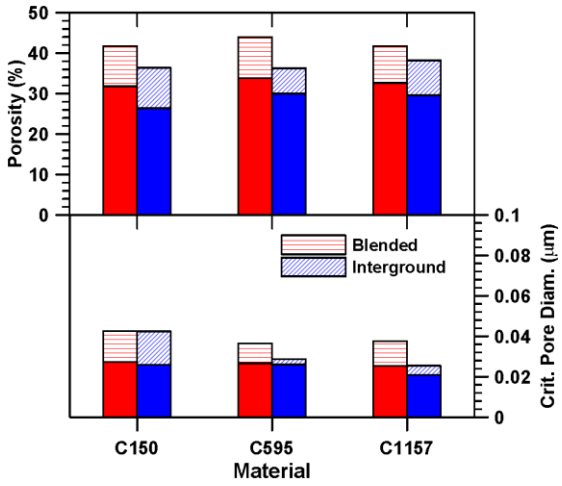

Figure 5-9: Comparison of porosity and critical pore diameter for PLCS investigated, patterned fill is at 3 days, solid is at 28 days.

From the lower panel in Figure 10, it is noted that the critical pore width is highest for the OPC and size matched limestone OPC blend samples at all ages, and lowest for the finer interground sample (C1157). It can also be seen from the lower panel in Figure 5-9 that the inclusion of size matched limestone has little influence on the critical pore diameter in the OPC system at early ages and results in only a slight increase at later ages. Further it is noted that the interground samples have a significantly lower critical pore diameter as compared to the blended samples at early ages, however at later ages the difference is seen to be much less significant. As noted previously, the critical pore diameter, is the diameter at which the intrusion rate of mercury into the sample is the highest, represented the threshold diameter when mercury percolates through the sample. Thus, it is thought to be

representative of the permeability of the sample, where a lower critical pore diameter would indicate a lower permeability, a factor that is critical to the durability of concrete due to ion permeability and the resultant corrosion. The lower critical pore diameter in interground samples as compared to their blended counterpart is likely due to the relative fineness of the limestone in the sample. The increased fineness in interground samples accelerates hydration and more effectively acts as a nucleation site for hydration products (Thomas, Jennings, and Chen 2009). These two factors result in a more refined pore structure, particularly at early ages, resulting in a decrease in the critical pore diameter. At later ages, the effect of limestone fineness is diminished as hydration proceeds, and the critical pore diameter becomes equivalent for all samples except the interground C1157 sample. This discrepancy is likely due to the difference in fineness between the size matched blended sample and interground sample, where the interground sample is noted to have an increased fineness as compared to the blended sample. This increased fineness results in a comparatively more reactive sample, resulting in a more refined pore structure at both early and later ages.

Studies have noted a strong relationship between the strength and porosity of cementitious samples, a similar relationship is noted in this study and is presented in Figure 5-10. A reduction in porosity is seen to result in a corresponding increase in strength. The increased scatter noted in this figure as opposed to that typically presented in strength-porosity relationships is likely due to the inclusion of soft limestone in the sample, a majority of which remains unreacted in the sample even at later ages as noted in Chapter 4. Further, it is noted that the sample with the lowest porosity, OPC, has lower strength than the interground blends at both early at later ages, despite the fact that they have a higher

porosity. This effect is likely due to the interground blends having a greater pore volume, but a pore structure that is more refined due to the inclusion of a limestone that is finer than OPC as discussed above, enhancing hydration product nucleation and accelerating the hydration reactions, refining the pore structure while the effective water-to-powder ratio concurrently increases porosity.

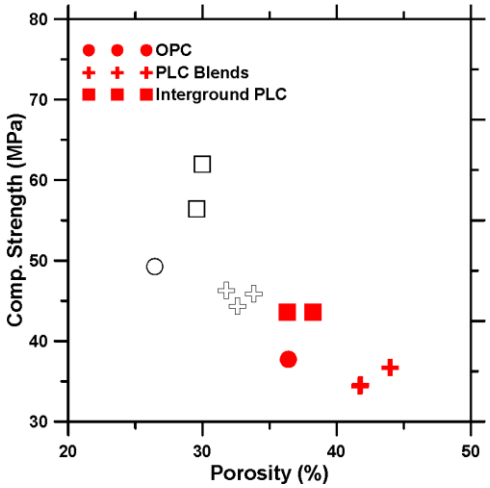

Figure 5-10: Strength versus porosity relationships at 3 days (solid fill) and 28 days (no fill).

To further explore the pore structure of these samples, the modified extruded pore size distribution and the volume of mercury retained after extrusion were determined as presented in Section 2.2.4. The results of these determinations are presented in Figures 5-11 and 5-12 respectively. From Figure 5-11, it is immediately evident that that samples with limestone included have a more significant volume extruded than OPC samples, as indicated by the difference between the volume remaining at the lowest diameter and volume remaining at the highest diameter, and the generally more flat shape of the OPC extrusion curve. Further, the blended mixes show higher total extruded volumes of mercury, as compared to the interground samples. The extruded quantity of mercury, has been shown to indicate the tortuosity and pore refinement of a sample (Salmas and

Androutsopoulos 2001), due to the fact that it is more difficult for mercury to be extruded from a more refined and tortuous structure, and thus a higher volume of mercury is retained in the sample. This indicates that interground limestone mixes likely have a more tortuous, refined pore structure then blended mixes, likely attributed to the increased presence of fine limestone as a result of intergrinding. Increased volume of fine limestone would accelerate early age hydration (D. Bentz et al. 2009a) and Chapter 4, and allow for increased microstructural packing. These results compare favorably with the intruded pore size distribution as presented in Figure 5-8, supporting the discussion above. The retained mercury volume fractions (upper panel in Figure 5-12(b)) further support these discussion, with interground mixes showing a higher volume retained than their blended counterpart. It is noted that the retained volume fraction is likely a better representation, as the total retained volume presented in the lower panel of Figure 5-12(b), indicates a reverse in trends, particularly at early ages. This effect is primarily attributed to the significantly higher volume of mercury intruded in the blended sample as compared to the interground sample, allowing for a larger overall quantity of mercury to be retained.

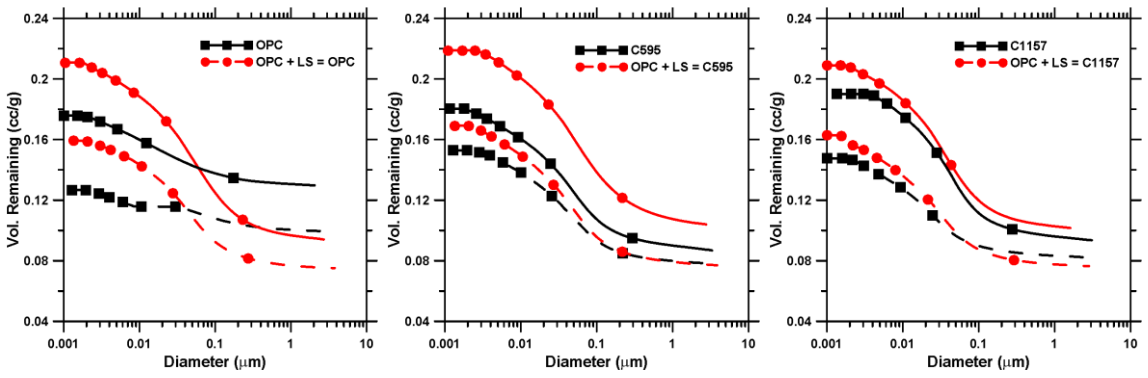

Figure 5-11 – Modified extrusion curves comparing interground and blended samples at 3 (solid line) and 28 (dashed line) days.

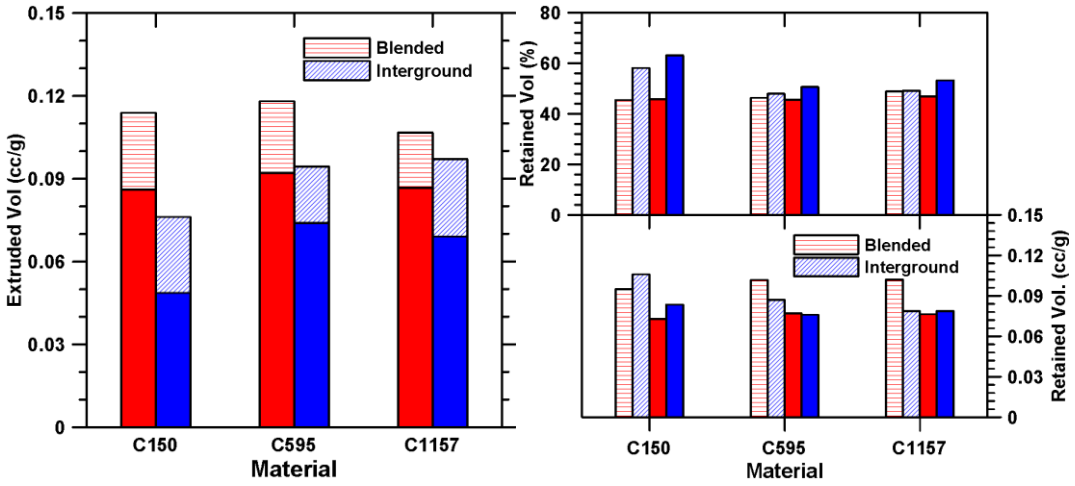

Figure 5-12: Comparison of interground and blended limestone cements, (a) volume extruded, and (b) volume and percent volume of intruded mercury retained; at 3 days (dashed fill) and 28 days (solid fill).

5.5 Conclusions

This paper reports on the effects of limestone and combinations of limestone and fly ash or metakaolin replacement on the pore structure of hardened cement pastes as determined by mercury intrusion investigations. The influence of limestone fineness in these systems is explored, in the context of porosity, critical pore diameter, and volume fraction of intruded mercury retained after the extrusion cycle is completed.

The replacement of portland cement by limestone indicates an increase in porosity regardless of limestone fineness. This effect is attributed to the increase in effective water-to-cement ratio resultant from limestone replacement in these mixtures.

With respect to other pore structure parameters, the critical pore diameter and the volume fraction retained, fine limestone is shown to have a beneficial influence on the pore structure of these systems, decreasing the critical pore diameter and increasing the volume retained. These factors indicate a more refined tortuous structure in these systems,

attributed to fine limestone particles acting as nucleation sites for hydration products and more effectively blocking connected paths through the structure.

Ternary blends of fly ash and limestone show increasing porosity with fly ash replacement or coarse limestone replacement. A synergistic interaction effect between fine limestone and fly ash is noted, resulting in a decrease in porosity and critical pore diameter and increase in volume retained as compared to binary fly ash-cement systems.

Ternary blends of fly ash and metakaolin indicate a strong influence of metakaolin, with the inclusion of metakaolin significantly decreasing the porosity and critical pore diameter while increasing the volume retained. A beneficial interaction effect is additionally noted for ternary blends of fine limestone and metakaolin on the pore structure of the pastes studied.

PART II – RHEOLOGY

6. THE RHEOLOGICAL PROPERTIES OF TERNARY BINDERS CONTAINING LIMESTONE AND METAKAOLIN OR FLY ASH

6.1 Introduction

Several studies have shown the beneficial effects of limestone additions on both the fresh and hardened properties of cementing systems (De Weerdt, Kjellsen, et al. 2011; Tennis, Thomas, and Weiss 2011; Hawkins, Tennis, and Detwiler 2003; D. Bentz et al. 2009b). The positive effects on the hardened properties are attributed to a combination of enhancing hydration through the filler effect, improved particle packing and the formation of carboaluminate phases (Lothenbach et al. 2008; Oey et al. 2012). However, limestone powders, based on their particle characteristics and interactions with other solids in the binder, can influence the fresh (rheological) properties of the paste fraction. Recent studies have demonstrated strategies to formulate ternary blends containing limestone and an aluminous cement replacement material such as metakaolin or fly ash without inducing any reductions in the mechanical properties of these mixtures, as compared to pure OPC formulations (De Weerdt, Haha, et al. 2011; De Weerdt et al. 2010). Thus, this work builds on prior efforts to determine if the benefits realized in hardened properties, may also be applicable to the fresh properties of these mixtures.

Several studies have evaluated the rheological properties of cementitious mixtures containing a variety of cement replacement materials (Park, Noh, and Park 2005; Ferraris, Obla, and Hill 2001; D. P. Bentz et al. 2012; D. P Bentz and Ferraris 2010; Hedda Vikan and Justnes 2007). The rheological parameters (yield stress and plastic viscosity, based on a Bingham or Herschel-Buckley representation) have been noted to be strongly dependent on the water-to-powder mass ratio, type/dosage of cement replacement materials used, and

the particle size distributions of the solids (Park, Noh, and Park 2005; Ferraris, Obla, and Hill 2001; D. P Bentz and Ferraris 2010; Hedda Vikan and Justnes 2007; D. P. Bentz et al. 2012).

This paper investigates the rheological properties of ternary blends containing limestone and metakaolin or fly ash, with special emphasis on quantifying the influence of:

Limestone particle size and dosage, and

Fly ash or metakaolin additions for pastes proportioned at a fixed water-to-solids ratio (by volume).

Experimental assessments of rheological properties are integrated with computational packing studies to elucidate the influences of particle number density and water film thickness. Overall, the results provide a clear understanding of the effects of limestone replacement in combination with fly ash or metakaolin on the fresh properties, thus enabling new strategies to proportion binder formulations which show comparable or superior properties to traditional OPC formulations as indicated in Chapter 4.

6.2 Experimental Program

6.2.1 Materials and Mixtures

The materials used include: a commercially available Type I/II ordinary portland cement (OPC) conforming to ASTM C150 ("ASTM C109 / C109M - 12 Standard Test Method for Compressive Strength of Hydraulic Cement Mortars (Using 2-In. or [50-Mm] Cube Specimens)" 2012), a Class F fly ash and metakaolin conforming to ASTM C618 ("ASTM C109-13. Standard Test Method for Compressive Strength of Hydraulic Cement Mortars Using 2-In. Cube Specimens" 2013), and a nominally pure limestone powder (purity >

95% $CaCO_3$, by mass) of three different median particle sizes denoted as 0.7 µm, 3 µm, and 15 µm, conforming to ASTM C568 ("ASTM C568 / C568M - 10. Standard Specification for Limestone Dimension Stone" 2012). Figure 6-1 shows the particle size distributions (PSD) of the limestone, metakaolin and fly ash, as measured using laser diffraction, along with their median particle sizes.

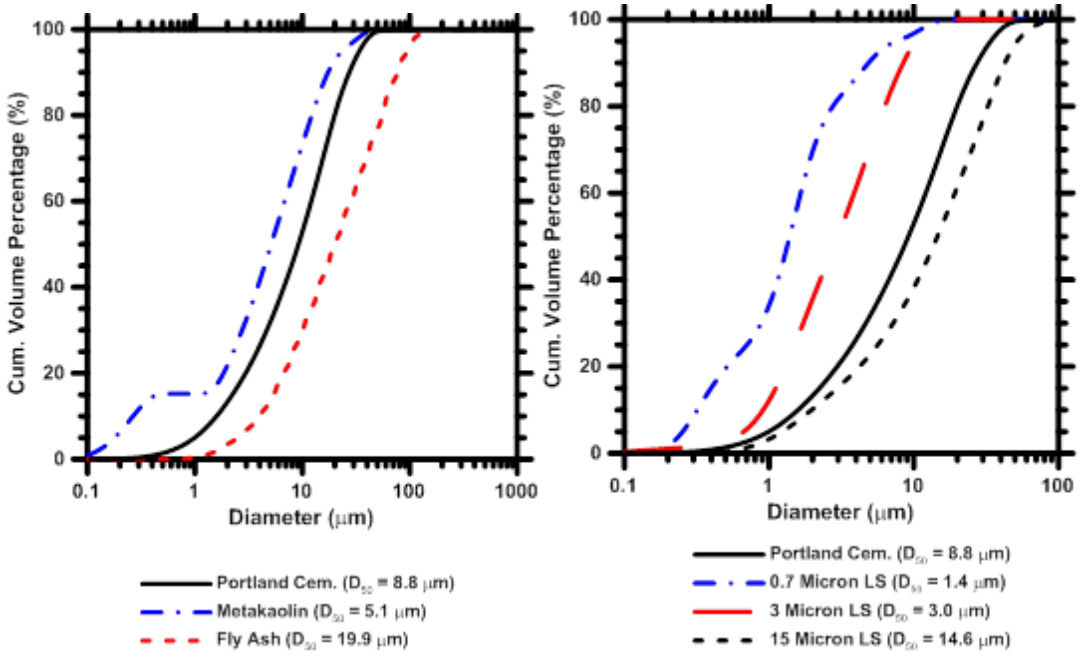

Figure 6-1: The particle size distributions (PSDs) of: (a) the OPC and limestone powders, and (b) the OPC, fly ash, and metakaolin powders.

The compositions of the portland cement and the cement replacement materials are presented in Table 6-1. Binary blends were prepared wherein: OPC was replaced by limestone of different particle sizes at levels ranging from 0-40%, by fly ash from 0-10% and by metakaolin from 0-10%; all by volume. Ternary blends containing limestone powder and fly ash or metakaolin were also prepared. Table 6-2 shows the proportions of the different mixtures evaluated. All pastes were proportioned at a fixed volumetric water-to-solids ratio, $(w/s)_v$ = 1.26 and/or 1.42, corresponding to a mass based water-to-solids

ratio $(w/s)_m$ = 0.40 and/or 0.45 so that the influences of the OPC replacement materials and their particle size distributions on the rheological properties could be consistently compared.

Table 6-1: Composition and specific surface areas (m^2/kg) of the materials used in this study as determined using XRF and the Blaine's air permeability apparatus per ASTM C205-11

Phase (%)	OPC	Class F Fly Ash	Metakaolin
SiO_2	21.06	58.4	51.7
Al_2O_3	3.86	23.8	43.2
Fe_2O_3	3.55	4.19	0.5
CaO	63.75	7.32	--
MgO	1.83	1.11	--
SO_3	2.93	0.44	--
Na_2O	0.12	1.43	--
K_2O	0.48	1.02	--
LOI	1.99	0.5	0.16
SSA (m^2/kg)	470	218	3255

Limestone powder contains 95-97% $CaCO_3$ as per the manufacturer. The Blaine specific surface areas are 4970 m^2/kg, 2400 m^2/kg, and 613 m^2/kg for the limestone powders having median particle sizes of 0.7 μm, 3 μm, and 15 μm respectively.

Table 6-2: The proportions of the paste mixtures evaluated in this study

		Replacement level (Vol. %)		
Mix Type	Volumetric Water-to-solids ratio $(w/s)_v$	Limestone (0.7, 3, and 15 μm)	MK	Fly Ash
OPC	1.26, 1.42	0	0	0
OPC + LS	1.26	0, 5, 10, 20, 30, 40	0	0
OPC + FA	1.42	0	0	5, 10, 20
OPC + MK	1.42	0	5, 10	0
OPC + LS + FA	1.26	10, 20	0	5, 10
OPC + LS + MK	1.42	10, 20	5, 10	0

6.2.2 Rheological Experiments

All powders were dry blended prior to wet mixing. Mixing was performed in accordance with ASTM C1738 ("ASTM C1738 - 11a. Standard Practice for High-Shear Mixing of Hydraulic Cement Paste" 2011) using a high shear mixer. The mixing sequence used was as follows: (i) the mixer was run at 4000 rpm for approximately 30 seconds while the blended powders and water are added, (ii) the mixer was run at 12000 rpm for 30 seconds, (iii) the mixing container was scraped and the paste allowed to rest, while covered for 2 minutes, (iv) the contents were mixed at 12000 rpm again for 90 seconds, and (v) a final round of hand mixing was carried out to verify the homogeneity of the paste Around 5 mL of paste was then discharged on to the rheometer using a disposable syringe. The time elapsed from water addition to the beginning of the rheological assessment was approximately 5 minutes.

The fresh properties of fresh pastes were evaluated using a rotational rheometer (TA Instruments AR2000 EX) in a parallel plate configuration, provided with Peltier elements

located within the bottom plate which were conditioned to 25 ± 0.5°C. To reduce slip on the plates, a serrated upper plate was used while the Peltier plate was covered with 150 grit adhesive backed, resin coated sandpaper (mean surface roughness of 16.89 μm). The upper plate used had a diameter of 50 mm, and the gap was set to 2 mm based on a series of trial mixtures that achieved consistent results over the range of fluidities considered (Ferraris 1999a). The rheological procedure consisted of a ramp up pre-shear phase from 5-to-100/s lasting around 90 seconds to homogenize the paste, followed by a ramp up from 5-to-100/s, followed immediately by a ramp down from 100-to-5/s. A step up, or step down shear rate of 10/s was implemented, as shown in Figure 6-2(a). Shear stress and shear rate data were extracted using TA Instruments' TRIOS software package. With the exception of the pre-shear range, at each step, data is acquired every second, until a steady state is achieved – as defined by three consecutive torque measurements within 5% of each other, at which time the experiment advances to the next shear rate. The time at each shear step is typically 5 seconds.

A non-Newtonian relationship between the shear stress and shear rate as shown in Figure 6-2(b) was used to interpret the measurements. As such, the shear stress-shear rate datasets for the descending (down ramp) curve were fitted using a least squares function corresponding to the Bingham model as shown in Equation 6-1 (Bingham 1922). The Bingham model is commonly used for the rheological characterization of cement pastes (D. P. Bentz et al. 2012; Ferraris, Obla, and Hill 2001; Banfill and others 2003; Ferraris 1999a; Park, Noh, and Park 2005) and a good linear fit (R^2 values > 0.95) between the shear stress and shear rate is obtained for the shear rate range between 10 and 100/s.

$$\tau = \tau_y + \mu_p \dot{\gamma} \qquad (6\text{-}1)$$

where τ is the shear stress, τ_y is the yield stress, μ_p is the plastic viscosity and $\dot{\gamma}$ is the shear rate. Based on the Bingham model, the yield stress is defined as the limiting shear stress at which the material begins to flow (the Y-intercept of the fit line in Figure 6-2(b) while the plastic viscosity denotes the resistance of the fluid to continued flow (Banfill and others 2003). All the pastes showed an essentially linear proportionality between the shear stress and shear rate for the range of shear rates selected, with a kink point (bi-linearity) being observed as very low shear rates are approached. Replicate measurements on at least three separately mixed pastes were carried out for each mixture, and coefficients of variation in the range of 7% for yield stress and 10% for plastic viscosity were quantified across all samples.

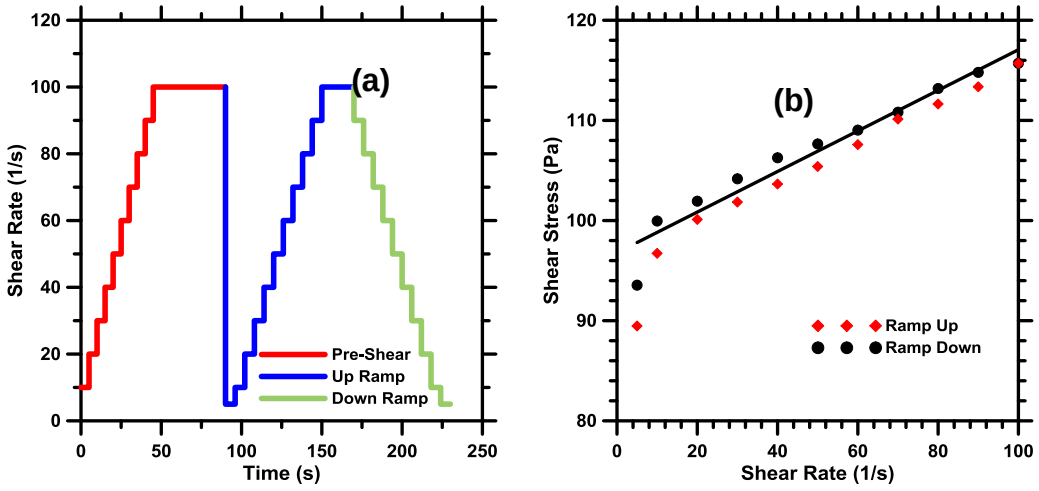

Figure 6-2: A schematic representation of the rheological procedure, and (b) a typical shear rate-shear stress relationship showing the ascending and descending curves. The linear fit of the data in the descending curve is used to extract the yield stress and plastic viscosity

6.2.3 Determination of Particle Number Density and Apparent Water Film Thickness

To correlate the rheological properties of the pastes to the water film thickness and the particle number density in a suspension, a series of calculations were carried out. First, to determine the particle number density and apparent water film thickness, a recursive, stochastic packing algorithm was implemented with periodic boundary conditions (Torquato 2001). The algorithm uses the measured particle size distributions and volume fractions of phases as inputs (cement, limestone, water, etc.), to pack spherical particles in a 3D-REV (representative element volume). The packing algorithm packs the REV while placing solid particles at random locations within the microstructure in relevance to two criteria: (i) size (largest to smallest), and the number of particles, determined from the particle size distributions, within the constraint that particles cannot be in contact, and (ii) satisfying the volume fractions of phases, as described by the input mixture proportions[1]. The particle numbers of all the blends studied were determined from the microstructural generations by counting the number of particles placed in the REV until the mixture-specific packing criteria are satisfied. The particle number density is then defined as the ratio of the number of particles packed to the volume of the unit cell that contains them. Three different REV sizes (200 μm, 400 μm, and 1000 μm cube) were used for the simulations, and the resultant particle number densities were only minimally influenced (within 5% of each other) by the chosen REV sizes. Hence the results in the remainder of

[1] The packing algorithm does not consider any agglomeration or dispersion effects, which would manifest in real systems. Thus the packing generations are illustrative and only for comparative purposes and is not a perfect recreation of reality.

the paper correspond to a REV of 400 x 400 x 400 μm^3. Figure 6-3(a) depicts a typical REV, and Figure 6-3(b) shows a representative 2-D slice from the REV.

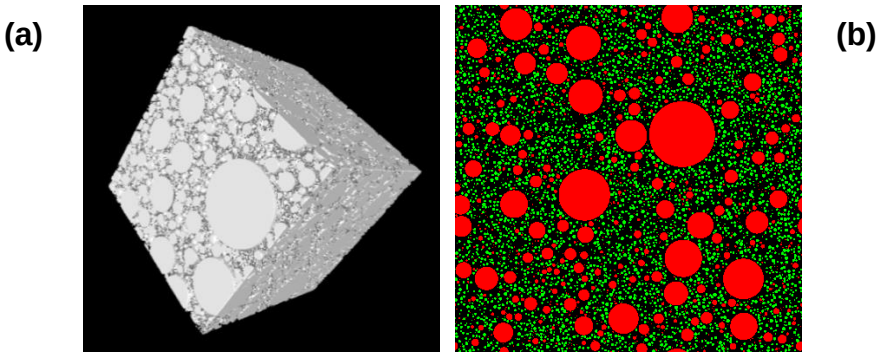

Figure 6-3: A simulated 3D microstructure generated using the packing algorithm and (b) a 2D slice captured from the 3D-REV.

Once the sought packing is achieved, solid-to-solid centroidal distances (center-to-center distance, since the particles are all spherical) in the desired REV are calculated as follows: (a) 100 particles are randomly selected in the microstructure, (b) for any particle p_i, the distance from its center to the centers of other particles that are located within a distance of 5 µm away from the surface of pi is calculated, and (c) the mean center-to-center distance is calculated by averaging the distances calculated as described in (b) for all 100 particles (Dale P. Bentz and Martys 1994). It should be noted that the selection of 100 random particles was made, as beyond this point the calculated centroidal distances between particles changed slightly, even if the number of analyzed particles was increased substantially (A. Kumar et al.). Figure 6-4 shows the centroidal distances between particles in the microstructure as a function of the limestone dosage for binary/ternary mixtures. The centroidal distance remains approximately invariant of the limestone content when cement is partially replaced by coarse limestone powder either in isolation or with fly ash/metakaolin, and drops significantly when a small amount of fine limestone powder

replaces cement. Upon further increases in the fine limestone content, the centroidal distance does not change appreciably. It should be noted that the centroidal distance is a measure of the interparticle spacing that dictates the yield stress and plastic viscosity of these pastes as discussed later.

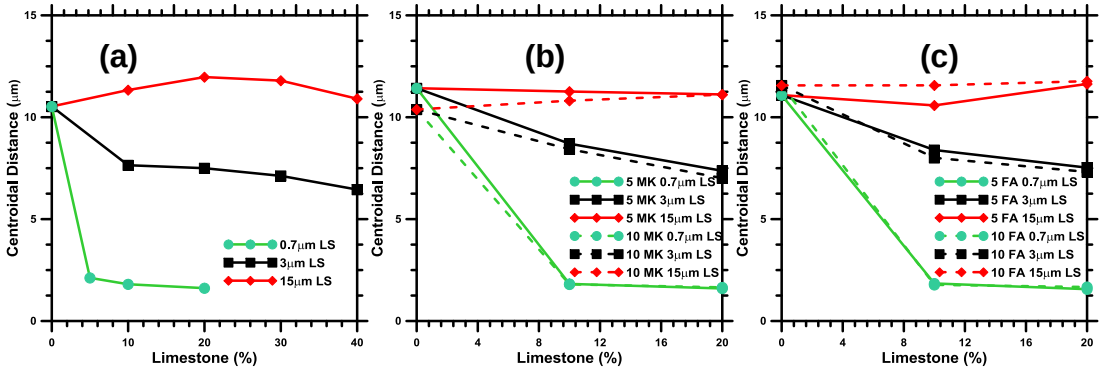

Figure 6-4: Centroidal distances as determined for: (a) binary blends containing limestone; (b) ternary blends containing limestone and metakaolin; and (c) ternary blends containing limestone and fly ash. The REV size is 400 x 400 x 400 μm^3

To determine the water film thickness, the "excess water" (w_{excess}) in the paste is quantified as:

$$w_{excess} = (w/s)_v - e_{solid} \tag{6-2}$$

where e_{solid} is the void ratio of the solid particles. The void ratio can be defined as:

$$e_{solid} = \frac{(1-\gamma)}{\gamma} \tag{6-3}$$

where γ is the maximum packing density of solid particles in the mixture, as obtained from the microstructural packing algorithm. The water film thickness (t_{film}) is obtained from (Fung and Kwan 2010):

$$t_{film} = \frac{w_{excess}}{SSA} \tag{6-4}$$

The specific surface area (SSA), i.e., the surface area of the solid particles divided by the total solid volume of each blend was determined using the measured particle size distributions for each constituent, in conjunction with a volumetric rule of mixtures (Dale P. Bentz 2007). The particles are assumed to be spherical. A comparison of the specific surface areas determined using Blaine's air permeability method and from the particle size distributions for a few selected powders showed a strong correlation, similar to (Garboczi and Bullard 2004). The calculation relevant to the maximum packing density of the solids (γ in Equation 6-3), being computationally intensive, was implemented only for a few "bounding" mixtures, and the corresponding water film thickness plotted as a function of $SSA/(w/s)_v$ is shown in Figure 6-5. The best fit relationship between these parameters was used to determine the water film thickness in the intermediate cementing blends.

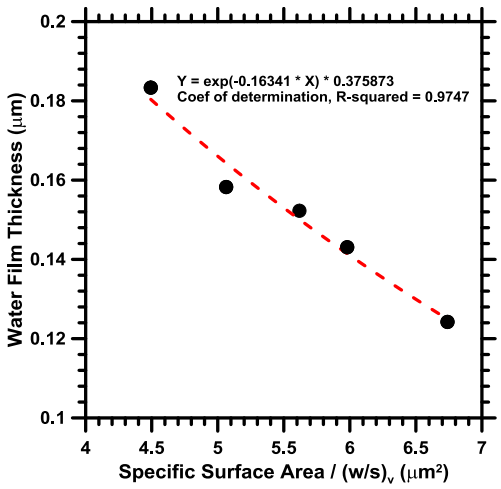

Figure 6-5: The relationship between the water film thickness and the ratio: $SSA/(w/s)_v$

6.3 Results and Discussions

The following section provides insights into the effects of OPC replacement by limestone, fly ash, metakaolin, or their combinations thereof, on the rheological characteristics of fresh paste systems. A Bingham model, shown in Equation (6-1) is used to interpret the

rheological response over the range of shear rates selected (Ferraris 1999a; Banfill and others 2003; Ferraris 1999b). It should be noted that the discussions are considered applicable only for the range of shear rates considered, i.e., between 5-to-100/s, and may be subject to change at other shear rates[2].

6.3.1 Rheological Studies of Limestone Powder Modified Cement Pastes

It is noted that as the median particle size of limestone is increased from 0.7 μm to 15 μm, there is a decrease in both the plastic viscosity and yield stress, as shown in Figure 6-6(a). In the case of 5% OPC replacement (by limestone), the yield stress reduces by around 20% with almost no reduction in the plastic viscosity, while at 20% OPC replacement there is a much larger decrease of almost 50% in both yield stress and plastic viscosity. A further reduction in yield stress is noted when the limestone particle size increases from 0.7-to-3 μm, but further increases in particle size do not produce further yield stress reductions at low levels of OPC replacement. Of course, at higher OPC replacement levels there is a continued decrease in yield stress with increasing particle size.

Except in the case of the 15 μm limestone, OPC replacement by limestone is noted to increase both the plastic viscosity and the yield stress, as observed in Figure 6-6(b). For example, in the case of pastes containing 0.7 μm limestone, the plastic viscosity almost doubles and the yield stress increases by a factor of around 1.5 over the OPC replacement range from 0-20%. On the other hand, for pastes containing 3 μm limestone, the yield stress and plastic viscosity increase by a factor of 3 as the OPC replacement level increases from 0-40%. However, for 15 μm limestone mixtures, both the plastic viscosity and yield stress

[2] It has been discussed that the yield stress could not be viewed as a realistic parameter of flow behavior because it likely vanishes at extremely low shear rates (Barnes 1999).

decrease slightly with increasing OPC replacement levels, when compared to the pure OPC paste. These observations indicate that, in general, particles coarser than the OPC decrease the yield stress and plastic viscosity while the presence of particles finer than the cement, induce an opposite effect.

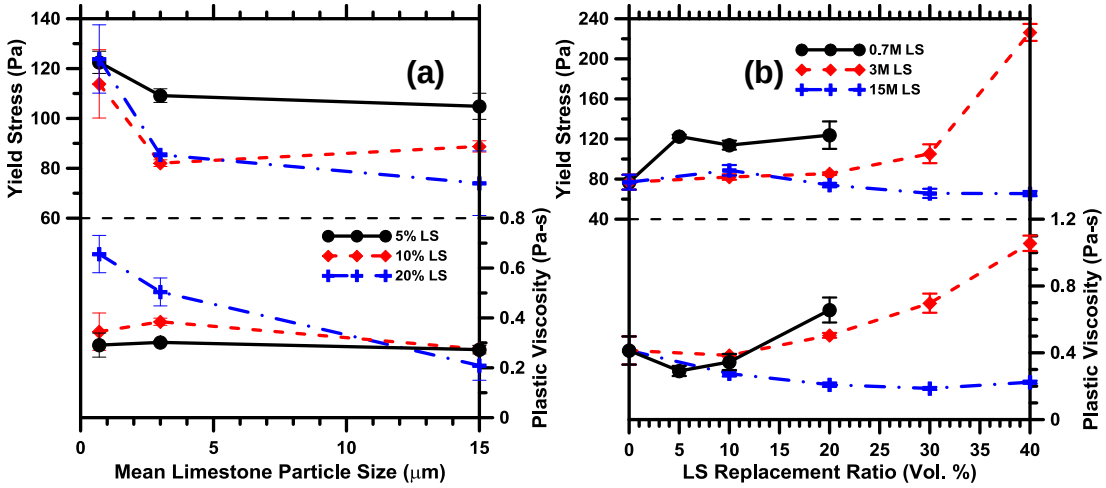

Figure 6-6: The influence of: (a) limestone particle size, and (b) level of replacement of OPC by limestone (volume basis) on the yield stress and plastic viscosity of the paste mixtures.

As such, the results suggest that when coarse limestone particles of approximately the same size as OPC particles are introduced, this results in an increase in particle spacing at a given (fixed) replacement ratio, which reduces the ability of the suspension to resist shear. Further, larger limestone particles exhibit a reduced water demand (Vuk et al. 2001; Hawkins, Tennis, and Detwiler 2003), due to a decrease in the available area on which water films may form (Tennis, Thomas, and Weiss 2011). Finally, the potential for agglomeration also reduces with increasing particle size, reducing the possibility of water remaining trapped within flocs, where it is unavailable to provide fluidity to the cement paste. This combination of effects explains why the yield stress and plastic viscosity depress, on OPC replacement by coarse limestone. On the other hand, in fresh pastes

containing fine limestone powders (0.7 and 3 μm), increasing OPC replacement by limestone produces the opposite effect. The addition of fine limestone powders results in an increased packing density of the paste, which decreases the interparticle spacing (Figure 6-4a) and increases the resistance of the suspension to applied shear. Moreover, in binary pastes containing 0.7 μm limestone, agglomeration and water film formation as expected to be substantial, and would decrease the amount of free water available in the paste (Sakai et al. 2009). This decrease in the free water content depresses fluidity as indicated by elevated plastic viscosities. It should be noted however, even in the case of well dispersed pastes (e.g., those containing a plasticizer), since fine limestone additions do in any event reduce interparticle spacing, mixtures containing such powders as OPC replacement materials are expected to consistently demonstrate higher yield stresses as compared to traditional pastes. However, the case of plastic viscosity in a well-dispersed case is not trivial because of competing effects. As such, while increasing the fine limestone content at a given $(w/s)_v$ will increase the specific surface area, the amount of excess water will also increase (since the void ratio of the solid particles is reduced). The water film thickness, and consequently the plastic viscosity could thus increase or decrease depending on whichever effect is dominant, and is likely a mixture specific effect.

6.3.2 Influence of Fly Ash and Metakaolin on the Rheological Properties of Pastes

The incorporation of aluminous materials such as fly ash or metakaolin has been found to beneficially influence the properties of limestone containing systems (De Weerdt, Haha, et al. 2011; De Weerdt, Kjellsen, et al. 2011; De Weerdt et al. 2010). Thus, before the rheological characteristics of the ternary systems are discussed, it is instructive to summarize the rheology of pastes containing fly ash or metakaolin.

Figure 6-7 presents the yield stress and plastic viscosity as a function of the fly ash or metakaolin content for the pastes evaluated in this study. For the fly ash modified pastes, while the yield stress and plastic viscosity are generally noted to decrease with increasing fly ash content, the opposite trend is noted in the case of metakaolin modified mixtures. These observations are in agreement with effects produced by fly ash and metakaolin on the workability of cementitious mixtures (Nehdi and Rahman 2004a; Moulin, Blanc, and Sorrentino 2001). First, the reduction in yield stress and plastic viscosity that is noted when fly ash replaces a part of the cement can be attributed to the spherical shape of fly ash particles (Kutchko and Kim 2006) and their consequent ability to impart fluidity to the paste . This effect is magnified due to the particle size distribution of the fly ash used, which being slightly coarser than the cement used, elevates the physical separation between neighboring particles, akin to the behavior of the paste with coarse limestone, which reduces the yield stress and plastic viscosity. The aberration in the trend of plastic viscosity at low replacement levels of fly ash is presumed to be a result of better particle packing facilitated by spherical ash particles (that increases the plastic viscosity), thus overcoming the effects of particle spacing and decreased surface friction. However, expected trends in the rheological parameters are restored at higher fly ash replacement levels.

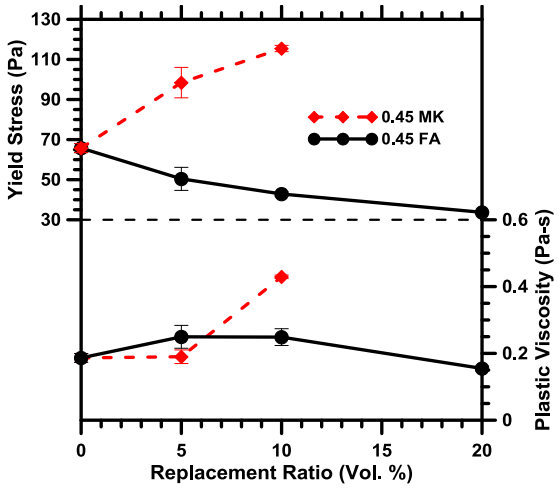

Figure 6-7: The influence of fly ash and metakaolin on the rheological properties of binary pastes

The contrast in the rheological behavior of metakaolin modified pastes when compared with the fly ash modified pastes is evident from Figure 6-7. Increasing the metakaolin content in the paste significantly increased both the yield stress and plastic viscosity. For example: while the plastic viscosity doubles, the yield stress increases 1.75 times as the metakaolin content is increased from 0-to-10%. This observation is attributed to the very high surface area of metakaolin (see shoulder in the PSD curve; Figure 6-1b), and the propensity of metakaolin fines to agglomerate (Sakai et al. 2009; Ambroise, Maximilien, and Pera 1994; Badogiannis et al. 2005). These effects would act to de-water the paste, causing large elevations in the measured yield stress and plastic viscosity.

6.3.3 Rheological Studies of Ternary Blends Containing Limestone

While the previous section quantify rheological evolutions in binary (i.e., cement + limestone, or cement + metakaolin or fly ash) mixtures, the current section expands this scope to include ternary combinations of these materials whose influences on yield stress and plastic viscosity of fresh pastes are unexpected and complex. The results are interpreted in broad conformity to the Bingham model of suspension flow.

6.3.3.1 Combined Effects of Limestone Particle Size and Addition of Fly Ash

Figure 6-8 presents the yield stress and plastic viscosity as a function of the limestone replacement level for pastes containing limestone of different particle sizes and either 5%-or-10% fly ash by volume. The influence of increasing limestone content on yield stress is complex. The yield stress is a function of, amongst other things: particle concentration (the number of particles in a unit volume), the overall solid surface area, and forces developed between particles under applied shear (Funk and Dinger 1994); with resistances generated between cement particles being more significant than those developed between limestone or fly ash particles; a function of particle shape/geometry. As a consequence, at low limestone and fly ash contents, while the particle concentration, packing fraction and surface area increase, the spacing between particles decreases[3]- more so for the smaller limestone particle sizes. While this effect results in negligible changes in yield stress at low replacement levels of limestone (10%) and low fly ash contents (5%), with increasing limestone replacement, the yield stress increases in growing proportion due to a reduction in the limestone particle size and increasing particle number density. It is unsurprising that coarse limestone additions result in yield stress reductions- a consequence of increased particle spacing, and reduced packing and surface areas. However, at higher fly ash contents (10%), the yield stress continuously decreases with an increase in the limestone content. While this reduction is expected for coarse limestone additions, even for fine limestone additions (i.e., 0.7 and 3 μm particles), the yield stress decreases. This latter observation is attributed to the elevated fly ash loading that further separates the solid

[3] The interparticle spacing between cement particles dominantly influences the yield stress as compared to the spacing between any of other particles, while their degree of contact influences the plastic viscosity.

grains and thus more than compensates for the increased particle concentration and specific surface area that is produced on fine particle additions.

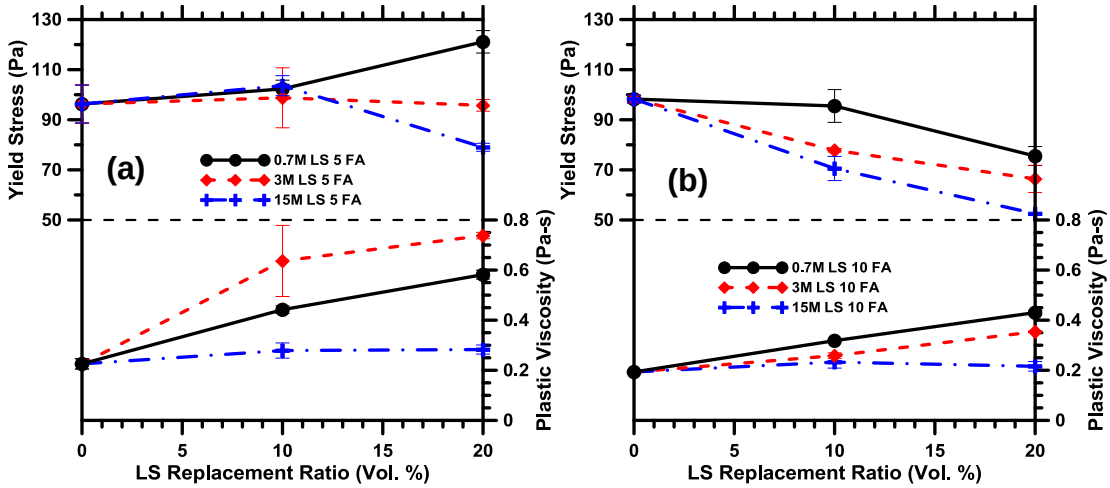

Figure 6-8: Influence of limestone dosage on measured rheological properties in limestone

Next, increasing limestone addition in fly ash blended pastes is noted to increase the plastic viscosity when fine limestone is used, and hold the plastic viscosity relatively unchanged when coarse limestone is used, as observed in the lower panels of Figure 6-8. This is in line with prior observations of plastic viscosity in binary (OPC + limestone) pastes shown in Figure 6-6(b) where coarse limestone additions are shown to render the plastic viscosity of the paste unchanged--- a function of negligible changes in the packing density and interparticle spacing (i.e., centroidal distances, Fig. 6-4a) - a point which is confirmed from the microstructural generations. Obviously then, fine limestone, by increasing the overall packing density and reducing particle spacing, increases the number of interparticle contacts and elevates the plastic viscosity. These effects are noted to be less significant with increasing fly ash contents as the spherical nature of fly ash particles likely compensates against other "viscosity enhancing" effects. For example: it has been rigorously demonstrated that particle shape dramatically influences the plastic viscosity of

suspensions (much more so than yield stress), with a unit volume of spherical particle additions reducing the plastic viscosity of the system by a much greater extent than an equal volume of cuboidal particle additions (Erdoğan et al. 2008).

6.3.3.2 Combined effects of limestone particle size and addition of metakaolin

Figure 6-9 presents the combined influence of metakaolin and limestone of different particle sizes on the yield stress and plastic viscosity of pastes. In general, for a fixed metakaolin content, an increasing limestone content decreases the yield stress and increases the plastic viscosity. Also, while fine limestone additions shows the most significant increase in plastic viscosity, coarse limestone additions shows the most significant decrease in the measured yield stress.

In ternary blends containing metakaolin, the yield stress is noted to decrease with an increase in the limestone content (OPC replacement) as shown in Figure 6-9. Previously, it has been shown that metakaolin additions (in isolation, Figure 6-7) and fine limestone additions (in isolation, Figure 6-6) act to elevate the yield stress, with yield stress reductions being noted only in the case of coarse limestone containing binary pastes. Hence the observation herein, of reducing yield stress with increasing limestone content in metakaolin modified pastes, requires more careful evaluation. While yield stress reductions in the case of coarse limestone additions can be easily explained as a consequence of enhanced particle spacing (as confirmed by the microstructural generations), in the case of fine limestone additions, it is expected that two competing effects operate. First, while fine limestone additions act to increase the packing density and hence yield stress, this action is offset by the second effect, i.e., electrostatic effects produced between the negatively

charged metakaolin and positively charged limestone particles, which enhances the interparticle spacing between the solids and thus reduces the yield stress (Board 1969).

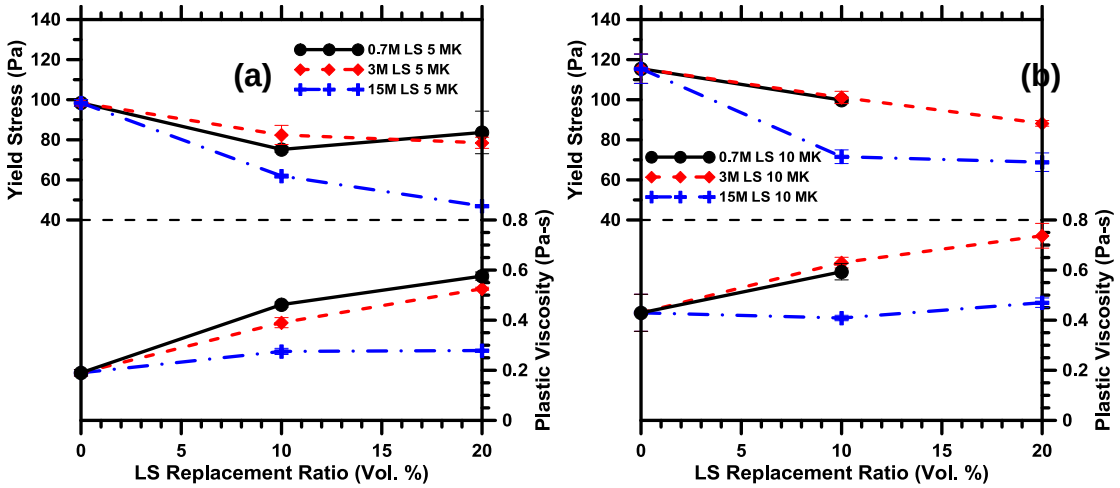

Figure 6-9: Influence of limestone dosage on the measured rheological properties of metakaolin blended pastes for: (a) 5% metakaolin, (b) 10% metakaolin.

The evolution of the plastic viscosity follows the same trends noted in the case of ternary blends containing fly ash. The coarse limestone pastes with metakaolin demonstrate plastic viscosities that are essentially invariant with the limestone dosage. Here, the drop in plastic viscosity noted in the case of binary pastes containing coarse limestone (Figure 6-6b) is compensated for by an increase in particle contacts caused by fine metakaolin additions, and substantial agglomeration of metakaolin fines - which acts to elevate the water demand and reduce fluidity. However, in the case of fine limestone-metakaolin pastes, the trends are similar to those observed in binary fine limestone pastes, however, with the contribution of metakaolin to elevating plastic viscosity in the abovementioned ways. A comparison between Figures 6-9(a) and (b) shows that the plastic viscosity increases with an increase in metakaolin content (contrast this to the decreasing plastic viscosities with increase in fly ash content – Figures 6-8 a/b), which justifies the perceived effects of metakaolin in cementing pastes.

6.3.4 Representing the Rheological Properties as Functions of the Mixture Parameters: Observations from Experiments and Microstructural Generations

The rheological response of particle suspensions in fluids such as cement pastes are influenced significantly by the particle size ranges and their distribution, volume fraction of particles and their interactions (Flatt and Bowen 2006; Buscall et al. 1987; Farris 1968; Chong, Christiansen, and Baer 2003; Olhero and Ferreira 2004; Lee et al. 2003; Zhou et al. 1999; D. P. Bentz et al. 2012). This section harmonizes the influence of particle number density, specific surface area of the solids (consisting of OPC, limestone, and fly ash/metakaolin), and the water film thickness on the yield stress and plastic viscosity of all mixtures studied. To facilitate an understanding of the influence of the particle number density (related to the volume fraction of particles in the suspension) and water film thickness, simulated microstructures consisting of spherical particles packed according to their PSDs and the specified mixture inputs, were used. It is anticipated that a better understanding of the combined influence of $(w/s)_v$ that influences the water film thickness, and the particle characteristics (number density and specific surface area) on the rheological characteristics will thus facilitate strategies to proportion binary and ternary blends that have beneficial fresh properties.

Figure 6-10 presents the relationship between the particle number density and the rheological parameters for several mixtures studied. Both the yield stress and plastic viscosity are correlated with the particle number density, though yield stress is in fact better correlated (D. P. Bentz et al. 2012). An increase in the particle number density corresponds to an increase in the packing fraction and a decrease in interparticle spacing; thus this representation clearly illustrates that the packing density of the suspension (i.e., a

combination of both the number and size of particles) is a substantial factor that influences the rheology of a fluid suspension, which supports the observations in (Flatt and Bowen 2007; Nicolas Roussel et al. 2010). The pastes containing metakaolin (Figure 6-10b) show much weaker particle number density – rheological parameter relationships, likely on account of complications including the effects of agglomeration and electrostatic interactions, which would not be accurately represented only by the particle number density. In fact, the divergence of the rheological parameters with solid volume fraction (or the particle number density) in the case of agglomerated systems has also been discussed in (Nicolas Roussel et al. 2010).

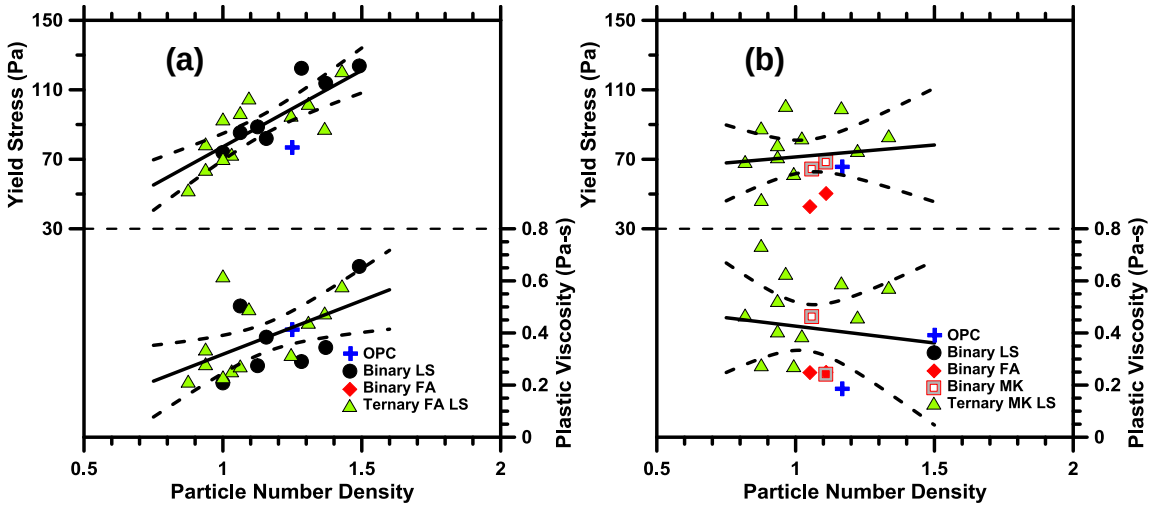

Figure 6-10: The influence of particle number density on the rheological properties of pastes with $(w/s)_v$ of: (a) 1.26 and (b) 1.42

Figure 6-11 represents the yield stress and plastic viscosity of all pastes as a function of the specific surface area of the particles in a given mixture. Similar to trend in the particle number density, as the specific surface area increases, the yield stress and plastic viscosity also increase (D. P. Bentz et al. 2012). The effects of increases in specific surface area on plastic viscosity are easily explained--- as the surface area increases (or the effective

particle size decreases), and interparticle spacing decreases, there is an increase in the number of interparticle contacts and interparticle friction, and thus plastic viscosity. Next, the trend in yield stress can be explained in terms of the two major effects that control yield stress: (1) packing density and (2) interparticle interactions. An increase in the specific surface area implies an increase in the packing density, decrease in interparticle spacing and increased interparticle interactions, which results in elevations in the yield stress. A yield stress model for suspensions reported in (Flatt and Bowen 2007; Flatt and Bowen 2006) predicts an inverse relationship between yield stress and particle size for suspensions (which equates to a direct relationship between yield stress and specific surface area as shown in Figure 6-11). The increased scatter seen at lower $(w/s)_v$ (upper panel of Figure 6-11a) is likely caused due to increased agglomeration at low $(w/s)_v$, which would have a significant influence on the free water availability, packing density, and interparticle spacing in these pastes. The specific surface areas shown here were obtained using the spherical particle assumption described in Section 6.2.3; however the use of Blaine's surface area also provided similar trends.

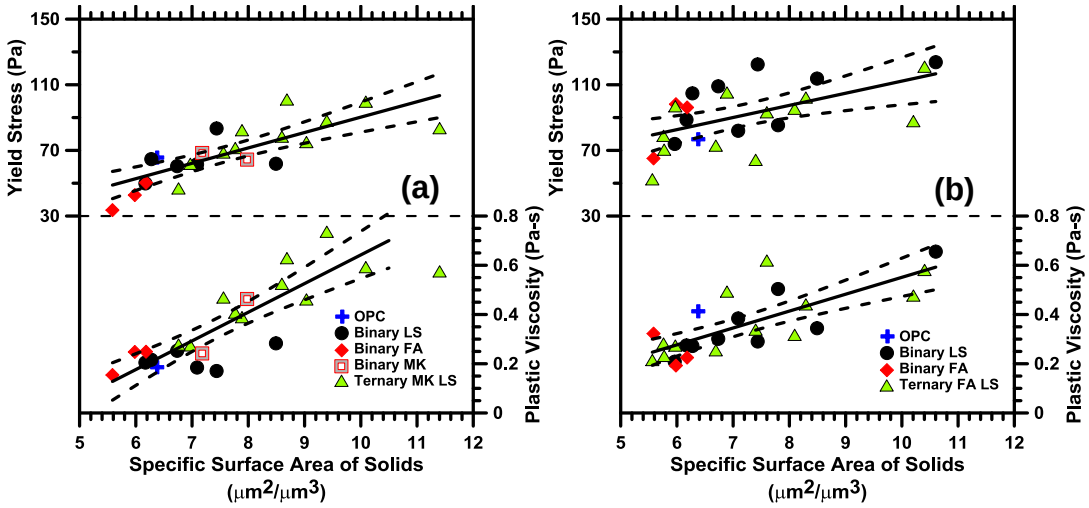

Figure 6-11: The influence of the specific surface area on the rheological properties of pastes with $(w/s)_v$ of: (a) 1.26 and (b) 1.42

The influence of the calculated water film thickness on the yield stress and plastic viscosity is shown in Figure 6-12. Since the water film thickness is inversely related to the specific surface area (Equation 6-4), the observed relationships of yield stress and plastic viscosity as a function of the film thickness are expected. An increasing thickness of water films around the particles then decreases the packing density and increases the interparticle spacing helping reduce both the yield stress and plastic viscosity. The water film thickness thus takes into account the combined effects of packing density and the surface area of solid particles.

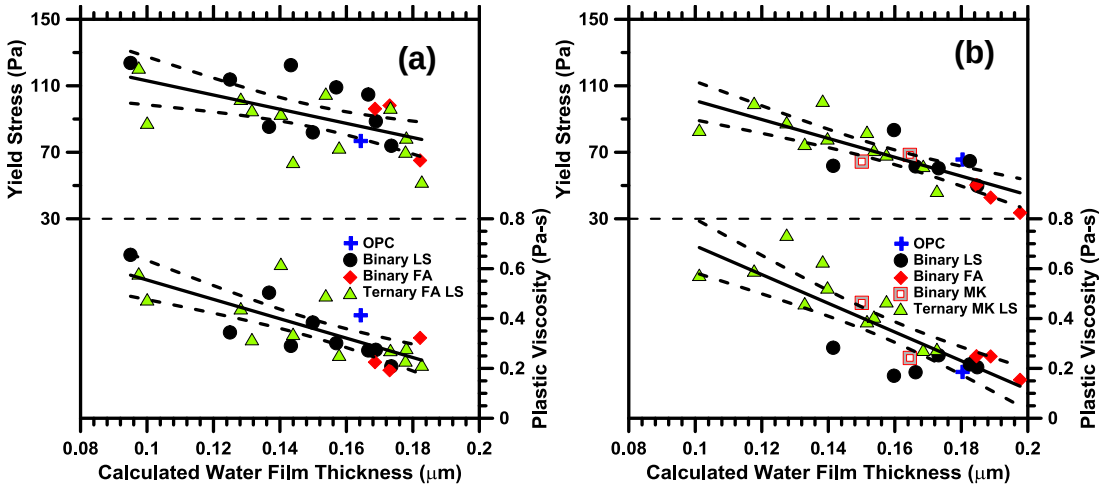

Figure 6-12: The influence of a calculated water film thickness on the rheological properties of cement pastes with $(w/s)_v$ of: (a) 1.26 and (b) 1.42.

In an effort to predict the apparent viscosities of suspensions as a function of particle loading, or to determine the maximum possible solid fraction, several equations have been proposed, starting from Einstein's equation (Skripkiūnas et al. 2005; Asaga and Roy 1980) to the Krieger-Dougherty (K-D) equation (Justnes and Vikan 2005; Krieger and Dougherty 1959), and other parametric models (Chong, Christiansen, and Baer 2003; Liu 2000). The apparent viscosity of a suspension (η_s) is defined as the ratio of the shear stress to the shear rate, for a specific shear rate. Dividing the apparent viscosity by the viscosity of the continuous phase (η_c) yields the apparent viscosity ratio or the relative viscosity (η_r). For the experimental datasets reported in this paper, i.e., for two different solid volume fractions (ϕ), and $(w/s)_v$, and the mixture specific maximum packing density ϕ_m, the Krieger-Dougherty equation (Equation 6-5), with only the intrinsic viscosity [η] as the variable parameter and Liu's model (Liu 2000) (Equation 6-6) which is a two-parameter (a and n) fitting model are used to compare the experimental and predicted apparent viscosities.

$$\eta_r = \frac{\eta_s}{\eta_c} = \left[1 - \frac{\phi}{\phi_m}\right]^{-[\eta]\phi_m} \quad (6\text{-}5)$$

$$\eta_r = \frac{\eta_s}{\eta_c} = [a(\phi_m - \phi)]^{-n} \quad (6\text{-}6)$$

The relationships between the experimentally determined apparent viscosity ratios and the apparent viscosity ratios calculated from the K-D equation (Equation 6-5) at each shear rate are shown in Figures 6-13a and b for pastes made using $(w/s)_v$ of 1.26 and 1.42 respectively. The apparent viscosity ratios were estimated from Equation 6-5 using a least squares minimization method which determined the intrinsic viscosity ([η]) at each shear rate for both the $(w/s)_v$ used. Note that no attempt was made to obtain different [η] values for the different mixtures, which would have reduced the scatter in the data. The [η] values ranged between 13.26±2.06 and 14.25±2.17 for the pastes of $(w/s)_v$ 1.26 and 1.42 respectively. For cementitious systems, the [η] values generally used are in the range of 4.0-6.0[4] (Justnes and Vikan 2005; Struble and Sun 1995); however the relationship between the experimental and calculated apparent viscosities did not conform to a 1:1 relationship when [η] values of that range were used. Such an observation has been recently reported in(D. P. Bentz et al. 2012).

[4] [η] = 2.5 for hard spheres, and increases with increase in aspect ratio of the particle (Wierenga and Philipse 1998)

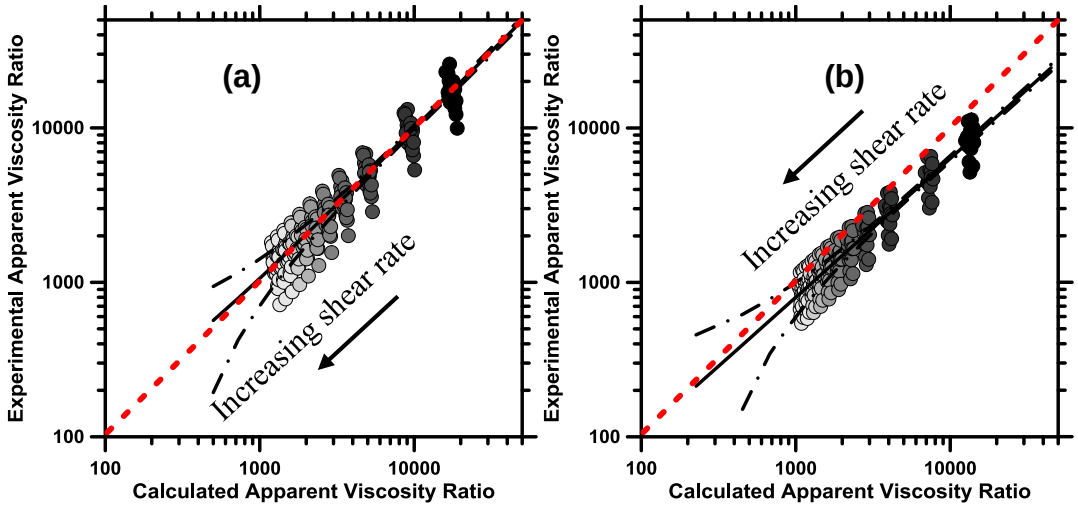

Figure 6-13: The apparent viscosity ratio for the pastes with $(w/s)_v$ of: (a) 1.26 (solid loading of 0.44) and (b) 1.42 (solid loading of 0.41) predicted using K-D equation (Equation 5). The constant η used in Equation (5) takes values of 13.26±2.06 and 14.25±2.17 for the $(w/s)_v$ 1.26 and 1.42 pastes respectively.

Figure 6-14 shows the experimental apparent viscosity ratios and those estimated using Liu's model (Equation 6) for all the pastes evaluated in this study. The estimated viscosity ratios were determined using a least squares minimization method and a numerical solver which resolved the fitting parameter a at each shear rate and $(w/s)_v$, while keeping the n value constant. Similar to the fitting of K-D equation in Figure 6-13, here also, no attempt was made to obtain customized a and n values for individual mixtures, in which case the scatter would have been greatly minimized. The a and n values used for the predictions shown in Figure 6-14 were 0.065±0.035 and 2.14 respectively. Least square minimization was also used to fit the data using {a; n} as {0.67±0.14; 6.0} and {0.34±0.11; 4.0} with limited changes in the predictive capability. Figure 6-14 shows a very similar trend to Figure 6-13, due to the similar nature of Equations 5 and 6. Both Figure 6-13 and 6-14 shows the significant influence of particle loading on the efficiency of apparent viscosity prediction models – a lower solid loading provides reduced scatter as shown in Figures 6-13(b) and 6-14(b).

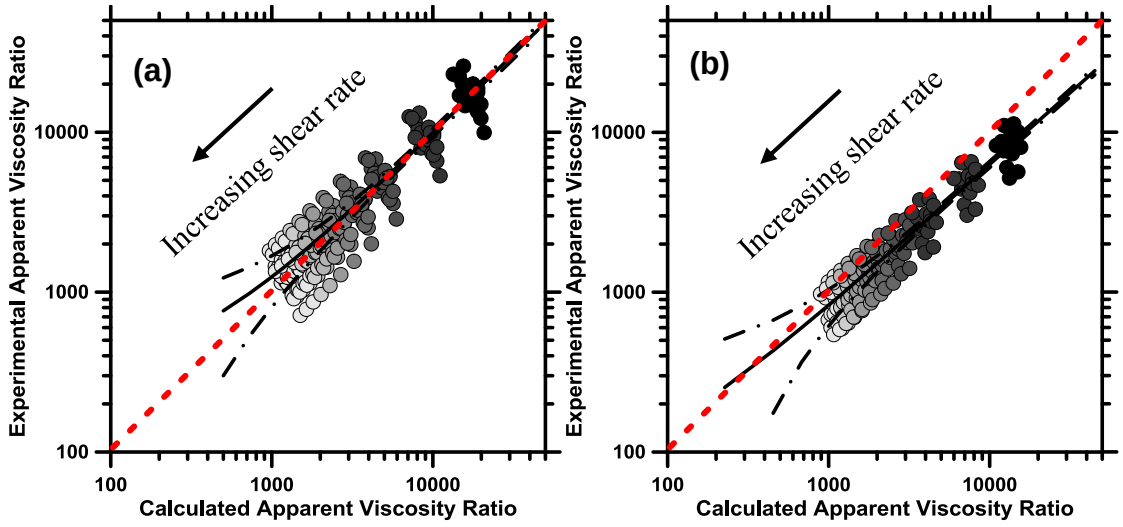

Figure 6-14: The apparent viscosity ratio for the pastes with $(w/s)_v$ of: (a) 1.26 (solid loading of 0.44) and (b) 1.42 (solid loading of 0.41) predicted using Liu's equation (Equation 6-6). The constants a and n used in Equation (6-6) take values of 0.065±0.035 and 2.14 respectively

Furthermore, it is noted that there exists a perfectly linear relationship ($R^2 = 0.99$) between the parameters a and n of Liu's model in the range investigated. This allows a more rigorous approach in using Liu's model for the apparent viscosity prediction of cementitious suspensions. The bounding values of the constant a are a very small number (very close to zero, but non-zero) and 1.0, and n can vary between 1.0 and a large number, e.g., close to 10 for the mixtures evaluated. As such, as a $\rightarrow$ 0, n $\rightarrow$1.0, resulting in a very high suspension viscosity, η_s. This is an indication of a high solid loading (approaching ϕ_m) in the suspension, suggesting that, in general, low values of a and n can be used when ϕ is high (in lower w/c mixtures). Conversely, when a $\rightarrow$ 1.0, and n approaches a high number, η_s tends to be very small, corresponding to a lower ϕ. Thus the fit parameters in Liu's equation can be chosen as a function of the solid volume in the suspension to obtain adequate predictions of the apparent viscosity. Conversely, based on the desired apparent viscosity, the particle loading (solid volume fraction) can be obtained from carefully

chosen constants. Another potential benefit of this approach, when well-calibrated, is its capability to predict the maximum solids concentration (ϕ_m). The measurement of this parameter is quite complex since it depends on the shape and size distribution of particles and computational methods that rely on a number of assumptions are generally used. However, it must be noted that the shear rate also needs consideration while choosing the constant a, where low values of a correspond to low shear rates.

6.4 Summary Conclusions

This study has reported the influence of binary blends of limestone, fly ash, or metakaolin and ternary blends of limestone and fly ash or metakaolin on the rheological properties of cement pastes. The Bingham model for fluid suspensions was used to interpret the material behavior. Replacement of OPC by coarse limestone powder (15 μm) depressed the yield stress and plastic viscosity of cement pastes, as attributed to a reduction in the packing density and specific surface area of solids and an increase in the particle spacing. Opposing effects in these parameters were noted when fine limestone powder (0.7 μm and 3 μm) is incorporated, resulting in higher yield stress and plastic viscosity. Binary blends containing fly ash behaved similar to those containing coarse limestone powder, whereas binary metakaolin blends demonstrated behavior similar to that of a fine limestone containing paste because of higher surface area and the agglomeration potential of metakaolin. In ternary blends containing limestone and fly ash or metakaolin, the plastic viscosity increased with increasing limestone content for fine limestone additions, as was the case for binary limestone blends, and remained unchanged for coarse limestone additions. The yield stress depression at higher fly ash contents even for pastes containing fine limestone powder results from the spherical geometry of fly ash particles that compensate for the

increased surface area and packing. In ternary blends containing metakaolin and fine limestone, the yield stress was noted to reduce with increasing limestone content. In this case, increases in the packing density effected by fine limestone additions were likely compensated by the electrostatic effects produced between metakaolin and limestone particles that enhance interparticle spacing.

The influence of particle number density, water film thickness and the specific surface area of the solids on the yield stress and plastic viscosity of suspensions containing binary or ternary blends containing size classified limestone powder has been quantified. The yield stress and plastic viscosity of all the pastes were found to increase with the particle number density and specific surface area, and decrease with water film thickness. A two-parameter model was used to relate the apparent viscosities to the solid volume fraction and maximum packing density, with a substantial predictive capability being realized.

7. THE RHEOLOGY OF CEMENTITIOUS SUSPENSIONS: A CLOSER LOOK AT EXPERIMENTAL PARAMETERS AND PROPERTY DETERMINATIONS USING COMMONLY USED RHEOLOGICAL MODELS.

7.1 Introduction

Rheological studies of concentrated suspensions of solid particles in a continuous liquid medium are commonly used to assess the characteristics of materials in industries ranging from food to pharmaceuticals to construction materials. The flow behavior of these concentrated suspensions is influenced by surface contacts between solid particles and interparticle forces such as van Der Waals and steric forces (Mueller, Llewellin, and Mader 2010). Rheological studies of cementitious suspensions provide an understanding of how these materials behave in the fresh state and serve to monitor structure development that dictates the development of the mechanical properties (Sant, Ferraris, and Weiss 2008). However, in order to apply rheological experiments to cementitious suspensions, it is important to clearly understand the influences of experimental parameters and the selected rheological model on both, measured and predicted characteristics of flow to establish their relevance and applicability.

Rheological experiments are typically carried out using a rotational rheometer, which monitors the change in torque required to change the shear rate (constant strain) or the change in strain required to change the torque (constant stress). There exist several experimental parameters of significance, including but not limited to: testing geometry (parallel plate, coaxial cylinder, cup and vane etc.), the gap between shearing surfaces, roughness of the shearing surfaces, testing temperature, and the state of dispersion determined by the particle characteristics and the mixing method. Models including

formulations by Bingham, Herschel-Bulkley, and/or Casson (Nehdi and Rahman 2004a; Ferraris 1999a; De Larrard, Ferraris, and Sedran 1998; Schwartzentruber, Le Roy, and Cordin 2006) are commonly applied to the shear stress-shear rate response to extract the rheological parameters that describe flow, e.g., plastic viscosity and yield stress.

Previous studies (Nehdi and Rahman 2004a; D. P. Bentz et al. 2012; Ferraris, Obla, and Hill 2001) have reported the influence of the experimental setup on the yield stress and plastic viscosity of cementitious suspensions extracted using a Bingham model. The plastic viscosity is a measure of the rate of increase in shear stress with increasing strain, and is thus a measure of the flowability of a fluid. The plastic viscosity of fluid suspensions is thought to be primarily influenced by interparticle friction and surface contacts (Banfill 2006), wherein decreasing the interparticle (friction) forces by increasing particle spacing (or by decreasing surface contacts) results in a decrease in plastic viscosity. The yield stress is a more complex parameter, defined as the non-zero (finite) stress at a "zero" strain rate[5]. Several methods have been proposed to determine the yield stress, including: an extended duration constant stress experiment (Møller, Mewis, and Bonn 2006), stress growth and strain reduction experiments (Cheng 1986), and oscillatory experiments (Nguyen and Boger 1992). Yield stress is typically determined in cementitious suspensions using strain reduction experiments with reverse extrapolation to a zero strain rate using a rheological model fit to the measured shear strain rate-shear stress dataset (Banfill 2006).

Yield stress has been attributed to the effects of both the surface contacts between particles which prevent flow (jamming) below a certain applied stress, as well as interparticle

[5] It should be noted that a "zero" strain rate does not practically exist. A non-zero strain rate (even if infinitesimally small) needs to be applied in order to obtain a resistance to flow (shear stress). The apparent "zero" strain rate is thus a mathematical simplification through which a value for the yield stress is obtained.

attractive forces (Funk and Dinger 1994; Lowke 2009; Mueller, Llewellin, and Mader 2010). Yield stress is commonly reported as the stress required to initiate flow of a fluid (Banfill 2006); however some authors distinguish between a dynamic yield stress and static yield stress (M.-H. Zhang et al. 2010). The dynamic yield stress is the stress required to maintain flow once it has commenced, while the static yield stress is the stress required to initiate flow from rest. This indicates that the dynamic yield stress is a model-dependent parameter, i.e. the choice of model can have a significant influence on the calculated yield stress, as can be seen from the data presented in (Nehdi and Rahman 2004a). This distinction is significant when comparative rheological studies of cementitious suspensions are to be performed, as selection of different shear rate ranges or models will result in substantial variations in the calculated yield stress, indicating that the dynamic yield stress is not a material parameter in the truest sense. This paper explores this idea in some detail in the context of cementing systems. Furthermore, an understanding of the influence of the shear history of the suspension, as represented using different mixing procedures is developed in addition to new evaluations of the influences of experimental parameters including: the gap between shearing surfaces and the surface roughness of the bottom plate on the measured rheological response.

7.2 Experimental Program

7.2.1 Materials

The materials used in this study are a commercially available Type I/II ordinary portland cement (OPC) conforming to ASTM C 150 ("ASTM C109 / C109M - 12 Standard Test Method for Compressive Strength of Hydraulic Cement Mortars (Using 2-In. or [50-Mm] Cube Specimens)" 2012), Class F fly ash conforming to ASTM C 618 ("ASTM C109-13.

Standard Test Method for Compressive Strength of Hydraulic Cement Mortars Using 2-In. Cube Specimens" 2013), and limestone powder of 3µm median particle size, conforming to ASTM C 568 ("ASTM C568 / C568M - 10. Standard Specification for Limestone Dimension Stone" 2012). The particle size distributions of these materials are presented in Figure 7-1 and their compositions in Table 7-1.

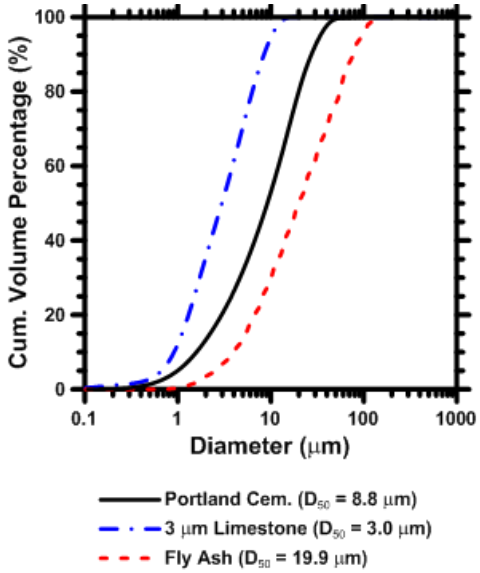

Figure 7-1: The particle size distributions of OPC, 3µm limestone, and fly ash, as measured using a light scattering analyzer.

Table 7-1: Oxide compositions and specific surface areas of the raw materials used in this study.

Material	SiO_2	Al_2O_3	Fe_2O_3	CaO	MgO	SO_3	Na_2O	K_2O	SSA
OPC	21.0%	3.86%	3.55%	63.8%	1.83%	2.93%	0.12%	0.48%	470 m^2/kg
Fly ash	58.4%	23.8%	4.19%	7.32%	1.11%	0.44%	1.43%	1.02%	218 m^2/kg

Limestone powder contains 95-97% $CaCO_3$ as per the manufacturer with a Blaine's specific surface area of 2396 m^2/kg.

For all the cementitious suspensions considered, cement was replaced by either limestone or fly ash on a volumetric basis to ensure that the comparisons are consistent. The

suspensions were prepared at a constant volumetric water-to-solid ratios, $(w/s)_v$, of 1.42, equivalent to mass-based water-to-solid ratio, $(w/s)_m$, of approximately 0.45. No chemical admixtures were used.

7.2.2 Experimental Parameters and Suspensions

The rheological response of the suspensions is considered in the context of 4 distinct parameters: (i) gap between the top and bottom plates in a parallel plate configuration (top plate diameter of 50 mm, serrated to a depth of 1.0 mm), (ii) roughness and surface treatment of the bottom plate[6] (serrated to a depth of 0.15mm, or resin-coated sandpaper[7] of mean surface roughness, MSR = 0.12mm or 0.017mm), (iii) type and speed of mixing of the suspension, and (iv) range of shear rates considered. Further details regarding the parameters are noted in Table 7-2. The suspensions consisted of: (i) OPC + water and (ii) OPC + limestone + water where the fine limestone ($d_{50} \approx 3\mu m$) replaced 10% of OPC by volume, and (iii) OPC + fly ash + water where fly ash replaced 10% OPC by volume. A gap of 2.0 mm, a bottom plate with 0.15 mm deep serrations, a shear rate of 5-to-100/s, and high-shear mixing corresponding to ASTM C 1738 ("ASTM C1738 - 11a. Standard Practice for High-Shear Mixing of Hydraulic Cement Paste" 2011) were used as the general "default" evaluation parameters.

[6] The influence of the surface condition of the Peltier plate on rheological measurements including the effects of slippage and plug flow have been reported elsewhere (Nehdi and Rahman 2004a; Banfill and others 2003).

[7] Care should be taken to ensure that the sandpaper is non-absorbent as otherwise it will result in changes in water availability and thus the rheological parameters.

Table 7-2: Details regarding experimental variables, their range, and the suspension characteristics

Variable	Levels of the variables	$(w/s)_v$	Cement replacement level (Vol. %)	
			Limestone	Fly Ash
Gap	1.0, 1.5, 2.0 mm	1.42	0, 10	0, 10
Surface condition	Serrated bottom plate (0.15 mm deep serrations), adhesive backed sand paper – 40, 150 grit (mean surface roughness = 0.12 mm and 0.017 mm)	1.42	0, 10	0, 10
Shear rate	5-100/s, 0.1-10/s, 0.1-100/s; See Figure 7-2	1.42	0, 10	0, 10
Mixing	4 different types, See Table 7-3	1.42	0, 10	0, 10

7.2.3 Mixing and Testing Procedure

All powders were dry blended prior to the addition of water. To investigate the effects of mixing on the rheological response, four different mixing procedures were used - three involving a high shear mixer and the fourth using a hand-held kitchen mixer. All the mixing procedures consisted of an initial powder addition phase, followed by initial mixing, a covered rest period, and final mixing. Table 7-3 illustrates the four different mixing procedures along with the mixing speeds, time, and rest durations. For all the three high shear mixing procedures, the powder blending speeds and the rest durations are the same. The differences lie in the initial mixing speed after adding water, and in the final mixing speed and its duration. The mixing condition of the highest intensity, both with respect to speed and duration is the one corresponding to ASTM C1738, and is described as 12-30-12-90. The first and third numbers represent the initial mixing speed after powder blending

and the final mixing speed after the rest period, in 1000x rpm (i.e., the number 12 in first and third positions in the above sequence indicates 12000 rpm), and the second and fourth numbers represent the duration (in seconds) of initial and final mixing steps respectively.

Table 7-3: Mixing procedures and corresponding details relevant to suspension preparation

Procedure type	**Description**	**Powder blending speed, rpm**	**Initial speed after mixing water, rpm(duration)**	**Rest period**	**Final mixing speed, rpm (duration)**
12-30-12-90	ASTM C 1738	4000	12000 (30s)	120s	12000 (90s)
12-30-12-30	Shorter duration during final mixing	4000	12000 (30s)	120s	12000 (30s)
4-30-4-30	Lower speeds and shorter durations during both initial and final mixing	4000	4000 (30s)	120s	4000 (30s)
Hand-held mixer	Lowest speeds and shorter durations during both initial and final mixing	-	- (30s)	120s	-- (30s)

In addition to the effects of mixing procedure, gap, and surface condition, the influence of the selected shear rate range on the rheological properties was also investigated. These experiments were of three different types: (i) a "normal" shear rate range between 5 and 100/s, typical of the range used in typical rheological studies of cement pastes (D. P. Bentz et al. 2012; Nehdi and Rahman 2004a), (ii) a "low" shear rate range, between 0.1 and 10/s, and (iii) a "wide" shear rate range, from 0.1 to 100/s, which encompasses both prior ranges.

All rheological sequences consisted of a ramp-up pre-shear phase lasting approximately 80s to homogenize the paste, an instantaneous ramp-down which is followed by a ramp-up, and then immediately followed by a ramp-down. The pre-shear, up-ramp, and down-ramp sequences for the three different shear rate ranges are shown in Figures 7-2(a)-(c).

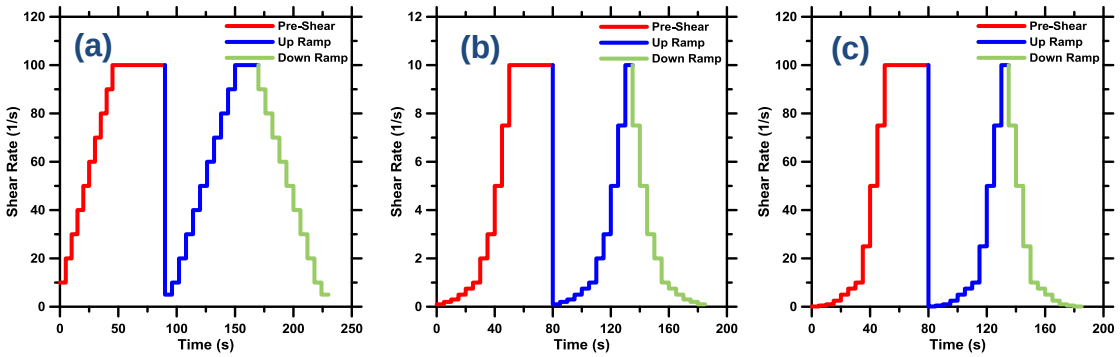

Figure 7-2: The rheological procedures applied over: (a) "normal" shear range, (b) "low" shear range, and (c) "wide" shear range

For all the experiments, the time elapsed from the addition of water to the powder, to the beginning of rheological measurements; including the time to set the gap, was about 5 minutes. Rheological measurements were carried out on samples of fresh cementitious suspensions using a rotational rheometer (TA Instruments AR2000EX) in a parallel plate configuration, provided with Peltier elements located in the bottom plate which were conditioned to 25±0.1 °C. Except during the pre-shear phase, data is collected every second at each step, until steady state has been achieved, as defined by three consecutive torque measurements within 5% of each other, at which time the experiment advances to the next shear rate. The time expended at each shear step in which data is collected is typically 5 seconds. The measured experimental values for shear stress and shear rate were extracted using the TA Instruments' TRIOS distribution.

The rheological model parameters for the "normal" shear rate range (5-100/s) were calculated using a least squares fitting to the Bingham model of the down-ramp data as shown in Equation 7-1 (Bingham 1922). The use of the Bingham model in this shear rate range is justified by the generally linear nature of the shear stress-shear rate response. The rheological parameters for the "wide" shear rate range (0.1-100/s) were calculated using a least squares fitting of the down-ramp data to two different models, sometimes referred to as generalized Bingham models: i.e., the Herschel-Bulkley model shown in Equation 7-2 (Herschel and Bulkley 1926), and the Casson model shown in Equation 7-3 (Casson 1959).

Bingham: $\tau = \tau_y + \eta_p \dot{\gamma}$ Equation (7-1)

Herschel-Bulkley: $\tau = \tau_y + K\dot{\gamma}^n$ Equation (7-2)

Casson: $\sqrt{\tau} = \sqrt{\tau_y} + \sqrt{\eta_\infty}\sqrt{\dot{\gamma}}$ Equation (7-3)

The latter models were used because of their ability to better capture non-linearities in the data that manifests at lower shear rates. In these equations, τ is the shear stress (in Pa), τ_y is the yield stress (in Pa), η_p is the plastic viscosity (in Pa.s), $\dot{\gamma}$ is the shear rate (in s^{-1}), K is the consistency index which is a measure of the average viscosity of the fluid, and n is the flow behavior index (Nehdi and Rahman 2004a; Herschel and Bulkley 1926), which ranges between 0-and-1 for shear thinning suspensions (Banfill 2006), and η_∞ (in Pa.s) is the viscosity at an infinite shear rate (A. Papo 1988) .

7.3 Results and Discussions

7.3.1 Influence of Gap between Parallel Plates on the Measured Rheological Properties

This section discusses the influence of the gap between the upper and lower parallel plates on the yield stress and plastic viscosity as determined using a Bingham model for a shear

rate of 5-to-100/s. All the other experimental variables were maintained at "default" levels as described in Section 7.2.2. The upper plate in the parallel plate configuration is set to three different gaps--- 1.0 mm, 1.5 mm, and 2.0 mm. In order to obtain consistent results, it has been reported that the gap should be at least an order of magnitude larger than the size of the largest characteristic inclusion phase in the suspension (Banfill 2003; Shaughnessy III and Clark 1988). The particle size distributions shown in Figure 7-1 confirm that this criterion is satisfied here. Moreover, the ideal gap also depends on the depth of the serrations in the upper and lower plates, and the plate diameter (Nehdi and Rahman 2004a; Ferraris 1999b). Given the depth of plate serrations and the different combinations of cement replacement materials used in this work, a minimum gap size of at least 1.0 mm was selected as noted in Chapter 6. The required gap also depends on the shear rate – larger shear rates are needed to ensure uniform flow across a larger gap, whereas larger shear rates in a smaller gap can cause flow instabilities due to the increased likelihood of turbulent flow, and an increased likelihood of particle contact with the shearing surfaces (Ferraris and Gaidis 1992).

Figure 7-3 presents the results for three different gaps for a plain OPC suspension and a suspension with 10% OPC (by volume) replaced by 3μm limestone, at a $(w/s)_v$ of 1.42. The general trend indicates that increasing the gap results in increasing yield stress. This response is consistent with the data presented in (Ferraris 1999a), but opposite of that reported in (Nehdi and Rahman 2004a). Additionally, increasing the gap results in a decrease in or relatively unchanged value of the plastic viscosity; in line with (Nehdi and Rahman 2004a). As shown in Figure 7-3, the effect of the gap on plastic viscosity is minimal for the plain OPC suspension and more pronounced in the case of the suspension

containing limestone. It is also observed that as the gap is decreased, the quality of fit becomes slightly poorer as indicated by lower coefficients of determination (R^2). Cementitious suspensions that do not contain rheology modifying chemical admixtures behave as shear thinning suspensions (Banfill 2006), where flow is enabled by the formation of shear bands within the suspension. The apparent viscosity thus decreases with increasing shear rates as these bands form (Mueller, Llewellin, and Mader 2010). This behavior may explain the apparently counterintuitive observation of increasing yield stress with increasing gap, as narrower gaps produce a larger number of turbid shear bands, while wider gaps produce fewer, but more intense shear bands (Herle, Fischer, and Windhab 2005). Furthermore, normal forces acting on the suspension that result from higher evaluation volumes with increasing gap, which increase sample weight, may result in increased interparticle forces that inhibit the ability of the paste to (initiate) flow, which also contributes to a higher observed yield stress.

The general decrease in plastic viscosity with increasing gap can be explained as follows: in particulate suspensions, increasing the gap results in an increased influence of concentration gradients (of the solid or liquid phases) along the height of the sample due to sedimentation of the particles (Bhatty and Banfill 1982) as well as decreased effects of confinement. This concentration gradient results in higher $(w/s)_v$ at specific locations along the height of the sample, which in turn decreases the measured plastic viscosity. This effect is enhanced in the presence as limestone, as the inclusion of limestone increases the spacing between cement particles by interrupting interparticle forces between the cement particles. This decrease in interparticle forces subsequently enhances the concentration gradient effect along the sample thickness.

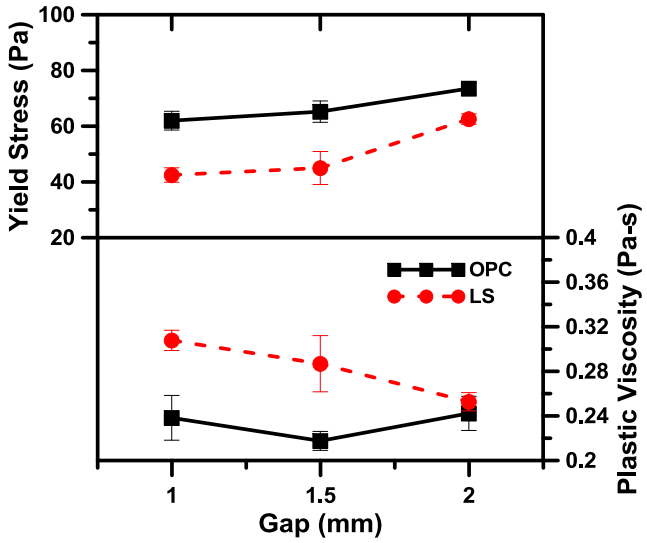

Figure 7-3: The influence of gap on the rheological properties, estimated using the Bingham model

7.3.2 Influence of the Surface Condition of the Bottom Plate

Measurement of rheological properties can be considerably influenced by the friction between the sample and the shearing surface. Several studies have shown that the use of a smooth shearing surface increases the likelihood of slippage and plug flow which can result in incorrect estimations of the rheological properties (Saak, Jennings, and Shah 2001; Mannheimer 1983; Banfill 2006). This section adds to this premise by studying the effects of surface roughness, as described by the mean surface roughness (MSR), which is the arithmetical mean height of the irregularities measured from the datum surface, on the rheological parameters as determined using the Bingham model (Equation 7-1). The bottom plate with 0.15 mm deep serrations has a MSR = 0.15mm, and the MSR values of the other surfaces (sandpaper) used are shown in Table 7-2.

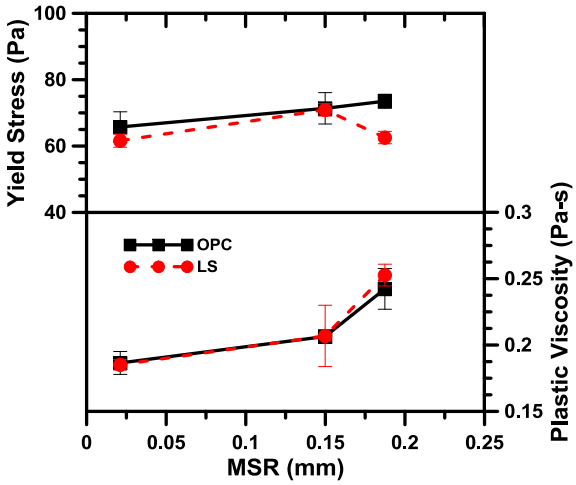

Figure 7-4: The influence of the surface condition of the bottom plate one the rheological properties as estimated using the Bingham model.

Figure 7-4 presents the influences of surface roughness on the rheological properties. Three surface conditions were used, ranging from a serrated bottom plate (MSR = 0.15mm) to 150 grit sandpaper (MSR = 0.017mm), at a constant gap value of 2.0 mm. In general, the yield stress and plastic viscosity increase with increasing MSR, as can be observed from Figure 7-4. It is important to note that, as the surface roughness increases, the likelihood of slip decreases. Since slip is caused due to a localized decrease in the solid concentration near the shearing surface (Saak, Jennings, and Shah 2001), the use of textured surfaces acts to maintain constant the solid fraction in the vicinity of these surfaces. Hence, as the roughness increases, the yield stress and more so, the plastic viscosity increases because of a reduction in slip at the shearing surface (Saak, Jennings, and Shah 2001; Mannheimer 1983).

7.3.3 Influence of Mixing Procedure on Rheological Properties as Estimated Using the Bingham Model

The shear history of fresh cementitious suspensions, which is attributed mainly to the mixing process, influences their rheological properties (Banfill 2006). Different mixing

methodologies influence suspension rheology due to their ability to induce varying levels of particulate dispersion, i.e., in controlling agglomeration and flocculation (Yang and Jennings 1995; Williams, Saak, and Jennings 1999). To better understand these effects, this section evaluates the influences of mixing procedure on the rheological parameters (yield stress and plastic viscosity) as determined using the Bingham model.

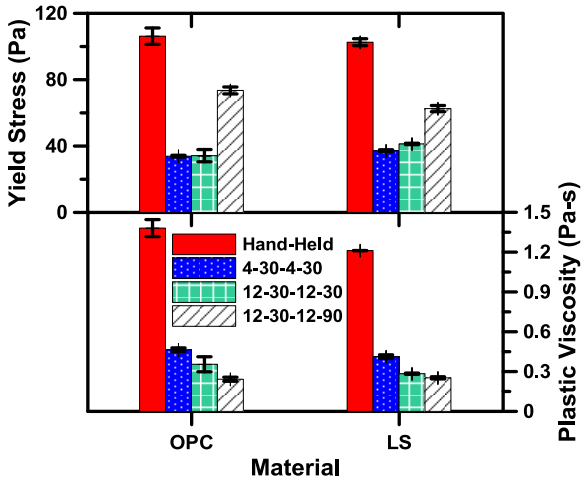

Figure 7-5: The influence of mixing procedure on the rheological properties as estimated using the Bingham model

The influence of mixing methodologies on measured rheological properties of OPC and 10% 3μm limestone containing suspensions is presented in Figure 7-5. It is evident that maintaining a consistent mixing procedure is critical when comparing rheological experiments. Both the yield stress and plastic viscosity are noticeably higher when a hand-held mixer is used, as compared to medium and high shear rate mixing using an industrial blender. This drastic increase in the yield stress occurs due to the fact that the hand-held mixer does not impose high enough shear rates to ensure proper dispersion of the particles and break up agglomerates. The inadequate dispersion, i.e., enhanced agglomeration, aids in the retention of free water within the flocs (Williams, Saak, and Jennings 1999; Sakai et al. 2009), and interparticle bond formation, all of which act to restrict the flow of the

suspension. In the case of mixing procedures that employ high shear rates, there is a consistent trend of decreasing plastic viscosity with increasing mixing intensity (both in terms of speed and duration). As the shear rate (i.e., the mixing speed) is increased, the mixing shifts from primarily extensive to intensive (Hetsroni 1982)[8], and thus particle dispersion increases and agglomerations are reduced or destroyed (Williams, Saak, and Jennings 1999; Tattersall and Banfill 1983; Yang and Jennings 1995). This results in a decrease in interparticle surface contacts and friction forces, thereby increasing the fluidity of the suspension. It is also notable that the influence of limestone addition varies across different mixing regimes. The plastic viscosity reduces on limestone incorporation across all mixing cases. On the other hand, the yield stress influence of limestone incorporation is inconsistent; both the lowest (hand-held) and highest (ASTM C1768) intensity mixing result in decreased yield stress while the intermediate levels show an increase in yield stress. This indicates that modifications to mixing procedures may produce different results, as well as different interpretations therein when comparing suspensions containing multiple solids with varying particle characteristics. While this could be attributed to competing effects of dispersion/agglomeration and bond destruction/formation, it is another example of yield stress being highly dependent on experimental parameters as will be discussed in the following section.

[8] It should be noted that extensive or distributive mixing causes a rearrangement of the components of the mixture and is responsible for the spatial (re)distribution of the particles within the fluid matrix while intensive or dispersive mixing normally involves a rupture of agglomerates through shear stresses at the particle/host fluid interface.

7.3.4 Influence of Shear Rate and Model Selection on Rheological Property

7.3.4.1 Shear Rate Range Effects

A discussion of the influence of shear rates on the yield stress and plastic viscosity as determined using the three shear rate ranges reported in Section 7.2.2: (a) 5-100/s, (b) 0.1-10/s, and (c) 0.1-100/s is presented here. While several different cementitious suspensions of $(w/s)_v = 1.42$ (including ternary blends of limestone of different particle sizes and fly ash) were evaluated, the results of three representative suspensions: (i) OPC, (ii) 10% OPC replaced by 3μm limestone, and (iii) 10% OPC replaced by fly ash, are presented in Figures 7-6 to 7-8. The datasets are plotted in both linear and logarithmic scales so as to appropriately elucidate the differences at lower shear rates. Note the appearance of a shear stress plateau at lower shear rates in the plot when the shear rate axis is plotted in the logarithmic scale, is similar in trend to that reported in (Schwartzentruber, Le Roy, and Cordin 2006). The fit lines shown on these plots are applicable for the Bingham model for the "normal" range which is generally linear (5-100/s) and the Herschel-Bulkley and Casson models on the "wide" shear range (0.1-100/s) as presented in Equations (7-1 to 7-3). The Herschel-Bulkley (H-B) model was not fit on datasets for the "normal" range, where the shear rate-shear stress response was quite linear because fitting the three-parameter H-B model (Equation 7-2) to a linear dataset does not provide unique fits, i.e., there exist multiple combinations of the parameters (i.e., even within the constraints such as $0 \leq n \leq 1.0$) with negligible least squares error and very high coefficients of determination[9]. The non-linearity of the data in the "wide" shear rate range experiments

[9] Many commercial equation-fitting programs pick one among the many possible combinations, based on the initial assumed values of the fitting parameters. While the use of H-B model has been suggested by some researchers over the Bingham model even in the event of a linear τ-γ relationship to avoid obtaining negative τ_0 values, this approach is not ideal. This section of the paper provides suggestions to overcome these artifacts of such "spurious curve fitting".

makes the use of H-B and Casson models applicable in such cases. Furthermore, the H-B model also does not provide a direct indication of the plastic viscosity of the suspension. Coefficients of determination (R^2) for these fits were always greater than 0.90, with the H-B model expectedly showing the highest R^2 values in many instances. While this aspect often favors the use of the H-B model for particulate suspension rheology (Atzeni, Massidda, and Sanna 1985; Kelessidis et al. 2006; Schwartzentruber, Le Roy, and Cordin 2006), key evidence provided later in the paper highlights inadequacies of this and other commonly used models in the context of rheological parameter (yield stress in particular) estimation and extraction.

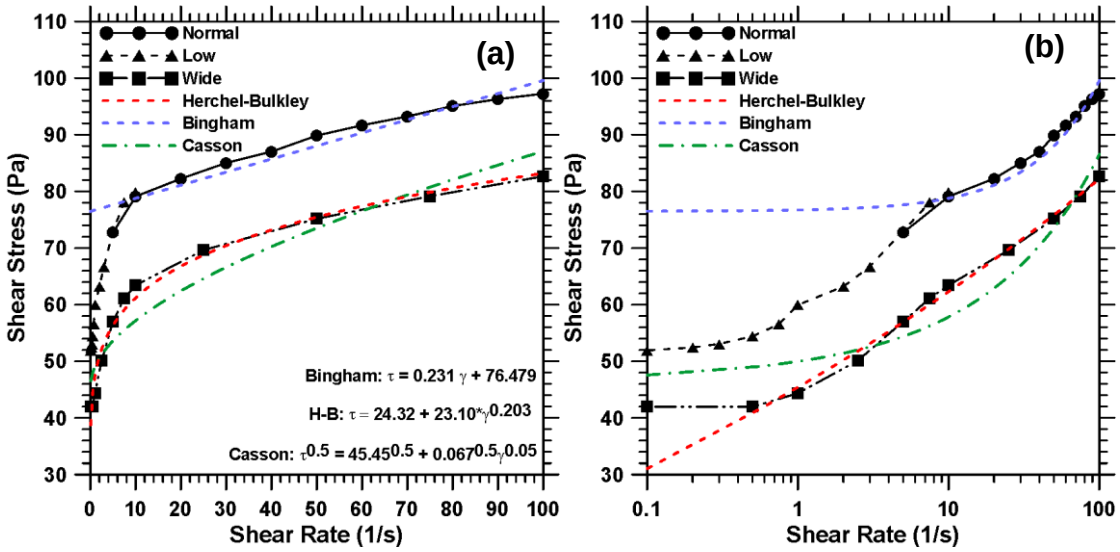

Figure 7-6: The influence of shear rate range and the selected model on rheological properties for the plain OPC suspension on: (a) linear scale, and (b) logarithmic scale

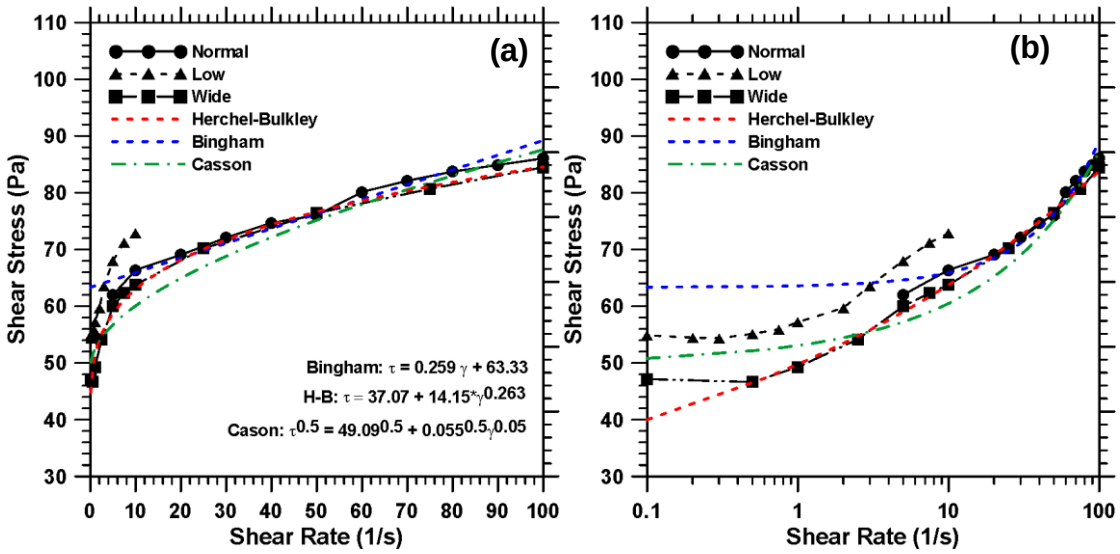

Figure 7-7: The influence of shear rate range and the selected model on the rheological properties for 10% 3 μm limestone containing suspension on: (a) linear scale, and (b) logarithmic scale.

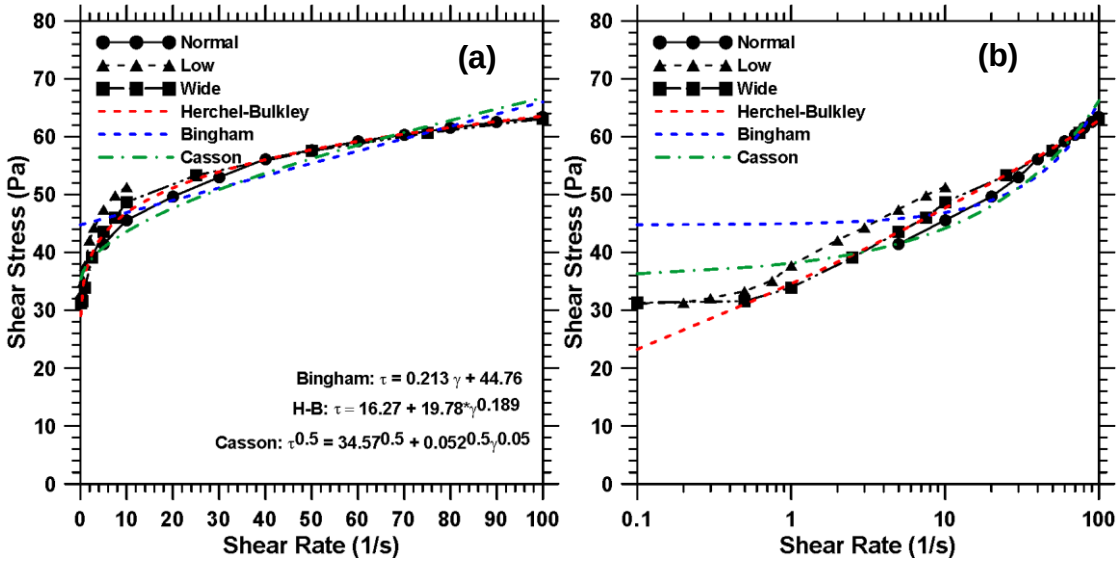

Figure 7-8: The influence of shear rate range and the selected model on the rheological properties for 10% fly ash containing suspension: (a) linear scale, and (b) logarithmic scale.

In Figure 7-6 which shows shear rate-shear stress relationships for OPC-water suspensions, there is a consistent shear stress offset of about 15 Pa between the "normal" and "wide" shear rate range data, which was observed in several repeat measurements. The suspensions containing 10% of limestone or fly ash (by volume) as cement replacement do not demonstrate this offset to such a degree, although an offset is present between the "low"

and “wide” shear rate range data. To investigate the origin of the stress offset between the “wide” and “normal” shear range data in Figure 7-6, an additional experiment was performed using another OPC suspension to determine if this effect may be specific to the cement used. The “normal” and “wide” experiments were then carried out as before, and an offset of about 7 Pa was noted. A “modified-wide” (wide-mod) experiment was added with the aim of maintaining an identical shear history between the “normal” and “wide-mod” data up to the peak stress value of the up-ramp. Thus, the pre-shear and up-ramp strain rates from Figure 7-2(a) (“normal”) and the down ramp strain rates from Figure 7-2(c) (“wide”) were used together to form the “modified-wide” experiment.

The shear rate-shear stress response of the suspension subjected to this regime, along with its response when subjected to the “normal” and “wide” shear rate ranges are presented in Figure 7-9. It is noted from this figure that the “wide-mod” range results in an almost identical peak shear stress as that in the “normal” shear rate range experiment, which is expected given the identical shear histories of the paste up to that point. After the point of maximum stress, in the down-ramp, the flow curves of the suspensions subjected to the “normal” and “wide-mod” regimes diverge, with the suspension subjected to the “wide-mod” regime experiencing less total strain (because of the reduced time – see Figure 7-2c) while showing a higher level of shear stress. This supports the idea that this stress offset is likely related to the differences in shear history of the suspension, wherein a reduction in the total strain experienced by the OPC suspension results in varying levels of structure build-up and breakdown as discussed in (Banfill and Saunders 1981). The offset is expected to be less significant in Figures 7-7 to 7-8, i.e., in the presence of limestone and fly ash as the relatively inert nature of these particles and their influences in aiding

suspension fluidity limits the role of structural build-up over the course of the experiment (Sant, Ferraris, and Weiss 2008).

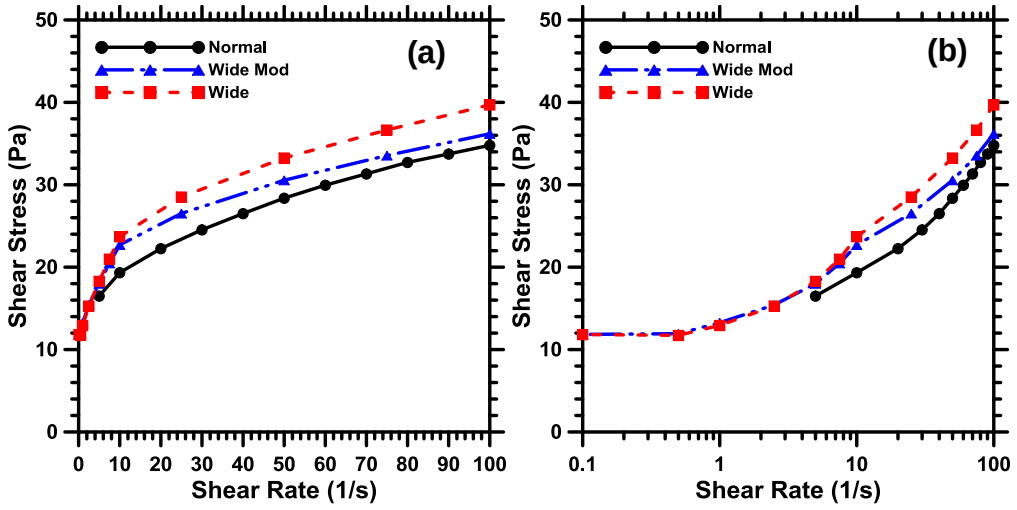

Figure 7-9: Investigations of shear stress offset using a "modified-wide" experiment on: (a) linear scale, and (b) logarithmic scale. The "modified-wide" evaluation is constructed by combining the "normal" and "wide" shear evaluation regimes.

The Bingham model has been shown to be applicable only over a limited range of shear rates (Barnes 1999; Bingham 1922), below which the shear rate-shear stress response becomes non-linear, as indicated by a downward curvature of the dataset, when the model breaks down. As such, its applicability to cementitious suspensions (Figures 7-5 to 7-8 and [5,23]) is clearly unreliable. The linear portion of the relationship between shear stress and shear rate, where the Bingham model is applicable, has been proposed to be similar to Region III in a typical creep curve (Barnes 1999), as shown in Figure 7-10(a). When low shear rates, typically below 1/s are used, as is the case in the "wide" and "low" ranges in Figures 7-6 to 7-8, a zone corresponding to a portion of Region II (i.e., constant shear stress with increasing shear rate – secondary creep) also emerges. Theoretically, if local particle densities were maintained in such a way that the shear bands remained intact at yet lower

shear rates – on the order to 10^{-3}-to-10^{-4} (below the torque limit of the rheometer), these rheological curves would take a form similar to that presented in (Barnes 1999) for Cheng's yield stress material (Cheng 1986) where Regions I-III are evident – i.e., the material changes from a Newtonian behavior through a power-law type region to another Newtonian-like behavior (Barnes 1999) with increase (or decrease) in shear rate.

In Figure 7-10(a), a portion of Region II is constructed using data from the wide shear rate measurements (solid circles) for 10% 3 μm limestone modified suspensions, while the remaining data (open circles) is estimated as noted in (Barnes 1999). Thus, if a portion of Region II is captured in addition to Region III by measuring the response at low enough shear rates (i.e., over a shear rate range of 0.1-to-100/s instead of 5-to100/s (Cheng 1986)), then the asymptotic value (i.e., 46 Pa in Figure 7-10a) can be considered to be representative of the dynamic or "apparent" yield stress of the material. The "wide" shear rate range considered in this study satisfies this criterion as it includes enough of Region II that the asymptotic yield stress value can be determined. Clearly, the yield stress (61 Pa) is overestimated by the Bingham model, due to the rheological response not being determined at low enough shear rates. The effects of H-B and Casson models will be discussed later in the paper.

To explore if the plateau region in the rheological response is particle independent, "wide" shear rate range rheological experiments were conducted using suspensions of the following materials: Type II/V cement, interground limestone cement, fly ash, and a steel slag. The $(w/s)_v$ ratios were varied so as to obtain a suspension that was stable, and not prone to overflow or segregate under applied shear. The shear stress-shear rate response for all these suspensions are shown in Figure 7-10(b). It is noted that, regardless of the

particle type, the shear stress plateau (Region II) which is indicative of the apparent yield stress is visible. In fly ash-water and slag-water suspensions, the plateau is present, but at very low shear rates, the shear stress tends to further increase, indicating a flow instability identified by the formation of shear bands (Olmsted 2008; Schall and van Hecke 2009). As presented, this curve is applicable for the *ramp down* of shear rates, and hence it is proposed that this behavior is indicative of the destruction of the shear bands that were formed at higher shear rates. This supports the idea that in suspensions with this behavior, the interparticle forces are insufficiently high, to prevent particles from settling into the region of shear band formation, increasing local particle density and thereby increasing the measured shear stress. However, the presence of a shear stress plateau in each of these suspensions provides: (1) a direct method for the accurate estimation of apparent yield stress and (2) indicates that this shear stress plateau response, is a generalized phenomenon.

Figures 7-6 to 7-8 illustrate the experimental independence of plastic viscosity irrespective of the shear rate range of the experiment. For example: the slopes of the shear stress-shear strain relations in Region III, irrespective of the shear history, are around 0.20 Pa.s, thus indicating that the plastic viscosity remains independent of the experimental methodology selected. As the three shear rate ranges (i.e., “normal”, “low”, and “wide”) impart different shear histories to the suspension, this shows that beyond a point, the rate of increase in stress with increase in strain (plastic viscosity) is reasonably independent of shear history.

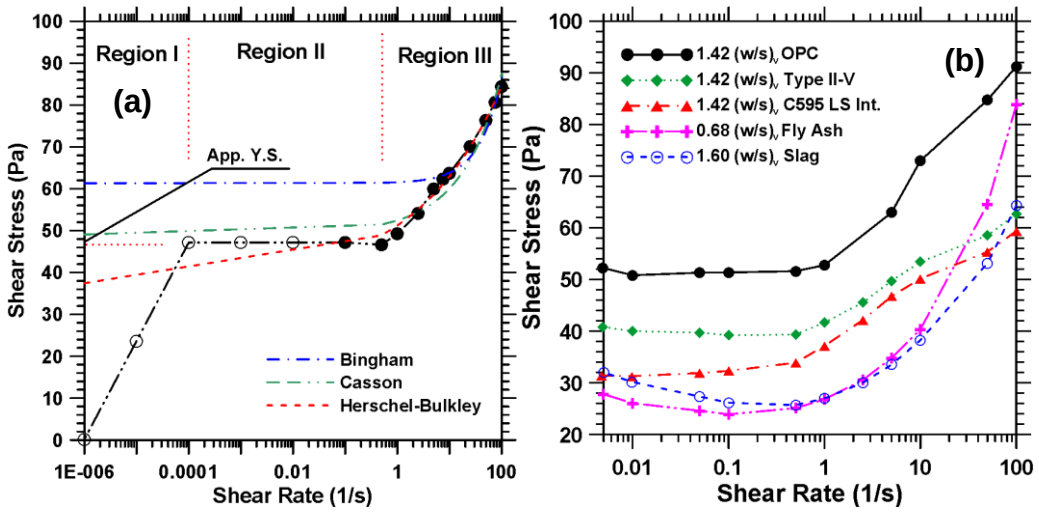

Figure 7-10: (a) The predicted shear rate vs. shear stress response extrapolated from data in Figure 7-9. Closed circles are measured data, open circles are extrapolated values. Results of the Bingham model are fit over the shear rate range of 5-100/s, and the Herschel-Bulkley and Casson models are fit over the shear rate range from 0.1-100/s and (b) shear stress-shear rate response for a number of particulate suspensions composed in water (three types of cement, fly ash, and slag) to demonstrate the existence of a stress plateau at low shear rates for various suspensions.

The apparent yield stress can be better identified using a viscosity-shear stress plot (see Figure 7-11), wherein the apparent yield stress is the point at which the viscosity drastically increases without any concomitant increase in stress, i.e., a value which is equal to that noted leftmost end of the stress plateau shown in Figures 7-6 to 7-8. It should be noted however, complications in precise identification of this point which indicates the yield stress and the lack of models to fit a wide enough range of the shear response have led to a series of deliberations on the applicability of yield stress to particulate suspensions (Astarita 1990; Evans 1992; Hartnett and Hu 1989; Barnes 1999; Barnes and Walters 1985; Cheng 1986).

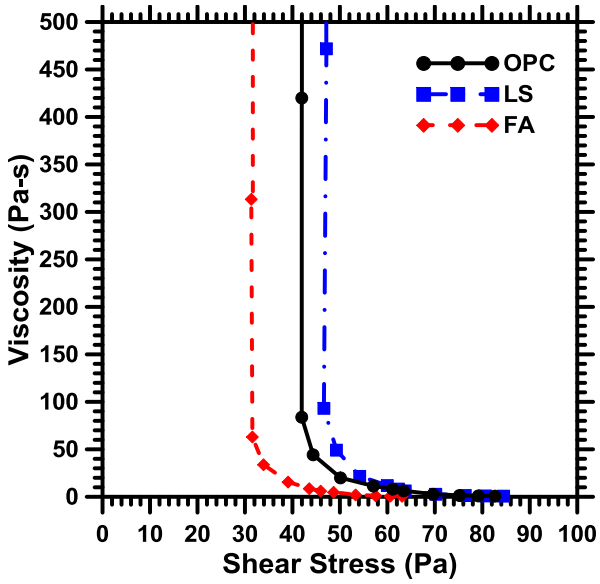

Figure 7-11: Viscosity-shear stress relationships for the suspensions evaluated, to illustrate the apparent yield stress.

7.3.4.2 Rheological Model Effects

To allow for a concise discussion of the influences of rheological models, the results of the "wide" shear rate range (0.1-100/s) experiments are re-plotted in Figures 7-12(a)-(c) for: (i) the OPC suspension, and the suspensions containing (ii) 10% of 3μm limestone and (iii) 10% of fly ash. Once again, the Bingham model is fit to the linear portion of the "wide" shear rate dataset (from 10-to-100/s), whereas the H-B and Casson models are fit to the entire shear rate range, i.e., from 0.1-to-100/s. The fit parameters and the apparent yield stress corresponding to the stress plateau are also denoted in the figures for all suspensions.

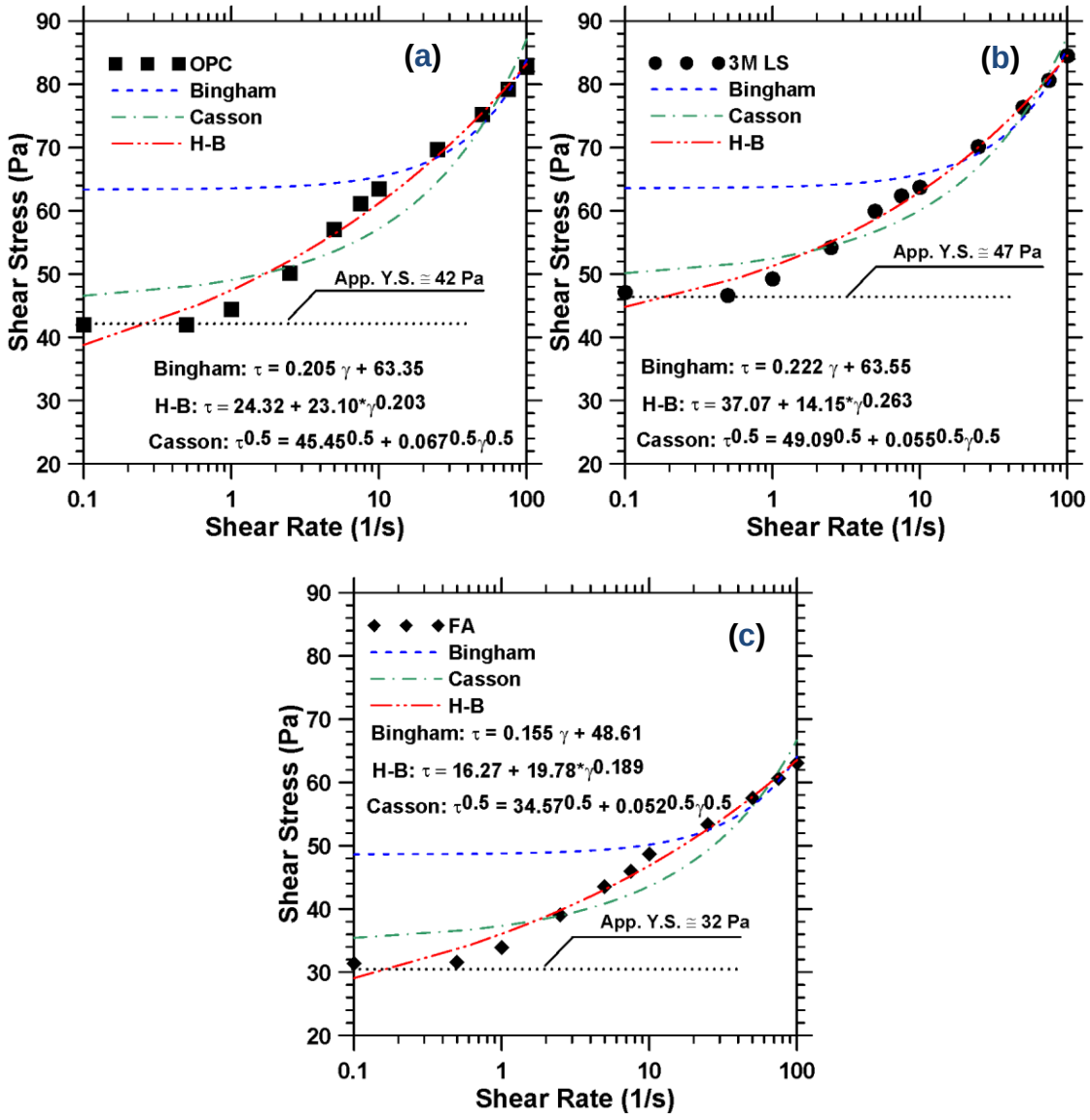

Figure 7-12: The influence of selected rheological model using "wide" shear rate range data on the estimated yield stress for: (a) OPC-water suspension, (b) 10% 3 μm limestone containing suspension, and (c) 10% fly ash containing suspension.

It is noted that the Bingham model significantly overestimates the apparent yield stress. The extent of overestimation is suspension specific, ranging from 35% for the limestone system to 50% for the fly ash and OPC systems. In general, the Casson model estimates the apparent yield stress accurately, though the quality of the fit as indicated by the R^2 value is poorer than the other models considered. Further, the second parameter in the

Casson model, i.e., η_∞, is not expected to be useful for cementitious suspensions given the lower bounds of shear rates experienced in practical applications (Ferraris 1999b). The Herschel-Bulkley model underestimates the yield stress for all suspensions to varying degrees: by approximately 40%, 20% and 50% for OPC, limestone, and fly ash systems respectively. Also, while the Herschel-Bulkley model provides a good fit to the data over the selected shear rate range and with the highest R^2 values of all models considered, concerns do exist. For example: a visual observation of the fits in Figure 7-12 shows an adequate match of the H-B model with the data including the Y-intercept (yield stress), however, when the model parameters are considered, the underestimation of yield stress is significant and on the order noted above. In general, it can be concluded that the true asymptote that is representative of the apparent yield stress lies between the τ_0 values predicted by the Bingham and H-B models.

To determine if the predictive capability of the H-B model could be improved, a series of experiments were conducted over a yet wider shear range rate (0.005-to-100/s) to better capture the stress plateau (Region II). Expectedly, the apparent yield stress predicted by the H-B model was shown to be refined by the addition of more data in the lower shear rate range. For example, the H-B yield stress was within 5% of the true asymptotic value for the case of OPC suspension. Moreover, increasing the number of data points obtained in the stress plateau (i.e., when much lower shear rate ranges are used), results in better the estimation of yield stress according to the H-B model. This shows that the use of H-B model to estimate yield stresses is unreliable when insufficient data in the lower shear rate range (significantly beyond the linear shear rate-stress response) is available, and the improved accuracy of this model in predicting the apparent yield stress is attributed

primarily to the statistical weighting resulting from including additional data at low shear rates. This is a significant aspect to consider if the H-B model is to be applied to estimate the rheological properties, in a comparative or absolute sense of cementing systems.

It is furthermore noted from Figure 7-12 that the influence of limestone incorporation on yield stress is different when different models (Equations 7-1 to 7-3) are used. The incorporation of 3μm limestone is shown to have a negligible effect on yield stress as compared to the OPC suspension when the Bingham model is used. However the apparent yield stress determined from the stress asymptote and the yield stresses estimated from the Casson and Herschel-Bulkley models are higher. In the case of fly ash modified suspension, all the models as well as the experimental asymptotic values show a decrease in yield stress when compared to the OPC paste, which is the trend expected due to the spherical nature of fly ash particles that enhance the fluidity of the suspension.

Thus and in general, the foregoing discussions illustrate the influence of a given rheological models on determining the flow characteristics of cementing suspensions and emphasize the effects of model selection and experimental parameters on the applicability, precision and reliability of a given model. This is significant, as erroneous selections can result in considerable imprecisions in yield stress determinations, though to a lesser extent in the case of plastic viscosity. Further, it illustrates that the yield stress determined from the Bingham model is likely not a true flow parameter, rather it is an artifact of model-based and experimental limitations. As such, its application may lead to incorrect conclusions when used in comparative studies of cementitious suspensions.

7.4 Applicability of Rheological Models in Fly Ash Geopolymer Suspensions

Rheological models such as Bingham, Herschel-Bulkley, and Casson, are commonly used to extract the rheological parameters of significance for cementitious systems. In order to use these models, it is critical that an understanding of their influences and applicability be confirmed. The aim of this section is to determine the applicability of the above mentioned models to fly ash based geopolymer systems. This work employs a similar approach as used previously with portland cement suspensions. In these studies, the Bingham (or Newtonian) model was fit to the linear portion of the "wide" shear rate data (shear rates ranging from approximately 5-to-100/s), while for Casson and Herschel-Bulkley models, the data was fit over the full range of the "wide" shear rate data. Figures 7-13 to 7-15 show the results of this analysis for various mixture constitutions of fly ash geopolymer suspensions.

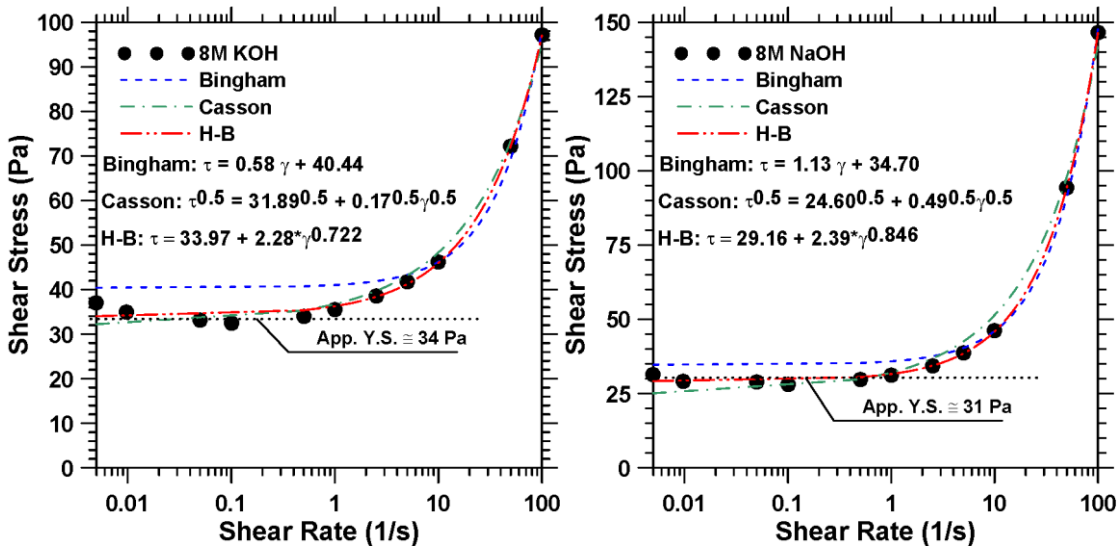

Figure 7-13: Investigation of model applicability for 0.35 $(a/p)_m$ hydroxide geopolymer suspensions: (a) 8M KOH, and (b) 8M NaOH.

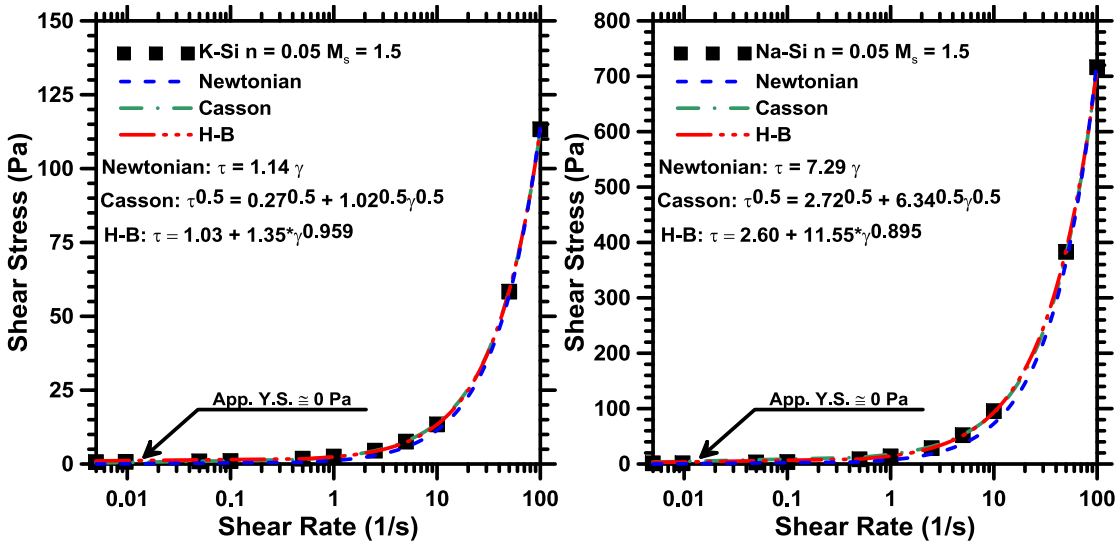

Figure 7-14: Investigation of model applicability for 0.20 $(a/p)_m$ silica hydroxide geopolymer suspensions with n = 0.05 and M_s = 1.5 : (a) potassium (b) sodium

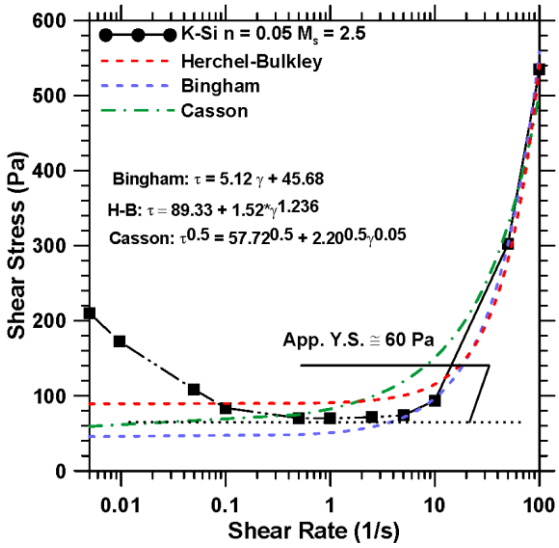

Figure 7-15: Investigation of model applicability for 0.20 $(a/p)_m$ potassium silicate geopolymer suspensions with n = 0.05 and M_s = 2.5

As can be seen from Figure 7-15, the hydroxide based geopolymer fly ash suspension, the Bingham model overestimates the apparent yield stress, although to a much lesser extent than OPC, while both Casson and Herschel-Bulkley models tend to predict it reasonably well. It is notable, however, that these models are fit to a wide range of shear rates, so the range of shear rates used needs to be considered when using a rheological model. The

coefficients of determination of all of the fits in Figure 7-15 were above 0.95, indicating that over the selected shear range all of the models provided a reasonable fit to the data. Based on these results, given that the shear rate range includes an appropriate number of points on the stress plateau, either the Herschel-Bulkley or the Casson model would be appropriate for the determination of yield stress. It is notable, that neither of these models provide an estimation of plastic viscosity, which may be a good indicator of the flowability of a suspension, thus given the shear rates commonly experienced by cementitious systems in mixing, determination of plastic viscosity (slope of the line) over the linear portion of the "wide" data is proposed to be a reasonable method for determining plastic viscosity.

7.5 Conclusions

This paper has presented a detailed study on the influence of experimental parameters and models on the rheological response of cement suspensions. The major findings of this study are:

- An increase in the Bingham yield stress and decrease in plastic viscosity was observed with increasing gap, attributable to changes in the local particle density and influence of increased particle contacts with the shearing surface. Increasing surface roughness (i.e., for the range studied), resulted in little change in the Bingham yield stress and increasing plastic viscosity.
- The shear history imparted to the paste through mixing was found to significantly influence the yield stress and plastic viscosity. With increasing mixing intensity, the plastic viscosity was noted to decrease due to the effectiveness of the mixing procedure in reducing the tendency of agglomeration in the paste.

- Modifying the shear rate range in the rheological experiments to include more data points at lower shear rates (0.5/s) revealed the existence of a well-defined shear stress plateau. This corresponds to a drastic increase in apparent viscosity with minimal increase in stress, and this value of the shear stress is recommended to be used as the apparent yield stress of the suspension. Significantly, such evaluations facilitate the model-less extraction of yield stress. However, plastic viscosities estimated as the slope of the line fit to the linear region of the shear stress-shear rate stress response were noted to be less influenced by shear rate effects.
- The influences and artifacts of the rheological model used in extraction of the apparent yield stress are highlighted. When compared to the value at the stress plateau, the Bingham and H-B models, overestimate and underestimate respectively, the apparent yield stress of a given cementitious suspension. The prediction of the Casson model was noted to be more accurate, but at the cost of a slightly poorer mathematical fit to the rheological dataset. The yield stress estimated by H-B model was found to be comparable to the (true) apparent yield stress noted from the shear stress asymptote when rheological evaluations were extended to much lower shear rates. This improvement is a function of the statistical weighting in the least squares fit, rather than an indicator of the H-B model to comprehensively estimation the flow response.

8. RHEOLOGICAL EVALUATION OF INTERGROUND AND BLENDED LIMESTONE-PORTLAND CEMENT SUSPENSIONS

8.1 Introduction

There continues to be a growing interest in the use of limestone as a cement replacement material to enhance portland cement concrete sustainability, acting as a filler by increasing particle packing and offsetting unhydrated cement in low water-to-cement concretes (V. Bonavetti et al. 2003), a location for cement hydration product nucleation (Caldarone and Zemajtis 2008; D. Bentz et al. 2009a; Hawkins, Tennis, and Detwiler 2003), and reacting to some extent with the aluminate phases in cements (De Weerdt, Haha, et al. 2011; Lothenbach et al. 2008). There are currently two strategies for replacing limestone by portland cement: (i) intergrinding the limestone with the clinker in a ball mill and (ii) mechanical mixing or blending of the cement with limestone. Blending of the limestone with portland cement will maintain the particle size distributions of the limestone and the portland cement in the composite mixture, while intergrinding limestone with portland cement clinker will result in a composite system where the two phases have differing particle size distributions. As limestone is known to be a softer material than clinker, intergrinding results in a limestone phase that is less fine than the clinker phase (Tsivilis, Voglis, and Photou 1999; Ludmilla Opoczky 1996), while blending will produce a PLC mix with a particle size distribution that is an average composition of the components included. Several studies have investigated the influence of limestone on the rheological performance of portland cement suspensions, including (Sakai et al. 2009; Mikanovic and Jolicoeur 2008; Hedda Vikan and Justnes 2007), and the work completed in Chapter 6. These studies have investigated the influence of fineness, superplasticizers, and

replacement ratio on the rheology of these systems. However, due to the fact that the limestone sizes that are either coarser or finer than OPC, the behavior of limestone in these systems is difficult to discern as it is confounded with the effects of changes in particle surface area and particle packing.

The current study aims to disconnect these two effects in exploring the exact nature of limestone in cementitious suspensions. Particle size distribution matched limestone is used in this study to minimize or eliminate these effects, making the exact influence of limestone on rheological performance clear, as well as allowing for the determination of causation of these effects. Rheological characterization of cementitious suspensions is commonly completed using strain or stress growth experiments, resulting in flow diagrams of the cement. From these diagrams, key rheological parameters such as apparent yield stress and plastic viscosity are extracted. The apparent yield stress is indicated by a non-zero stress at a zero strain rate and the plastic viscosity is a measure of the strain rate increase required for a unit increase in stress. The current work determines the apparent yield stress using the stress plateau method presented in (Barnes 1999) and in Chapter 7, and the plastic viscosity from the linear portion of the flow curve. The apparent yield stress has been shown to be primarily influenced by particle effects, such as jamming, particle spacing, surface area and roughness (D. P. Bentz et al. 2012; Erdoğan et al. 2008) and Chapter 6, and interparticle dispersion forces (van der Waals and electrostatic repulsive forces) (Flatt 2004; Mikanovic et al. 2006). The interaction potential between particles in a colloidal suspension is governed by DLVO theory (named for Derjaguin, Landau, Verwey, and Overbeek), which states there are competing effects of electrostatic repulsive forces. Electrostatic repulsive forces originate from the adsorbed ions in the diffuse layer of the

electric double layer (EDL). Wherein the EDL is defined by an inner stern layer of tightly held ions with opposite charge of the surface of the particle and the more weakly held ions in the diffuse outer layer with ions with the same charge as the particle surface. The electrostatic repulsive effects have been shown to be proportional to $\exp[-\kappa(r-2a)]$ (Hunter and White 1987; Neubauer, Yang, and Jennings 1998), where r is the distance from the center of the particle, κ is the Debye length, and a is the particle diameter. Van der waals forces, on the other hand have been shown to be proportional to $1/r^2$, and thus do not fall off as quickly as electrostatic repulsive forces. Further, it is noted that van der Waals forces between the same material are always attractive, while between two different materials they may be repulsive. Above a certain particle concentration, called the coagulation limit, the effect of the attractive forces dominate over the electrostatic repulsive forces, and it has been shown the cementitious suspensions are commonly above this limit (Neubauer, Yang, and Jennings 1998; Yang, Neubauer, and Jennings 1997). Though cementitious suspensions have larger particles than would generally be considered colloidal, the DLVO theory is likely still applicable. Further, the influence of Brownian motion in cementitious suspensions is likely minimal due to the relative size of the particles present in the suspension. The plastic viscosity, on the other hand, is more strongly influenced by solid loading and particle separation, as it is a measure of resistance to flow once it has commenced.

8.2 Experimental Program

8.2.1 Materials

Two Interground PLCs were used in this study, one conforming to ASTM C1157 ("ASTM C1157/C1157M-11 Standard Performance Specification for Hydraulic Cement" 2013) and

the other to ASTM C595 ("ASTM C595/595M-13 Standard Specification for Blended Hydraulic Cements" 2013) with the former being the finer of the two. The control portland cement used in this study was Type I/II, conforming to ASTM C150 ("ASTM C150 / C150M - 12. Standard Specification for Portland Cement" 2012), which was the parent cement used to generate the interground PLCs. Additionally, limestone of four different median particle sizes (0.7, 3, 10, and 15 μm) were used in this study to generate the blended mixes. The purity of the limestone used in this study is greater than 95% $CaCO_3$. A class F fly ash was used to investigate the flow characteristics of ternary blends of these systems. The compositions of these materials are presented in Table 8-1.

Table 8-1: Oxide composition of experimental materials, and material median particle size

Material	**SiO_2**	**Al_2O_3**	**Fe_2O_3**	**CaO**	**MgO**	**SO_3**	**D_{50}**
OPC (ASTM C150)	19.60	4.09	3.39	63.21	3.37	3.17	12.4
PLC (ASTM C595)	18.57	3.80	2.99	63.87	2.93	3.15	11.3
PLC (ASTM C1157)	18.57	3.84	3.11	63.59	3.38	3.23	8.3
Fly Ash (ASTM C	58.40	23.80	4.19	7.32	1.11	0.44	19.9

The particle size distributions (PSDs) of the raw materials used in this study are presented in Figure 8-1. OPC-limestone blends were prepared to match the PSDs of the two PLCs and the parent OPC, using the same limestone replacement ratio as in the PLCs (11.1% by mass; 13.8% by volume). A least-squares fitting and error minimization procedure was adopted to obtain the amounts of limestone particles of each median sizes required to match the PSD curves of the OPC or PLCs. The PSDs (both cumulative and differential) of these blended systems as compared to the PLC or OPC they are matched with are presented in Figure 8-2. It is notable that the blended mixtures were able to reasonably match the size

distribution of the interground material except for the case of the C1157 PLC, where the interground material is notably finer than the blend.

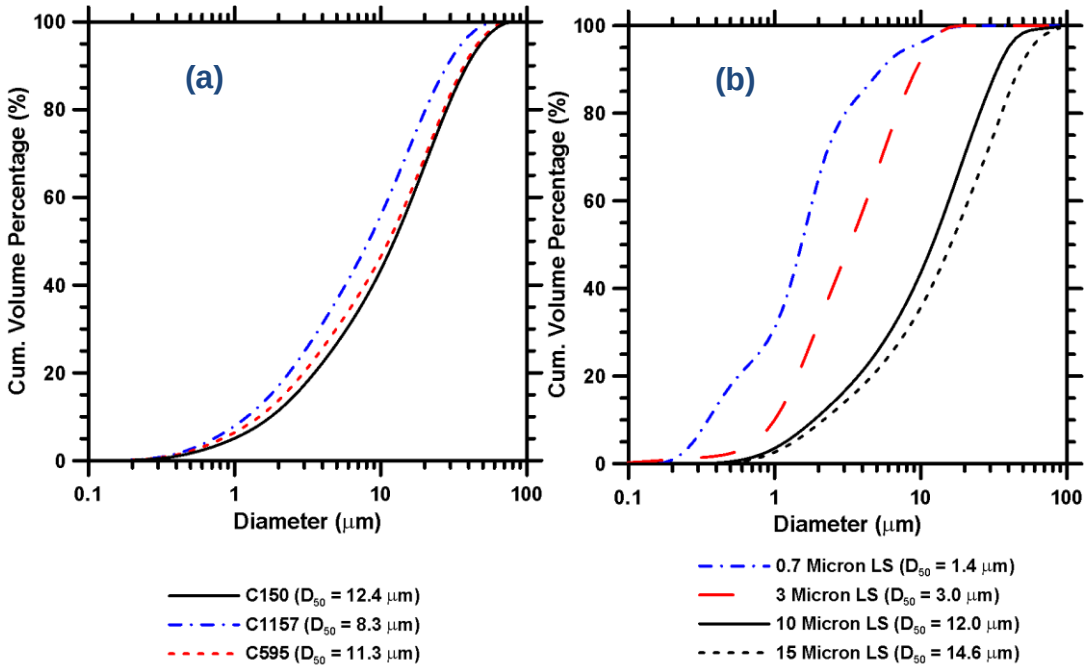

Figure 8-1: Particle size distribution of (a) cements, and (b) limestones used in this study.

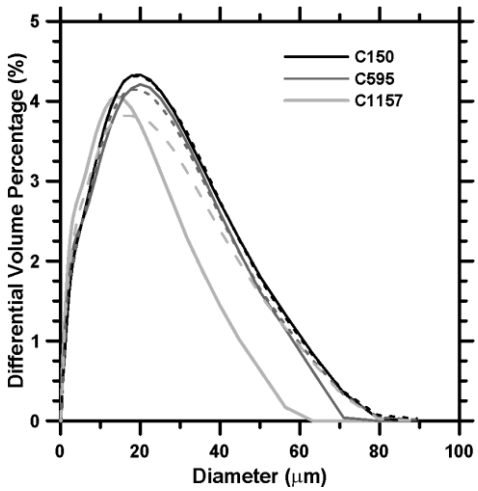

Figure 8-2: Particle size distribution interground limestone-cements (solid lines) as compared to blended mixes (dashed lines).

8.2.2 Experimental Parameters

Suspensions were prepared using a constant volumetric water-to-solids ratio (w/s) of 1.42, which corresponds to a mass based w/s ratio of 0.45 for OPC suspensions, and a slightly higher mass-based w/s for blends of limestone or fly ash due to the lower specific gravity of these replacement materials. The constant volumetric ratio was used as the flow behavior of concentrated suspensions is heavily influenced by the volume fraction of solids (Chong, Christiansen, and Baer 2003; Jeffrey and Acrivos 1976). The specimens were mixed in accordance with ASTM C1738 ("ASTM C1738 - 11a. Standard Practice for High-Shear Mixing of Hydraulic Cement Paste" 2011), using a low shear rate of 5000 RPM for initial mixing, followed by a 30 second period at a high shear rate of 12000 RPM, a two minute covered rest period, and a 90 second final mixing at the high shear rate.

Two different rheological experiments were conducted as part of this study, the first a typical shear rate ramp study similar to the one developed in Chapter 7, using the parallel plate configuration, and the second a stress growth, low-amplitude oscillatory shear study using a concentric cylinder configuration. Both studies were completed with a TA Instruments AR 2000EX stress controlled dynamic shear rheometer, and rheological parameters (stress, strain rate, storage modulus, and loss modulus) were extracted using the TA Instruments Trios software package. The shear rate ramp study was conducted using a 50 mm parallel plate configuration with the Peltier plate conditioned to a surface temperature of 25±0.1 °C. The surface of the upper geometry was serrated to a depth of 1mm and the surface of the lower geometry (Peltier cover plate) was serrated to a depth of 0.15 mm to prevent slip at the shearing surface. Slip causes local particle concentration changes near the shearing surface, potentially resulting in significant underestimation of

the rheological properties (Mannheimer 1983; Saak, Jennings, and Shah 2001). The gap between the upper and lower plates was set to 2 mm, as this was found to achieve good results as indicated in Chapters 6 and 7. The oscillatory shear study was performed using a concentric cylinder configuration with a constant gap between the surface of the bob and cylinder of 1.07 mm. The surface of the bob and cylinder were grit-blasted to minimize the effects of slip.

The experimental procedure used in the shear rate ramp experiment consists of a step-up pre-shear to homogenize the sample, followed by a ramp-up and ramp-down of shear rates. Data acquisition was completed during only the final ramp-up and ramp-down phases of the study, while only the data from the down-ramp portion was used for the extraction of rheological parameters used in this study. A graphical representation of the experimental sequence is presented in Figure 8-3. The range of shear rates used in this study were from 0.005/s to 100/s, with three points investigated per decade. At each step, data is collected every second. Each step was terminated once a steady state has been achieved, as indicated by a difference in torque of less than 5% over 5 consecutive readings, with a maximum step length of 10 seconds. The typical duration of the rheological experiment was 3 minutes, while the total duration of the experiment from water addition to completion was approximately 7 minutes. This experimental scheme minimizes the experimental duration; as cement hydration is a time-dependent process, minimal experiment duration is crucial to allow for the assumption that minimal dissolution and hydration occurs during the experiment. The oscillatory shear experiment consisted of a stress growth experiment beginning at a stress of 0.001 Pa and ending at 50 Pa, at a constant oscillatory frequency of 1 Hz, with the ending stress determined based on the maximum yield stress as

determined from the parallel plate rheological studies to approximate the linear viscoelastic regime of the material.

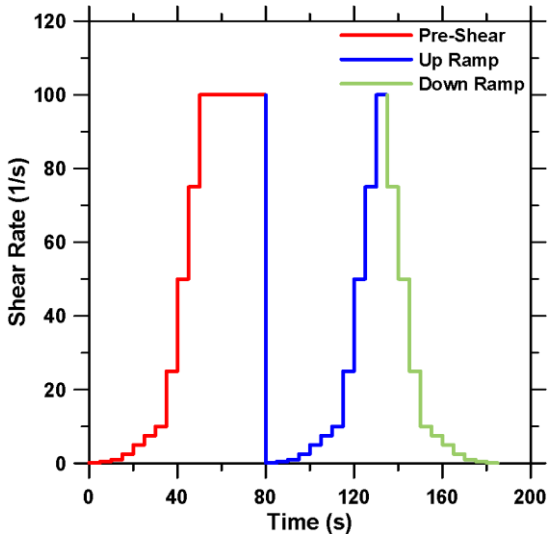

Figure 8-3: The Rheological Procedure for Shear Ramp Study

Rheological parameters (apparent yield stress and plastic viscosity) for the shear strain rate growth experiment were extracted using the method presented in Chapter 7. The yield stress is determined as the stress value indicated by the stress plateau, and the plastic viscosity is determined as the slope of the best fit line for the linear portion of rheological data above a strain rate of 5/s. This method was shown to be more consistent than using any of the commonly used rheological models such as Bingham or Herschel-Bulkley for cementitious suspensions. A typical flow diagram showing the parameter extraction methodology is presented in Figure 8-4.

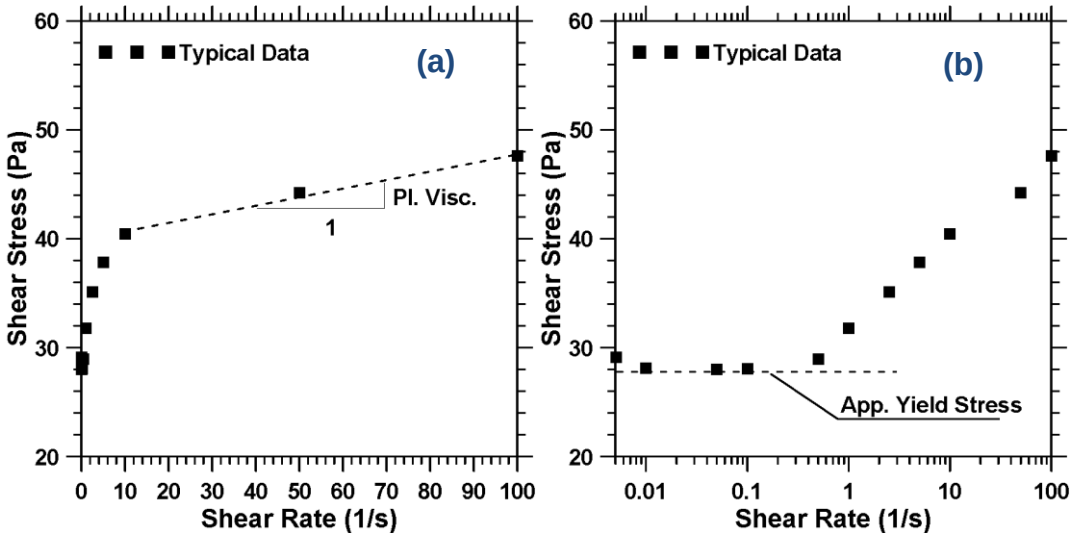

Figure 8-4: Method of rheological parameter extraction used in shear ramp study

8.3 Results and Discussions

8.3.1 Rheological Response of Portland Limestone-Cement Blends

This section describes the results of the study on the influence of different levels of PSD-matched limestone replacement on the rheological behavior of portland cement suspensions. The PSD-matching approach allows the effects of particle packing and arrangement to be discounted, thereby facilitating a more unbiased investigation of the nature of limestone in these suspensions. Figure 8-5 shows the shear rate-shear stress and shear rate-apparent viscosity (flow curves) relationships for the suspensions constituted of OPC and OPC-limestone blend where 11% of OPC (by mass) is replaced by PSD-matched limestone.

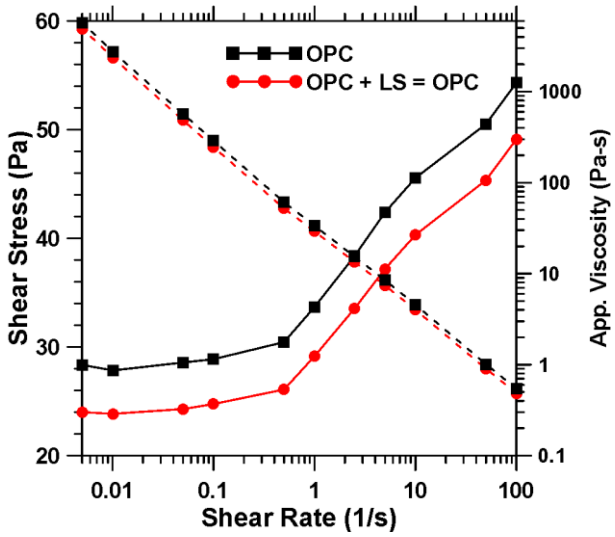

Figure 8-5: Representative flow curves for OPC and OPC-limestone suspension (OPC replacement by PSD-matched limestone 11.8% by mass)

Immediately noted from this figure is the fact that the inclusions of PSD-matched limestone in a portland cement suspension induces minimal changes on the plastic viscosity (as noted by the nearly parallel lines in Figure 8-5, and a reduction in the apparent yield stress of about the same magnitude as the volumetric limestone replacement level in the system. The rheological performance of portland cement suspensions has been shown to be strongly influenced by solid loading, fineness and the size distribution of the particles (D. P. Bentz et al. 2012) and Chapter 6, and the surface interaction between cement particles. As discussed previously dispersion (van der Waals) forces exist between cement particles, and above the coagulation limit will dominate over electrostatic repulsive forces (Lesko et al. 2001; Gmira et al. 2004; Flatt 2004). Aqueous suspensions of calcium carbonate at a high pH have similarly been shown to develop large dispersion forces, indicative of coagulation (Mikanovic et al. 2006). The minimal changes in plastic viscosity in this system suggest that these dispersion forces are less significant in the flow of suspensions once sufficient flow has been initiated. This concept can be intuitively confirmed by

considering the negligible influence of superplasticizers on the plastic viscosity of portland cement suspensions (Banfill 2006), where the adsorption of superplasticizers on the surface of cement particles result in a decrease in interparticle attractive forces, decreasing the apparent yield stress but resulting in minimal changes in the plastic viscosity. The slight influence of superplasticizers on plastic viscosity in portland cement suspensions is attributed to the destruction of agglomerations which releases water so as to be available to enhance fluidity (Sakai et al. 2009). Thus, plastic viscosity, which is a measure of the rate of resistance to flow as the strain rate is increased, would be expected to be more heavily influenced by the nature of the suspending fluid and the solid fraction and size distribution of the particles present (D. P. Bentz et al. 2012; Grzeszczyk and Lipowski 1997). As the particle size distribution and solid loading are equivalent in the mixtures considered here, the plastic viscosity is not significantly influenced by the inclusion of limestone.

The apparent yield stress, on the other hand, is a measure of the resistance to initiate flow, and is thus more strongly influenced by dispersion and jamming forces. Rheological behavior of cementitious suspensions have been shown to depend significantly on the interparticle spacing of cement grains (D. P. Bentz et al. 2012), which would have a direct effect on the magnitude of the forces listed above. Increasing the spacing by the inclusion of a higher volume of water or a reduction in surface area more significantly decreases the electrostatic repulsive forces as compared to van der Waals dispersion forces, thereby increasing the interparticle attractive forces between cement particles, resulting in a reduction in the apparent yield stress. Thus, it is proposed that, as smaller volumes of PSD-matched limestone replaces cement in the suspension, the magnitude of the dispersion

forces between limestone and cement are lower than those between the cement particles. The limestone thus acts to increase the interparticle spacing between cement grains, reducing the interparticle attractive forces and thereby decreasing the apparent yield stress.

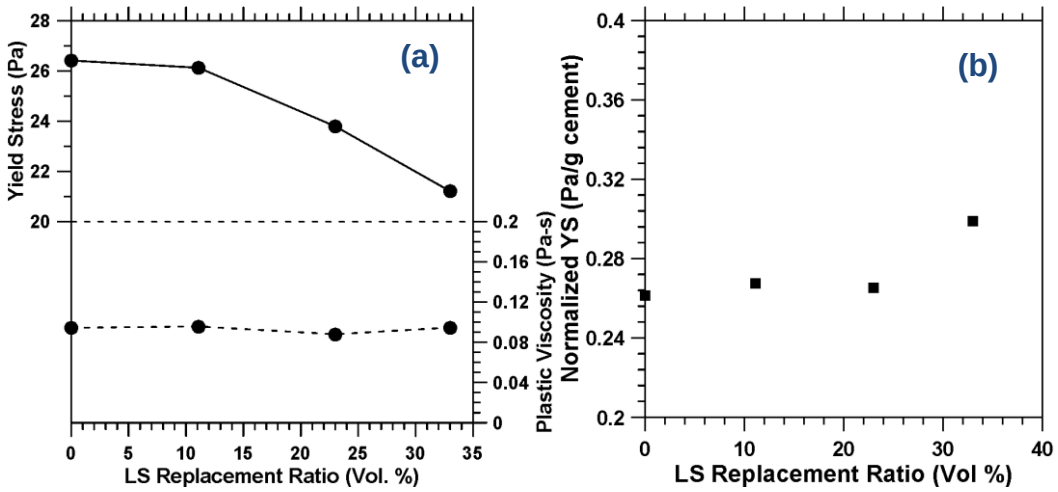

Figure 8-6: Influence of the content of PSD-matched limestone on determined rheological properties of the suspension.

To further investigate the influence of varying levels of PSD-matched limestone on the rheological properties of portland cement suspensions, a study was performed at additional PSD-matched limestone contents of 23 and 33% by volume (20 and 30% by mass) while maintaining the same volumetric water to solids ratio of 1.42. Figure 8-6(a) depicts the apparent yield stress and plastic viscosity of these suspensions as a function of the PSD-matched limestone content in the system. Noted from this figure is a similar influence as seen in Figure 8-5, with a constant plastic viscosity regardless of the limestone content (within the range of replacement studied) and a continuing decrease in apparent yield stress as the limestone content is increased. This supports the idea that plastic viscosity is more heavily influenced by the particle size distribution and the surface area of particles present in the suspension. Even as more limestone replaces cement in the suspension, the composite PSD and the specific surface areas remain relatively unchanged, resulting in

unchanged plastic viscosity. The apparent yield stress, on the other hand, is more strongly influenced by dispersion forces between cement particles. These results support the discussions above, wherein the van der Waals forces between limestone and cement particles are significantly lower than those between cement particles, and thus increasing the limestone content in the suspension at a constant solid loading with an unchanged PSD results in a continued reduction in interparticle forces, and subsequent reduction in the apparent yield stress.

Figure 8-6(b) shows the yield stress of these suspensions normalized by the mass of cement and plotted against the volumetric limestone content. The normalized yield stress is found to remain relatively constant at lower limestone contents, but increases as the replacement level increases beyond a certain value. At low OPC replacement levels, cement-cement and cement-limestone particle contacts would likely dominate. The unchanged normalized yield stresses at lower replacement levels supports the idea that interparticle attractive forces between limestone and cement particles is likely negligible as compared to those between cement particles. However, as the limestone content increases further, limestone-limestone contacts become increasingly prevalent. It has been shown that suspensions of limestone result in similar dispersion forces as suspensions of cement (Mikanovic et al. 2006), and when the limestone-limestone contacts in the suspension become more prevalent, the normalized apparent yield stress increases.

8.3.2 Comparing the Rheological Parameters of Interground PLC and PSD-Matched OPC-Limestone Blends

8.3.2.1 Yield Stress and Plastic Viscosity

Rheological studies were performed on the interground PLCs and PSD-matched OPC-limestone blends as presented in Section 8.2. The blends were proportioned to match the PSD of the parent OPC and both the interground PLCs (Figure 8-2) with the same volumetric OPC replacement level as the interground PLCs (13.8% by volume). The interground PLCs represented here are the limestone cements directly obtained from the manufacturer while the blended systems are obtained by blending the parent OPC used to produce the interground PLCs with limestone of different median particle sizes so as to match the PSDs of the respective PLCs. The rheological parameters (apparent yield stress and plastic viscosity) were extracted using the methodology presented in Section 8.2 are shown in Figure 8-7.

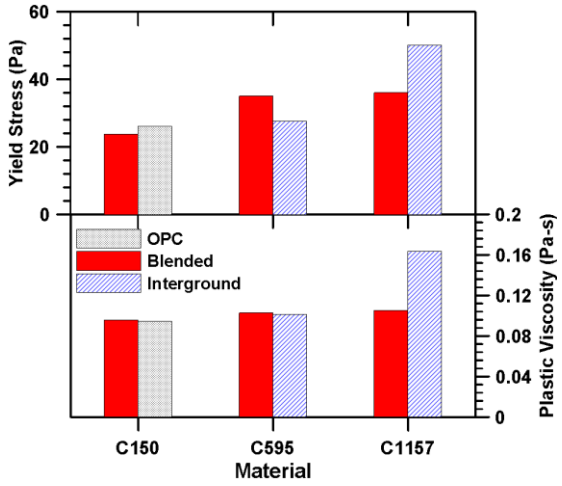

Figure 8-7: Yield stress and plastic viscosity of the PLC suspensions along with those of PSD-matched OPC-limestone blends corresponding to pure OPC and the PLCs.

Several important observations can be made from this figure: (i) the plastic viscosity is approximately constant regardless of whether the mixture is blended or interground, with the exception of the interground C1157 PLC suspension, (ii) the interground C1157 PLC suspensions have both higher apparent yield stress and plastic viscosity, and (iii) the C595 blended suspension has a higher apparent yield stress as compared to the corresponding interground PLC suspension.

The first two phenomena can be explained as follows. The constant plastic viscosity across all C150 OPC suspensions (the parent OPC and the equivalent blended system) and C595 PLC and the equivalent blended systems as well as the blended suspension equivalent to C1157 PLC is due to the similar PSD and specific surface area as presented in Figure 8-2 and Table 8-1 respectively. As discussed previously, consistent PSDs and specific surface areas yield consistent plastic viscosity results if all the other experimental variables are held constant, attributable to the constant water film thicknesses around the particles in these suspensions. Achieving a reasonable PSD match with the finer C1157 interground PLC was not possible with the sizes of limestone used in this study, as discussed in Section 8.2. Thus the finer C1157 interground suspension shows a higher plastic viscosity as compared to the other suspensions. The finer interground mixture has a larger surface area than the corresponding blended mixture which is coarser, resulting in a decrease in water film thickness and subsequent increase in plastic viscosity. The higher fineness of the C1157 PLC similarly results in a significant increase in apparent yield stress for this suspension as compared to the other suspensions. The increased fineness decreases particle separation, which increases dispersion forces, and consequently the apparent yield stress.

These results are similar to the observations on the influence of the fineness of limestone powder on OPC suspension rheology which has been reported in detail in Chapter 6.

The third observation, i.e., the C595 PLC suspension has a lower apparent yield stress as compared to the equivalent blended suspension, can be explained by considering the relative size distributions of limestone and cement in the blend. The similarities in PSDs of the blended and the interground systems (Figure 8-2) combined with constant volume ratios of limestone leads to the expectation that the apparent yield stress and plastic viscosity in these suspensions would be equivalent. However, intergrinding limestone with portland cement clinker will result in a finer limestone phase and a coarser cement phase in the blended cement due to the relative softness of limestone as compared to portland cement clinker (Tsivilis, Voglis, and Photou 1999). The results from the PSD-matched OPC-limestone blends in Section 8.3.1 indicate that the interparticle attractive forces between limestone and cement are lower than those between the cement grains, resulting in a reduction in yield stress as PSD-matched limestone replaces OPC. Thus, the coarser cement particles in the C595 PLC mixture would result in a decrease in the cement particle contacts as compared to the equivalent blended mixture, which subsequently reduces the interparticle attractive forces and decreases the apparent yield stress.

8.3.2.2 Observations from Oscillatory Shear Stress Ramp Experiments

In addition to parallel plate rheological experiments described in the previous section, small amplitude oscillatory stress growth experiments were also performed on suspensions of interground PLC and PSD-matched OPC-limestone blends. Oscillatory stress growth experiments are used to extract the storage and loss moduli, which are the elastic and viscous components of a viscoelastic material respectively, as a function of applied stress.

The typical shape of the moduli-shear stress relationships is a horizontal moduli plateau, followed by a significant reduction over a rather small range of stress, indicative of structural breakdown (Asaga and Roy 1980), and followed by a plateau at a lower moduli level. Figure 8-8 shows the relationships between the shear stress and storage/loss moduli for the OPC and PLC suspensions along with those for the PSD-matched OPC-limestone blends corresponding to the pure OPC or the selected PLCs.

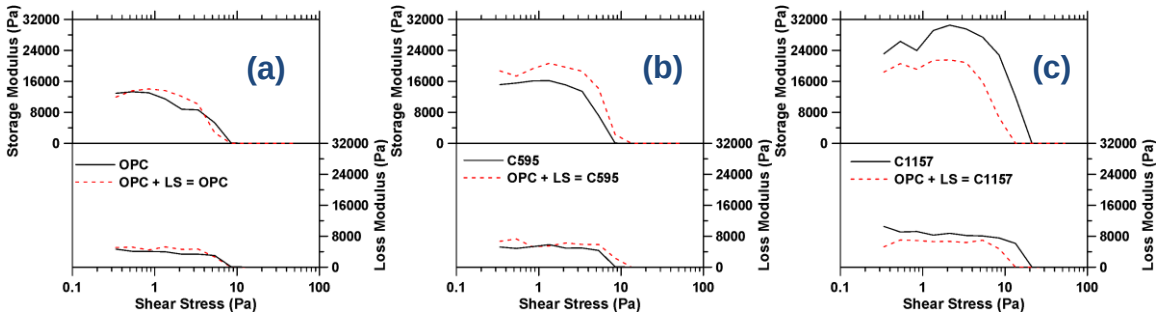

Figure 8-8: Relationship between shear stress and storage or loss moduli of suspensions: (a) pure OPC and the OPC-limestone blend with same PSD as OPC; (b) C595 PLC and OPC-limestone blend with the same PSD as C595 PLC; and (c) C1157 PLC and OPC-limestone blend with the same PSD as C1157 PLC.

Comparing Figures 8-8(a)-(c), it can be noticed that the storage and loss moduli of the suspensions in the linear viscoelastic regime (defined as the regime over which the moduli is independent of stress (Barnes, Non-Newtonian, and Mechanics 2000) as observed from the plateau region in these figures) can be expressed as OPC < C595 < C1157, for both the OPC and the interground PLCs and the blends that match the PSDs of these materials. The increase in moduli corresponds with an increase in the fineness of the cementitious system, where the OPC is least fine and the C1157 PLC is the finest as indicated in the PSD curves presented in Figures 8-1 and 8-2. Further, this trend is consistent with the apparent yield stress results presented in Figure 8-6.

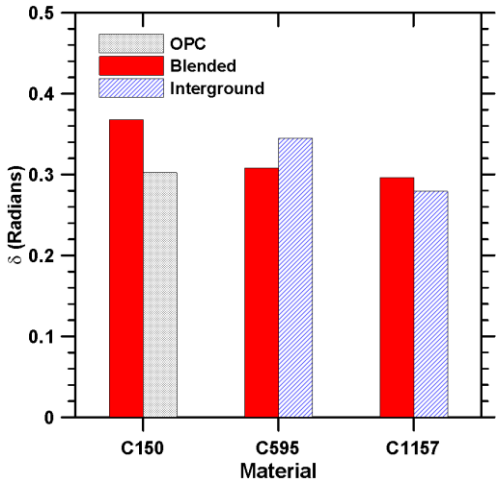

Figure 8-9: Viscoelastic phase angle (δ) for investigated suspensions.

To allow for further discussions on the viscoelastic nature of these suspensions, it is useful to investigate their relative influences on the viscoelastic phase angle δ, defined as:

$$\frac{G''}{G'} = \tan\delta \qquad \text{(Eq. 8-1)}$$

The phase angle represents the ratio of the viscous to elastic portions of the material, with a lower value representing a more solid, or elastic behavior, and a higher value indicating a more liquid or viscous response. Thus, a phase angle of 1 would represent a Newtonian fluid and a phase angle of 0 would represent a perfectly elastic solid. The elastic portion of the response is dominated primarily by interparticle contacts and interparticle forces. Figure 8-9 shows the phase angles for all the suspensions evaluated here, and it can be noticed that the trend is consistent with the observations in Figure 8-6, with the C1157 PLC suspension showing the lowest phase angle, and the PSD-matched OPC-limestone blend equivalent to the pure OPC showing the highest. Comparing the pure OPC suspension to the PSD-matched blend corresponding to OPC, there is a noted increase in the phase angle for the blended suspension. As the PSDs are similar and solid loading is the same in both

these suspensions, this effect can be attributed solely to changes in the interparticle forces in these mixtures. This result further confirms the discussions on limestone-cement dispersion forces presented earlier, where the inclusion of a relatively small fraction of PSD-matched limestone results in a more fluid behavior, attributed to a reduction in interparticle attractive forces in the particle network due to lower limestone-cement dispersion forces. The lower phase angle in the C595 equivalent blended suspension as compared to the interground C595 suspension can similarly be attributed to the particle sizes of cement and limestone as discussed previously. Finally, the lower phase angle in the interground C1157 suspension as compared to all other suspensions can be attributed to the finer particle size distribution in this suspension, which would act to decrease particle spacing and increase particle contacts thereby increasing the interparticle attractive forces and allowing the suspension to behave in a more solid-like manner.

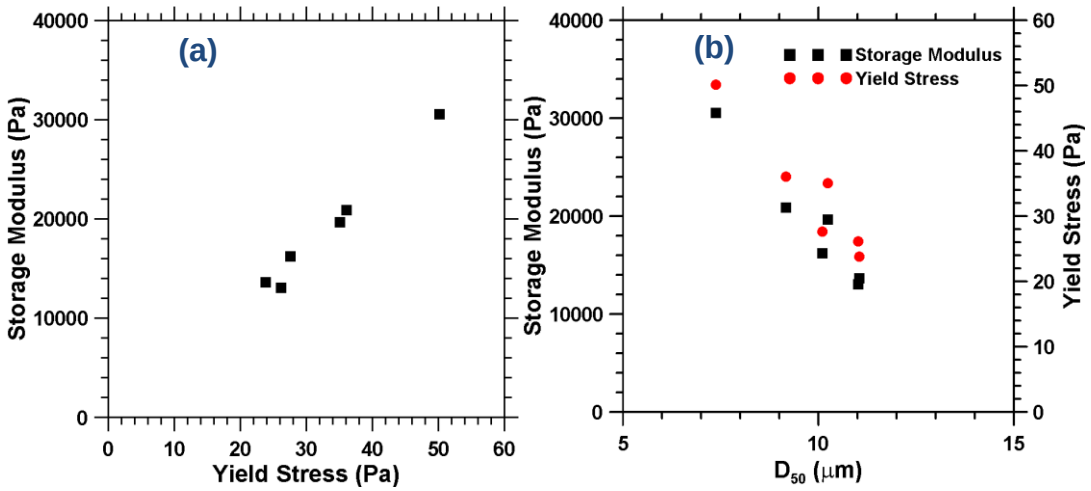

Figure 8-10: (a) Relationship between yield stress and storage modulus in linear viscoelastic regime, and (b) effect of median particle size on yield stress and storage modulus.

Comparisons of the viscoelastic response to the flow response from the strain growth experiments indicate a very strong correlation between the storage modulus and the yield

stress as indicated in Figure 8-10(a). This relationship is one that is expected, as a higher storage modulus would indicate a more elastic behavior, which in turn indicates a more structured network with higher interparticle attractive forces, and consequently a higher apparent yield stress. The good correlation between the storage modulus and yield stress also confirms the accuracy of the determination of apparent yield stress from the plateau of shear stress-shear rate relationship at lower shear rates rather than the use of simplified models.

Figure 8-10(b) illustrates the influence of median particle size (D_{50}) on both the storage modulus and yield stress of the suspensions. A relatively strong correlation is noted in this figure; however there is some degree of scatter. As the median particle size increases, the water film thickness on the surface of the suspended particles would increase, resulting in increased particle separation and a reduction on the interparticle attractive forces. These results are consistent with those in (D. P. Bentz et al. 2012) and Chapter 6, which indicate that the rheological properties of suspensions are strongly influenced by the sizes of the suspended particles. However, it needs to be remembered that the viscoelastic and yield stress response are also influenced by the particle interactions in these suspensions. Thus, the scatter in this figure is likely attributed to changes in interparticle forces in the particle network resulting from the replacement of OPC with limestone. As described in detail previously through deductions from experimental observations, limestone-cement particle interaction effects have been illustrated to be lower than cement-cement interaction, which justifies the changes in the yield stress and viscoelastic response of these binder systems despite comparable PSDs.

8.3.3 Influence of Fly Ash on the Rheological Performance of PLC Suspensions

Rheological performance of OPC and interground PLCs were studied with an additional replacement by fly ash at a volumetric ratio of 10% using the parallel plate configuration and the experimental procedure presented in Section 8.2. The determined rheological properties as a result of this study are presented in Figure 8-11. The incorporation of fly ash in these systems results in a reduction of both the plastic viscosity and apparent yield stress, as expected. The inclusion fly ash, with a median particle size (D_{50}) of 19.9 μm, which is coarser than OPC, replaces OPC or PLC both having smaller D_{50} values than fly ash, resulting in decreased overall surface area of the particles. This, in turn, results in an increase in the water-film-thickness around particles, reducing interparticle forces and increasing particle separation (Fung and Kwan 2010). These effects, in additional with the spherical shape effect of fly ash, result in a decrease in both plastic viscosity and apparent yield stress.

Further noted from this figure is the plastic viscosity remains relatively constant across all of the blends similar to the results shown in Figure 7-6, with the exception of the finer interground C1157 PLC. This divergence is attributed to the higher fineness of this mixture. Similarly, apparent yield stress is also seen to maintain similar trends as that of systems without limestone (Section 8.3.2.1). It is shown that the incorporation of fly ash in these systems generally reduces the rheological parameters as expected, but do not change the overall nature of the suspension.

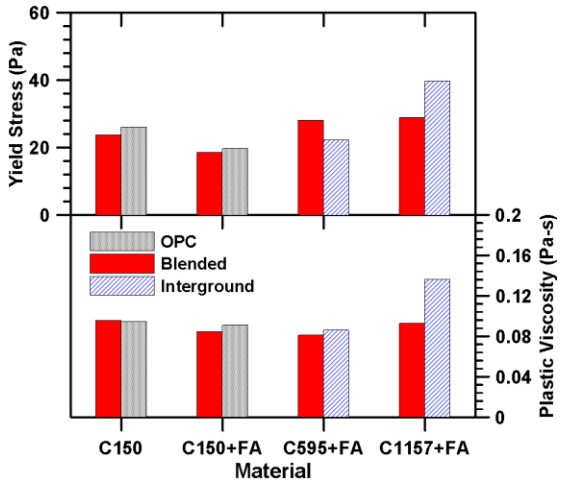

Figure 8-11: Influence of fly ash addition on the rheological properties of blended and interground limestone-cement suspensions.

8.4 Conclusions

This paper extensively studies the rheological influences of limestone inclusion in portland cement suspensions. The effects of packing and surface area changes have been disconnected from these influences by using PSD matched limestone replacement. It is noted in this study that the inclusion of limestone results in a diminished apparent yield stress due to decreased interparticle dispersion forces. The cause of this is due to lower electrostatic attractive forces between limestone and cement particles as compared to between cement particles. This phenomena is confirmed through viscoelastic testing of the suspensions. It is further noted that interground PLC blends are likely to have lower apparent yield stresses and more fluid-like behavior than blended PLC suspensions of the same size distribution. This is attributed to the fact that softer limestone is more readily ground than portland cement clinker, resulting in a finer limestone phase in the PLC. This decreases the yield stress as compared to the blended mixture due to the larger cement particles present decreasing surface contacts between cement particles and lowering the net interparticle attractive forces in the network. Finally, the use of the stress plateau method

for yield stress determinations is confirmed as reliable, by relating the apparent yield stress to the viscoelastic response.

9. OBSERVATIONS ON THE RHEOLOGICAL RESPONSE OF ALKALI ACTIVATED FLY ASH SUSPENSIONS: THE ROLE OF ACTIVATOR TYPE AND CONCENTRATION

9.1 Introduction

Ordinary portland cement (OPC) based concrete is one of the most widely used materials globally, and production of OPC has been shown to require a significant quantity of energy and release significant quantities of CO_2. One of the sustainable alternatives to OPC that has been gaining attention is the use of geopolymeric or alkali activated materials, where alumino-siliceous waste/by-product materials such as fly ash or slag can be activated using alkalis to create a binding medium that is X-ray amorphous and has a three-dimensional network structure (Puertas and Fernández-Jiménez 2003; Palomo, Grutzeck, and Blanco 1999; Škvára et al. 2009). The formation of the binding gel is a complex process including the dissolution process where some Si and Al from the source materials are dissolved by the highly alkaline solution, precipitation of aluminosilicate gel, and further polymerization and condensation to develop the final microstructure (Davidovits 1999; Davidovits 2005). Geopolymeric systems are reported to demonstrate similar or superior mechanical and durability properties compared to OPC-based concretes (Bernal, Mejía de Gutiérrez, and Provis 2012; Bijen 1996; Fernández-Jiménez, Garcia-Lodeiro, and Palomo 2007). Geopolymers based on coal fly ash are of particular interest because of the potential utilization of a waste material that is available in large quantities as well as the beneficial properties of the resulting binder (Provis et al. 2007).

While several studies have examined the mechanical and durability properties of fly ash-based geopolymeric systems, there have been scant studies on aspects related to their

fundamental rheological response. A few studies have investigated the flow behavior of fly ash-based geopolymeric systems using conventional concrete workability techniques (Qing-Hua and Sarkar 1994; Poulesquen, Frizon, and Lambertin 2013b) and investigated the influence of admixtures (superplasticizers and retarders) (Termkhajornkit and Nawa 2004; Criado et al. 2009; Burgos-Montes et al. 2012; Palacios et al. 2009b) on the rheology of these systems. Studies on the influence of superplasticizers on the flowability of geopolymer suspensions have generally found mixed results (Palacios et al. 2009b; Criado et al. 2009), indicating that the nature of these suspensions is likely different from that of OPC suspensions.

This paper aims to develop a fundamental understanding of the rheological nature of these systems and explore the influence of activator type and composition on their rheological properties. Two different classes of activators are used in this study where Class F fly ash is used as the source material: (i) sodium or potassium-hydroxide solutions, and (ii) sodium or potassium-silicate solutions with different SiO_2-Na_2O ratios (M_s) and Na_2O-to-powder ratios (n). The main rheological parameters considered are the yield stress and plastic viscosity of the suspensions determined using the well-known Bingham model. Obtaining a detailed understanding of the rheological influences of alkali cation type and activation solution viscosity is emphasized. Additionally an in-depth investigation of the rheological nature of these suspensions is also attempted using a wider shear range method developed previously (Vance, Sant, and Neithalath), where model-less estimations of rheological parameters are achieved. This experimental approach is used to compare the rheological nature of these suspensions to those of OPC-water suspensions. Limited shear stress growth

rheological studies are described in an effort to discern the transition between Newtonian and non-Newtonian behaviors with changing silicate activator chemistry.

9.2 Experimental Program

9.2.1 Experimental Parameters

A Class F fly ash conforming to ASTM C 618 ("ASTM C109-13. Standard Test Method for Compressive Strength of Hydraulic Cement Mortars Using 2-In. Cube Specimens" 2013) was used as the starting material. The chemical composition of fly ash is shown in Table 9-1. The specific surface area of fly ash was measured as 218 m^2/kg using Blaine's air permeability apparatus. The median particle size, measured using the dynamic light scattering method was 19.9 μm.

Table 9-1: Chemical Composition and Physical Properties of Fly Ash

SiO_2	Al_2O_3	Fe_2O_3	CaO	MgO	SO_3	Na_2O	K_2O	LOI	SSA
58.4%	23.8%	4.19%	7.32%	1.11%	0.44%	1.43%	1.02%	0.5%	218 m^2/kg

The activators used were hydroxide or silicate solutions of Na or K. The concentration of NaOH and KOH solutions used was 4M and 8M. The activation solution[10]-to-fly ash ratio (mass-basis) used was 0.35 corresponding to a volumetric ratio of activation solution-to-powder $(a_s/p)_v$ of between 0.85 and 0.90. The Na- and K-silicate solutions for activation were proportioned considering two parameters: (i) n – the ratio of Na_2O in the activator to the total fly ash content; and (ii) M_s – the ratio of SiO_2-to-Na_2O in the activator. Two different n values were used: 0.03 and 0.05. The mass-based M_s values of the as-obtained

[10] The ***"activation solution"*** refers to the solution of water and the alkali activating chemical: alkali hydroxide or alkali silicates in which the fly ash is suspended. It is noted that when silicate-based activators are used, this includes the solids content in the activator solution, water content in the activator solution, and the additional water required to obtain the desired water-to-powder ratio. In other words, i.e. the activation solution is the suspending fluid.

Na- and K-silicates were 3.22 and 2.10 respectively, which corresponds to mole-based values of 3.32 and 3.29. The solids content in both the silicate solutions were approximately 36%. Requisite amounts of NaOH or KOH were added to the silicate solutions to adjust the M_s (mole-based) to 2.5 or 1.5 for both Na- and K-silicate solutions. M_s values in this range have been shown to be necessary to induce sufficient activation and strength development (Ravikumar and Neithalath 2012b; Ravikumar and Neithalath 2012a). For the Na- and K-silicate activated fly ashes, the mass-based water-to-solids ratio - $(w/s)_m$ - used was 0.20 and 0.25 which corresponds to a $(a_s/p)_v$ between 0.59 and 0.74 and between 0.72 and 0.88 respectively. The solids in $(w/s)_m$ consists of fly ash, the solid fraction of the K- or Na-silicate activator, and the solid fraction of the alkali hydroxide used to adjust the M_s, and the liquid consists of the water in the activator solution and the water added to achieve at the desired $(w/s)_m$. In order to facilitate comparisons between the rheological performances of these suspensions, it is may be necessary to consider the binder loading on a volume basis. Hence in the discussion section, the actual volume-based activation solution-to-powder ratios - $(a_s/p)_v$ for the corresponding $(w/s)_m$ are used. An OPC suspension proportioned at a mass-based water-to-cement ratio (w/c) of 0.45 (which corresponds to a w/c of 1.42 on a volume-basis), was also proportioned so as to provide a point of comparison of fly ash geopolymer rheology to those of commonly used OPC systems.

9.2.2 Mixing and Testing Procedure

Liquid activators were prepared prior to mixing with the binder (fly ash), and allowed to cool down for a period of 3 to 4 hours to ambient temperature (22 ± 2^oC) as measured with an infrared thermometer. For the rheological studies of activation solutions, approximately

12 mL of solution was placed using a disposable syringe in a TA Instruments AR2000EX rheometer in the concentric cylinder configuration, in which both the cup and bob were textured, to reduce slip. The gap between the concentric cylinders was fixed at 1.0 mm. For studies of fresh geopolymer suspensions, approximately 200 g of the suspension was mixed using a kitchen blender as follows: (1) initial hand mixing to disperse the powder in the activation solution and to ensure that particles do not adhere to the edges of mixing container, (2) mixing in the blender at high speed for 30s, (3) 30s covered rest period, and (4) final mixing at high speed in the blender for 30s. This mixing sequence is a modification to ASTM C1738 ("ASTM C1738 - 11a. Standard Practice for High-Shear Mixing of Hydraulic Cement Paste" 2011) which provides recommendations for measurements of cement paste rheology (Nehdi and Rahman 2004b); but demonstrated to provide similar fluidity and mixing consistency. After mixing, approximately 6 mL of sample was extracted using a disposable syringe and placed between in the rheometer in the parallel plate configuration. The gap between the top and bottom plates parallel plates (top plate diameter of 50 mm, serrated to a depth of 1.0 mm) was set to 2.0 mm during the experiments, as this gap has been noted to provide consistent results in cementitious suspensions as shown in Chapters 5 and 6. The bottom plate was serrated to a depth of 0.15 mm. The rheological studies were carried out with the Peltier plate set to a temperature of 25±0.1 °C. The approximate time from the addition of the activation solution to the start of the rheological experiment was 150s. Treatment and conditioning of experimental data was carried out for shear stress and shear rates using the TA Instruments TRIOS software package.

The general experimental procedure consists of varying the shear rate as follows: (1) a stepped ramp-up pre-shear phase, (2) a subsequent stepped ramp-up, and (3) a stepped ramp-down phase. The actual data acquisition is carried out during steps (2) and (3). Shear stress values are recorded every second, with a given shear step being terminated when a steady state has been achieved, as defined by 3 consecutive measurements within 5% of each other. For all the studies, the values used in determining rheological properties are the steady state values of shear stress and the related shear rate in the down ramp. Two different rheological evaluations are conducted. The shear rate range used for the rheological studies of activation solutions and the suspension was 5-to-100/s, hereinafter referred to as the "normal" shear rate range. This is the shear rate range that is used in a majority of rheological studies on cementitious suspensions (Banfill 2006; Nehdi and Rahman 2004b). For the comparative study of geopolymer and cementitious suspensions, a "wide" shear rate range: 0.005-to-100/s was used. The "wide" experiment follows a similar procedure as that used in Chapter 6 in an effort to characterize and adequately model the stress plateau which only manifests are very lower shear rates (Barnes 1999). A graphical representation of the two rheological procedures used in this study is presented in Figure 9-1. In addition, an oscillatory shear stress growth study was carried out to investigate the unexpected Newtonian behavior when an activation solution with a low(er) M_s was used. Here, a coaxial cylinder geometry was used with an oscillatory frequency of 1 Hz and a stress range from 0.005 Pa to 50 Pa was employed. Stress ranges below 0.1 Pa resulted in torque readings that were close to the torque limit of the instrument, resulting in significant data scatter and thus such data is disregarded in the analysis.

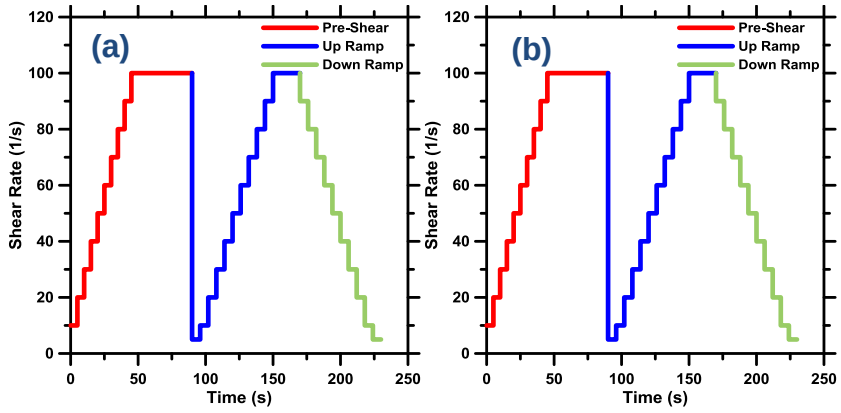

Figure 9-1: Rheological procedure: (a) "normal" shear range and (b) "wide" shear range

The viscosity of the activation solutions was determined by fitting the rheological data to the Newtonian flow model shown in Equation 9-1. The rheological model parameters for the "normal" shear rate range (5-to-100/s) for geopolymer suspensions was calculated by fitting the down-ramp data to the Bingham model shown in Equation 9-2 (Bingham 1922). The use of Bingham and Newtonian models and their adequacy (or lack thereof) is better considered by analysis of additional data provided via "wide" shear rate range studies. In the equations below, τ is the shear stress (Pa), τ_y is the yield stress (Pa), η_p is the plastic viscosity (Pa.s), and $\dot{\gamma}$ is the shear rate (s^{-1}).

Newtonian: $\tau = \eta_a \dot{\gamma}$ Equation (9-1)

Bingham: $\tau = \tau_y + \eta_p \dot{\gamma}$ Equation (9-2)

9.3 Results and Discussions

This section discusses the influence of the type and chemistry of the alkaline activation solution on the rheological parameters of fly ash suspensions determined using the Bingham model. The solution is also evaluated in itself to account for the influences of ion

concentrations on solution viscosity, which in turn influences the rheological properties of the suspension.

9.3.1 Rheological Behavior of the Activation Solutions

The rheology of the activation solutions was evaluated in the "normal" shear rate range (5-to-100/s). 4M and 8M NaOH and KOH solutions were used to explore the influence of concentration and cation type on flow properties. Additional experiments were carried out using Na-and-K- silicate solutions to investigate the influence of n, M_s and cation type on solution rheology, and for comparison with hydroxide solutions. Expectedly, all of the activation solutions demonstrated Newtonian behavior over the range of shear rates investigated. A typical flow diagram of an activation solution is presented in Figure 9-2.

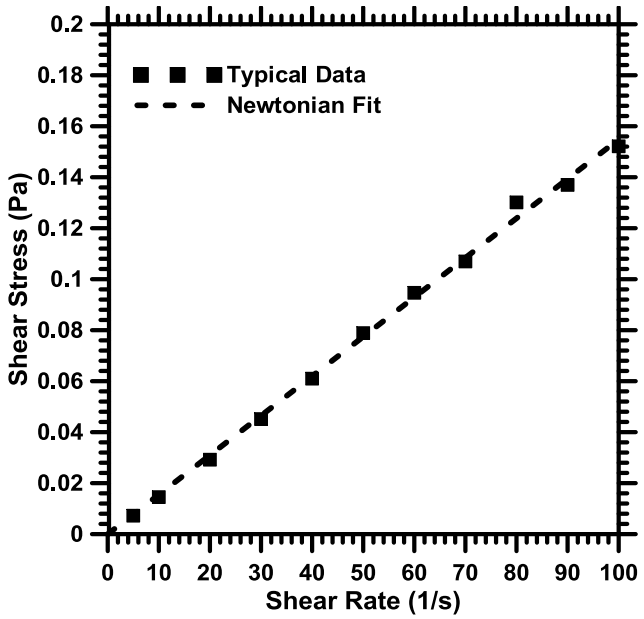

Figure 9-2: A typical shear rate-stress plot of activator solutions and the corresponding Newtonian least squares best fit

The influences of alkali cation, molarity, and n and M_s respectively on the solution viscosity are presented in Figures 9-3(a-b). For reference, the viscosity of water at 25°C is approximately 8.9×10^{-4} Pa.s. Na-containing solutions demonstrate higher viscosities than

the K-containing ones over all values of n and M_s considered, which is in line with reported literature (Provis and Van Deventer 2009).

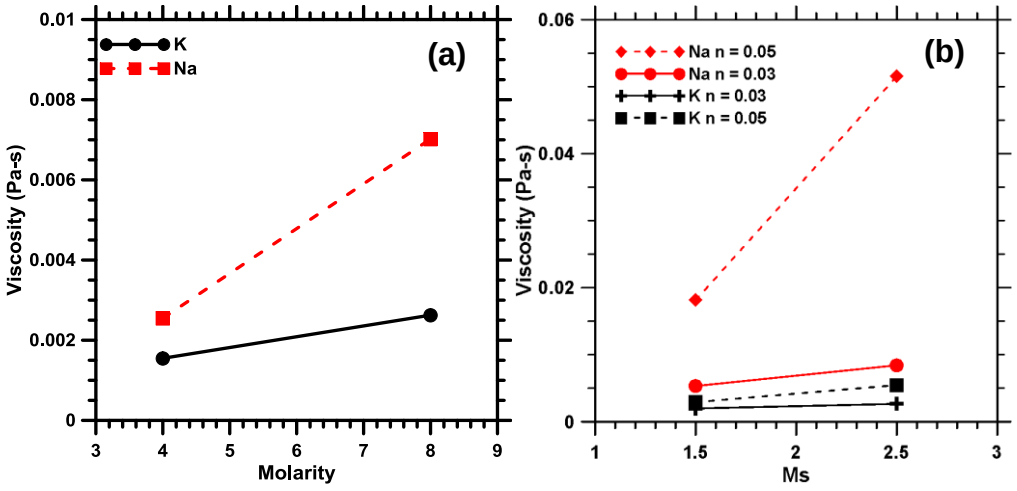

Figure 9-3: Influence of: (a) molarity of KOH and NaOH solutions on its viscosity, and (b) n, M_s of K-silicate and Na-silicate activators on its viscosity. The viscosities were extracted using a Newtonian model.

From Figure 9-3(a) two obvious trends emerge: increasing concentration increases the solution viscosity regardless of the cation type, and Na-based activators result in significantly higher viscosities compared to K-based activators, at equivalent concentrations. As an example: at a concentration of 8 mol/L, the viscosity of the NaOH solution is 3 times higher than the corresponding KOH solution. The viscosity of aqueous solutions is described by ion-ion interactions and ion-dipole forces. As the ionic concentration increases, the influence of ion-dipole forces increases, resulting in an increase in the measured viscosity. The higher charge density of Na^+ ions results in higher ion-dipole forces in the NaOH solution, thereby increasing their viscosity relative to the KOH solution.

When silicate bearing activators are used, a similar trend with respect to the alkali cation is noted (Figure 9-3b). In addition, a general increase in viscosity with increasing M_s and

n is observed, with the effect once again being more noticeable for the Na cation than for K. NMR studies of concentrated alkali silicate solutions have indicated the presence of colloidal Si-O-H-M complexes (where M denotes Na or K species) on the order of 0.6 nm in size, which form aggregates on the order of a few nm (Stebbins, Farnan, and Xue 1992; Tognonvi et al. 2010), the presence of which increases the solution viscosity (Brady 1993). The quantity/size of these colloidal species and aggregates likely increases with M_s due to an increased Si (i.e., complex) content and the reduced abundance of OH^- species to break Si-O-Si bonds (Iler 1979), which in turn results in an increase in the solution viscosity (Svensson, Sjöberg, and Öhman 1986; Wijnen et al. 1989). The influence of n on the solution viscosity can be explained as follows. An increase in n increases the ionic concentration of Na or K, as well as an increase of Si in the solution, resulting in increased ion-dipole forces as well as increased quantity of Si-O-H-M complexes. In addition, to obtain identical n and M_s values for Na and K silicate solutions, more Na-silicate is needed (than K-Silicate) due to the lower molecular weight of sodium. This results in inequivalent ion-dipole forces in these solutions, as a result of which Na-bearing silicate solution show higher viscosities. Figure 9-3(b) also shows that, with an increasing value of n, the viscosity enhancement is higher with increasing M_s when Na^+ is the cation in solution. This behavior is attributed to the more significant influence of ion-dipole forces with more charge dense Na^+ ions combined with higher colloidal species concentration.

9.3.2 Rheological Behavior of Fly Ash Suspensions Activated with NaOH or KOH

Rheological studies were performed on suspensions where fly ash was dispersed in NaOH or KOH solutions (4M and 8M) using the "normal" shear rate range as described in Section 9.2. From Figure 9-4 it is observed that increasing the activation solution concentration

results in an increase in the plastic viscosity and yield stress of the suspensions. This behavior is primarily attributed to the increase in the viscosity of the activation solution with concentration. Similarly, the effect of the cation on the rheological performance of the suspension can also be related to the rheology of the medium in which the fly ash is dispersed. As seen in Figure 9-3(a), NaOH solutions demonstrate higher viscosity than the KOH solutions. The steeper slope associated with the change in plastic viscosity of the fly ash-NaOH suspension as compared to the fly ash-KOH suspension when the concentration increases also mimics trends in the viscosity of the activation solution. Yield stress, however, increases at a greater rate with an increase in activation solution concentration when fly ash is dispersed in KOH. At lower concentrations, the yield stress of the fly ash-NaOH suspension is higher than that of the fly ash-KOH suspension, while at higher concentrations, the yield stress values of the two suspensions are similar. The yield stress of a suspension is influenced by several competing effects: (i) the viscosity of the fluid, (ii) interparticle forces (interaction potential or steric forces and van der Waals forces), and (iii) the influence of particle jamming (Lowke 2009; Barnes 1999). As the volume fraction of solids (fly ash) is similar for all these mixtures and the fly ash particles are spherical, the influence of particle jamming can be ignored in comparative evaluations. Similarly, particle spacing also will be approximately similar across these suspensions, and thus the influence of van Der Waals forces is likely redundant. The yield stress can be considered to be proportional to the inverse square of particle separation (van der Waals forces) minus the square of the interaction potential (zeta potential) (Scales et al. 1998). Increased particle separation will decrease the effect of van Der Waals forces, while a higher net surface charge on the particles will increase the repulsive force between particles, both

effects resulting in a decrease in yield stress. This behavior can be conceptually verified by considering the surface interaction effect that results from the use of superplasticizers in cementitious suspensions (Adriano Papo and Piani 2004). Based on the above analysis, there are two remaining influences which may be attributable to the relative increase in yield stress with increasing molarity: interaction potential and viscosity of the activation solution. Studies have shown the zeta-potential of fly ash is dependent on ion type, ion concentration and the pH of the suspending solution (Nägele 1986; Nägele and Schneider 1989). In solutions of NaOH and KOH, the zeta potential of fly ash has been shown to be negative, with those in NaOH solutions showing a larger net potential (Nägele 1986). This behavior is attributed to the enhanced adsorption of K^+ on the fly ash particle surfaces than Na^+ ions (Franks 2002), resulting in a less negative surface charge as the K^+ concentration is increased. As the zeta potential decreases, the yield stress increases due to a decreased repulsive force between fly ash particles. The smaller increase in yield stress in NaOH solutions as compared to KOH solutions with increasing molarity can thus be attributed to the greater net surface charge of fly ash particles in NaOH that result in more significant repulsive forces.

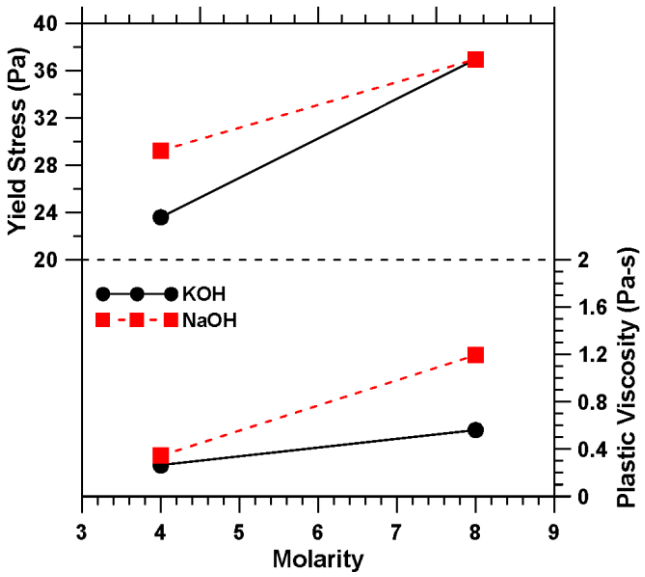

Figure 9-4: Influence of molarity of KOH and NaOH on the rheological properties determined using the Bingham model

9.3.3 Rheological Behavior of Fly Ash Suspensions Activated Using Na- or K-Silicates

The following discussions highlight the major factors influencing the rheological parameters of fly ash suspensions activated using Na- or K-silicate solutions. Two key factors are identified and explored: (i) the viscosity of the suspending media as dictated by the M_s of the activator and n of the suspension, and (ii) the volume of activation solution present.

9.3.3.1 Influence of n, M_s, and $(w/s)_m$

Rheological studies were performed on suspensions where fly ash was dispersed in Na- or K-silicate solutions. For the silicate based activators, MOH was added to reduce the M_s of the as-obtained silicate solutions to the desired values (1.5 and 2.5 in this study). The rheological studies were performed using the "normal" shear rate range as described in Section 9.2. Figures 9-5 and 9-6 show the influence of n and M_s on the yield stress and plastic viscosity of fly ash-K silicate and fly ash-Na silicate suspensions respectively for two different $(w/s)_m$ – 0.20 (Figures 9-5(a) and 9-6(a)) and 0.25 (Figures 9-5(b) and 9-6(b))

corresponding to $(w/s)_v$ ratios of between 0.57 and 0.74 and between 0.72 and 0.88 for $(w/s)_m$ ratios of 0.20 and 0.25 respectively. For the Na-silicate activated case, a suspension at a $(w/s)_m$ of 0.20 could not be proportioned with an n-value of 0.05 and M_s of 2.5 because the water from the silicate activators themselves produced a $(w/s)_m$ higher than 0.20. Increasing the $(w/s)_m$ from 0.20 to 0.25 results in a drastic decrease in the yield stress and plastic viscosity as would be expected. Increasing the amount of suspending fluid in a suspension increases the particle spacing, thereby increasing the fluid film thickness between/around the particles, and thus decreasing yield stress and plastic viscosity. Increasing the water content also reduces the alkali ion concentration in the solution which reduces the viscosity of the activation solution, further contributing to a decrease in the values of the rheological parameters.

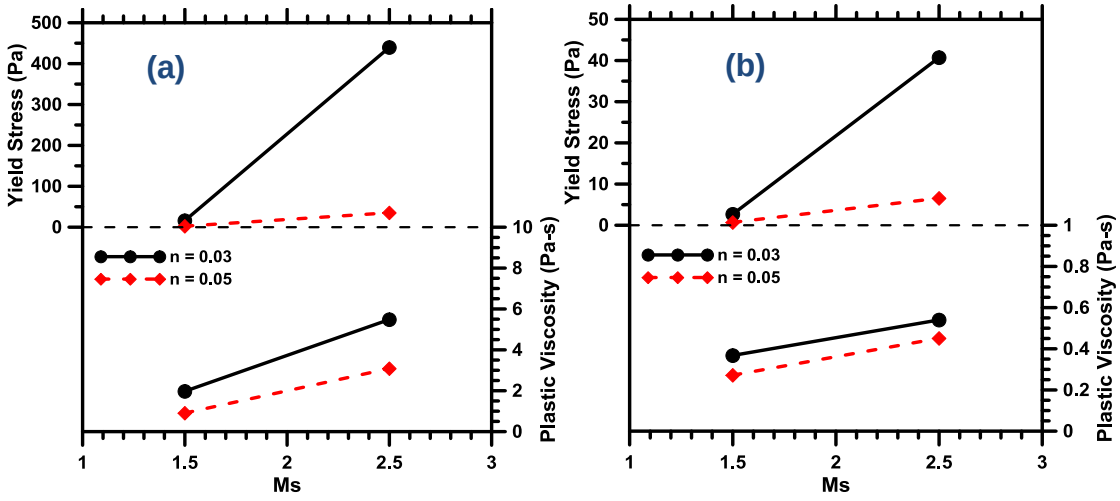

Figure 9-5: Influence of M_s on the rheological properties of fly ash-K silicate suspensions determined using the Bingham model for: (a) 0.20 $(w/s)_m$ and (b) 0.25 $(w/s)_m$. Note the difference in the ranges of yield stress and plastic viscosity with changing $(w/s)_m$. The Y-axis scales are different in both these graphs.

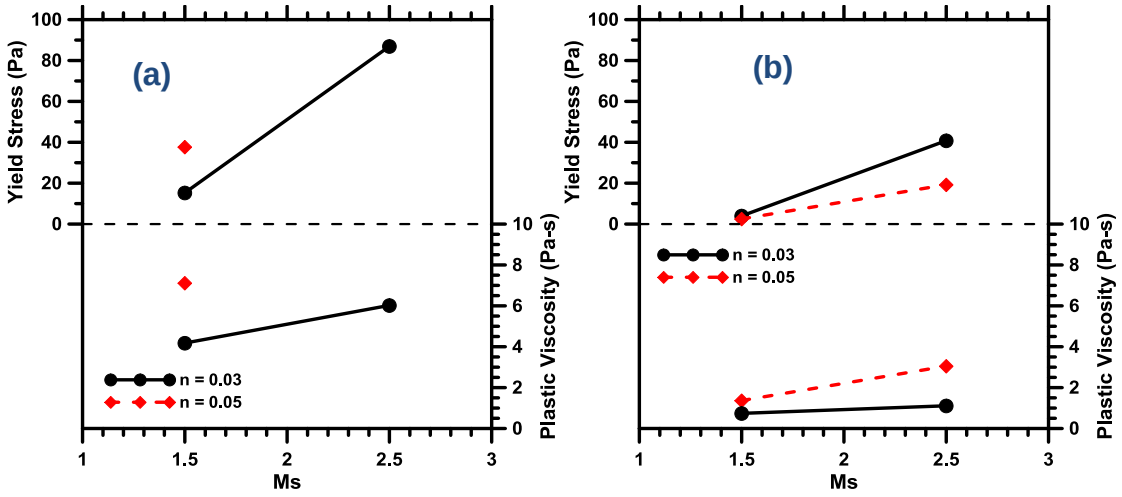

Figure 9-6: Influence of M_s on the rheological properties of fly ash-Na silicate suspensions determined using the Bingham model for: (a) 0.20 $(w/s)_m$ and (b) 0.25 $(w/s)_m$. At a $(w/s)_m$ of 0.20, a fly ash-Na silicate suspension with an M_s of 2.5 and n of 0.05 was not possible because it would have meant removing water from the activators to obtain the desired $(w/s)_m$.

Several key observations are noted that are typical of these figures: (i) increasing M_s results in increases in yield stress and plastic viscosity , (ii) a lower n-value results in more significant enhancements in yield stress as M_s is increased, and (iii) at low values of M_s the yield stress approaches zero indicating a transition to Newtonian behavior. The increase in the yield stress and plastic viscosity with increasing M_s may be partially attributed to the increase in activation solution viscosity with M_s as noted in Figure 9-3. The latter observations which demand careful examination are explored in the forthcoming sections.

When Figures 9-5 and 9-6 are compared, the following important observations can be made: (i) at a lower $(w/s)_m$ and higher M_s, the yield stress of the fly ash-K silicate suspension is about 5 times higher than that of the fly ash-Na silicate suspension, while the values are comparable at a higher (w/s)m; and (ii) increasing the (w/s)m results in a 10-fold reduction in plastic viscosity especially at higher Ms for the fly ash-K silicate suspension while the reduction is only 2-fold for the fly ash-Na silicate suspension. These

observations support the idea that flow parameters are influenced to a great extent by the adsorption of cations on particle surfaces. At higher (w/s)m, the surface adsorption of ions and van Der Waals forces become less significant as the particle spacing increases, and thus the influence of the alkali cation from the activation solution is reduced. In addition, Na-based fly ash suspensions demonstrate similar or higher yield stress as compared to K-based suspensions. Increasing the n-value is shown to decrease both the yield stress and plastic viscosity in K-based suspensions, while generally increasing those values in Na-based suspensions (except for the fly ash-Na silicate suspension with an Ms of 2.5 at a (w/s)m of 0.25). The increased rheological properties in Na silicate-fly ash suspensions as compared to K silicate-fly ash suspensions can be primarily attributed to the significantly greater viscosity of the Na-based suspensions as compared to K-based suspensions as noted in Figure 9-3. Further, in K silicate-fly ash suspensions, the behavior is Newtonian (zero yield stress) at low Ms values regardless of (w/s)m ratio, whereas the Na-silicate suspensions exhibit the Newtonian behavior only at the higher (w/s)m. The shift to a Newtonian flow regime at low Ms values is explored in detail in a later section.

9.3.3.2 Dependence of rheological parameters on the volumetric activator solution-binder ratio

The $(w/s)_m$ ratio is a mass-based ratio of the water in the activator (along with any additional water added) to the total solids (the binder material, fly ash in this case and the solids present in any of the activating chemicals) in the suspension. The $(a_s/b)_V$ ratio, on the other hand, is the volumetric ratio of the activation solution to the binder. The activation solution implicitly includes the dissolved solids present in the solution: both the silicate solutions used in this study have the same solids content. The use of $(a_s/b)_V$ ratio, rather

than $(w/s)_m$ (which is an easier proportioning parameter for practical applications) is deemed to be appropriate because the rheological characteristics of suspensions are typically dependent on the volume of suspending fluid present, the size, shape, and concentration of the suspended particles (Santamaria-Holek and Mendoza 2010; D. P. Bentz et al. 2012; Mueller, Llewellin, and Mader 2010; Sweeny and Geckler 1954; Jeffrey and Acrivos 1976), and the rheological properties of the suspending medium (Kamal and Mutel 1985; Krieger and Dougherty 1959; Barnes 1989). It is further notable that the use of a constant $(w/s)_m$ while modifying the n and M_s values will not result in a constant $(a_s/b)_V$ due to the influence of changing amounts of MOH added to the activator solution to maintain the desired M_s. Generally, increasing either M_s or n will increase the $(a_s/b)_V$ ratio due to an increase in solids present in the activator, requiring an increase in solution volume to maintain a constant $(w/s)_m$ ratio. Thus, at the same $(w/s)_m$ ratio, an activation solution with a higher n and/or M_s will have both a higher $(a_s/b)_V$ ratio and a higher added M^+ ionic concentration.

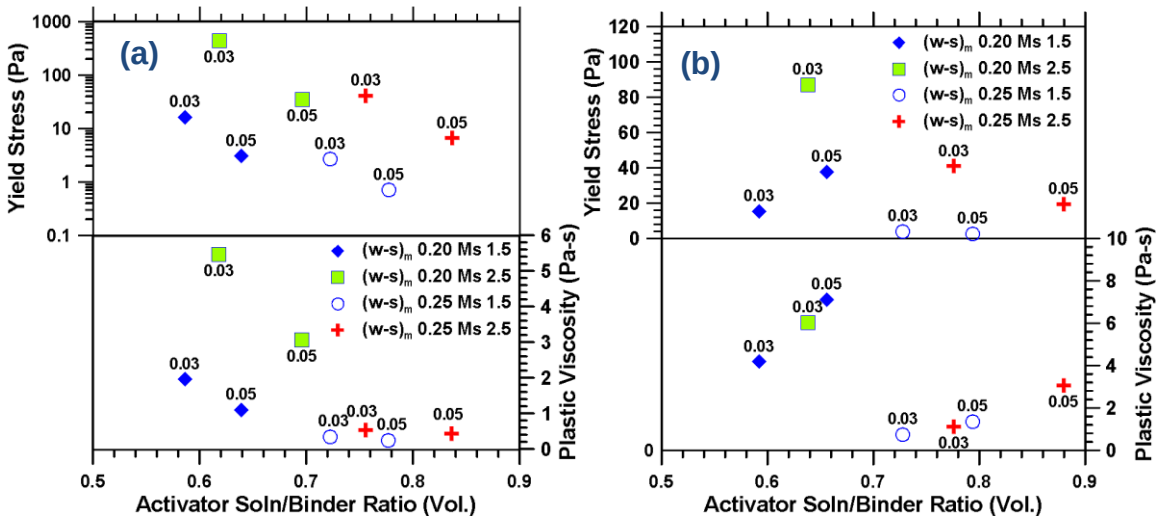

Figure 9-7: Influence of $(a_s/b)_V$ ratio on rheological properties for: (a) fly ash-K silicate suspensions, and (b) fly ash-Na silicate suspensions (label in parentheses is the n-value).

Figures 9-7(a) and (b) illustrate the influence of $(a_s/b)_v$ on the yield stress and plastic viscosity of Na- and K-silicate activated fly ash suspensions respectively. In general, the yield stress and plastic viscosity decreases for all the suspensions as the $(a_s/b)_v$ increases, attributable to the reduction in particle concentration. This is a trend that is expected, as in the case of OPC when the $(w/p)_v$ is increased (Ferraris 1999b). For both K- and Na-based suspensions, with an increase in M_s, at the same n value, it is observed that both the yield stress and plastic viscosity increases. One can also notice that, for the same n value, the $(a_s/b)_v$ is higher at a higher M_s. The increase in rheological parameters is despite this fact, indicating other underlying phenomena, which will be discussed later in this paper. At the same $(w/s)_m$ and M_s, the rheological parameters decrease with an increase in the n value, which is attributable to the increased amount of MOH solution added to increase n, and the consequent reduction in the volume fraction of solids provided by the activator. The only exception is the Na silicate-fly ash suspension at an M_s of 1.5 and $(w/s)_m$ of 0.20 (a_s/b of 0.66) where an increase in n increases both the yield stress and plastic viscosity despite the

fact that increasing n results in an increase in the volume of activator solution. This inconsistency can be primarily attributed to more significant changes in the Na-based activator solution viscosity as noted previously in Figure 9-3. Further, the increase in plastic viscosity with increasing $(a_s/b)_V$ in Na-silicate fly ash suspensions could have been augmented by the higher concentration of Na^+ present which decreases the absolute surface charge of fly ash and thus the steric forces.

To further investigate possible influences in these suspensions, and disconnect the influence of solids content provided by the activator on the rheological parameters, suspensions of fly ash in potassium silicate activator solutions were prepared where a constant $(a_s/b)_V$ ratio of 0.72 was maintained while varying M_s and n. The results of this experiment are presented in Figure 9-8 which shows the yield stress and plastic viscosity of the suspensions and the activation solution viscosity as a function of M_s. Similar trends as shown in Figure 9-5 earlier are noted here, where increasing M_s results in increased determined rheological properties. However, at a constant $(a_s/b)_V$, increasing n increases both yield stress and plastic viscosity, especially at the higher M_s value. This is opposite to what was observed in Figure 9-7(a) where the influence of n and $(a_s/b)_V$ were confounded. It is noted from this figure that there is a strong correlation between the trends of activation solution viscosity and the plastic viscosity of the resultant suspension. This indicates that the dominant influences in suspension viscosity in these systems are likely the viscosity of the solution itself and the solids loading of the suspension. Yield stress is also found to demonstrate similar trends as the activation solution viscosity when plotted as a function of M_s, for the suspension with an n value of 0.05. However, at an n value of 0.03 the activation solution viscosity barely changes with M_s whereas the yield stress increase is

significant. It can thus be postulated with reasonable certainty that the activation solution viscosity is a less dominant influence on yield stress, and effects such as particle surface charge effects are more dominant. Yield stress of activated fly ash suspensions is thus dominated by influences of solid loading and particle interactions as is the general case for particulate suspensions, while the plastic viscosity is more strongly influenced by activation solution viscosity and solids loading.

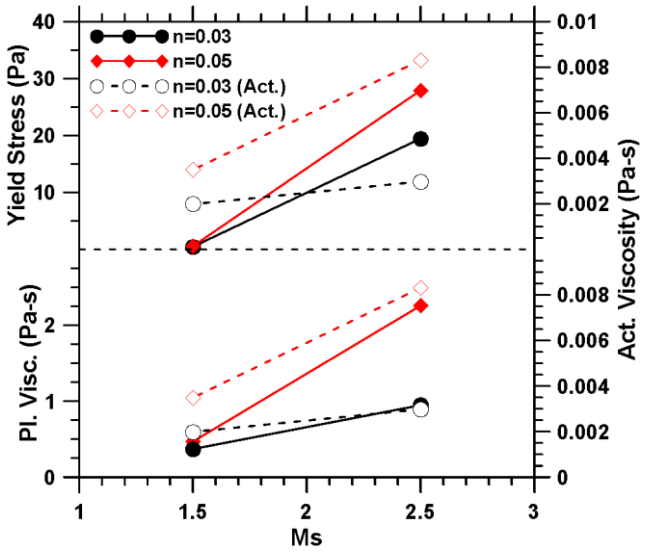

Figure 9-8: Investigation of influence of n and M_s at a constant $(a_s/b)_V$ ratio of 0.72. Solid lines represent the determined suspension rheological parameters, dashed lines represent rheological properties of activation solution.

9.3.4 Rheological Response of Suspensions under Extended Shear Rates

9.3.4.1 Comparison of Activated Fly Ash Suspension to OPC-Water Suspensions

The purpose of this section is to investigate the differences and/or similarities in rheological behavior of suspensions of fly ash particles in an alkaline activator to ordinary portland cement (OPC) particles in water. The experiments for this study, including that for the Type I/II OPC suspension were completed using the "wide" rheological procedure as presented in Section 9.2. This procedure allows for a model-less estimation of apparent

yield stress (Barnes 1999) based on the stress plateau that is not discerned in the typical shear rate ranges employed in rheological studies of cementitious systems as illustrated in Chapter 7. Figures 9-9 and 9-10 present the flow (shear stress-shear rate) curves plotted in both linear and logarithmic scales to allow for more in-depth discussion of the rheological response of these suspensions. The suspending liquid content in all these mixtures are different and have been selected so as to obtain flow curves that occur over roughly similar stress ranges (in a strain rate range of 5-100/s that is used in conventional rheological studies of cementitious suspensions) to facilitate effective comparisons.

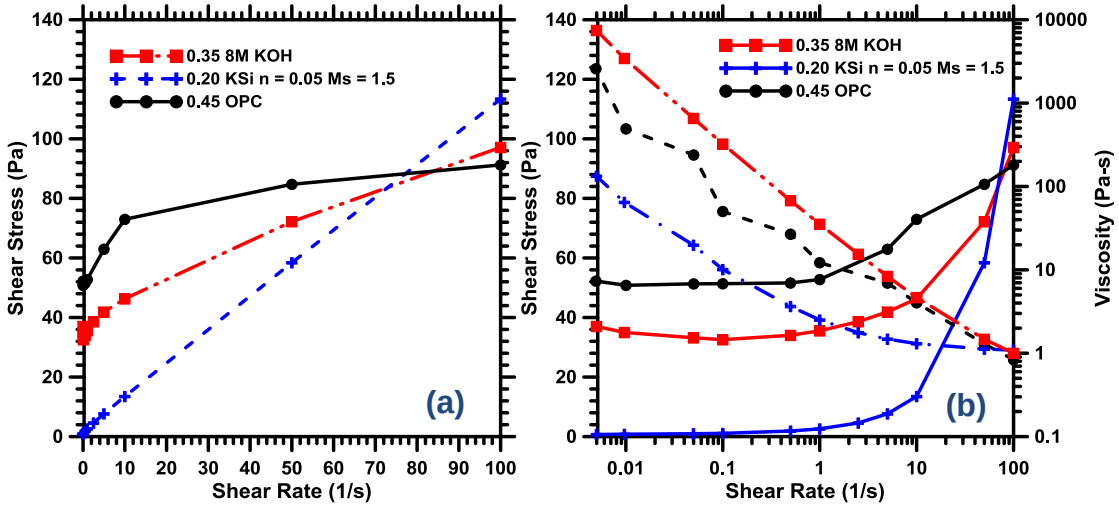

Figure 9-9: Comparison of rheological response of fly ash suspensions in KOH and K-silicate solutions and portland cement-water suspension: (a) shear stress response in linear scale and (b) shear stress (solid) and viscosity response (dashed) in log scale

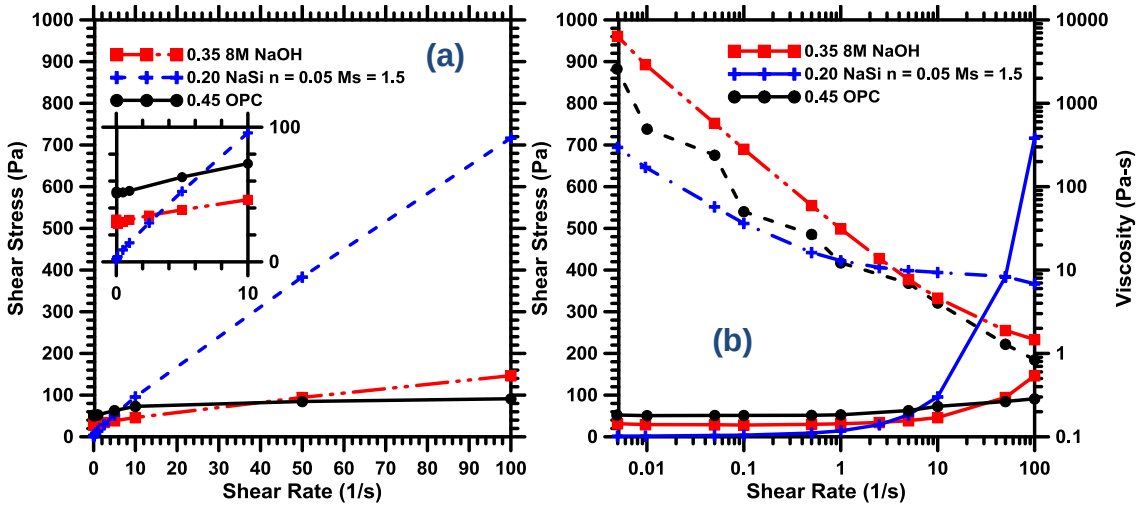

Figure 9-10: Comparison of rheological response of fly ash suspensions in NaOH and Na-silicate solutions and portland cement-water suspension: (a) shear stress response in linear scale and (b) shear stress (solid) and viscosity (dashed) response in log scale

It is immediately evident from both Figures 9-9 and 9-10 that the general shear rate-shear stress response of the fly ash-MOH suspensions is quite similar to that of the portland cement-water suspension. In both cases there is a stress plateau at lower shear rates (< 1/s) indicating an apparent yield stress (Barnes 1999; Cheng 1986), which is preceded by a linear portion at relatively constant slope from shear rates of about 10 to 100/s. In the linear scale, both KOH and NaOH based suspensions show the typical downward trend at low shear rates that has been documented in several other publications of cementitious material rheology (Atzeni, Massidda, and Sanna 1985) and Chapter 6. In the KOH-fly ash suspension, there is a noted upward trend in shear stress at the very low end of shear rates along the stress plateau region. This is indicative of flow instabilities associated with localized particle diffusion and reorganization (Schall and van Hecke 2009). As shear is applied to a suspension, particle localized particle rearrangement occurs to enable flow, at very low shear rates, there is insufficient strain to maintain the localized changes in particle

density, which is indicated by an instability in the flow curve. The existence of the this trend in K-based suspensions and its absence in Na-based suspensions supports the presence of a higher surface charge on fly ash particles in K-based suspensions as compared to Na-based suspensions. This larger surface charge promotes the fly ash particles to move into the less concentrated region and to a less organized state to achieve a state of minimized energy. This behavior results in an increased resistance to flow of the suspension indicated by an increase in stress (Schall and van Hecke 2009; Callaghan 2008).

9.3.4.2 Discussions on the changes in rheological response with activator M_s

The behavior of the silicate based activator suspensions is noted to be quite different. As noted in the previous section, the suspension behaves in a nearly Newtonian fashion at an M_s value of 1.5. While the OPC and hydroxide-based suspensions demonstrate a viscosity range of about 4 orders of magnitude from the highest to lowest shear rate, the viscosity of the silicate based suspensions only increase by 2 orders of magnitude over the same shear rate range, as can be observed from Figures 9-9(b) and 9-10(b). Further, in the log scale, the viscosity-shear rate relationships of the OPC-water and fly ash-MOH suspensions appear relatively linear; while the silicate based suspensions demonstrate a viscosity asymptote at higher shear rates. To investigate the cause of this behavior, an additional rheological experiment was conducted using a mixture of fly ash and water with the same mass-based liquid to powder ratio as used in the silicate based activator experiments. The results of this experiment are presented in Figure 9-11.

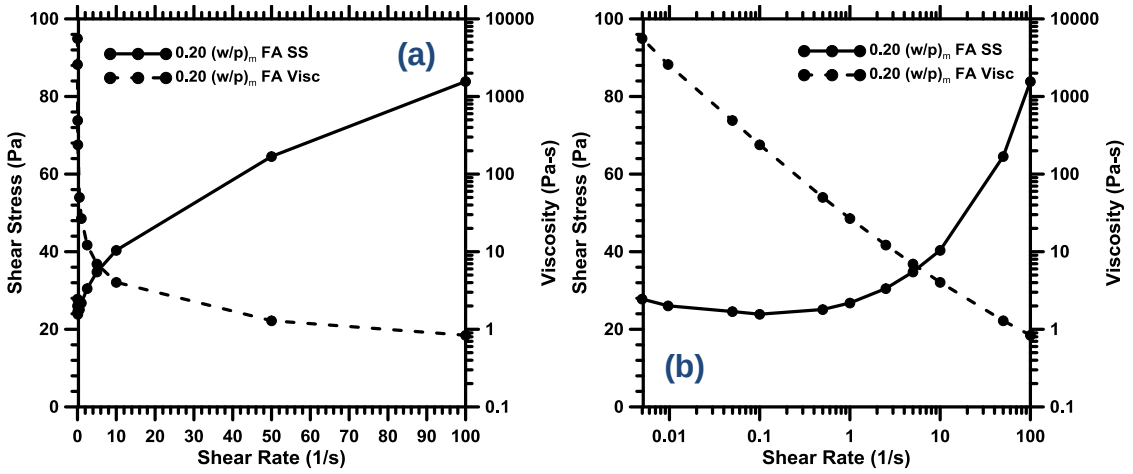

Figure 9-11: Rheological study of 0.20 $(w/s)_m$ suspension of fly ash and water: (a) linear scale and (b) logarithmic scale

The fly ash-water suspension indicates a rheological behavior that bears more resemblance to that of the fly ash-MOH or OPC-water suspensions. In this case, a noted stress plateau and an increase in viscosity by almost 4 orders of magnitude over the range of shear rates investigated are observed. Given that the activation solutions in these suspensions have viscosities of 0.0017 and 0.0054 Pa-s (Figure 9-3) for potassium silicate and sodium silicate respectively, which are meaningfully greater than that of water (approximately 0.00089 Pa-s at 25 °C), this behavior is somewhat counterintuitive. It can be noted from Figures 9-5 and 9-6 that at higher values of M_s, in all suspensions investigated, the existence of an apparent yield stress is observed; i.e., the fly ash suspensions employing activators of higher M_s are non-Newtonian. As the Newtonian behavior is not present in fly ash-water suspensions, and it disappears at a higher value of M_s, this indicates a clear influence of the siliceous species and the free M^+ ion concentration present in the suspension. Additional experiments were conducted at M_s values of 1.0 and 2.0 to investigate the range in which this phenomenon is present, and the results are presented in Figure 9-12. At low M_s values (1.0 and 1.5), the Newtonian shift is visible with the absence of a stress plateau in Figure

9-12(a), while at larger M_s values, the behavior transitions to non-Newtonian as a stress plateau is formed. It is possible that the increased quantity of hydroxide ions present in the solutions at lower values of M_s, results in a decreased polymerization of the colloidal silica species as discussed previously. This in turn results in colloidal species that react in a fashion similar to superplasticizers in cement. The shift in the order of magnitude of viscosity increase indicates a shift towards shear thickening behavior (Adriano Papo and Piani 2004; Lootens et al. 2004).

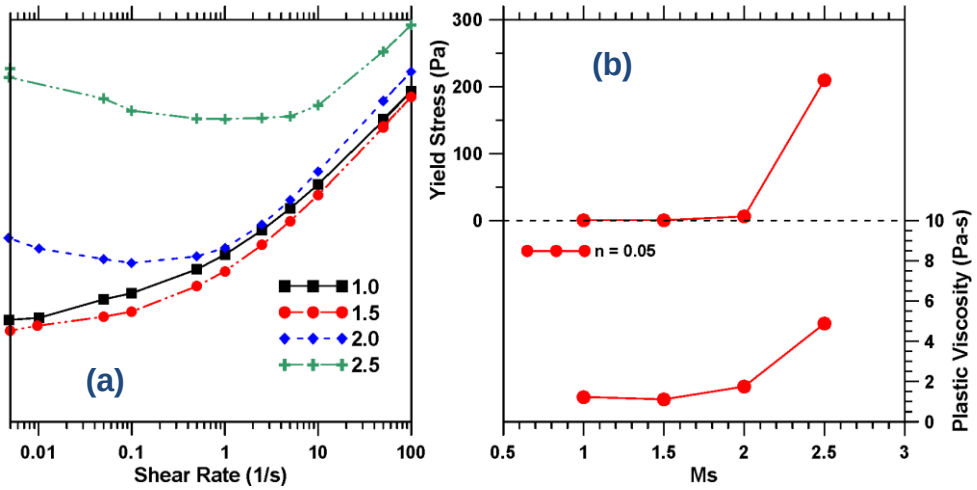

Figure 9-12: Rheological study of 0.25 $(w/s)_m$ K-Si fly ash suspension at varying M_s: (a) flow curve in logarithmic scale and (b) influence of M_s on determined rheological properties

9.3.4.3 Response of different activator M_s: Shear stress growth experiments

A small amplitude oscillatory shear stress growth experiment was carried out on the fly ash - silicate suspensions corresponding to a $(w/s)_m$ of 0.25. The results of this experiment are presented in Figure 9-13 which also shows the influence of reducing M_s on the rheological behavior of the system. Noted from this figure is the significant change in behavior for the suspensions at a low M_s with respect to both the storage and loss moduli. The storage modulus (G') and loss modulus (G'') are related to the elastic and viscous portions of a

viscoelastic material respectively (Barnes, Non-Newtonian, and Mechanics 2000; Nehdi and Rahman 2004b). The expected trend in cementitious suspensions is a plateau region at low stress indicative of the linear viscoelastic region, followed by a significant decrease in both the storage and loss moduli at higher stresses, which indicates structural breakdown of the suspension (Nehdi and Rahman 2004b). This low stress plateau is noted in all suspensions investigated except the K-Si suspension at an M_s of 1.5, which is likely present at a further lower stress than that investigated in this study. Performing this experiment at further lower stresses resulted in increased data scatter due to the fact that the measured stresses were nearing the torque limit of the instrument, and hence they are not presented here. At lower M_s values, the critical linear viscoelastic stress is shifted drastically to the left, and the height of the plateau region is an order of magnitude lower. The significantly higher storage modulus for the higher activator M_s suspension indicates a more structurally organized system, which supports the observations and explanations discussed earlier. At an M_s value of 1.5 there is a change in behavior of the suspension, possibly attributed to the charged colloidal siliceous species present in this system, or extreme surface charge effects on the fly ash particles. Further, the drastic decrease in magnitude of the stress plateau and leftward shift of the critical linear viscoelastic stress is indicative of a behavior similar to that observed in OPC suspensions in the presence of high-range water reducing admixtures (Nehdi and Rahman 2004b). A lower stress plateau is indicative of well-dispersed particles in a suspension with a less defined networked structure, likely caused by increased repulsive forces between fly ash particles. The exact nature of this phenomena requires future investigation, particularly in the context of understanding the speciation of alkali-silicate activator solutions. Given the noted inconsistencies in the use of

superplasticizers in geopolymer suspensions (Palacios et al. 2009b), an understanding of this phenomena may allow for optimization of the flow properties of geopolymer concretes without the use of chemical admixtures.

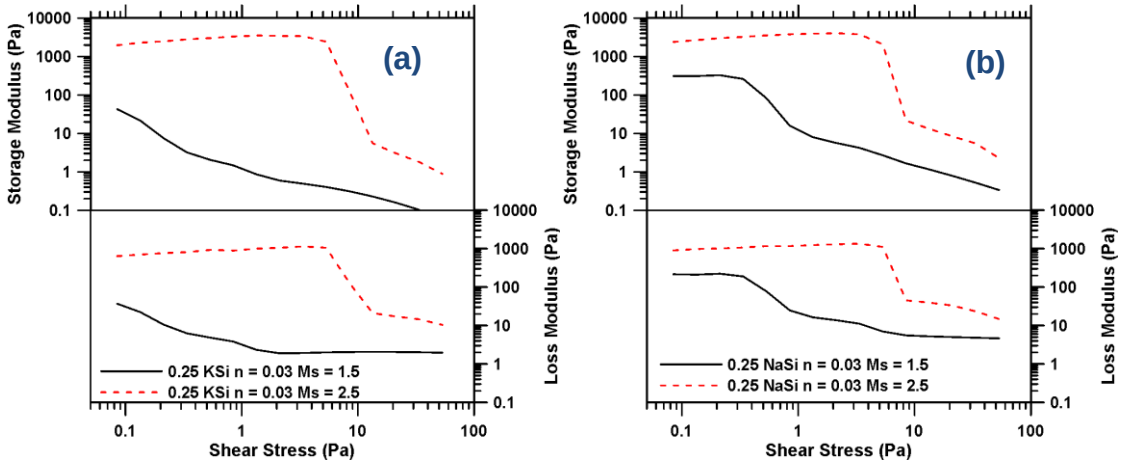

Figure 9-13: Oscillatory shear study of 0.25 $(w/s)_m$ fly ash suspensions with (a) K-Si based activator, and (b) Na-Si based activator

9.4 Conclusions

The influence of activator type and concentration on the rheological characteristics of fly ash suspension is reported in this paper. Hydroxides and silicates of Na and K were used as the activation solutions, the viscosities of which increased with molarity (for hydroxides) or M_s (for silicates), with the Na-based activators demonstrating increased viscosity. The rheological properties of NaOH or KOH activated fly ash were found to be primarily influenced by the changes in the viscosity of the suspending fluid and surface charge of the fly ash particles. Na-based suspensions demonstrated a large increase in viscosity due to the more significant increase in the viscosity of the suspending fluid while K-based suspensions showed a more significant increase in yield stress, attributed to the greater adsorption of weakly hydrated K^+ ions onto the surface of the fly ash particles, reducing the repulsive effect between fly ash particles.

The rheological response of fly ash-alkali silicate suspensions were found to be more complex. The yield stress and plastic viscosity of suspensions were observed to increase with M_s with the yield stress tending to zero (approaching a Newtonian behavior) at low activator M_s values. Increasing the water-to-solids ratio and/or the n value of the suspension resulted in significantly different yield stress and plastic viscosity trends for the Na- and K-based suspensions, pointing to the influence of both the activation solution viscosity and cationic adsorption on the fly ash particle surfaces that greatly influence the suspension rheology. Experiments on suspensions with controlled activation solution-to-binder ratios (volume-basis) showed the influence of several key parameters on the rheological properties. The plastic viscosity was found to be influenced strongly by the solid loading and the activation solution viscosity, while yield stress appears to be less influenced by activation solution viscosity and more strongly influenced by interaction effects produced by the surface charges on the fly ash particles, which are dependent on the cationic type.

In silicate based suspensions, at low M_s values, the suspension demonstrated a transition to a Newtonian behavior, with a zero yield stress. While the OPC and hydroxide-based suspensions demonstrated a viscosity range of about 4 orders of magnitude from the highest to lowest shear rate (100/s to 0.005/s), the viscosity of the silicate based suspensions increased by only 2 orders of magnitude over the same shear rate range. The fly ash-water suspension also behaved similar to the OPC-water and fly ash-MOH suspensions. A small amplitude oscillatory stress growth experiment showed that the critical linear viscoelastic stress plateau shifts to much lower shear stress ranges, and the storage/loss moduli reduces at lower M_s values, akin to the response of superplasticized cementitious suspensions. The exact nature of this transition is not fully understood and requires additional work.

Rheological Characterization of Fresh Alkali Activated Slag Suspensions: Influence of Activator Type

9.5 Introduction

Geopolymers are a type of gel binders that was first introduced by Davidovits in 1970 (4). These materials are referred to using several names: (i) alkali-activated-cement (5), (ii) inorganic polymer (6), (iii) geopolymer (4,7–10), and (iv) pozzolonas. These products can be synthesized at room temperature by mixing reactive aluminosilicate materials with strong alkaline solutions. These solution activators generally include hydroxides, silicates, carbonates, aluminates etc. (such as NaOH, KOH, Na_2SiO_3, K_2SiO_3 etc.). The aluminosilicate raw materials predominantly used are fly ash (class C and F), slag, metakaolin etc. Although in our study we have used configurations of slags prominently, some with combination of slag and fly ash as well. Geopolymers based on coal fly ash display superior paste workability with less water, which may result in improved mechanical properties (11). There has been some work done on the effects of admixtures on geopolymer systems (12–15). Although very less research in rheology has been carried out to study the effect of activator on the raw material and the resultant constitution of the paste obtained (16,17).

Millions of tons of metallurgical slags, consisting mainly of silicate and glassy phases, are produced every year. The generation of slags reaches almost 15% of the quantity of metal produced (18–20). On rapidly chilling the molten slag with by immersion in water, a vitreous phase of Ca-Al-Mg silicate fine grain is obtained having more cementations properties. Slag contains much reactive SiO_2 and Al_2O_3, and thus can prove to be a better raw material to synthesize high value geopolymer. Large quantities of slags are still disposed of in surface dumps or under the sea in several countries (8,21).

The current study aims to explore the rheological performance of slag based geopolymer materials activated using solutions of sodium or potassium hydroxide as well as sodium or potassium silicate. An understanding of the effects of activator constitution of the flow properties of these suspensions provides insight into preferential activator methodologies with respect to concrete workability, as well as gives insight into the nature of fresh geopolymer materials. A review of the literature has found very little work done on the influence of activator type and constitution on the rheological properties of these pastes (15,16). This paper aims to add to the understanding of these systems as well as determine the influence of activator type and constitution on the rheological properties of these systems. The current study has three primary goals with respect to blast furnace slag based geopolymeric suspensions: (Part 1) to determine the influence of activator type and chemical constitution on the rheological properties in the fresh state and (Part 2) to examine the nature of the rheological properties of these systems as compared with portland cement and fly ash based suspensions.

9.6 Experimental Program

9.6.1 Experimental Materials

A low calcium slag was used for all experiments. Two different slags were used, the first for the "Normal" range studies and the second for the "Wide" studies. The chemical composition of these slags is presented in Table 10-1. Additionally, a fly ash was used for rheological investigation of fly ash-slag mixtures. It is notable, that due to the flash setting behavior of some alkali-activated slag systems, particularly with the second slag with higher magnesium content, some rheological experiments could not be completed for certain mixtures. Two different types of activators were used in this study, hydroxide based

activators and silicate based activators. The hydroxide based activators were composed of Na- or KOH at molar ratios of 4 and 8. The mass-based activator solution-to-powder ratio of these mixtures was fixed at 0.60 which corresponds to a volumetric activator-to-powder ratio of between approximately 1.60 and 1.70. The silicate activators were composed of Na or K-silicates with additional added NaOH or KOH to modify the sodium contents. The sodium silicate was E-sodium silicate and the potassium silicate was KASIL 33, both supplied by PQ Corporation.

Table 9-2: Chemical composition of study materials

Mat.	SiO_2	Al_2O_3	Fe_2O_3	CaO	MgO	SO_3	Na_2O	K_2O	LOI	SSA
Slag 1	39.4 %	6.9%	0.4%	38.0 %	8.5%	2.09 %	1.7%		3.0 %	487 m^2/kg
Slag 2	39.4 %	8.5%	0.4%	35.5 %	12.63 %	2.89 %		0.39 %		487 m^2/kg
FA	58.4 %	23.8 %	4.19 %	7.32 %	1.11%	0.44 %	1.43 %	1.02 %	0.5 %	218 m^2/kg

The sodium and potassium silicate solutions for activation were proportioned considering two parameters: (i) n – the ratio of M_2O in the activator to the total fly ash content; and (ii) M_s – the ratio of SiO_2 to M_2O in the activator. Two different n values were used: 0.03 and 0.05. The mass-based M_s values of the as-obtained Na- and K-silicates were 3.22 and 2.10 respectively, which corresponds to mole-based values of 3.32 and 3.29. The solids content in the silicate solutions were approximately 36%. Requisite amounts of NaOH or KOH were added to the silicate solutions to bring the M_s (mole-based) values down to 2.5 or 1.5 for both Na- and K-silicate solutions. M_s values in this range were found to be necessary to ensure sufficient activation and strength development. For the Na- and K-silicate activated slag, the mass-based water-to-solids ratios - $(w/s)_m$ - used were 0.35 and 0.40

which corresponds to a $(a_s/p)_v$ of between 1.09 and 1.39 and between 1.10 and 1.44 for 0.20 and 0.25 mixtures of K- and Na-silicate respectively.

9.6.2 Mixing and Testing Procedure

The experimental design has been divided into two distinct studies, the first a study using typical shear rate ranges common in rheological studies of cementitious systems (REF), and the second an exploration of these systems over wider shear rates to determine the accuracy of model prediction and to more thoroughly compare these materials with portland cement based materials as presented in Chapter 7.

Liquid activators were prepared prior to mixing with the binder (slag), and allowed to cool to room temperature prior to use, typically a period of 3-4 hours. For rheological studies of the activators, approximately 12 mL of solution was extracted using a disposable syringe and placed in the rheometer geometry as soon as the solution had achieved room temperature as measured by an infrared thermometer. For investigation of the fresh geopolymer solutions, approximately 200g of the suspension was prepared and mixed in a kitchen blender at the high setting using the following sequence: (1) initial hand mix to disperse powder in activator and assure no powder has stuck to edges of mixing container, (2) mixing in blender on high for 30 seconds, (3) 30 second covered rest period, and (4) final mixing at high in blender for 30 seconds. This mixing sequence was selected as a modification to the ASTM C1738 procedure, as it showed similar results, and the reduced size of the kitchen blender versus the high shear blender allowed for significant material savings. After mixing was completed, approximately 6mL of sample was extracted using a disposable syringe and placed immediately in a TA Instruments AR2000EX rotational rheometer configured for the given experiment. For the characterization of the activator

solutions, a concentric cylinder geometry was used, with the surfaces of both the cup and bob roughened by grit blasting to reduce the influence of slip. The gap for the concentric cylinder experiment is fixed at 1.0 mm. For all other experiments, a 50mm diameter parallel plate configuration was used with a serrated surface on both the geometry and the Peltier plate (serration depth of 0.15mm on the Peltier plate and 1.0 mm on the geometry). The gap for these experiments was set to 2.0 mm as this was found to be a reasonable gap for rheological measurements of cement pastes of similar fluidity in a recent study (22). The Peltier plate surface temperature was set to 25±0.1 °C. The approximate time from the addition of the activator to the start of the rheological experiment was two and a half minutes. Experimental values for shear stress and shear rate were extracted using TA Instruments' TRIOS software package.

The general rheological experiment for these studies consist of varying the shear rate using: (1) a stepped ramp up pre-shear, (2) a subsequent stepped ramp up, and (3) a stepped ramp down. At each step except during the pre-shear, shear stress values are recorded every second, with the step termination criteria set at the point at which steady state has been achieved defined by 3 consecutive measurements within 5% of each other. For all studies, the values used in determining rheological properties are the steady state values of shear stress and the related shear rate. Two different rheological experiments were conducted for this project. All samples prepared for Part 1 including the rheological investigation of the activators were conducted using a "normal" rheological procedure consisting of shear rate ranges from 5 to 100/s, while the Part 2 comparative study of geopolymer and cement pastes was conducted with a "wide" study with shear rates from 0.005 to 100/s. The "wide" experiment was implemented to more thoroughly investigate the influence of shear rates

and to assess the presence of the stress plateau reported in Chapter 7. A graphical representation of the two rheological procedures used in this study is presented in Figure 10-1.

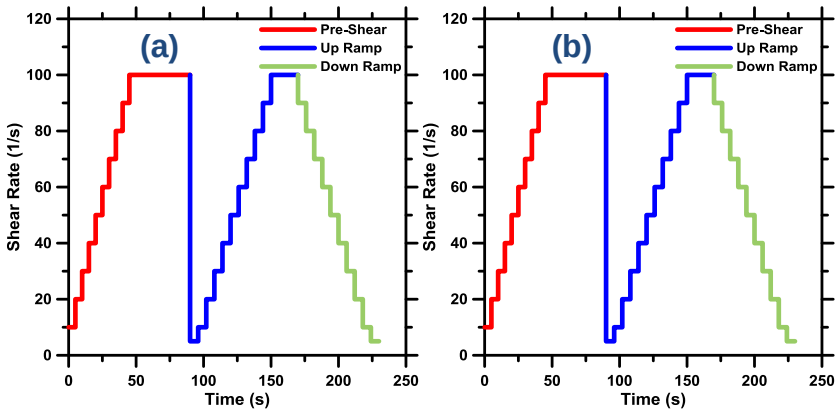

Figure 9-14: Rheological procedure: (a) "normal" shear range, (b) "wide" shear range

The rheological model parameters for the "normal" shear rate range (5-100/s) of the slag suspensions were calculated using a least squares fitting to the Bingham model of the down-ramp data as shown in Equation 10-2 (23). The average viscosity for the activator solutions was determined using a least squares fit to the Newtonian model presented in Equation 1. The use of Bingham and Newtonian models in this shear rate range can be justified by the generally linear nature of the shear stress-shear rate response. In these equations, τ is the shear stress (in Pa), τ_y is the yield stress (in Pa), η_a is the average viscosity (in Pa.s), η_p is the plastic viscosity (in Pa.s), and $\dot{\gamma}$ is the shear rate (in s^{-1}).

Newtonian: $\tau = \eta_a \dot{\gamma}$ Equation (10-1)

Bingham: $\tau = \tau_y + \eta_p \dot{\gamma}$ Equation (10-2)

9.7 Results and Discussions

This section discusses the influence of the constitution of the alkali activator solution on determined rheological parameters extracted using the Bingham model. Rheological studies of the activator solution itself, as well as the influences of the activator solution on the resultant slag geopolymer suspension are presented.

9.7.1 Rheological Behavior of Activated Solution

A rheological study of the activator solutions were performed using the "normal" procedure as discussed in Section 2 and the concentric cylinder geometry. Sodium and potassium based activators were examined to explore the influence of molarity as well as alkali ion on the rheological properties of the activator solutions. Additionally, experiments were completed on both sodium and potassium silicate solutions to investigate the influence of n, M_s and alkali ion on the rheological properties of these solutions. All of the activator solutions investigated indicated Newtonian behavior over the range of shear rates investigated, indicating, as would be expected for an aqueous solution, the lack of a yield stress. The average viscosity was extracted using a least squares fit to the Newtonian model (Equation 10-1), with a stress intercept set to zero. A typical flow diagram of this activator study is presented in Figure 10-2, indicating Newtonian behavior.

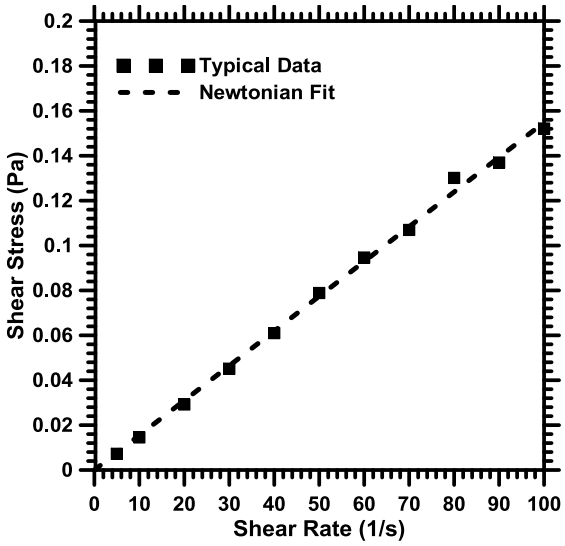

Figure 9-15: Typical results of activator rheology showing Newtonian least squares best fit

The influences of alkali cation, molarity, and n and M_s respectively on the determined average viscosity of the activator solutions is presented in Figure 9-3. For reference, the viscosity of water at 25 °C is approximately 8.9e-4 Pa-s, thus potassium based activator solutions at low M_s and high $(w/p)_m$ are comparable to the characteristics of water, while all other activator solutions indicate average viscosities which are significantly higher as compared to water.

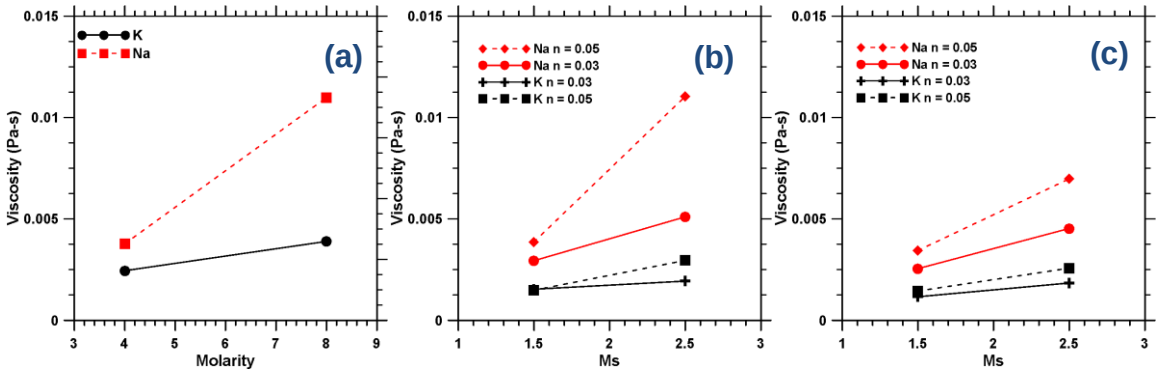

Figure 9-16: Activator rheology, viscosity determined using a Newtonian model, (a) influence of molarity on KOH and NaOH activator solutions, and influence of n and M_s on KOH and NaOH silicate activators for: (b) 0.35, and (c) 0.40 $(w\text{-}s)_m$ activators.

The results presented are similar to those in a companion study on fly ash geopolymer suspensions reported in Chapter 9, as would be expected. For a more thorough discussion of changes in rheological behavior in the activator solutions the author directs the readers to Chapter 9. However, it is generally noted that increasing the molarity in hydroxide based solutions result in an increase in average viscosity, further this increase is more substantial in Na based solutions. This behavior is attributed to the greater charge density of the Na^+ ions in solution which results in more significant ion-dipole forces as compared to the less charge dense K^+ ions. With alkali-silicate solutions, it is noted that an increase in M_s corresponds with an increase in activator viscosity. It has been reported that both ionic and colloidal silica species are present in these solutions (24,25). Decreasing the M_s of the solution requires the increased inclusion of alkali-hydroxide, the presence of these hydroxides break Si-O-Si chains in the polymerized colloidal species, resulting in decreased molecular size and decreased polymerization. This subsequently results in a decrease in determined activator viscosity, due to decreased colloidal particle size. Alternatively, as the n-value is decreased, this indicates an increase in silicon, which would result in an increase in colloidal molecule concentration and increase the activator viscosity. Comparing the values for Na and K-based solutions in alkali-silica solutions, Na-based solutions are noted to have significantly higher determined viscosities at the same value of n and M_s. This behavior is attributed to the fact that due to the relative molecular weights of the two alkali elements, there is a significantly higher ionic quantity of Na required as compared to K, when combined with the fact that sodium ions are more charge dense, results in significantly higher determined rheological properties.

9.7.2 Rheological Behavior of Fresh Slag Suspensions Activated Using KOH or NaOH

Rheological studies of fresh slag suspensions were performed with plain cation-hydroxide based activators. These studies were performed using the "Normal" shear rate range as presented in Section 10.2, with rheological parameters determined using a least squares fit of the Bingham model (Equation 10-2).

The results of rheological studies of hydroxide based slag geopolymers are presented in Figure 10-4. Notable from this figure are the generally increasing trends in both plastic viscosity and yield stress with increasing molarity. Further, at all levels tested, sodium based suspensions have a higher determined yield stress and plastic viscosity than potassium-based suspensions. For both potassium and sodium based activator solutions, yield stress is noted to increase at approximately the same rate, while plastic viscosity increases more drastically in the case of sodium based activator solutions.

The yield stress of concentrated suspensions is dictated by particle interactions, interparticle forces (Van der Waals and steric), and the viscosity of the suspending fluid (26–30). As the volume of suspending fluid is roughly constant in these experiments, the effects of particle interactions and Van der Waals forces can be neglected from this comparative discussion. The increase in yield stress with increasing M_s can thus be partially attributed to the increase in activator viscosity as presented in Figure 10-2. It is, however, noted from Figure 10-2 that Na-based suspensions show a significantly higher increase in activator viscosity as compared to K-based suspensions. As the upper panel in Figure 10-4 indicates a consistent increase between Na and K-based suspensions, there is clearly a secondary effect present. Based on the above listed influences on yield stress, it is clear that this effect is interparticle steric (repulsive) forces. Zeta potential studies of the

slag at a neutral pH indicate that it possesses a negative surface charge under these conditions, which is in general agreement with the literature (31,32). Zeta potential studies of these suspensions under the experimental conditions of this study were not possible due to the extremely high pH of the system (on the order of 14) and particle concentrations in excess of the instrument specifications. Thus, zeta potential studies were performed on a significantly more dilute solution with a pH of about 10, these results cannot conclusively be used to verify the behavior of these suspensions in this study, as the ion concentrations would be 4 orders of magnitude greater, however they generally indicate that K-based suspensions have a lower absolute surface charge (closer to zero) than Na-based suspensions. This result is consistent with that reported by (33), where the poorly hydrated K^+ ion adsorbs more readily on the surface of the particle resulting in a more significant change in surface charge in the presence of K^+ ions as compared to the well hydrated Na^+ ions. Thus, the consistent trend with respect to yield stress can be explained as follows. In Na-based suspensions, increasing the molarity results in an increase in activator viscosity and a negligible change in slag particle surface charge, thus the more significant increase in activator viscosity is counteracted by the large interparticle repulsive forces between slag particles. Conversely, in K-based suspensions the diminished increase in activator viscosity is supplemented by the diminished influence of steric forces due to a decrease in the absolute surface charge of the slag particles, which results in a decrease in repulsive forces between slag particles.

The determined plastic viscosity results in the lower panel of Figure 10-4 indicate a trend that is similar in nature to the viscosity of the activator solutions presented in Figure 10-2. Increasing the molarity of the solution results in a more significant increase in plastic

viscosity for Na-based solutions than for K-based solutions. With increasing molarity from 4 to 8, the activator viscosity is noted to increase by a factor of approximately 1.6 and 2.7 for K and Na-based solutions respectively. The plastic viscosity of these suspensions is similarly shown to increase by a factor of 1.5 and 3.3 for K and Na-based suspensions respectively. This similar trend indicates that the influence of activator viscosity is likely a dominant effect on plastic viscosity for these suspensions.

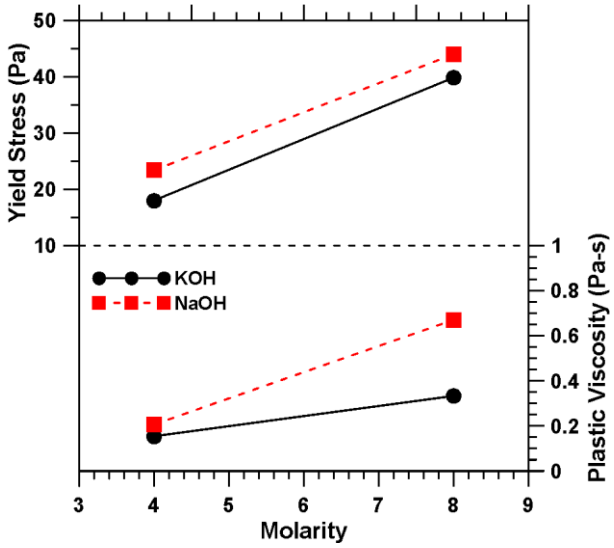

Figure 9-17: Influence of molarity of KOH and NaOH activators on determined rheological properties using the Bingham model for 0.60 $(a/p)_m$

9.7.3 Rheological Behavior of Fresh Slag Suspensions Activated Using K-Si or Na-Si

Results of a similar study using silicate based activators are presented in Figures 10-5 and 10-6. For both activator types, increasing the activator water-to-solids ratio $(w/s)_m$ results in a decreased determined yield stress and plastic viscosity as would be expected. Increasing the quantity of a fluid in a suspension increases particle spacing, thereby increasing the activator film thickness, which decreases the particle interactions resulting in a decrease in determined yield stress and plastic viscosity. Further, an increase in $(w/s)_m$ ratio corresponds to a decrease in activator viscosity as presented in Figure 10-2, which

would further increase flowability of the paste. With the exception of the Na-based suspension at a $(w/s)_m$ of 0.40, increasing the M_s value leads to an increase in estimated plastic viscosity and yield stress. In all suspensions, increasing the n-value is shown to decrease the yield stress. These increases in plastic viscosity and yield stress can be partially attributed to the increase in activator solution viscosities as presented in Figure 10-2. However, the presence of a decrease in plastic viscosity for some solutions indicates the presence of multiple phenomena.

Increasing the value of n, on the other hand, is shown to generate varying effects. For all suspensions yield stress is increased with decreasing n-value, while plastic viscosity is increased for K-based suspensions and decreased for Na-based suspensions with increasing n. It is noted that as the n-value is increased, the viscosity of the activator solution is increased as well, thus an increase in yield stress of the suspension would be expected. This indicates competing effects present, identified as the activator solution volume, the activator solution viscosity, and the repulsive forces between slag particles and charged colloidal and ionic siliceous species present in the activator solution. Increasing the n-value increases the activator viscosity, but also concurrently increases the volumetric ratio of activator solution to powder as well as the quantity of silicon present in the activator solution.

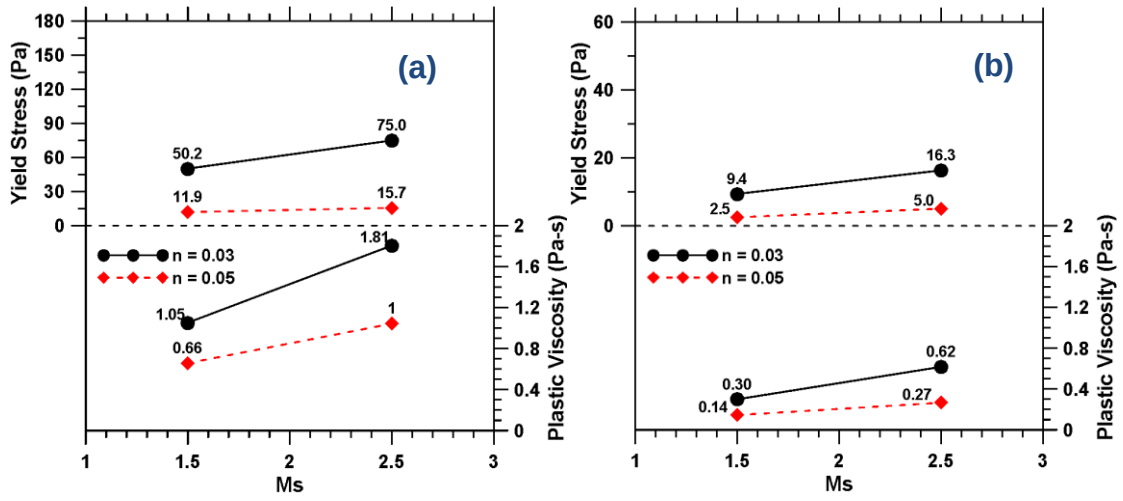

Figure 9-18: Influence of M_s in K-Si activated pastes on determined rheological properties using the Bingham model for: (a) 0.35 $(w/s)_m$ and (b) 0.40 $(w/s)_m$

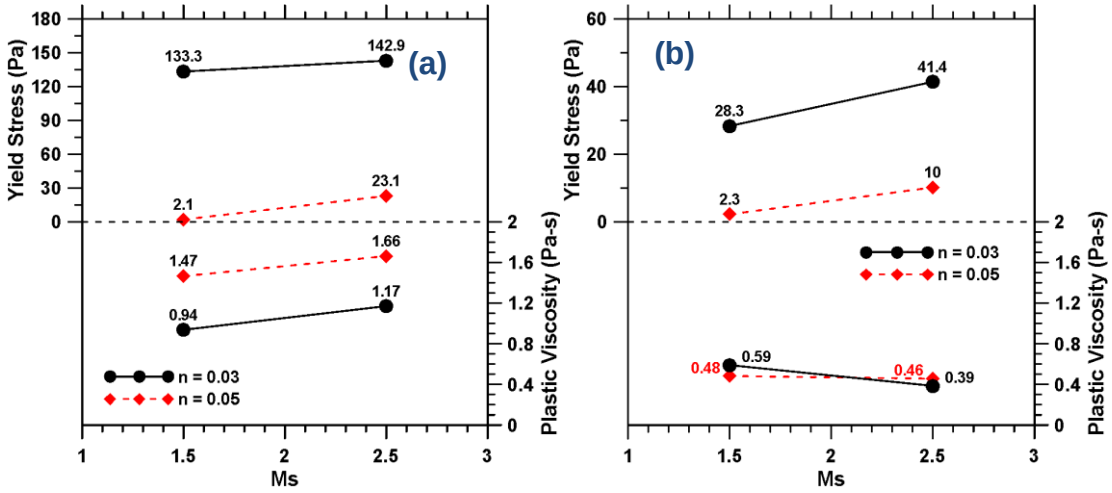

Figure 9-19: Influence of M_s in Na-Si activated pastes on determined rheological properties using the Bingham model for: (a) 0.35 $(w/s)_m$ and (b) 0.40 $(w/s)_m$

Similar to the fly ash suspensions investigated in Chapter 9, several of the suspensions at an M_s of 1.5 indicated a behavior that was approximately Newtonian as illustrated by the near zero yield stresses in Figures 10-5 and 10-6. However, unlike with the fly ash based suspensions, this Newtonian behavior was only noted at an n value of 0.05. Similar to the fly ash suspensions in Chapter 9, the Newtonian slag suspensions indicated a shift in the apparent viscosity trend, which is again similar to that seen in portland cement suspensions

with superplasticizers present. This indicates that this Newtonian shift may be resultant from the presence of charged siliceous species present in the activator solution acting to repulse slag particles and decrease the influence of agglomeration formation thereby increasing the available free solution and increasing the flowability of the paste.

Further notable from Figures 10-5 and 10-6 is the increase in flowability of the suspension when silicates are present as compared to without (Figure 10-4). For the suspensions investigated, the volumetric activator solution to powder ratio for hydroxide based suspensions is approximately 1.6, while for silicate based suspensions it varies from approximately 1.2 to 1.4 at a $(w/s)_m$ of 0.40. Comparing Figure 10-4 with Figures 10-5(b) and 10-6(b), it is noted that all of the silicate based suspensions had comparable or lower determined rheological properties, while the volume of the suspending fluid was *lower*. This effect may be partially attributed to the fact that the viscosity of these activating solutions at a $(w/s)_m$ of 0.40 was considerably lower for silicate based activators as compared to pure hydroxide based activators. The increased flowability of silicate based suspensions compared to hydroxide based suspensions may also be attributed to the charge of the siliceous species present in the activator solution and the increased absolute surface charge of the slag particles in the presence of siliceous species resulting in increased steric forces between slag particles.

To further explore the nature of these suspensions, Figure 10-7 presents the results of the above data plotted against the activator solution to powder ratio $(A_s/p)_V$. It is notable that this ratio is different from the $(w/s)_m$ ratio in that it is the volumetric ratio of the total activator solution (including dissolved solids) to the volume of powder added, while the $(w/s)_m$ ratio is the mass ratio of water to all solids added (including those added in the

activator). The $(A_s/p)_V$ ratio is a more appropriate ratio for these studies as rheological performance of suspensions is strongly influenced by the volumetric ratio of the suspending solution to the suspending particles. Figure 10-7 illustrates an expected trend in these suspensions of decreasing measured rheological properties with increasing $(A_s/p)_V$, as an increased volume of suspending solution increases particle spacing and decreases particle interaction. However, this trend is not as consistent as would be expected with increasing volume of solution for typical suspensions. For K-silicate suspensions (Figure 10-7(a)), the trend is quite consistent for both determined yield stress and plastic viscosity, with two approximately parallel lines as the volume of activator solution is increased, with the higher offset line noted to be the values at the higher M_s. This offset may be partially attributed to changes in the viscosity of the activator solution as presented in Figure 10-2. Increasing M_s is noted to increase the viscosity of the activator, which would subsequently decrease the flowability of the suspension. For Na-silicate suspensions (Figure 10-7(b)), the trend is less consistent. Yield stress continues to show a generally decreasing trend with increasing $(A_s/p)_V$, however as Figure 10-7(b), there is a noted increase in scatter. The two points that deviate most significantly from this trend are noted to again be at n-values of 0.05 and M_s values of 1.5, the points that indicate a transition to Newtonian behavior. The increase in scatter may also be attributed to the more significant influence of activator viscosity. Similarly, the plastic viscosity figure for Na-silicate suspensions show increased scatter with respect to $(A_s/p)_V$, though the general trend is decreasing plastic viscosity with increasing $(A_s/p)_V$. As previously noted, unlike for K-silicate suspensions, increasing the n-value increases the plastic viscosity, a behavior indicating a more significant influence of activator viscosity and a decreased influence of ion adsorption on the surface of slag.

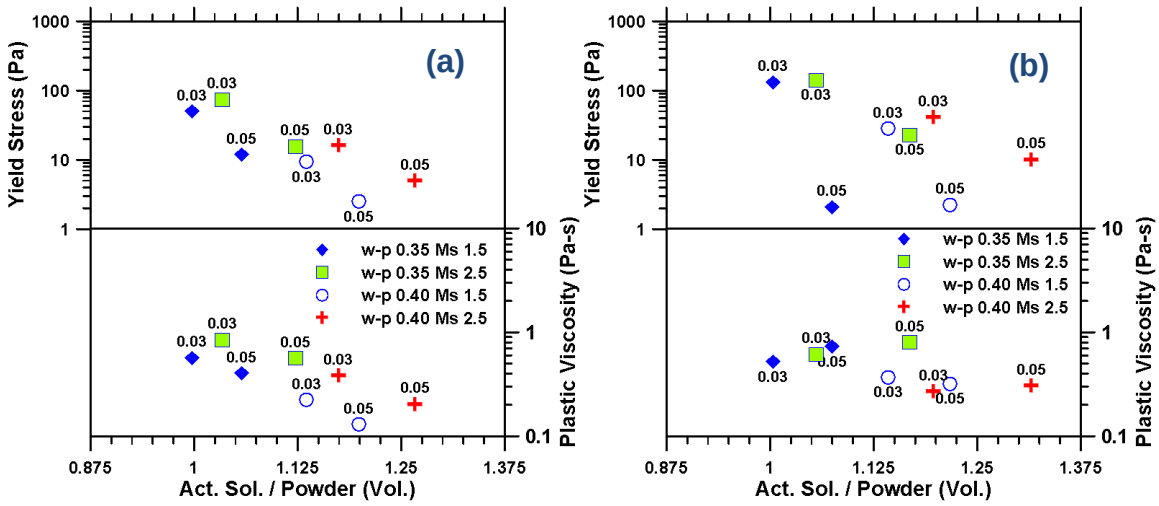

Figure 9-20: Influence of $(A_s/p)_V$ ratio of suspension on determined rheological properties for: (a) K-silicate, and (b) Na-silicate suspensions

9.7.4 Influence of Fly Ash Addition on Determined Rheological Properties of Slag Based Geopolymers

Rheological studies of fly ash-slag blended suspensions (50% by volume slag) were performed using the rheological procedure as described in Figure 10-1 and rheological parameters were extracted using the Bingham model (Equation 10-2). The results of this study are presented in Figure 10-8. All experiments were performed at an n-value of 0.05 and $(w/s)_m$ ratio varying from 0.30 to 0.35. The results of 0.35 $(w/s)_m$ plain slag are presented for reference. It is evident from this figure that the inclusion of fly ash results in a significant depression of yield stress at the same $(w/s)_m$ ratio, and a reduction even at the lower $(w/s)_m$ ratio of 0.30. It is also noted to decrease the determined plastic viscosity at the same $(w/s)_m$ ratio. For K-silicate suspensions (Figure 10-8(a)), the yield stress can be seen to shift from a Bingham to Newtonian behavior when fly ash is added to the suspension at an M_s of 1.5. The reduction in yield stress is attributed to the inclusion of approximately spherical fly ash particles, which results in a reduction of surface area and a subsequent increase in activator-film-thickness. Studies of fly ash suspensions indicate

Newtonian behavior at an M_s value of 1.5 as noted in Chapter 9, thus the inclusion of fly ash promotes the shift to this behavior. This behavior importantly illustrates that the surface charge of fly ash and slag in these suspensions is likely of the same sign, otherwise addition of fly ash would likely have shown yield stress increases due to the presence of interparticle attractive forces between particles with opposite surface charges. Plastic viscosity similarly decreases to the increased flowability of the solution resultant from the inclusion of spherical fly ash particles with a lower surface area increasing the amount of free suspending solution present and decreasing particle contacts.

Similarly, for Na-silicate suspensions (Figure 10-7(b)) both the yield stress is seen to decrease at either $(w/s)_m$ ratio studied and the plastic viscosity is shown to decrease at the same $(w/s)_m$ ratio. However, the reduction is not as significant at the low M_s when compared to K-silicate suspensions. This is due to the fact that the Newtonian behavior is already present in slag suspensions at this $(w/s)_m$, n-value and M_s (Figure 10-6(b)). As with K-silicate suspensions, the changes in yield stress and plastic viscosity with fly ash addition are attributed to the decrease in surface area and inclusion of the spherical fly ash particles which enhance flow. Similarly, the decrease upon fly ash addition indicates a likely same sign of surface charge for fly ash and slag in these Na-silicate solutions.

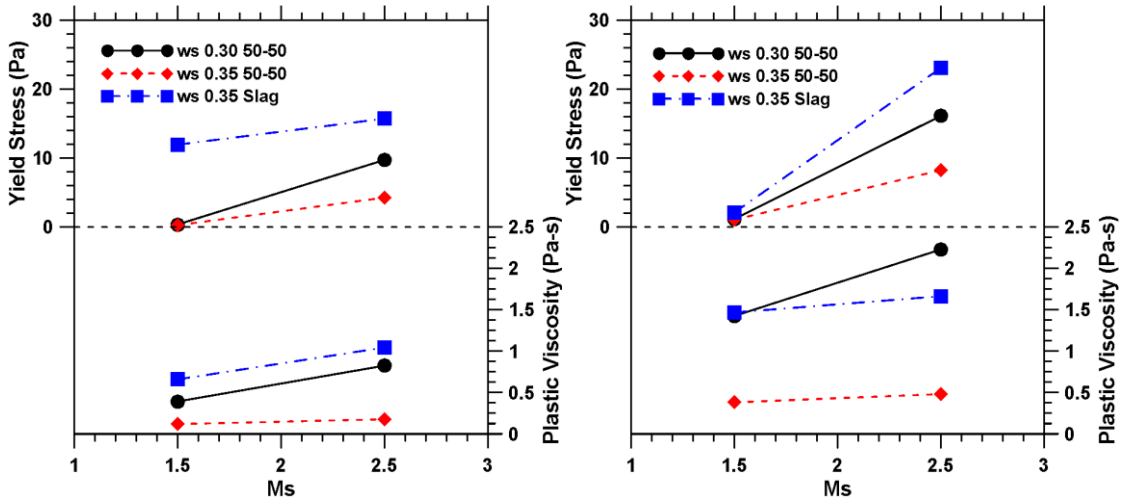

Figure 9-21: Influence of fly ash addition at 50% mass ratio for (a) K-Si and (b) Na-Si at $(w/s)_m$ ratios of 0.30 and 0.35, n-value of 0.05, and M_s ratio at 1.5 and 2.5. Results for slag at 0.35 with same n and M_s values included for reference.

9.8 Conclusions

This paper reports on the influence of activator constitution and type on the determined rheological properties of fresh slag geopolymer and slag-fly ash blended geopolymer suspensions. Hydroxide based activators and silicate based activators are used. The following phenomena are noted:

The rheological characteristics of the activator solutions are influenced by both selected cation and concentration. Sodium based geopolymer activator solutions showed higher average viscosities than potassium based activators.

Increasing molarity in hydroxide based geopolymer suspensions results in increased yield stress and plastic viscosity. This is attributed primarily to decreased flowability of the suspending fluid and in the case of less well hydrated potassium cations, an influence of decreasing the negative surface charge of fly ash as the cations are adsorbed on the surface of the fly ash particles.

Silicate based suspensions illustrate a more complex behavior. At intermediate M_s values the fluid behavior transitions to Newtonian, with a very low yield stress, the existing of a similar behavior in fly ash based geopolymer suspensions indicate that this effect is likely due to the chemical composition of the activator solution and may be related to the presence of highly charged colloidal siliceous species present acting to disperse slag particles. However, the nature of this phenomena requires further exploration.

10. CONCLUSIONS

10.1 Part I Conclusion

The use of limestone as portland cement replacement is thoroughly investigated from an early age hydration and pore structure perspective with and without the inclusion of additional alumina. Several key aspects are noted:

- There is a noted size effect of limestone inclusion, when limestone which is as coarse as OPC is used, it acts primarily as a filler, leading to a reduction in desired mechanical properties and pore structure characteristics, with no noted hydration benefits. This effect is attributed to a dilution of OPC in the system. Fine limestone illustrates more beneficial properties, enhancing the tortuosity and accelerating hydration product formation, with minimized impacts on strength.
- The addition of alumina (fly ash or metakaolin) in limestone replacement systems is shown to be beneficial with respect to hydration product formation, hydration, and pore structure.

10.2 Part II Conclusion

The rheological characterization of various cementitious materials brought about explorations of several key phenomena in these systems:

- The influence of dispersion, electrostatic repulsive forces, and solid loading are found to be dominant on the determined apparent yield stress. Plastic viscosity, on the other hand, is not particularly influenced by interparticle forces, however is more strongly influenced by the viscosity of the suspending solution.

- A yield stress plateau method is used and confirmed to be reliable for determination of rheological properties in concentrated suspensions, it is shown to be less prone to error than other commonly used models.
- The influence of limestone in cementitious systems is fully explored, it is noted that limestone inclusion decreases net interparticle attractive forces in the particle network, decreasing the yield stress when all other suspension parameters are held constant. The size effect is crucial to suspensions, where despite the increase in attractive forces, inclusion of fine limestone increases determined rheological properties due to increased surface area and decreased particle spacing and water film thickness.

10.3 Future Work

The following is a brief overview of proposed activities to continue the work in this dissertation

- Further investigation of the rheological nature of concentrated suspensions, including effects of particle self-diffusion and localized areas of lower particle concentration. These effects influence the flow of cementitious suspensions, and may have influences on later age durability characteristics.
- Investigations of the chemical nature of alkali activator solutions, including investigations of their nature and the chemical species present in the solutions. This exploration will provide insight into the Newtonian transition noted in some alkali activated geopolymer suspensions.
- Further investigation of the pore structure of portland limestone cement systems, including investigations of potential synergistic benefits of inclusion of alumina sources in these mixtures. Impedance spectroscopy and thermoporometry will provide additional insight into the nature of these hardened pastes.

- Investigating the use of rheometry to determine the time dependent viscoelastic property development of cementitious pastes using oscillatory shear techniques.

BIBLIOGRAPHY

Alonso, C, C Andrade, M Castellote, and P Castro. 2000. "Chloride Threshold Values to Depassivate Reinforcing Bars Embedded in a Standardized OPC Mortar." *Cement and Concrete Research* 30 (7): 1047–55. doi:10.1016/S0008-8846(00)00265-9.

Ambroise, J., S. Maximilien, and J. Pera. 1994. "Properties of Metakaolin Blended Cements." *Advanced Cement Based Materials* 1 (4): 161–68.

Antoni, M., J. Rossen, F. Martirena, and K. Scrivener. 2012. "Cement Substitution by a Combination of Metakaolin and Limestone." *Cement and Concrete Research* 42 (12): 1579–89. doi:10.1016/j.cemconres.2012.09.006.

Asaga, K., and D.M. Roy. 1980. "Rheological Properties of Cement Mixes: IV. Effects of Superplasticizers on Viscosity and Yield Stress." *Cement and Concrete Research* 10 (2): 287–95. doi:10.1016/0008-8846(80)90085-X.

Astarita, Gianni. 1990. "Letter to the Editor: The Engineering Reality of the Yield Stress." *Journal of Rheology* 34: 275.

"ASTM C109 / C109M - 12 Standard Test Method for Compressive Strength of Hydraulic Cement Mortars (Using 2-In. or [50-Mm] Cube Specimens)." 2012. In ASTM International, West Conshohocken, PA.

"ASTM C109-13. Standard Test Method for Compressive Strength of Hydraulic Cement Mortars Using 2-In. Cube Specimens." 2013. In ASTM International, West Conshohocken, PA.

"ASTM C1157/C1157M-11 Standard Performance Specification for Hydraulic Cement." 2013. In ASTM International, West Conshohocken, PA.

"ASTM C143 - 12. Standard Test Method for Slump of Hydraulic-Cement Concrete." 2012. In ASTM International, West Conshohocken, PA.

"ASTM C150 / C150M - 12. Standard Specification for Portland Cement." 2012. In ASTM International, West Conshohocken, PA.

"ASTM C1738 - 11a. Standard Practice for High-Shear Mixing of Hydraulic Cement Paste." 2011. In ASTM International, West Conshohocken, PA.

"ASTM C568 / C568M - 10. Standard Specification for Limestone Dimension Stone." 2012. In ASTM International, West Conshohocken, PA.

"ASTM C595/595M-13 Standard Specification for Blended Hydraulic Cements." 2013. In ASTM International, West Conshohocken, PA.

Atahan, Hakan Nuri, Osman Nuri Oktar, and Mehmet Ali Tasdemir. 2009. "Effects of Water–cement Ratio and Curing Time on the Critical Pore Width of Hardened Cement Paste." *Construction and Building Materials* 23 (3): 1196–1200.

Atzeni, C., L. Massidda, and U. Sanna. 1985. "Comparison between Rheological Models for Portland Cement Pastes." *Cement and Concrete Research* 15 (3): 511–19. doi:16/0008-8846(85)90125-5.

Badogiannis, E., G. Kakali, G. Dimopoulou, E. Chaniotakis, and S. Tsivilis. 2005. "Metakaolin as a Main Cement Constituent. Exploitation of Poor Greek Kaolins." *Cement and Concrete Composites* 27 (2): 197–203.

Bágel', L'., and V. Živica. 1997. "Relationship between Pore Structure and Permeability of Hardened Cement Mortars: On the Choice of Effective Pore Structure Parameter." *Cement and Concrete Research* 27 (8): 1225–35. doi:10.1016/S0008-8846(97)00111-7.

Bager, Dirch H., and Erik J. Sellevold. 1975. "Mercury Porosimetry of Hardened Cement Paste: The Influence of Particle Size." *Cement and Concrete Research* 5 (2): 171–77.

Bakharev, T., J. G. Sanjayan, and Y. B. Cheng. 2000. "Effect of Admixtures on Properties of Alkali-Activated Slag Concrete." *Cement and Concrete Research* 30 (9): 1367–74.

Banfill, P. F. G. 2003. "Rheology of Fresh Cement and Concrete - A Review." In Durban.

———. 2006. "Rheology of Fresh Cement and Concrete." *Rheology Reviews* 2006: 61.

Banfill, P. F. G., and others. 2003. "The Rheology of Fresh Cement and Concrete-a Review." In *Proceedings of the 11th International Cement Chemistry Congress*, 50–62.

Banfill, P.F.G., and D.C. Saunders. 1981. "On the Viscometric Examination of Cement Pastes." *Cement and Concrete Research* 11 (3): 363–70. doi:10.1016/0008-8846(81)90108-3.

Barnes, H. A, Institute of Non-Newtonian, and Fluid Mechanics. 2000. *A Handbook of Elementary Rheology*. Univ. of Wales, Institute of Non-Newtonian Fluid Mechanics.

Barnes, H. A. 1989. "Shear-Thickening ('dilatancy') in Suspensions of Nonaggregating Solid Particles Dispersed in Newtonian Liquids." *Journal of Rheology* 33: 329.

———. 1999. "The Yield Stress—a Review or 'παντα Pε$ιota$'—everything Flows?" *Journal of Non-Newtonian Fluid Mechanics* 81 (1): 133–78.

Barnes, H. A., and K. Walters. 1985. "The Yield Stress Myth?" *Rheologica Acta* 24 (4): 323–26.

Bayod, Elena, Ene Pilman Willers, and Eva Tornberg. 2008. "Rheological and Structural Characterization of Tomato Paste and Its Influence on the Quality of Ketchup." *LWT-Food Science and Technology* 41 (7): 1289–1300.

Beaudoin, J. J. 1979. "Porosity Measurement of Some Hydrated Cementitious Systems by High Pressure Mercury Intrusion-Microstructural Limitations." *Cement and Concrete Research* 9 (6): 771–81. doi:10.1016/0008-8846(79)90073-5.

Bensted, John. 1999. "Thaumasite -- Background and Nature in Deterioration of Cements, Mortars and Concretes." *Cement and Concrete Composites* 21 (2): 117–21. doi:16/S0958-9465(97)00076-0.

Bentz, D., E. F Irassar, B. Bucher, and W. J Weiss. 2009a. “Limestone Fillers Conserve Cement: Part 1: An Analysis Based on Powers Model.” *Concrete International* 31 (11): 41–46.

———. 2009b. “Limestone Fillers Conserve Cement; Part 2: Durability Issues and the Effects of Limestone Fineness on Mixtures.” *Concrete International* 31 (12): 35–39.

Bentz, D. P, and C. F Ferraris. 2010. “Rheology and Setting of High Volume Fly Ash Mixtures.” *Cement and Concrete Composites* 32 (4): 265–70.

Bentz, D. P., C. F. Ferraris, M. A. Galler, A. S. Hansen, and J. M. Guynn. 2012. “Influence of Particle Size Distributions on Yield Stress and Viscosity of Cement–fly Ash Pastes.” *Cement and Concrete Research*. http://www.sciencedirect.com/science/article/pii/S0008884611002912.

Bentz, D. P., T. Sato, I. de la Varga, and W. J. Weiss. 2011. “Fine Limestone Additions to Regulate Setting in High Volume Fly Ash Mixtures.” *Cement and Concrete Composites*. http://www.sciencedirect.com.ezproxy1.lib.asu.edu/science/article/pii/S0958946511001612.

Bentz, D.P. 2005. “Replacement of ‘Coarse’ Cement Particles by Inert Fillers in Low W/c Ratio Concretes: II. Experimental Validation.” *Cement and Concrete Research* 35 (1): 185–88. doi:16/j.cemconres.2004.09.003.

Bentz, Dale P. 2006. “Influence of Water-to-Cement Ratio on Hydration Kinetics: Simple Models Based on Spatial Considerations.” *Cement and Concrete Research* 36 (2): 238–44. doi:10.1016/j.cemconres.2005.04.014.

———. 2007. “Cement Hydration: Building Bridges and Dams at the Microstructure Level.” *Materials and Structures* 40 (4): 397–404.

Bentz, Dale P., Edward J. Garboczi, Claus J. Haecker, and Ole M. Jensen. 1999. “Effects of Cement Particle Size Distribution on Performance Properties of Portland Cement-Based Materials.” *Cement and Concrete Research* 29 (10): 1663–71. doi:10.1016/S0008-8846(99)00163-5.

Bentz, Dale P., and Nicos S. Martys. 1994. “Hydraulic Radius and Transport in Reconstructed Model Three-Dimensional Porous Media.” *Transport in Porous Media* 17 (3): 221–38.

Bentz, Dale P., and Max A. Peltz. 2008. “Reducing Thermal and Autogenous Shrinkage Contributions to Early-Age Cracking.” *ACI Materials Journal* 105 (4). http://www.concrete.org/Publications/ACIMaterialsJournal/ACIJournalSearch.aspx?m=details&ID=19904.

Bernal, Susan A., Ruby Mejía de Gutiérrez, and John L. Provis. 2012. “Engineering and Durability Properties of Concretes Based on Alkali-Activated Granulated Blast Furnace Slag/metakaolin Blends.” *Construction and Building Materials* 33: 99–108.

Bhatty, J.I., and P.F.G. Banfill. 1982. “Sedimentation Behaviour in Cement Pastes Subjected to Continuous Shear in Rotational Viscometers.” *Cement and Concrete Research* 12 (1): 69–78. doi:10.1016/0008-8846(82)90100-4.

Bijen, Jan. 1996. “Benefits of Slag and Fly Ash.” *Construction and Building Materials* 10 (5): 309–14.

Bingham, E. C. 1922. “Fluidity and Plasticity.” http://orton.catie.ac.cr/cgi-bin/wxis.exe/?IsisScript=BFHIA.xis&method=post&formato=2&cantidad=1&expresion=mfn=011959.

Board, National Research Council (U S.) Building Research Advisory. 1969. *Chemical Soil Stabilization*. National Academies.

Bonavetti, V., H. Donza, G. Menéndez, O. Cabrera, and E. F. Irassar. 2003. “Limestone Filler Cement in Low W/c Concrete: A Rational Use of Energy.” *Cement and Concrete Research* 33 (6): 865–71. doi:16/S0008-8846(02)01087-6.

Bonavetti, V. L., V. F. Rahhal, and E. F. Irassar. 2001. “Studies on the Carboaluminate Formation in Limestone Filler-Blended Cements.” *Cement and Concrete Research* 31 (6): 853–59. doi:16/S0008-8846(01)00491-4.

Brady, John F. 1993. “The Rheological Behavior of Concentrated Colloidal Dispersions.” *Journal of Chemical Physics* 99 (1): 567–81.

Bullard, Jeffrey W., Hamlin M. Jennings, Richard A. Livingston, Andre Nonat, George W. Scherer, Jeffrey S. Schweitzer, Karen L. Scrivener, and Jeffrey J. Thomas. 2011. “Mechanisms of Cement Hydration.” *Cement and Concrete Research* 41 (12): 1208–23.

Burgos-Montes, Olga, Marta Palacios, Patricia Rivilla, and Francisca Puertas. 2012. “Compatibility between Superplasticizer Admixtures and Cements with Mineral Additions.” *Construction and Building Materials* 31: 300–309.

Buscall, R., P. D. A. Mills, R. F. Stewart, D. Sutton, L. R. White, and G. E. Yates. 1987. “The Rheology of Strongly-Flocculated Suspensions.” *Journal of Non-Newtonian Fluid Mechanics* 24 (2): 183–202.

C. F Ferraris, and de Larrard, Francois. “Testing and Modelling of Fresh Concrete Rheology”. National Institute of Standards and Technology.

Caldarone, M. A., and J. Z. Zemajtis. 2008. “Effect of Use of Limestone on Various Properties of Portland Cement–Part II”. PCA R & D SN 2891a. Skokie (IL): Portland Cement Association. http://trid.trb.org/view.aspx?id=844287.

Callaghan, Paul T. 2008. “Rheo NMR and Shear Banding.” *Rheologica Acta* 47 (3): 243–55.

Cam, Hieu T., and Narayanan Neithalath. 2010. “Moisture and Ionic Transport in Concretes Containing Coarse Limestone Powder.” *Cement and Concrete Composites* 32 (7): 486–96. doi:16/j.cemconcomp.2010.04.002.

Casson, N. 1959. “A Flow Equation for Pigment-Oil Suspensions of the Printing Ink Type.” *Rheology of Disperse Systems* 84.

Cerny, L. C., F. B. Cook, and C. C. Walker. 1962. “Rheology of Blood.” *American Journal of Physiology–Legacy Content* 202 (6): 1188–94.

Cheng, D. C.-H. 1986. “Yield Stress: A Time-Dependent Property and How to Measure It.” *Rheologica Acta* 25 (5): 542–54. doi:10.1007/BF01774406.

Chindaprasirt, Prinya, Chai Jaturapitakkul, and Theerawat Sinsiri. 2005. “Effect of Fly Ash Fineness on Compressive Strength and Pore Size of Blended Cement Paste.” *Cement and Concrete Composites* 27 (4): 425–28. doi:10.1016/j.cemconcomp.2004.07.003.

Chomton, G., and P. J. Valyer. 1972. “Applied Rheology of Asphalt Mixes Practical Application.” In *Presented at the Third International Conference on the Structural Design of Asphalt Pavements, Grosvenor House, Park Lane, London, England, Sept. 11-15, 1972.* Vol. 1. http://trid.trb.org/view.aspx?id=138840.

Chong, J. S., E. B. Christiansen, and A. D. Baer. 2003. “Rheology of Concentrated Suspensions.” *Journal of Applied Polymer Science* 15 (8): 2007–21.

Cook, Raymond A., and Kenneth C. Hover. 1999. “Mercury Porosimetry of Hardened Cement Pastes.” *Cement and Concrete Research* 29 (6): 933–43.

Criado, M., A. Palomo, A. Fernández-Jiménez, and P. F. G. Banfill. 2009. “Alkali Activated Fly Ash: Effect of Admixtures on Paste Rheology.” *Rheologica Acta* 48 (4): 447–55.

Daimon, M., and D. M. Roy. 1979. “Rheological Properties of Cement Mixes: II. Zeta Potential and Preliminary Viscosity Studies.” *Cement and Concrete Research* 9 (1): 103–9. doi:10.1016/0008-8846(79)90100-5.

Davidovits, Joseph. 1991. “Geopolymers.” *Journal of Thermal Analysis and Calorimetry* 37 (8): 1633–56.

———. 1999. “Chemistry of Geopolymeric Systems, Terminology.” In *Geopolymer*, 99:9–40.

———. 2005. “Geopolymer Chemistry and Sustainable Development. The Poly (sialate) Terminology: A Very Useful and Simple Model for the Promotion and Understanding of Green-Chemistry.” In *Proceedings of 2005 Geopolymer Conference*, 1:9–15.

De Larrard, F., C. F. Ferraris, and T. Sedran. 1998. “Fresh Concrete: A Herschel-Bulkley Material.” *Materials and Structures* 31 (7): 494–98.

De Weerdt, K., M. Ben Haha, G. Le Saout, K.O. Kjellsen, H. Justnes, and B. Lothenbach. 2011. “Hydration Mechanisms of Ternary Portland Cements Containing Limestone Powder and Fly Ash.” *Cement and Concrete Research* 41 (3): 279–91. doi:16/j.cemconres.2010.11.014.

De Weerdt, K., H. Justnes, K. O. Kjellsen, and E. Sellevold. 2010. “Fly Ash-Limestone Ternary Composite Cements: Synergetic Effect at 28 Days.” *Nordic Concrete Research* 42 (2): 51–70.

De Weerdt, K., K.O. Kjellsen, E. Sellevold, and H. Justnes. 2011. “Synergy between Fly Ash and Limestone Powder in Ternary Cements.” *Cement and Concrete Composites* 33 (1): 30–38. doi:16/j.cemconcomp.2010.09.006.

Deschner, F., F. Winnefeld, B. Lothenbach, S. Seufert, P. Schwesig, S. Dittrich, F. Goetz-Neunhoeffer, and J. Neubauer. 2012. “Hydration of Portland Cement with High Replacement by Siliceous Fly Ash.” *Cement and Concrete Research*. http://www.sciencedirect.com/science/article/pii/S0008884612001585.

Dhir, R. K., M. C. Limbachiya, M. J. McCarthy, and A. Chaipanich. 2007. “Evaluation of Portland Limestone Cements for Use in Concrete Construction.” *Materials and Structures* 40 (5): 459–73.

Dintenfass, Leopold. 1976. *Rheology of Blood in Diagnostic and Preventive Medicine: An Introduction to Clinical Haemorheology*. Butterworths London, Boston. http://www.getcited.org/pub/101581210.

Dweck, Jo, Pedro Mauricio Buchler, Antonio Carlos Vieira Coelho, and Frank K. Cartledge. 2000. “Hydration of a Portland Cement Blended with Calcium Carbonate.” *Thermochimica Acta* 346 (1-2): 105–13. doi:16/S0040-6031(99)00369-X.

Elkhadiri, I, A Diouri, A Boukhari, J Aride, and F Puertas. 2002. “Mechanical Behaviour of Various Mortars Made by Combined Fly Ash and Limestone in Moroccan Portland Cement.” *Cement and Concrete Research* 32 (10): 1597–1603. doi:10.1016/S0008-8846(02)00834-7.

Erdoğan, S. T., N. S. Martys, C. F. Ferraris, and D. W. Fowler. 2008. “Influence of the Shape and Roughness of Inclusions on the Rheological Properties of a Cementitious Suspension.” *Cement and Concrete Composites* 30 (5): 393–402.

Evans, Ian David. 1992. “Letter to the Editor: On the Nature of the Yield Stress.” *Journal of Rheology* 36: 1313.

Fajun, Wei, Michael W. Grutzeck, and Della M. Roy. 1985. “The Retarding Effects of Fly Ash upon the Hydration of Cement Pastes: The First 24 Hours.” *Cement and Concrete Research* 15 (1): 174–84. doi:10.1016/0008-8846(85)90024-9.

Farris, R. J. 1968. “Prediction of the Viscosity of Multimodal Suspensions from Unimodal Viscosity Data.” *Journal of Rheology* 12: 281.

Felekoğlu, B., K. Tosun, B. Baradan, A. Altun, and B. Uyulgan. 2006. “The Effect of Fly Ash and Limestone Fillers on the Viscosity and Compressive Strength of Self-Compacting Repair Mortars.” *Cement and Concrete Research* 36 (9): 1719–26.

Fernández-Jiménez, Ana, I. Garcia-Lodeiro, and A. Palomo. 2007. “Durability of Alkali-Activated Fly Ash Cementitious Materials.” *Journal of Materials Science* 42 (9): 3055–65.

Ferraris, C. F. 1999a. “Measurement of the Rheological Properties of Cement Paste: A New Approach.” In *PRO 5: International RILEM Conference on The Role of Admixtures in High Performance Concrete*, 5:333.

———. 1999b. “Measurement of the Rheological Properties of High Performance Concrete: State of the Art Report.” *JOURNAL OF RESEARCH-NATIONAL INSTITUTE OF STANDARDS AND TECHNOLOGY* 104 (5): 461–78.

Ferraris, C. F., and J. M. Gaidis. 1992. “Connection between the Rheology of Concrete and Rheology of Cement Paste.” *ACI Materials Journal* 89 (4). http://www.concrete.org/PUBS/JOURNALS/OLJDetails.asp?Home=MJ&ID=2575.

Ferraris, C. F., K. H. Obla, and R. Hill. 2001. “The Influence of Mineral Admixtures on the Rheology of Cement Paste and Concrete.” *Cement and Concrete Research* 31 (2): 245–55.

Flatt, Robert J. 2004. “Dispersion Forces in Cement Suspensions.” *Cement and Concrete Research* 34 (3): 399–408.

Flatt, Robert J., and Paul Bowen. 2006. “Yodel: A Yield Stress Model for Suspensions.” *Journal of the American Ceramic Society* 89 (4): 1244–56.

———. 2007. “Yield Stress of Multimodal Powder Suspensions: An Extension of the YODEL (Yield Stress mODEL).” *Journal of the American Ceramic Society* 90 (4): 1038–44.

Fraay, A. L. A., J. M. Bijen, and Y. M. de Haan. 1989. “The Reaction of Fly Ash in Concrete a Critical Examination.” *Cement and Concrete Research* 19 (2): 235–46. doi:10.1016/0008-8846(89)90088-4.

Franks, George V. 2002. “Zeta Potentials and Yield Stresses of Silica Suspensions in Concentrated Monovalent Electrolytes: Isoelectric Point Shift and Additional Attraction.” *Journal of Colloid and Interface Science* 249 (1): 44–51.

Frías, M., M. I. Sánchez de Rojas, and J. Cabrera. 2000. “The Effect That the Pozzolanic Reaction of Metakaolin Has on the Heat Evolution in Metakaolin-Cement Mortars.” *Cement and Concrete Research* 30 (2): 209–16. doi:10.1016/S0008-8846(99)00231-8.

Frías, Moisés, and Joseph Cabrera. 2000. “Pore Size Distribution and Degree of Hydration of Metakaolin–cement Pastes.” *Cement and Concrete Research* 30 (4): 561–69. doi:10.1016/S0008-8846(00)00203-9.

Fung, W. W. S., and A. K. H. Kwan. 2010. “Role of Water Film Thickness in Rheology of CSF Mortar.” *Cement and Concrete Composites* 32 (4): 255–64.

Funk, J. E., and D. R. Dinger. 1994. *Predictive Process Control of Crowded Particulate Suspensions: Applied to Ceramic Manufacturing*. Springer. http://books.google.com/books?hl=en&lr=&id=xq5KAsfGQ_YC&oi=fnd&pg=PR9&dq=Predictive+process+control+of+crowded+particulate+suspensions,+Kluwer++funk&ots=6tj4Nms5wo&sig=bxnc4XKtpf4DwvlY0M7LSS1Kx08.

Gallé, C. 2001. “Effect of Drying on Cement-Based Materials Pore Structure as Identified by Mercury Intrusion Porosimetry: A Comparative Study between Oven-, Vacuum-, and Freeze-Drying.” *Cement and Concrete Research* 31 (10): 1467–77. doi:10.1016/S0008-8846(01)00594-4.

Garboczi, E. J., and J. W. Bullard. 2004. “Shape Analysis of a Reference Cement.” *Cement and Concrete Research* 34 (10): 1933–37.

Gaskins, Frederick H., John G. Brodnyan, Wladimir Philippoff, and Edmund Thelen. 1960. “The Rheology of Asphalt. II. Flow Characteristics of Asphalt.” *Journal of Rheology* 4: 265–78.

Geiker, Mette, Erik Pram Nielsen, and Duncan Herfort. 2007. “Prediction of Chloride Ingress and Binding in Cement Paste.” *Materials and Structures* 40 (4): 405–17.

Gmira, A., M. Zabat, RJ-M. Pellenq, and H. Van Damme. 2004. “Microscopic Physical Basis of the Poromechanical Behavior of Cement-Based Materials.” *Materials and Structures* 37 (1): 3–14.

Government of Canada, Natural Resources Canada. 2009. “Energy Consumption Benchmark Guide: Cement Clinker Production | Office of Energy Efficiency.” April 22. http://oee.nrcan.gc.ca/publications/industrial/6527.

Grzeszczyk, S., and G. Lipowski. 1997. “Effect of Content and Particle Size Distribution of High-Calcium Fly Ash on the Rheological Properties of Cement Pastes.” *Cement and Concrete Research* 27 (6): 907–16.

Halamickova, Pavla, Rachel J. Detwiler, Dale P. Bentz, and Edward J. Garboczi. 1995. “Water Permeability and Chloride Ion Diffusion in Portland Cement Mortars: Relationship to Sand Content and Critical Pore Diameter.” *Cement and Concrete Research* 25 (4): 790–802. doi:10.1016/0008-8846(95)00069-O.

Hartnett, James P., and Robert YZ Hu. 1989. “Technical Note: The Yield Stress—an Engineering Reality.” *Journal of Rheology* 33: 671.

Hartshorn, S. A., J. H. Sharp, and R. N. Swamy. 1999. “Thaumasite Formation in Portland-Limestone Cement Pastes.” *Cement and Concrete Research* 29 (8): 1331–40.

Hawkins, P., P. Tennis, and R. Detwiler. 2003. “The Use of Limestone in Portland Cement: A State-of-the-Art Review.” *EB227, Portland Cement Association, Skokie, IL* 44.

Hendriks, C. A., E. Worrell, D. De Jager, K. Blok, and P. Riemer. 2002. “Emission Reduction of Greenhouse Gases from the Cement Industry.” *International Energy Agency (IEA)*. http://www.moleconomics.org/files/sustainability%20documents/EmissionReductionofGreenhouseGasesfromtheCementIndustry.pdf.

Herle, Vishweshwara, Peter Fischer, and Erich J. Windhab. 2005. “Stress Driven Shear Bands and the Effect of Confinement on Their Structures A Rheological, Flow Visualization, and Rheo-SALS Study.” *Langmuir* 21 (20): 9051–57.

Herschel, W. H., and R. Bulkley. 1926. “Measurement of Consistency as Applied to Rubber-Benzene Solutions.” In *Proceedings of the American Society for the Testing of Materials*, 26:621–33.

Hetsroni, Gad. 1982. “Handbook of Multiphase Systems.” http://www.osti.gov/energycitations/product.biblio.jsp?osti_id=5474196.

Hooton, R. D. 1990. “Effects of Carbonate Additions on Heat of Hydration and Sulfate Resistance of Portland Cements.” *Carbonate Additions to Cement*, 73.

Hoshino, Seiichi, Kazuo Yamada, and Hiroshi Hirao. 2006. “XRD/Rietveld Analysis of the Hydration and Strength Development of Slag and Limestone Blended Cement.” *Journal of Advanced Concrete Technology* 4 (3): 357–67.

Hunter, Robert J., and Lee R. White. 1987. *Foundations of Colloid Science*. Clarendon Press.

Iler, Ralph K. 1979. “The Chemistry of Silica: Solubility, Polymerization, Colloid and Surface Properties, and Biochemistry.” http://www.lavoisier.fr/livre/notice.asp?ouvrage=1353889.

Ingram, K., M. Poslusny, K. Daugherty, W. Rowe, P. Klieger, and R. D. Hooton. 1990. “Carboaluminate Reactions as Influenced by Limestone Additions.” *Proc Carbonate Additions to Cement* 1064: 14–23.

Ipavec, A., R. Gabrovsek, T. Vuk, V. Kacivc, J. Macek, and A. Meden. 2011. “Carboaluminate Phases Formation During the Hydration of Calcite-Containing Portland Cement.” *Journal of the American Ceramic Society* 94 (4): 1238–42.

Irassar, E. F. 2001. “Mechanical Properties and Durability of Concrete Made with Portland Limestone Cement.” *ACI Special Publication* 202. http://www.concrete.org/Publications/GetArticle.aspx?m=icap&pubID=10798.

Irassar, E.F., D. Violini, V.F. Rahhal, C. Milanesi, M.A. Trezza, and V.L. Bonavetti. 2011. “Influence of Limestone Content, Gypsum Content and Fineness on Early Age Properties of Portland Limestone Cement Produced by Inter-Grinding.” *Cement and Concrete Composites* 33 (2): 192–200. doi:16/j.cemconcomp.2010.10.001.

Jeffrey, D. J., and Andreas Acrivos. 1976. “The Rheological Properties of Suspensions of Rigid Particles.” *AIChE Journal* 22 (3): 417–32.

Justnes, Harald. 2003. “Thaumasite Formed by Sulfate Attack on Mortar with Limestone Filler.” *Cement and Concrete Composites* 25 (8): 955–59. doi:16/S0958-9465(03)00120-3.

Justnes, Harald, and Hedda Vikan. 2005. “Viscosity of Cement Slurries as a Function of Solids Content.” *Ann. Trans. Nordic Rheology Soc* 13: 75–82.

Kadri, E. H., S. Kenai, K. Ezziane, R. Siddique, and G. De Schutter. 2011. “Influence of Metakaolin and Silica Fume on the Heat of Hydration and Compressive Strength Development of Mortar.” *Applied Clay Science*. http://www.sciencedirect.com.ezproxy1.lib.asu.edu/science/article/pii/S0169131711002171.

Kakali, G., S. Tsivilis, E. Aggeli, and M. Bati. 2000. “Hydration Products of C3A, C3S and Portland Cement in the Presence of CaCO3.” *Cement and Concrete Research* 30 (7): 1073–77. doi:16/S0008-8846(00)00292-1.

Kakali, G., S. Tsivilis, A. Skaropoulou, J. H. Sharp, and R. N. Swamy. 2003. “Parameters Affecting Thaumasite Formation in Limestone Cement Mortar.” *Cement and Concrete Composites* 25 (8): 977–81.

Kamal, M.R., and A. Mutel. 1985. “Rheological Properties of Suspensions in Newtonian and Non-Newtonian Fluids.” *Journal of Polymer Engineering* 5 (4): 293–382. doi:10.1515/POLYENG.1985.5.4.293.

Kelessidis, V. C., R. Maglione, C. Tsamantaki, and Y. Aspirtakis. 2006. “Optimal Determination of Rheological Parameters for Herschel–Bulkley Drilling Fluids and Impact on Pressure Drop, Velocity Profiles and Penetration Rates during Drilling.” *Journal of Petroleum Science and Engineering* 53 (3): 203–24.

Koch, Gerhardus H., Michiel PH Brongers, Neil G. Thompson, Y. Paul Virmani, and Joe H. Payer. 2002. “Corrosion Cost and Preventive Strategies in the United States.” http://trid.trb.org/view.aspx?id=707382.

Krieger, Irvin M., and Thomas J. Dougherty. 1959. “A Mechanism for Non-Newtonian Flow in Suspensions of Rigid Spheres.” *Transactions of the Society of Rheology* 3 (1): 137–52.

Kumar, A., T. Oey, S Kim, Thomas, D, Badran, S, Li, J, Fernandes, F, Neithalath, N, and Sant, G. “Simple Methods to Estimate the Influence of Limestone Fillers on Reaction and Property Evaluation in Cementitious Materials.” *Submitted to Cement and Concrete Research*.

Kumar, Rakesh, and B. Bhattacharjee. 2003. “Study on Some Factors Affecting the Results in the Use of MIP Method in Concrete Research.” *Cement and Concrete Research* 33 (3): 417–24.

Kutchko, Barbara G., and Ann G. Kim. 2006. “Fly Ash Characterization by SEM–EDS.” *Fuel* 85 (17–18): 2537–44. doi:10.1016/j.fuel.2006.05.016.

Lachemi, M., K. M. A. Hossain, V. Lambros, P. -C. Nkinamubanzi, and N. Bouzoubaâ. 2004. “Performance of New Viscosity Modifying Admixtures in Enhancing the Rheological Properties of Cement Paste.” *Cement and Concrete Research* 34 (2): 185–93. doi:16/S0008-8846(03)00233-3.

Lagier, F., and K. E. Kurtis. 2007. “Influence of Portland Cement Composition on Early Age Reactions with Metakaolin.” *Cement and Concrete Research* 37 (10): 1411–17.

Langan, B.W., K. Weng, and M.A. Ward. 2002. “Effect of Silica Fume and Fly Ash on Heat of Hydration of Portland Cement.” *Cement and Concrete Research* 32 (7): 1045–51. doi:10.1016/S0008-8846(02)00742-1.

Lee, S. H., H. J. Kim, E. Sakai, and M. Daimon. 2003. “Effect of Particle Size Distribution of Fly Ash–cement System on the Fluidity of Cement Pastes.” *Cement and Concrete Research* 33 (5): 763–68.

Lesko, Samuel, Eric Lesniewska, André Nonat, Jean-Claude Mutin, and Jean-Pierre Goudonnet. 2001. “Investigation by Atomic Force Microscopy of Forces at the Origin of Cement Cohesion.” *Ultramicroscopy* 86 (1): 11–21.

Liu, Dean-Mo. 2000. “Particle Packing and Rheological Property of Highly-Concentrated Ceramic Suspensions: Φm Determination and Viscosity Prediction.” *Journal of Materials Science* 35 (21): 5503–7.

Livesey, P. 1991. “Performance of Limestone-Filled Cements.” In *BLENDED CEMENTS IN CONSTRUCTION. PAPERS PRESENTED AT THE INTERNATIONAL CONFERENCE, UNIVERSITY OF SHEFFIELD, UK, 9-12 SEPTEMBER 1991*. http://trid.trb.org/view.aspx?id=376797.

Loose, W., and S. Hess. 1989. “Rheology of Dense Model Fluids via Nonequilibrium Molecular Dynamics: Shear Thinning and Ordering Transition.” *Rheologica Acta* 28 (2): 91–101.

Lootens, D., P. Hébraud, E. Lécolier, and H. Van Damme. 2004. “Gelation, Shear-Thinning and Shear-Thickening in Cement Slurries.” *Oil & Gas Science and Technology* 59 (1): 31–40.

Lothenbach, Barbara, Gwenn Le Saout, Emmanuel Gallucci, and Karen Scrivener. 2008. “Influence of Limestone on the Hydration of Portland Cements.” *Cement and Concrete Research* 38 (6): 848–60. doi:16/j.cemconres.2008.01.002.

Lowke, D. 2009. “Interparticle Forces and Rheology of Cement Based Suspensions.” In *Nanotechnology in Construction 3*, 295–301. Springer. http://link.springer.com/chapter/10.1007/978-3-642-00980-8_39.

Mannheimer, R. J. 1983. “Effect Of Slip On The Flow Properties Of Cement Slurries.” In *Annual Meeting Papers, Divison of Production*. http://www.onepetro.org/mslib/servlet/onepetropreview?id=API-83-H001.

Marsh, B. K., and R. L. Day. 1988. “Pozzolanic and Cementitious Reactions of Fly Ash in Blended Cement Pastes.” *Cement and Concrete Research* 18 (2): 301–10.

Matschei, T., B. Lothenbach, and F. P. Glasser. 2007a. “The AFm Phase in Portland Cement.” *Cement and Concrete Research* 37 (2): 118–30. doi:10.1016/j.cemconres.2006.10.010.

Matschei, T., B. Lothenbach, and F.P. Glasser. 2007b. “The Role of Calcium Carbonate in Cement Hydration.” *Cement and Concrete Research* 37 (4): 551–58. doi:16/j.cemconres.2006.10.013.

Mehta, P. Kumar, and Paulo J. M. Monteiro. 2005. *Concrete : Microstructure, Properties, and Materials*. Blacklick, OH, USA: McGraw-Hill Professional Publishing. http://site.ebrary.com/lib/asulib/docDetail.action?docID=10196829.

Mehta, P.K. 2002. “Greeningof the Concrete Industry for Sustainable Development.” *Concrete International*, 23.

Menéndez, G, V Bonavetti, and E. F Irassar. 2003. “Strength Development of Ternary Blended Cement with Limestone Filler and Blast-Furnace Slag.” *Cement and Concrete Composites* 25 (1): 61–67. doi:10.1016/S0958-9465(01)00056-7.

Mikanovic, Nikola, and Carmel Jolicoeur. 2008. “Influence of Superplasticizers on the Rheology and Stability of Limestone and Cement Pastes.” *Cement and Concrete Research* 38 (7): 907–19. doi:16/j.cemconres.2008.01.015.

Mikanovic, Nikola, Kamal Khayat, Monique Pagé, and Carmel Jolicoeur. 2006. "Aqueous CaCO< Sub> 3</sub> Dispersions as Reference Systems for Early-Age Cementitious Materials." *Colloids and Surfaces A: Physicochemical and Engineering Aspects* 291 (1): 202–11.

Møller, Peder CF, Jan Mewis, and Daniel Bonn. 2006. "Yield Stress and Thixotropy: On the Difficulty of Measuring Yield Stresses in Practice." *Soft Matter* 2 (4): 274–83.

Moon, J., J. E. Oh, M. Balonis, F. P. Glasser, S. M. Clark, and P. J. M. Monteiro. 2011. "High Pressure Study of Low Compressibility Tetracalcium Aluminum Carbonate Hydrates 3CaO· Al2O3·CaCO3· 11H2O." *Cement and Concrete Research*. http://www.sciencedirect.com/science/article/pii/S0008884611002262.

Moreno, M., W. Morris, M. G. Alvarez, and G. S. Duffó. 2004. "Corrosion of Reinforcing Steel in Simulated Concrete Pore Solutions: Effect of Carbonation and Chloride Content." *Corrosion Science* 46 (11): 2681–99. doi:10.1016/j.corsci.2004.03.013.

Moulin, E, P Blanc, and D Sorrentino. 2001. "Influence of Key Cement Chemical Parameters on the Properties of Metakaolin Blended Cements." *Cement and Concrete Composites* 23 (6): 463–69. doi:10.1016/S0958-9465(00)00093-7.

Mueller, S., E. W. Llewellin, and H. M. Mader. 2010. "The Rheology of Suspensions of Solid Particles." *Proceedings of the Royal Society A: Mathematical, Physical and Engineering Science* 466 (2116): 1201–28. doi:10.1098/rspa.2009.0445.

Nägele, E. 1986. "The Zeta-Potential of Cement: Part II: Effect of pH-Value." *Cement and Concrete Research* 16 (6): 853–63.

Nägele, E., and U. Schneider. 1989. "The Zeta-Potential of Blast Furnace Slag and Fly Ash." *Cement and Concrete Research* 19 (5): 811–20.

Nehdi, M., and M. -A. Rahman. 2004a. "Estimating Rheological Properties of Cement Pastes Using Various Rheological Models for Different Test Geometry, Gap and Surface Friction." *Cement and Concrete Research* 34 (11): 1993–2007. doi:16/j.cemconres.2004.02.020.

Nehdi, M., and M.-A. Rahman. 2004b. "Effect of Geometry and Surface Friction of Test Accessory on Oscillatory Rheological Properties of Cement Pastes." *ACI Materials Journal* 101 (5). http://www.concrete.org/PUBS/JOURNALS/OLJDetails.asp?Home=MJ&ID=13428.

Neubauer, Christopher M, Ming Yang, and Hamlin M Jennings. 1998. "Interparticle Potential and Sedimentation Behavior of Cement Suspensions: Effects of Admixtures." *Advanced Cement Based Materials* 8 (1): 17–27. doi:10.1016/S1065-7355(98)00005-4.

Nguyen, Q. D., and D. V. Boger. 1992. "Measuring the Flow Properties of Yield Stress Fluids." *Annual Review of Fluid Mechanics* 24 (1): 47–88.

Oey, T., A. Kumar, J.W. Bullard, N. Neithalath, and G. Sant. 2012. “The Filler Effect: The Influence of Filler Content and Surface Area on Cementitious Reaction Rates.”

Olhero, S. M., and J. M. F. Ferreira. 2004. “Influence of Particle Size Distribution on Rheology and Particle Packing of Silica-Based Suspensions.” *Powder Technology* 139 (1): 69–75.

Olmsted, Peter D. 2008. “Perspectives on Shear Banding in Complex Fluids.” *Rheologica Acta* 47 (3): 283–300.

Opoczky, L. 1992. “Progress of Particle Size Distribution during the Intergrinding of a Clinker-Limestone Mixture.” *ZEMENT KALK GIPS* 45: 648–648.

Opoczky, Ludmilla. 1996. “Grinding Technical Questions of Producing Composite Cement.” *International Journal of Mineral Processing* 44: 395–404.

Palacios, M., Y. F. Houst, P. Bowen, and F. Puertas. 2009a. “Adsorption of Superplasticizer Admixtures on Alkali-Activated Slag Pastes.” *Cement and Concrete Research* 39 (8): 670–77.

———. 2009b. “Adsorption of Superplasticizer Admixtures on Alkali-Activated Slag Pastes.” *Cement and Concrete Research* 39 (8): 670–77.

Palacios, M., and F. Puertas. 2005. “Effect of Superplasticizer and Shrinkage-Reducing Admixtures on Alkali-Activated Slag Pastes and Mortars.” *Cement and Concrete Research* 35 (7): 1358–67.

Palomo, A., M. W. Grutzeck, and M. T. Blanco. 1999. “Alkali-Activated Fly Ashes: A Cement for the Future.” *Cement and Concrete Research* 29 (8): 1323–29.

Papo, A. 1988. “Rheological Models for Cement Pastes.” *Materials and Structures* 21 (1): 41–46.

Papo, Adriano, and Luciano Piani. 2004. “Effect of Various Superplasticizers on the Rheological Properties of Portland Cement Pastes.” *Cement and Concrete Research* 34 (11): 2097–2101.

Park, C.K., M.H. Noh, and T.H. Park. 2005. “Rheological Properties of Cementitious Materials Containing Mineral Admixtures.” *Cement and Concrete Research* 35 (5): 842–49. doi:16/j.cemconres.2004.11.002.

Péra, Jean, Sophie Husson, and Bernard Guilhot. 1999. “Influence of Finely Ground Limestone on Cement Hydration.” *Cement and Concrete Composites* 21 (2): 99–105. doi:16/S0958-9465(98)00020-1.

Phair, J. W., J. D. Smith, and J. S. J. Van Deventer. 2003. “Characteristics of Aluminosilicate Hydrogels Related to Commercial ‘Geopolymers.’” *Materials Letters* 57 (28): 4356–67.

Pipilikaki, P., and M. Beazi-Katsioti. 2009. “The Assessment of Porosity and Pore Size Distribution of Limestone Portland Cement Pastes.” *Construction and Building Materials* 23 (5). Compatibility of Plasters and Renders on Salt Loaded Substrates: 1966–70. doi:10.1016/j.conbuildmat.2008.08.028.

Poon, C. S., L. Lam, S. C. Kou, Y. L. Wong, and R. Wong. 2001. “Rate of Pozzolanic Reaction of Metakaolin in High-Performance Cement Pastes.” *Cement and Concrete Research* 31 (9): 1301–6.

Popescu, C. D., M. Muntean, and J. H. Sharp. 2003. “Industrial Trial Production of Low Energy Belite Cement.” *Cement and Concrete Composites* 25 (7): 689–93. doi:10.1016/S0958-9465(02)00097-5.

Poslinski, A. J., M. E. Ryan, R. K. Gupta, S. G. Seshadri, and F. J. Frechette. 1988. “Rheological Behavior of Filled Polymeric Systems I. Yield Stress and Shear-Thinning Effects.” *Journal of Rheology (1978-Present)* 32 (7): 703–35.

Poulesquen, A., F. Frizon, and D. Lambertin. 2013. “Rheological Behavior of Alkali-Activated Metakaolin during Geopolymerization.” In *Cement-Based Materials for Nuclear Waste Storage*, 225–38. Springer. http://link.springer.com/chapter/10.1007/978-1-4614-3445-0_20.

Powers, T.C., and T.L. Brownyard. 1947. “Studies of the Physical Properties of Hardened Portland Cement Paste.” In *Journal Proceedings*, 43:549–602.

Provis, John L., Yolandi Muntingh, Redmond R. Lloyd, Hua Xu, Louise M. Keyte, Leon Lorenzen, Pavel V. Krivenko, Jannie SJ van Deventer, and UKRAINE Kiev. 2007. “Will Geopolymers Stand the Test of Time?” *Developments in Porous, Biological and Geopolymer Ceramics: Ceramic Engineering and Science Proceedings*, 235.

Provis, John L., and Jan Stephanus Jakob Van Deventer. 2009. *Geopolymers: Structure, Processing, Properties and Industrial Applications*. Woodhead Cambridge, UK. http://www.lavoisier.fr/livre/notice.asp?ouvrage=1862690.

Puertas, F., and A. Fernández-Jiménez. 2003. “Mineralogical and Microstructural Characterisation of Alkali-Activated Fly Ash/slag Pastes.” *Cement and Concrete Composites* 25 (3): 287–92.

Qing-Hua, C., and S. L. Sarkar. 1994. “A Study of Rheological and Mechanical Properties of Mixed Alkali Activated Slag Pastes.” *Advanced Cement Based Materials* 1 (4): 178–84.

Ramachandran, V. S. 1988. “Thermal Analyses of Cement Components Hydrated in the Presence of Calcium Carbonate.” *Thermochimica Acta* 127: 385–94.

Ravikumar, Deepak, and Narayanan Neithalath. 2012a. “Reaction Kinetics in Sodium Silicate Powder and Liquid Activated Slag Binders Evaluated Using Isothermal Calorimetry.” *Thermochimica Acta*. http://www.sciencedirect.com/science/article/pii/S0040603112003437.

———. 2012b. “Effects of Activator Characteristics on the Reaction Product Formation in Slag Binders Activated Using Alkali Silicate Powder and NaOH.” *Cement and Concrete Composites* 34 (7): 809–18. doi:10.1016/j.cemconcomp.2012.03.006.

Roussel, N., and P. Coussot. 2005. “‘Fifty-Cent Rheometer’ for Yield Stress Measurements: From Slump to Spreading Flow.” *Journal of Rheology (1978-Present)* 49 (3): 705–18. doi:10.1122/1.1879041.

Roussel, Nicolas. 2006. “Correlation between Yield Stress and Slump: Comparison between Numerical Simulations and Concrete Rheometers Results.” *Materials and Structures* 39 (4): 501–9.

Roussel, Nicolas, Anael Lemaître, Robert J. Flatt, and Philippe Coussot. 2010. “Steady State Flow of Cement Suspensions: A Micromechanical State of the Art.” *Cement and Concrete Research* 40 (1): 77–84.

Saak, Aaron W., Hamlin M. Jennings, and Surendra P. Shah. 2001. “The Influence of Wall Slip on Yield Stress and Viscoelastic Measurements of Cement Paste.” *Cement and Concrete Research* 31 (2): 205–12.

———. 2004. “A Generalized Approach for the Determination of Yield Stress by Slump and Slump Flow.” *Cement and Concrete Research* 34 (3): 363–71.

Sabir, B. B, S Wild, and J Bai. 2001. “Metakaolin and Calcined Clays as Pozzolans for Concrete: A Review.” *Cement and Concrete Composites* 23 (6). Metakaolin and Calcined Clays: 441–54. doi:10.1016/S0958-9465(00)00092-5.

Sakai, E., K. Masuda, Y. Kakinuma, and Y. Aikawa. 2009. “Effects of Shape and Packing Density of Powder Particles on the Fluidity of Cement Pastes with Limestone Powder.” *Journal of Advanced Concrete Technology* 7 (3): 347–54.

Sakai, E., S. Miyahara, S. Ohsawa, S. H. Lee, and M. Daimon. 2005. “Hydration of Fly Ash Cement.” *Cement and Concrete Research* 35 (6): 1135–40.

Salmas, Constantinos E., and George P. Androutsopoulos. 2001. “A Novel Pore Structure Tortuosity Concept Based on Nitrogen Sorption Hysteresis Data.” *Industrial & Engineering Chemistry Research* 40 (2): 721–30.

Sánchez de Rojas, M. I., M. P. Luxán, M. Frías, and N. García. 1993. “The Influence of Different Additions on Portland Cement Hydration Heat.” *Cement and Concrete Research* 23 (1): 46–54. doi:10.1016/0008-8846(93)90134-U.

Sant, Gaurav, Chiara F. Ferraris, and Jason Weiss. 2008. “Rheological Properties of Cement Pastes: A Discussion of Structure Formation and Mechanical Property Development.” *Cement and Concrete Research* 38 (11): 1286–96. doi:16/j.cemconres.2008.06.008.

Santamaria-Holek, I., and Carlos I. Mendoza. 2010. “The Rheology of Concentrated Suspensions of Arbitrarily-Shaped Particles.” *arXiv:1005.5707 [cond-Mat]*, May. http://arxiv.org/abs/1005.5707.

Scales, Peter J., Stephen B. Johnson, Thomas W. Healy, and Prakash C. Kapur. 1998. “Shear Yield Stress of Partially Flocculated Colloidal Suspensions.” *AIChE Journal* 44 (3): 538–44.

Schall, Peter, and Martin van Hecke. 2009. “Shear Bands in Matter with Granularity.” *Annual Review of Fluid Mechanics* 42 (1): 67.

Schwartzentruber, L. D’Aloia, R. Le Roy, and J. Cordin. 2006. “Rheological Behaviour of Fresh Cement Pastes Formulated from a Self Compacting Concrete (SCC).” *Cement and Concrete Research* 36 (7): 1203–13. doi:16/j.cemconres.2004.10.036.

Shaughnessy III, Richard, and Peter E. Clark. 1988. “The Rheological Behavior of Fresh Cement Pastes.” *Cement and Concrete Research* 18 (3): 327–41.

Shaw, D. 1992. *Introduction to Colloid and Surface Chemistry*. Butterworth-Heinemann. http://store.elsevier.com/product.jsp?isbn=9780750611824&gdftrk=gdfV26763_a_7c349_a_7c883_a_7c9780750611824&mckv=dvgJdFEm_dc&pcrid=34261229472&gclid=CI728JnH7b0CFVKFfgodPrMAHA.

Skripkiūnas, Gintautas, Mindaugas Dauksys, Arminas Stuopys, and Rimantas Levinskas. 2005. “The Influence of Cement Particles Shape and Concentration on the Rheological Properties of Cement Slurry.” *Materials Science (Medziagotyra)* 11 (2). http://internet.ktu.lt/lt/mokslas/zurnalai/medz/pdf/medz0-81/10%20Skripkiuno%20str%20150-158.pdf.

Škvára, František, Lubomír Kopecký, Vít Šmilauer, and Zdeněk Bittnar. 2009. “Material and Structural Characterization of Alkali Activated Low-Calcium Brown Coal Fly Ash.” *Journal of Hazardous Materials* 168 (2–3): 711–20. doi:10.1016/j.jhazmat.2009.02.089.

Soroka, I., and N. Setter. 1977. “The Effect of Fillers on Strength of Cement Mortars.” *Cement and Concrete Research* 7 (4): 449–56.

Soroka, I., and N. Stern. 1976. “Calcareous Fillers and the Compressive Strength of Portland Cement.” *Cement and Concrete Research* 6 (3): 367–76. doi:16/0008-8846(76)90099-5.

Stebbins, Jonathan F., Ian Farnan, and Xianyu Xue. 1992. “The Structure and Dynamics of Alkali Silicate Liquids: A View from NMR Spectroscopy.” *Chemical Geology* 96 (3): 371–85.

Steffe, James Freeman. 1996. *Rheological Methods in Food Process Engineering*. Freeman press. http://books.google.com/books?hl=en&lr=&id=LrrdONuST9kC&oi=fnd&pg=PR9&dq=rheology+of+catsup&ots=kYZPqy7ae0&sig=xDl3z2hvuWFQAaOFUavtQEGFCuw.

Struble, Leslie, and Guo-Kuang Sun. 1995. “Viscosity of Portland Cement Paste as a Function of Concentration.” *Advanced Cement Based Materials* 2 (2): 62–69.

Svensson, Ingvar L., Staffan Sjöberg, and Lars-Olof Öhman. 1986. “Polysilicate Equilibria in Concentrated Sodium Silicate Solutions.” *J. Chem. Soc., Faraday Trans. 1* 82 (12): 3635–46.

Sweeny, Keith H., and Richard D. Geckler. 1954. “The Rheology of Suspensions.” *Journal of Applied Physics* 25 (9): 1135–44. doi:doi:10.1063/1.1721828.

Tattersall, Geoffrey Howarth, and P. F. G. Banfill. 1983. *The Rheology of Fresh Concrete*. Monograph. http://trid.trb.org/view.aspx?id=199391.

Taylor, H. F. W. 1997. *Cement Chemistry*. Thomas Telford. http://books.google.com/books?hl=en&lr=&id=1BOETtwi7mMC&oi=fnd&pg=PA1&dq=taylor+h.f.w.+cement+chemistry+second+edition+thomas+telford&ots=6XveOt_Tuz&sig=4uomsHTLnBj1RXtnwKOXAPWJQLc.

Tennis, P., M.D.A. Thomas, and W.J. Weiss. 2011. *State-of-the-Art Report on Use of Limestone in Cements at Levels of up to 15%, SN3148*. Skokie, Illinois, USA: Portland Cement Association.

Termkhajornkit, Pipat, and Toyoharu Nawa. 2004. "The Fluidity of Fly Ash–cement Paste Containing Naphthalene Sulfonate Superplasticizer." *Cement and Concrete Research* 34 (6): 1017–24.

Texas Department of Transportation. 2012. "Where Has the Fly Ash Gone?" April. http://ftp.dot.state.tx.us/pub/txdot-info/cst/tips/fly_ash_0412.pdf.

Thomas, Jeffrey J., Hamlin M. Jennings, and Jeffrey J. Chen. 2009. "Influence of Nucleation Seeding on the Hydration Mechanisms of Tricalcium Silicate and Cement." *The Journal of Physical Chemistry C* 113 (11): 4327–34.

Tognonvi, Monique Tohoué, Dominique Massiot, André Lecomte, Sylvie Rossignol, and Jean-Pierre Bonnet. 2010. "Identification of Solvated Species Present in Concentrated and Dilute Sodium Silicate Solutions by Combined< Sup> 29</sup> Si NMR and SAXS Studies." *Journal of Colloid and Interface Science* 352 (2): 309–15.

Torquato, Salvatore. 2001. *Random Heterogeneous Materials: Microstructure and Macroscopic Properties*. Vol. 16. Springer. http://books.google.com/books?hl=en&lr=&id=PhG_X4-8DPAC&oi=fnd&pg=PA1&dq=Torquato,+S.,+Random+Heterogeneous+Materials:+Microstructure+and+Macroscopic+Properties,+New+York,+Springer,+2002&ots=SY79oX84qP&sig=IEz4lfxhdGIT2r4mE4Q_O_xJ250.

Tsivilis, S., G. Batis, E. Chaniotakis, Gr. Grigoriadis, and D. Theodossis. 2000. "Properties and Behavior of Limestone Cement Concrete and Mortar." *Cement and Concrete Research* 30 (10): 1679–83. doi:10.1016/S0008-8846(00)00372-0.

Tsivilis, S., E. Chaniotakis, E. Badogiannis, G. Pahoulas, and A. Ilias. 1999. "A Study on the Parameters Affecting the Properties of Portland Limestone Cements." *Cement and Concrete Composites* 21 (2): 107–16. doi:16/S0958-9465(98)00031-6.

Tsivilis, S., E. Chaniotakis, G. Batis, C. Meletiou, V. Kasselouri, G. Kakali, A. Sakellariou, G. Pavlakis, and C. Psimadas. 1999. "The Effect of Clinker and Limestone Quality on the Gas Permeability, Water Absorption and Pore Structure of Limestone Cement Concrete." *Cement and Concrete Composites* 21 (2): 139–46. doi:16/S0958-9465(98)00037-7.

Tsivilis, S., J. Tsantilas, G. Kakali, E. Chaniotakis, and A. Sakellariou. 2003. "The Permeability of Portland Limestone Cement Concrete." *Cement and Concrete Research* 33 (9): 1465–71. doi:16/S0008-8846(03)00092-9.

Tsivilis, S., N. Voglis, and J. Photou. 1999. "A Study of the Intergrinding of Clinker and Limestone." *Minerals Engineering* 12 (7): 837–40.

Vance, Kirk, Aditya Kumar, Gaurav Sant, and Narayanan Neithalath. 2013. "The Rheological Properties of Ternary Binders Containing Portland Cement, Limestone and Metakaolin or Fly Ash." *Cement and Concrete Research*

Submitted for Review. doi:10.1016/j.cemconcomp.2013.03.028. http://www.sciencedirect.com/science/article/pii/S0958946513000474.

Vance, Kirk, Gaurav Sant, and Narayanan Neithalath. “Rheology of Cement Pastes: A Closer Look at Experimental Parameters and Property Determination Using Common Rheological Models.” *Cement and Concrete Research* Submitted.

Vikan, H., H. Justnes, F. Winnefeld, and R. Figi. 2007. “Correlating Cement Characteristics with Rheology of Paste.” *Cement and Concrete Research* 37 (11): 1502–11. doi:16/j.cemconres.2007.08.011.

Vikan, Hedda, and Harald Justnes. 2007. “Rheology of Cementitious Paste with Silica Fume or Limestone.” *Cement and Concrete Research* 37 (11): 1512–17. doi:16/j.cemconres.2007.08.012.

Voglis, N., G. Kakali, E. Chaniotakis, and S. Tsivilis. 2005. “Portland-Limestone Cements. Their Properties and Hydration Compared to Those of Other Composite Cements.” *Cement and Concrete Composites* 27 (2): 191–96. doi:16/j.cemconcomp.2004.02.006.

Vuk, T., V. Tinta, R. Gabrovsek, and V. Kaucic. 2001. “The Effects of Limestone Addition, Clinker Type and Fineness on Properties of Portland Cement.” *Cement and Concrete Research* 31 (1): 135–39. doi:16/S0008-8846(00)00427-0.

Washburn, Edward W. 1921. “Note on a Method of Determining the Distribution of Pore Sizes in a Porous Material.” *Proceedings of the National Academy of Sciences of the United States of America*, 115–16.

Wierenga, Anieke M., and Albert P. Philipse. 1998. “Low-Shear Viscosity of Isotropic Dispersions of (Brownian) Rods and Fibres; a Review of Theory and Experiments.” *Colloids and Surfaces A: Physicochemical and Engineering Aspects* 137 (1): 355–72.

Wijnen, PWJG, T. P. M. Beelen, J. W. De Haan, C. P. J. Rummens, L. J. M. Van de Ven, and R. A. Van Santen. 1989. “Silica Gel Dissolution in Aqueous Alkali Metal Hydroxides Studied By< Sup> 29</sup> Si□ NMR.” *Journal of Non-Crystalline Solids* 109 (1): 85–94.

Wild, S., and J. M. Khatib. 1997. “Portlandite Consumption in Metakaolin Cement Pastes and Mortars.” *Cement and Concrete Research* 27 (1): 137–46. doi:10.1016/S0008-8846(96)00187-1.

Wild, S., J. M. Khatib, and A. Jones. 1996. “Relative Strength, Pozzolanic Activity and Cement Hydration in Superplasticised Metakaolin Concrete.” *Cement and Concrete Research* 26 (10): 1537–44. doi:10.1016/0008-8846(96)00148-2.

Williams, David A., Aaron W. Saak, and Hamlin M. Jennings. 1999. “The Influence of Mixing on the Rheology of Fresh Cement Paste.” *Cement and Concrete Research* 29 (9): 1491–96.

Winslow, Douglas N., and S. Diamond. 1970. “A Mercury Porosimetry Study of the Porosity in Portland Cement.” *Journal of Materials*. http://trid.trb.org/view.aspx?id=96627.

Worrell, E., L. Price, N. Martin, C. Hendriks, and L. O. Meida. 2001. “Carbon Dioxide Emissions from the Global Cement Industry 1.” *Annual Review of Energy and the Environment* 26 (1): 303–29.

Yahia, A., M. Tanimura, and Y. Shimoyama. 2005. “Rheological Properties of Highly Flowable Mortar Containing Limestone Filler-Effect of Powder Content and W/C Ratio.” *Cement and Concrete Research* 35 (3): 532–39.

Yang, M., and H.M. Jennings. 1995. “Influences of Mixing Methods on the Microstructure and Rheological Behavior of Cement Paste.” *Advanced Cement Based Materials* 2 (2): 70–78. doi:10.1016/1065-7355(95)90027-6.

Yang, M., C. M. Neubauer, and H. M. Jennings. 1997. “Interparticle Potential and Sedimentation Behavior of Cement Suspensions: Review and Results from Paste.” *Advanced Cement Based Materials* 5 (1): 1–7. doi:10.1016/S1065-7355(97)90009-2.

Ye, G., X. Liu, G. De Schutter, A. -M. Poppe, and L. Taerwe. 2007. “Influence of Limestone Powder Used as Filler in SCC on Hydration and Microstructure of Cement Pastes.” *Cement and Concrete Composites* 29 (2): 94–102. doi:10.1016/j.cemconcomp.2006.09.003.

Yuan, Qiang, Caijun Shi, Geert De Schutter, Katrien Audenaert, and Dehua Deng. 2009. “Chloride Binding of Cement-Based Materials Subjected to External Chloride Environment–a Review.” *Construction and Building Materials* 23 (1): 1–13.

Yunovich, M., and N. G. Thompson. 2003. “CORROSION OF HIGHWAY BRIDGES: ECONOMIC IMPACT AND CONTROL METHODOLOGIES.” *Concrete International* 25 (1). http://trid.trb.org/view.aspx?id=732496.

Zeng, Qiang, Kefei Li, Teddy Fen-Chong, and Patrick Dangla. 2012. “Analysis of Pore Structure, Contact Angle and Pore Entrapment of Blended Cement Pastes from Mercury Porosimetry Data.” *Cement and Concrete Composites* 34 (9): 1053–60. doi:10.1016/j.cemconcomp.2012.06.005.

Zhang, Min-Hong, Chiara F. Ferraris, Huaning Zhu, Vincent Picandet, Max A. Peltz, Paul Stutzman, and Daniel De Kee. 2010. “Measurement of Yield Stress for Concentrated Suspensions Using a Plate Device.” *Materials and Structures* 43 (1-2): 47–62.

Zhang, Xiong, and Jihong Han. 2000. “The Effect of Ultra-Fine Admixture on the Rheological Property of Cement Paste.” *Cement and Concrete Research* 30 (5): 827–30. doi:10.1016/S0008-8846(00)00236-2.

Zhou, Zhongwu, Michael J. Solomon, Peter J. Scales, and David V. Boger. 1999. “The Yield Stress of Concentrated Flocculated Suspensions of Size Distributed Particles.” *Journal of Rheology* 43: 651.